Dissertation zur Erlangung des Doktorgrades

der Fakultät für Chemie und Pharmazie

der Ludwig-Maximilians-Universität München

Identification and characterization of conformation-specific cytoplasmic integrin interactors

Hui-yuan Tseng

aus

Tainan, Taiwan

2015

Erklärung
Diese Dissertation wurde im Sinne von § 7 der Promotionsordnung vom 28. November 2011 von Herrn Prof. Dr. Reinhard Fässler betreut.

Eidesstattliche Versicherung

Diese Dissertation wurde eigenständig und ohne unerlaubte Hilfe erarbeitet.

München, ……

_____

(Hui-yuan Tseng)

Dissertation eingereicht am 17.08.2015
1. Gutachterin / 1. Gutachter: Prof. Dr. Reinhard Fässler
2. Gutachterin / 2. Gutachter: Prof. Dr. Christian Wahl-Schott
Mündliche Prüfung am 16.11.2015

Table of contents

List of publications

This thesis is based on the following publications, which are referred to in the text by their Roman numerals (I-V):

I. **Hui-yuan Tseng**, Ralph T. Böttcher1, Anna V. Samarelli, Tilman Ziegler, Nagarjuna Nagaraj, Charles R. Sanders, Roy Zent, and Reinhard Fässler **A proteomic approach reveals conformation specific cytoplasmic integrin interactors.** (*Manuscript in progress*)

II. Ralph Thomas Böttcher, Christopher Stremmel, Alexander Meves, Hannelore Meyer, Moritz Widmaier, **Hui-Yuan Tseng** and Reinhard Fässler. **Sorting nexin 17 prevents lysosomal degradation of β1integrins by binding to the β1-integrin tail.** Nat Cell Biol. 2012 14(6):584-92

III. **Hui-Yuan Tseng**, Niko Thorausch, Tilman Ziegler, Alexander Meves, Reinhard Fässler, and Ralph T. Böttcher. **Sorting nexin 31 binds multiple β integrin cytoplasmic domains and regulates β1 integrin surface levels and stability.** J Mol Biol. 2014 Sep 9;426(18):3180-94

The following publications were not the focus of my project but I contributed to them

IV. Zhiqi Sun, **Hui-Yuan Tseng**, Sally J. Deeb, Dirk Dedden, Maik Veelders, Naoko Mizuno, Matthias Mann, Reinhard Fässler. **Kank family proteins comprise a novel type of talin activator.** (*Manuscript in progress*)

V. Eugenia M. Yazlovitskaya , **Hui-yuan Tseng**, Olga Viquez, Tianxiang Tu, Glenda Mernaugh, Karen Riggins, Vito Quaranta, Peter Yurchenco, Arnoud Sonnenberg, Ralph T. Böttcher, Ambra Pozzi, Roy Zent. **Integrin α3β1 regulates kidney collecting duct development via TRAF6-dependent K63-linked polyubiquitination of Akt.** Mol. Biol. Cell May 15, 2015 vol. 26 no. 10 1857-1874

Abbreviations

aa	amino acid
ACAP1	ANK repeat and PH domain-containing protein1
ADAM	a disintegrin and metalloproteinase
ADMIDAS	adjacent to metal-ion-dependent adhesion site
Akt	RAC-alpha serine/threonine-protein kinase
ANK	Ankrin repeat
AP-2	adaptor protein-2
CDC42	cell division cycle 42
CMC	critical micelle concentration
Col	Collagen
CD	Collecting duct
cyto	cytoplasmic
D6PC	dihexanoylphosphatidylcholine
Dab-2	Disabled 2
DMPC	dimyristoylphosphatidylcholine
DOK1	Docking protein 1
DPC	Dodecylphosphocholine
ECM	extracellular matrix
EE	early endosome
EGF	epidermal growth factor
EM	electron microscopy
ER	endoplasmic reticulum
ESCRT	endosomal sorting complex required for transport
FA	focal adhesion
FAK	focal adhesion kinase
FB	fibrillar adhesion
FERM	4.1, Ezrin, Radixin, and Moesin
Fg	fibrinogen
FN	fibronectin
GAP	GTPase activating proteins

GDI	guanine nucleotide dissociation inhibitors
GEF	guanine nucleotide exchange factors
GFOGER	Glycine (G), phenylalanine (F),hydroxyproline (O), glutamic acid (E), arginine(R)
IBS	integrin-binding site
ICAM	intercellular cell adhesion molecule
Ig	immunoglobin
ILK	Integrin-linked kinase
IPP	ILK-parvin-pinch
KO	knockout
LE	late endosome
LAD	leukocyte adhesion deficiency
LIMBS	ligand-induced metal ion binding site
LCP1	lymphocyte cytosolic protein 1
LN	laminin
MDGI	mammary-derived growth inhibitor
MFGE8	milk fat globule-EGF factor 8
MIDAS	metal-ion-dependent adhesion site
MMP	matrix metalloproteinase
mTORC2	mammalian target of rapamycin complex 2
PDK1	phosphoinositol dependent kinase 1
PH	pleckstin homology
PI3K	Phosphatidylinositol 3-kinase
PIPKIγ	phosphatidylinositol 4-phosphate 5-kinase type Iγ
PKD1	protein kinase D1
PNRC	perinuclear recycling compartments
PSI	plexin, semaphorins, and integrins
PTB	phosphotyrosine-binding
PTEN	Phosphatase and tensin homolog
Rac1	Rasrelated C3 botulinum toxin substrate 1
RE	recycling endosome
RGD	arginine-glycine-aspartate

RhoA	Ras homologous
SHARPIN	SHANK-associated RH-domain containing protein
TGF-β	transforming growth factor β
TM	transmembrane
TNF	tumor necrosis factor
TRAF6	TNF receptor-associated factor 6
UB	ureteric bud
VCAM-1	vascular cell adhesion molecule-1
VN	vitronectin

Summary

Integrins are heterodimeric transmembrane proteins, composed of α and β subunits. A characterisitc feature of all integrin subunits except one is the presence of a short cytoplasmic domain that lacks enzymatic activity and actin binding sites. As a result integrins rely on the recruitment of proteins to their cytoplasmic tails to regulate their ligand binding affinity, to establish a connection to the actin cytoskeleton, to initiate intracellular signaling and even to regulate their intracellular protein trafficking. Thus, the cytoplasmic integrin interactors are crucial for the integrin's ability to regulate various cellular functions, including cell migration, cell spreading, and cell survival.

Integrins undergo allosteric conformational changes characterized by altered affinity for their ligands through binding of the intracellular proteins talin and kindlin to the cytoplasmic tails of β integrins (inside-out activation). In their inactive state transmembrane and cytoplasmic (TMcyto) domains of the two integrin subunits are associated, while they become separated upon integrin activation. There is growing evidence that integrin inactivation might not be the default state but is actively regulated by the binding of intracellular integrin inactivators. Such inactivators may deactivate integrins or lock integrins in an inactive state thereby establishing a regulatory mechanism to efficiently prevent unwanted integrin activation. Furthermore, interactors of inactive integrins would also allow cells to distinguish between active and inactive integrins in other processes such as integrin biosynthesis and intracellular integrin trafficking.

We hypothesized such cytoplasmic proteins exist and specifically interact with integrin heterodimers in their low-affinity conformation by binding to the associated α-β integrin tails. Recently, filamin A has been shown to interact with both α and β tails to retain integrins in an inactive state thereby preventing unwanted integrin activation, which is particularly important for cells of hematopoietic origin such as leukocytes. However, filamin A is the only tail interactor so far to fulfil this criteria.

In my PhD thesis, I aimed to identify specific and common interacting partners of α and β subunits of different integrin heterodimers (α5, αIIb, αM and β1, β2, β3) and to characterize conformation-specific integrin tail interactors of αMβ2 integrins in an unbiased proteomics approach (**Paper I**). To achieve this I modified commonly used

pull-down protocols in two ways: (i) I incorporated recombinant integrin α or TMcyto β domains into bicelles as membrane-mimicking system to strengthen the interaction of proteins that require interaction with the plasma membrane to bind integrins. Several integrin tail binding proteins such as talin, kindlin and ILK depend on the interaction with the plasma membrane for proper integrin binding and function. (ii) I engineered recombinant proteins by fusing the TMcyto tails to the Fos and Jun dimerization domains as 'velcro' to obtain stably associated dimers that mimic the inactive integrin conformation.

Single α- and β subunits as well as the αMβ2-TMcyto complexes were incorporated into bicelles and used as baits to pull down interacting proteins from bone marrow derived macrophage cell lysates, which were analyzed by high-resolution mass spectrometry. This approach allowed me to systemically identify and compare cytoplasmic interactors of the single α- and β integrin subunits and proteins binding preferentially to dimerized αMβ2 integrin tails.

Candidate proteins were further characterized for their involvement in the regulation of integrin activation, signalling and integrin trafficking. The protein KN motif and ankyrin repeat domains 2 (Kank2) was pulled-down with β1 integrin tails and my initial analysis indicated that Kank2 localized at focal adhesion and Kank2 depletion in fibroblasts increases cell migration speed. This project was continued by the PhD student Zhiqi Sun under the supervision of Prof. Dr. Reinhard Fässler (**Paper IV**). I selected one protein that showed increased binding to the associated αMβ2 dimer compared to the single subunits, lymphocyte cytosolic protein 1 (LCP1). Regarding, LCP1 we were able to show that LCP1 co-IPs strong with αMβ2 integrins in resting macrophages while activation of the macrophages leads to reduced LCP1-αMβ2 interaction confirming our proteomics data of preferential LCP1 binding to the associated (inactive) αMβ2 integrin tails. Knock-down of LCP1 in macrophage cells (Raw264.7) and in differentiated neutrophils (PLB-985) increases αMβ2 surface levels and enhances cell adhesion of non-activated macrophages (**paper I**) indicating a role of LCP1 in regulating integrin surface levels and/or integrin activation.

In the second paper, we described a novel cytoplasmic β1 integrin interactor, sorting nexin 17 (SNX17), and its role in the regulation of β1 integrin stabilization. SNX17

directly binds to the membrane-distal NxxY motif of β1 integrin tails in early endosomes to prevent β1 integrin degradation and thereby enables integrin recycling back to the cell surface. Depletion of SNX17 or disruption of the SNX17-β1 integrin interaction causes rapid degradation of integrins and decreases migration speed of fibroblast on fibronectin-coated surfaces. Thus, the membrane distal NxxY motif of the β1 integrin tail is part of a spatial-temporally controlled series of β1 integrin-protein interactions that controls β1 integrin activation and signaling at the plasma membrane and subsequently their sorting from early endosomes back to the plasma membrane.

We showed that the interaction of SNX17 with β1 integrin tails is mediated by the SNX17-FERM (4.1, Ezrin, Radixin, and Moesin) domain (**paper II**). As the mammalian genome encodes for three SNXs proteins that harbour FERM domain, SNX17, SNX27, and SNX31, the other FERM-SNX family members could also bind β integrin tails to regulate integrin functions. However, we could show that only SNX17 and SNX31 but not SNX27 interact with multiple integrin β tails in early endosome in a phosphatidylinositol 3-kinase-dependent manner (**paper III**). This interaction depends on the FERM domain within the SNX proteins and the conserved NxxY motif in the β integrin tails. Consequently, SNX31 can rescue the reduced β1 integrin surface levels and stability in SNX17-depleted cells. While SNX17 is ubiquitously expressed, SNX31 is an integrin trafficking regulator with a restricted expressed pattern, expressed mainly in bladder and melanoma tissue.

Finally, in the proteomics integrin interactor screen, I identified the ubiquitin-modifying enzyme TNF receptor-associated factor 6 (TRAF6) as an interactor with the integrin β1 subunit. In parallel, Dr. Roy Zent (Vanderbilt University, USA) showed that integrin α3β1 modulates Akt activation in the developing collecting system and that Akt activation is PI3K-independent but requires K63-linked polyubiquitination. Together with the Zent group we showed that integrin α3β1-dependent K63-linked polyubiquitination of Akt is mediated by TRAF6. The role of TRAF6 in collecting duct development in kidney was further supported in TRAF6-deficient mice, which displayed similar kidney defects as α3 integrin knockout mice (**paper V**).

Introduction

1. The integrin receptor family

Multicellular organisms assemble cells and extracellular matrices (ECM) into distinct organs and tissues using different sets of adhesion molecules. Integrins are a major class of transmembrane cell adhesion receptors in metazoan cells conserved from sponges, corals, nematodes, and echinoderms to mammals (Burke, 1999; Hynes, 2002; van der Flier and Sonnenberg, 2001). Integrins exist as non-covalently interacting heterodimers with one α and one β subunit. Structurally they consist of three major parts: (1) a large extracellular domain, (2) a single-membrane-spanning transmembrane (TM) domain, (3) and a generally short cytoplasmic tail between 40 and 60 amino acids (except β4 integrin which has a long tail of 1018 amino acids).

One of the main roles of integrins is to link the ECM to the actin cytoskeleton. The extracellular domain binds to ECM proteins such as collagens and fibronectins, or to cellular counter-receptors like vascular cell adhesion molecule-1 (VCAM-1) and the intercellular cell adhesion molecule (ICAM) family on adjacent cell surfaces (Hynes, 2002; Plow et al., 2000) while the cytoplasmic tail binds to adaptor proteins to create the linkage between integrins and the actin cytoskeleton. Apart from adhesion and linkage to cytoskeleton, integrins also modulate different signal transduction pathways to control a wide range of biological and cellular events including cell adhesion, migration, proliferation, cell differentiation, and apoptosis, which are crucial for embryonic development and homeostasis of multicellular organisms (Giancotti and Ruoslahti, 1999). Based on the ability to ‘integrate’ cues from the extracellular ligands with the cells’ interior cytoskeleton, the term ‘integrin’ was coined (Tamkun et al., 1986). Notably, integrins do no possess enzymatic activity or actin-binding domains but serve as a hub to assemble and cluster adaptor and regulatory proteins in response to external or internal signals. In addition, the interaction of intracellular proteins with integrin cytoplasmic tails can induce conformational changes in the ectodomain characterized by altered affinity for their ligands (‘inside-out’ signalling). Thus, the cytoplasmic tail of integrins and their binding partners are crucial for the unique ability of integrins to signal bi-directionally across the plasma membrane.

1.1 Integrins and their ligands

Mammals express 18 α and 8 β subunits, which combine to form 24 integrin heterodimers. Heterodimerization takes place in the endoplasmic reticulum (ER) and is a pre-requisite for integrin transport to the cell surface (Rosa and McEver, 1989). The different combinations of αβ integrin heterodimers are characterized by distinct ligand binding specificity and tissue distribution. Integrins can be grouped into four classes depending on their binding specificity: 1. RGD (arginine, glycine, aspartate)-binding integrins. 2. Collagen (Col)-binding integrins. 3 Laminin (LN)-binding integrins. 4. Leukocyte-specific integrins (Figure 1 and Table 1):

1. RGD-binding integrins bind to ECM molecules, which contain exposed RGD motifs such as fibronectin (FN), vitronectin (VN), fibrinogen (Fg). This group includes all five αV heterodimers (αvβ1, αvβ3, αvβ5, αvβ6 and αvβ8); two β1 integrins (α5β1, α8β1), and the platelet integrin αIIbβ3. Additionally, β1 integrin also dimerizes with α4 and α9 subunits, which binds to the functionally related Leu-Asp-Val (LDV) motif. These receptors recognize both FN and Ig-superfamily proteins such as VCAM-1.
2. Collagen (Col)-binding integrins consists of the β1 heterodimers α1β1, α2β1, α10β1 and α11β1. They recognize Gly-Phe-Hyp-Gly-Glu-Arg (GFOGER; O represent Hydroxyproline) peptides. The different heterodimers vary in their preference to different Col types. Importantly, all of these α-subunits contain a special αI domain in their extracellular domain, critical for ligand binding (discuss in section 1.3).
3. Laminin (LN)-binding integrins consist of α3β1, α6β1, α7β1, and α6β4 integrins. The binding motif in LN recognized by the integrins varies depending on the integrin heterodimer (Humphries et al., 2006).
4. Leukocyte-specific integrins atr defined by their specific expression in leucocytes to establish cell-cell contacts with endothelial cells by interacting with cellular counter-receptors such as ICAM and VCAM (Hynes, 2002; Ley et al., 2007). This group consists of β2 integrin-containing family αLβ2, αMβ2, αXβ2, αDβ2 as well as α4β7 and αEβ7 (specific for E-Cadherin). Similar to the Col receptors, the leukocyte-specific integrins evolved by the insertion of the αI-domain.

Besides the classical integrin ligands, additional integrin ligands also have been described (Table 1). These ligands include ADAM family members interacting with

α4β1, α5β1, α6β1, α9β1, αVβ3 and αVβ6, which are involved in ECM remodeling during cell adhesion and migration (Legate and Fassler, 2009). Proteolysis derived protein products, such as Endostatin (from Col XVIII), endorepellin (from perlecan, known as heparin sulfate proteoglycan 2) tumstatin (from Col α3) (Bix and Iozzo, 2005; Wickstrom and Keski-Oja, 2005), Milk fat globule-EGF factor 8 (MFGE8) and complement factor iC3b participate in phagocytosis of apoptotic cells and pathogens. More of these integrin ligands, along with their respective integrin partners, are known (Table 1 (Humphries et al., 2006).)

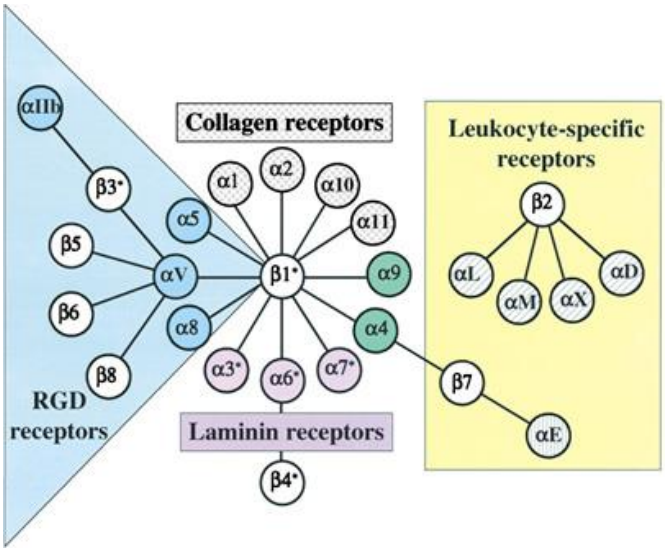

Figure 1. Mammalian integrin receptor family and their main ligands. 8 β subunits can associate with 18 α subunits to form 24 distinct integrin heterodimers. The αβ subunit combination determines the ligand-binding specificity. Many cell types express more than one integrin heterodimer.
(taken from Hynes 2002)

Table 1 Characteristics of human integrin heterodimers (modified from Barczyk et al., 2010)

Integrin heterodimer	α subunit characteristics	αI	Ligands	Additional ligands
α1β1 (CD49a, VLA1)	1151 aa		collagens (collagen IV > collagen I > collagen IX)	Semaphorin 7A
α2β1 (CD29b, VLA2)	1181 aa		collagens (collagen I > collagen IV; collagen IX)	E-cadherin, endorepellin
α3β1 (CD49c, VLA3)	1051 aa, splice variants α3A, α3B	V	laminins (LN-511 > LN-332 > LN-211)	
α4β1 (CD49d, VLA4)	1038 aa		fibronectin, VCAM-1	
α5β1 (CD49e, VLA5)	1049 aa	V	fibronectin (RGD)	endostatin
α6β1 (CD49f, VLA6)	1073 aa, splice variants α6A, α6B	V	laminins (LN-511 > LN-332 > LN-211 > LN-411)	
α7β1	1137 aa, splice variants α7X1, α7X2	V	α7X1β1: laminins (LN-511 > LN-211 > LN-411 > LN-111) α7X2β1: laminins (LN-111 > LN-211 > LN-511)	
α8β1	1025 aa	V	fibronectin, vitronectin, nephronectin (RGD)	
α9β1	1035 aa		tenascin-C, VEGF-C, VEGF-D	osteopontin
α10β1	1167 aa		collagens (collagen IV > collagenVI > collagen II; collagen IX)	
α11β1	1188 aa		collagens (collagen I > collagen IV; collagen IX)	
αLβ2 (CD11a, LFA1)	1170 aa		ICAM-1, -2, -3, -5	
αMβ2(CD11b,MAC1)	1153 aa		iC3b, fibrinogen + more	
αXβ2(CD11c)	1163 aa		iC3b, fibrinogen + more	
αDβ2(CD11d)	1162 aa		ICAM-3, VCAM-1	
αIIbβ3 (CD42,GpIIb)	1039 aa	V	fibrinogen, fibronectin (RGD)	
αVβ1	1048 aa	V	fibronectin, vitronectin (RGD)	
αVβ3		V	vitronectin, fibrinogen, fibronectin (RGD)	tumstatin
αVβ5		V	vitronectin (RGD)	
αVβ6		V	fibronectin, TGF-β-LAP (RGD)	
αVβ8		V	vitronectin, TGF-β-LAP (RGD)	
αEβ7(CD103,HML1)	1178 aa	V	E-cadherin	
α4β7			MadCAM-1, fibronectin, VCAM-1	
α6β4		V	laminins (LN-332, LN511)	

Table 1 (continue) (Modified from Barczyk et al., 2010)

Integrin β chain	β subunit characteristics	Notes
β1 (CD29, GpIIa)	798 aa, splice variants β1A-D	Splice variants β1B and β1C not present in mice, minor variants with unclear function
β2 (CD18)	769 aa	
β3 (CD61, GpIIIa)	788 aa, splice variants β3A, β3B, and β3C	β3A major form
β4 (CD104,TSP-180)	1875 aa, splice variants β4A-E	β4A and β4B major forms, similar function
β5	799 aa, splice variants β5A, β5B	Both splice variants have similar functions
β6	788 aa	
β7	798 aa	(LPAM-1, βP)
β8	769 aa	

Cells frequently express splice variants of integrins contributing to the complexity of the integrin family. Variable sequences have been found in the extracellular domain of many integrin subunits that might regulate integrin activity or ligand-binding affinity while cytoplasmic variation affect integrin activity, connection to cytoskeleton, and signaling. The integrin heterodimers and their splice variants are expressed in distinct tissues and embryonic developmental stages suggesting vital functions although not all the functions of these splice variants are well-characterized (de Melker and Sonnenberg, 1999; van der Flier and Sonnenberg, 2001). Best characterized examples are the four cytoplasmic β1 subunit variants: β1A, β1B, β1C, and β1D. β1A is ubiquitously expressed in all tissues except mature cardiac and skeletal muscle, in which β1D is expressed instead. Splice variants β1B and β1C are not present in mice and their function is still unclear. Expression using genetically modified mice revealed different roles of β1A and β1D in embryonic development. Expression of β1D instead of β1A leads to early embryonic lethality, while replacement of β1D with β1A in mice causes mild abnormalities in striated muscles (Baudoin et al., 1998) indicating a non-substitutable role of β1A during development.

1.2 Integrin and mouse development

Integrins have multiple functions, which are reflected by the diversity of phenotypes observed in mice lacking individual α or β subunits (Table 2) despite the fact that integrins have overlapping ligand preferences (Bouvard et al., 2013; Hynes, 2002). This diversity originates from the different spatial and temporal expression pattern, different functional regulation and different signaling properties of individual integrin heterodimers. Genetic ablation of β1 integrin leads to peri-implantation lethality characterized by a failure of the inner cell mass (ICM) to form (Fassler et al., 1995; Stephens et al., 1995). The α4, α5, and αv integrin KO phenotypes are less severe but still embryonic lethal at different developmental stages: α5 KO embryos die between embryonic day 9.5 (E9.5) and E10 due to extraembryonic and embryonic vascular defects (Yang et al., 1993); α4 deletion leads to death between day E11 and E14 as the result from the defective choriallantois fusion and abnormal cardiac development (Yang et al., 1995); αv KO embryos die between E10 and E12 because of a placental defects or cleft palate and massive hemorrhages (Bader et al., 1998). The KOs of α3, α6, α8, β4, or β8 are lethal perinatal due to various phenotypes (See Table 2). Genetic deletion of other integrins leads to the defects in hematopoietic cell function (α2, αIIb, αL, αM, αE, β2, β3 and β7), inflammation (β6), angiogenesis (α1 and β3) and muscular dystrophy (α7).

KO mice serve as models for abnormal integrin functions, which are the underlying cause of several human diseases. Glanzmann thrombosthenia is a human disorder characterized by platelet dysfunction and bleeding caused in some patients by mutations in αIIb and β3 integrin subunits. Deletion of both integrins in mice also results in defective platelet aggregation (Hodivala-Dilke et al., 1999; Hogg and Bates, 2000; Tronik-Le Roux et al., 2000). Ablation of β2 integrin in mice mimics the adhesion defects detectable in human leukocyte adhesion deficiency (LAD)-I patients (Hogg and Bates, 2000; Scharffetter-Kochanek et al., 1998). LAD is currently divided into three subtypes, LAD-I, -II and –III. LAD-I results from mutations in the β2 integrin subunit (Kishimoto et al., 1987). Leukocytes from these patients either lack the integrin heterodimers such as αMβ2 and αLβ2 or express only very low levels preventing firm adhesion. LAD-III is also known as LAD-I variant is characterized by LAD-I like immunodeficiency and additional

Glanzmann's thrombasthenia-like bleedings. Mutations within the *KIND-3* gene (see section 2.1.1) are responsible for LAD-III, resulting in the combined defects in β1, β2, and β3 integrin activation in all hematopoietic cells. Whilst defects in integrin function are the underlying causes of LAD-I and –III, defects in the posttranslational fucosylation of selectin ligands lead to a loss of selectin ligands on the cell surface dramatically reducing leukocyte rolling and resulting in LAD-II (Schmidt et al., 2013).

Finally, mutations in α6 and β4 in humans result in junctional epidermolysis bullosa with skin blistering (Takizawa et al., 1997; Vidal et al., 1995). These phenotypes can be also observed in α6 (Georges-Labouesse et al., 1996) or β4 (van der Neut et al., 1996) integrin KO mice.

1.3 Integrin structure and activity

Structurally, each integrin subunit consists of a large extracellular domain (80-150kDa), a single strand spanning the membrane and a short cytoplasmic tail of about 20-50 amino acids (aa). The only exception is the β4 integrin subunit with a long cytoplasmic domain of 1072 residues (Wegener and Campbell, 2008). The cytoplasmic tail domains of β subunits except β4 are highly conserved, while the α-subunit tails are more divergent.

A unique feature of integrin heterodimers is their ability to regulate their affinity for ligands through an allosteric conformational switch by converting the unbound form of integrins from the low affinity (the "inactive" state; bent extracellular domain, associated TM domains and cytoplasmic tails) via an intermediate ligand binding affinity (or primed state) to the ligand-bound, high affinity (the "active" state; extended extracellular domain, separated TM domains and cytoplasmic tails) state. Long-range allosteric rearrangements underlie the transitions between these states that allow integrins to signal bi-directionally across the plasma membrane (section 2). A large number of structural studies revealed the mechanism of ligand-binding and affinity regulation including crystal structures of the complete αvβ3 (Xiong et al., 2001; Xiong et al., 2002), αIIbβ3 (Zhu et al., 2008) and αxβ2 (Xie et al., 2010) extracellular domains and of different integrin fragments. Crystal structures were strengthened by NMR and electron microscopy (EM)-imaging of complete extracellular domains as well as full

length αIIbβ3 integrins embedded in nanodiscs (section 5.3) (reviewed in (Campbell and Humphries, 2011)). The following chapters describe the three main integrin domains in more detail:

Table 2 Integrin knockout mice: phenotypes and the connection to human disease. (taken from Bouvard et al., 2012)

Integrin subunit	Mouse phenotype	Effects of loss	Link to human disease
α1	Viable, fertile	Defects in collagen synthesis, tumour angiogenesis, small kidneys, skin hardening	Unknown
α2	Viable, fertile	Defects in platelet adhesion, mammary ductal branching and kidney development	Unknown
α3	Perinatal lethal	Defects in kidney and lung development, skin blistering	Interstitial lung disease, nephrotic syndrome, epidermolysis bullosa
α4	Embryonic lethal	Defects in placenta formation, cardiac development and haematopoietic cell maintenance and homing	Unknown
α5	Embryonic lethal	Defects in neural crest cell survival and mesoderm formation	Unknown
α6	Perinatal lethal	Defects in brain cortex organization, skin blistering	Junctional epidermolysis bullosa with pyloric stenosis
α7	Perinatal lethal	Defects in vascular development and placenta formation, muscular dystrophy	Muscular dystrophy
α8	Perinatal lethal	Kidney defects, deafness	Unknown
α9	Perinatal lethal	Defects in lymphatic valve formation and in the development of the lymphatic system, congenital chylothorax*	Congenital chylothorax
α10	Viable, fertile	Dwarfism, mild chondrodysplasia	Unknown
α11	Viable, fertile	Dwarfism, increase mortality, defective incisor eruption	Unknown
αv	Embryonic or perinatal lethal	Defects in placenta formation and in CNS and GI blood cell development, cleft palate	Unknown
αx	Viable, fertile	T cell defects, increased susceptibility to bacterial infections	Systemic lupus erythematosus
αL	Viable, fertile	Impaired leucocyte recruitment and tumour rejection, defects in osteoclast development	Psoriasis
αD	Viable, fertile	Increased susceptibility to bacterial infections	Unknown
αM	Viable, fertile	Impaired phagocytosis and PMN apoptosis, obesity, defective mast cell development	Systemic lupus erythematosus
αE	Viable, fertile	Reduced lymphocyte numbers	Unknown
αIIb	Viable, fertile	Platelet abnormalities	Glanzmann's thrombasthenia, thrombocytopenia
β1	Embryonic lethal	Inner cell mass deterioration	Unknown
β2	Viable, fertile	Impaired leucocyte migration, skin infections, osteoporosis	LADI
β3	Viable, fertile	Platelet abnormalities, bone defects	Glanzmann's thrombasthenia, thrombocytopenia
β4	Perinatal lethal	Skin blistering	Epidermolysis bullosa
β5	Viable, fertile	No apparent phenotype	Unknown
β6	Viable, fertile	TGFβ activation defect, juvenile baldness, asthma, periodontal disease	Asthma
β7	Viable, fertile	Immunological defects	Inflammatory bowel disease
β8	Embryonic or perinatal lethal	Defects in placenta and in CNS and GI blood cell development, cleft palate	Unknown

1.3.1 Extracellular domain

The first crystal structure of an integrin extracellular domain (integrin αVβ3) showed that the heterodimer assembles into an ovoid "head" and two "legs" and that it is severely bent at a defined region in its legs, reflecting an unusual flexibility that was thought to be connected to integrin regulation (Xiong et al., 2001). The domains within α and β integrin subunits were defined after this structure. The α subunits generally contain a β propeller head domain, a Thigh domain followed by two Calf domains, which share structural similarities to immunoglobulin β-sandwich folds (Figure 2). These domains bear relatively less structural flexibility. An important flexible interface is located between the Calf-1 and Thigh domain connect by a small Ca^{2+} binding loop, termed ‘genu’ as a joint, which extends in switchblade model of integrin activation (see below). Furthermore, as indicated in the previous chapter some α subunits (α1, α2, α10, α11, αL, αM, αX, αD) carry an additional insertion of ligand binding competent αI domain (Figure 2B), a 200 aa insertion into second and third β-sheet of the β propeller, also known as von Willebrand factor A domain, which is associated to ligand binding affinity (see below).

The structure of β integrin subunits are more sophisticated. They consist of a PSI (plexin, semaphorins, and integrins) domain inserted by a hybrid domain, which is inserted by a ligand binding βI domain forming the headpiece (Figure 2). The βI domain includes two segments: the first forms the interface with the β-propeller in α subunit and the second is essential for specific ligand binding, known as the specificity determining loop (SDL). While the headpiece is relatively stiff, the leg piece is structurally flexible and consists of four tandem cysteine-rich EGF-like repeats interconnected with disulfide bond and a membrane proximal β tail domain (Figure 2). Highest flexibility is observed between EGF-1 and EGF-2, which are in close proximity to the ‘genu’ of α subunits and critically contribute to ligand binding through unbending of the integrin headpiece.

The αI and βI domains are structurally homologous. Both domains harbor a conserved ‘metal-ion-dependent adhesion site’ (MIDAS), which is occupied by Mg^{2+} under physiological conditions (Xia and Springer, 2014). In integrins composed of an αI domain-containing α subunit, the ligand binding will be mediated by the αI domain while the ligand binding site of the βI domain is associated to a β-propeller in the α subunit

(Figure 2B) (Zhu et al., 2013). The MIDAS in the βI-domain is flanked by two additional Ca^{2+} binding sites, which participate in integrin-ligand affinity regulation: ADMIDAS (adjacent to metal-ion-dependent adhesion site) and LIMBS (ligand-induced metal ion binding site or Synergistic Metal ion Binding site (SyMBS)). ADMIDAS has inhibitory effect and LIMBS is named because this site is only formed after ligand binding and functions to stabilize ligand binding. Owing to the existence of these sites, integrin activation is influenced by divalent cations: (1) Mg^{2+} has an activatory role (contributed to MIDAS). (2) High concentrations of Ca^{2+} (>1mM) negatively affects ligand binding and (due to inhibitory effect by ADMIDAS) (3) it is speculated that Mn^{2+} induces a high affinity integrin confirmation through replacement of Ca^{2+} at the ADMIDAS site of the βI domain although the underlying mechanism is still not clear. Conversely, incubation of cells with metal ion chelators, for example EDTA, affects integrin activity in a concentration dependent manner as well. At intermediate concentrations, EDTA causes inhibitory effect (probably through removal Mg^{2+} from MIDAS) while it activates integrins at higher concentrations (likely chelates Ca^{2+} ions) (Humphries et al., 2003; Springer et al., 2008; Wegener and Campbell, 2008; Xia and Springer, 2014; Zhu et al., 2013).

The structural analysis of integrin heterodimers revealed the integrin atomic structure and also the conformational changes accompanied by ligand binding. Although controversies remain, it is generally believed that the extracellular domain of integrins reversibly shifts between three (only two in α5β1) conformations with different ligand binding affinities: a bent conformation (low-affinity for ligand, not observed in α5β1), a half-extended (intermediate affinity), and an extended (high-affinity) conformation. The bent conformation has been observed for the ectodomains of αVβ3, αLβ2 and αXβ2 integrins in electron micrograph by negative staining when the C-termini were clasped or when samples were prepared in Ca^{2+}-containing buffer (Nishida et al., 2006; Takagi et al., 2002), while α5β1 integrin prepared with same clasped C-termini revealed only extended conformers (Takagi et al., 2001) indicating integrin heterodimer dependent differences. This raises the question whether all integrin heterodimers adopt a bent conformation. Notably, the images of the bent conformers were obtained by EM-negative staining of the extracellular domain but without taking contributions of the transmembrane and cytoplasmic regions into consideration. Other factors, such as

differences in the sample preparation, sampling bias in EM, distinct lipid usage might also explain discrepancies between different structural studies. For example, cyro-EM data shows the inactive αIIbβ3 integrins isolated from platelet expose an intermediate conformation between bent and extended forms (Adair and Yeager, 2002), while αIIbβ3 integrins inserted into liposomes showed a bent conformation in the presence and absence of Mn^{2+} activation. (Ye et al., 2008). Additional EM study revealed that by embedding full length αIIbβ3 into nanodisc (see section 5.2), they adopt an open conformation when activated by talin head (Ye et al., 2010). This study agrees with a shift in the conformation equilibrium from bent to extended conformations of integrins.

Despite the controversial studies it is believed that the shift from bent (intermediated in α5β1) to extended conformation (integrin activation) is possibly induced by the binding of extracellular ligand or mainly regulated by the binding of integrin activator proteins talin and kindlin (inside-out signaling, see section 2.1). Two models have been proposed to illustrate the underlying structural changes during integrin activation: in the deadbolt model, integrin ligand-binding occurs before extension of integrin extracellular domain while it happens after extension in the switchblade model.

In the low affinity conformation, the headpiece of the integrin folds over its legs at the genu and faces down towards the plasma membrane (Figure 2A-1 and 2B-1). The ‘switchblade’ model states that during the transition from a bent to the extended conformation, the separation of the cytoplasmic and TM domain causes a switchblade-like knee extension of the bent integrin, which leads to the dislocation from the EGF-like repeats within the β leg. In turn, an outward motion of the hybrid domain occurs, making an obtuse angle with the βI domain leading to the "opening" of the ligand binding pocket on extracellular domain to allow ligand binding (Figure 2). In contrast, the ‘deadbolt’ model does not require unbending but, upon a piston-like movement in the tilt of the TM domains that results in sliding of the extracellular legs of α and β subunits. As a result the interaction between headpiece and β legs is disrupted just beyond the membrane and ligand binding site of the head domain (Arnaout et al., 2005; Askari et al., 2009; Wegener and Campbell, 2008; Zhu et al., 2008).

In the case of αLβ2 integrin, the ligand binding affinities increase from 2mM for the bend conformation up to 200nM in the active, extended conformation (Carman and Springer, 2003). The strong differences in the ligand binding affinities and their tight regulation is especially important for integrins expressed in hematopoietic cells as 'unwanted' ligand interactions could lead to catastrophic effects such as blood clotting. In contrast, such a tight control might not be essential for adherent cell types such as fibroblasts. Indeed, the clasped α5β1 integrin, adopt a non-bent conformation with high affinity to FN (35nM) under non-stimulation condition which only slightly increases to 6.3nM upon transition into the unclasped, fully extended conformation (Takagi et al., 2001).

1.3.2 Transmembrane and cytoplasmic domains

Conformational changes of the integrin TM domain are crucial to transmit signals between the extracellular environment and the intracellular compartment across the plasma membrane and to mediate integrin activation as well. Therefore, much effort has been devoted to understand the TM domain structure to comprehend the undergoing structural changes during integrin activation and integrin-mediated signaling. Unfortunately, there is still no high resolution X-ray crystal structure available for the TM segments. Among all integrins, the TM domain of αIIbβ3 has been studied most extensively. Recent structures of αIIb and β3 integrins TM regions incorporated into bicelles model membranes have been solved by NMR separately and in a heterodimeric complex (Lau et al., 2008a; Lau et al., 2009; Lau et al., 2008b). Notably, earlier NMR studies using micelles could not detect the α-β interaction (Li et al., 2001) while it is successfully detected with lipid bicelles (see also section 5.2) as a membrane mimicking system (Lau et al., 2009). Meanwhile, a similar structure as αIIbβ3 embedded in bicelles (Lau et al., 2009) was also obtained for the TM region of αIIbβ3 using disulfide-based distance restraints combined with protein modeling (Zhu et al., 2009).

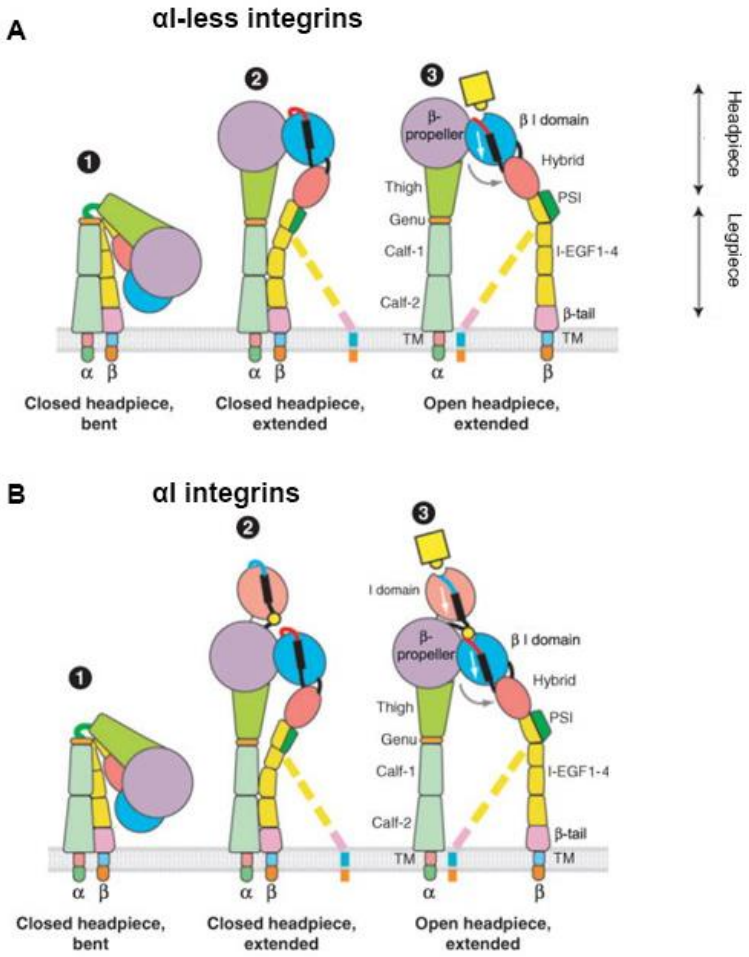

Figure 2. The structure of integrin heterodimers. The scheme depicts the integrin structure in in αI-less (A) and αI containing (B) integrins in low (1), intermediate (2) and high affinity state (3) and illustrates the domain rearrangement during activation. In the bent/inactive state (A-1, B-1), the orientation and closed conformation of the headpiece resulting in no ligand binding which is stabilized by tight interaction of the hybrid domain and the integrin leg regions. In A-2 and B-2, the integrin adopts an extended, ligand binding competent conformation. Ligand binding induces further conformational changes in the headpiece, resulting in an “open-extended” conformation coupled to the hybrid domain via pistoning of the βI-α7-helix (black cylinder), leading to hybrid domain swing out and stabilization of the “open” high affinity conformation (A-3, B-3). The proposed predominant orientation of the flexible β subunit lower legs is shown, whereas the less predominant is indicated with dashed lines. (modified from Shatti et al., 2010)

The sequences of the TM regions are well-conserved among integrins suggesting that the interactions between consensus reciprocal groups on α and β helices are essential for integrin heterodimer formation (Figure 3A-B). In the NMR

structure of the αIIbβ3 TM complex embedded in bicelles, the 24 aa long αIIb helix is perpendicular into the membrane, whereas the 29 aa β3 helix is ~25° tilted to enable the side chains of its hydrophobic residues to embed into membrane (Lau et al., 2009). Indeed, NMR analysis of TM domains of αIIbβ3 integrins successfully detected the association of αIIb and β3 (Lau et al., 2009). Two interaction areas are observed in (1) the 'outer membrane clasp (OMC)' formed by the interaction of conserved glycine residues, αIIb G972/G976 and β3 G708 allowing close helix packing. (2) The 'inner membrane clasp' (IMC) is established by an unusual αIIb backbone reversal that packs a consecutive hydrophobic interaction of Phe residues (αIIb F992-F993) against the β3 TM helix (β3 L712, W715, K716, I719) promoting the electrostatic bridge between αIIb R995 and β3 D723 residues (Fig. 3C-D) (Lau et al., 2009). This αIIb-D723/ β3-R995 salt bridge has previously been proposed to explain the stabilizing effect of these residues on the αIIbβ3 integrin inactive state (Hughes et al., 1996).

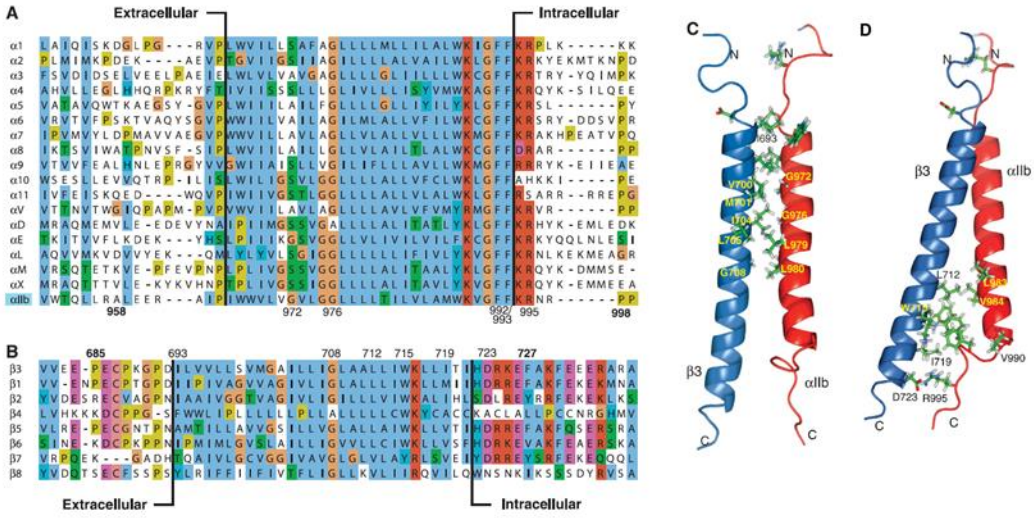

Figure 3. Interactions of TM regions of integrin heterodimers. Sequence alignment of the transmembrane segments of all human integrin subunits (A) α and (B) β. Interactions of the TM segment of αIIbβ3 integrin in the **(C)** outer- or **(D)** inner- plasma membrane clasp. The structures were predicted by NMR for the resting conformation of αIIbβ3 integrins embedded in a bicellar lipid environment. (modified from Lau et al., 2009)

Several mutational studies of the integrin transmembrane domains and molecular modeling experiments indicate that dissociation of the α-β integrin transmembrane domains results in integrin activation. Mutations in β3 TM domain, G708N, G708L and G708I, or the αIIb subunits (G972 or G976 in GxxxG motif in to bulky aa, Leu or Asn) activate αIIbβ3 integrin and increase ligand binding affinity (Li et al., 2003; Luo et al., 2005; Partridge et al., 2005). These studies suggest that the helical packing of OMC interaction in TM regions requires Gly residues from both α and β subunit to stabilize integrin in low affinity conformation. In contrast, the introduction of an artificial disulfide bond in TM region of αIIbβ3 integrin prevents separation of the TM domains and inhibits integrin activation (Luo et al., 2004).

The integrin cytoplasmic tails are generally short, except for the β4 subunit. Nevertheless, given that these tails are the initiation-point of integrin activation induced by binding of intracellular proteins ('inside-out' activation, see section 2.1), the structure of the cytoplasmic domains, especially αIIbβ3 integrins, has been characterized. Several NMR structures of the heterodimeric αIIbβ3 cyto domain are available, which show a great amount of structural variety. Interactions between αIIb and β3 integrin tails were not detected in solution (Ulmer et al., 2001) and with αIIbβ3 TM-Cyto constructs embedded into micelles (Li et al., 2001), while another study using purified recombinant αIIb and β3 cytoplasmic domain proteins detected weak α-β interaction (Vinogradova et al., 2002). The explanation for this inconsistency might be an inherent structural flexibility of integrin tails, which only form transient structures or stay unstructured in the absence of binding partners. This flexibility might explain how integrin tails are capable of serving as a hot-spot for a multitude (approximately 232 proteins associated both directly and indirectly with integrins) of structurally divergent adaptor and signaling proteins to bind and regulate different functions (Winograd-Katz et al., 2014). Two conserved interaction motifs in the β subunits stand out: the membrane proximal NPxY and membrane distal NxxY motif, which are critically important for integrin activation, signaling and trafficking. Both are recognition sequences for phosphotyrosine-binding (PTB) domain containing proteins (Calderwood et al., 2003) and mutations in these sequences in mice lead to early embryonic lethality due to impaired integrin function (Czuchra et al., 2006). In contrast, the sequences of α subunits are highly divergent

except for a conserved GFFKR motif (or even GFFxR sequence) close to the transmembrane domain, which is part of the IMC (Figure 3D).

Importantly, the interaction between arginine (conserved GFFKR) in the α subunits and aspartic acid (conserved HDR(R/K)E) in the β subunits are proposed to form a salt bridge to maintain αIIbβ3 integrins in the inactive state (Hughes et al., 1996). During integrin activation, this salt bridge and the Van der Waal-like inter-subunit interactions between TM regions are disrupted (Luo et al., 2004; Vinogradova et al., 2002). However, the salt bridge is functionally not important for all integrin heterodimers as knock in mice with an aspartic acid to alanine exchange in the salt bridge of β1 integrin (i.e. D759A) show no obvious phenotype regarding integrin activation, adhesion, spreading, and migration *in vitro* (Czuchra et al., 2006).

In summary, it is believed that the dissociation of integrin TM-cyto domains is a key step for integrin activation. In the inactive state, integrins allow interactions of two distinct association motifs (OMC and IMC) as well as salt bridge between Arginine residue in α subunit and Aspartic acid in β subunit to retain the inactive state. Once integrins are activated, the TM-cyto domains also disassociate. In line, mutations mentioned above disrupt these associations leading to integrin activation. However, structural and mutagenesis studies are mainly done in αIIbβ3 integrins so far. Given the reason that the differences between structures of extracellular domains we know so far (for instance, α5β1 (Takagi et al., 2001) and αVβ3 (Takagi et al., 2002)), there might be also heterodimer specific differences.

2. Bi-directional regulation of integrin signaling

Integrins have the unusual property to transmit signals bi-directionally across the cell membrane. The extracellular conformation and ligand-binding affinity can be adjusted through interaction of intracellular ligands with integrin tails, a process called ‘inside-out’ signaling or integrin activation. Conversely, binding of extracellular ligands to the integrin extracellular domain allows integrins to transmit signals into cells through the recruitment of adaptor and signaling molecules which regulate various cell functions such as adhesion, polarity, migration and cell division. This process is referred to as

'outside-in' signaling. Thus, integrins have the ability to signal in both directions (bi-directionally) across the plasma membrane.

2.1 Inside-out signaling

The affinity regulation of integrins for their ligands is a tightly controlled process. This is particularly crucial and well-described in cells of hematopoietic lineages such as platelets or leukocytes. In non-activated cells of the hematopoietic system it is assumed that integrins are inactive with a bent conformation which does not allow integrins to engage their extracellular ligands. Upon cell stimulation by different cues, proteins are triggered to bind to the integrin tails in their low affinity conformation inducing conformational changes that lead to integrin activation and ligand binding. The molecular mechanism of inside-out integrin activation are extensively studied and two integrin interacting proteins, talin and kindlin take center stage as important regulators of integrin activation. A rare hematopoietic disease LAD-III is linked to kindlin. LAD-III patients are suffered immunodeficiency and hemorrhages due to combined defects in the activation of β1, β2, and β3 integrins on leukocytes and platelets owing to *KINDLIN-3* gene mutations (Kuijpers et al., 2009; Malinin et al., 2009; Svensson et al., 2009; Zimmerman, 2009). The other two LAD subtypes have been described above (section 1.2).

2.1.1 Talin, kindlins, and integrin activation

Talin

Talin was first identified in membrane ruffles and focal adhesions around 30 years ago as interaction partner of two other focal adhesion proteins, vinculin and integrins (Burridge and Connell, 1983). The vertebrate genome codes for two closely related talins: talin1 and talin2 (74% identical) with overlapping but distinct functions. In mammalian cells, talin1 is ubiquitously expressed, being most abundant in the heart and scarce in brain while talin2 is enriched in the heart and brain with lower levels detected in the skeletal muscle, liver and lung. In addition, different splicing variants of talin2 are expressed in every tissue examined (Debrand et al., 2009).

Talin consists of 2541 aa (~270kDa) and is highly conserved throughout metazoans. It contains a globular head domain (~50kDa) linked to a carboxyl-terminal

flexible region composed of a series of helical bundles known as rod domain (~220kDa). The head domain is formed by a N-terminal FERM (4.1, Ezrin, Radixin, and Moesin) domain, which can be further divided into three subdomains (F1, F2, F3) and an extra F0 subdomain, which is not present in classical FERM domains (Figure 4A). The F3 domain harbors a PTB-like domain that interacts with the proximal NPxY motif of β integrin tails (integrin-binding site-1, IBS1) (Anthis et al., 2009; Calderwood et al., 2002), the phosphatidylinositol 4-phosphate 5-kinase type Iγ (PIPKIγ) (de Pereda et al., 2005) and the hyaluronan receptor layilin (Wegener et al., 2008). Focal adhesion kinase (FAK) (Lawson et al., 2012) and Rac1-GEF T Lymphoma Invasion and Metastasis (TIAM1) (Wang et al., 2012a) also have been shown to interact with F3 domain. Meanwhile, the helical rod domain contains 11 binding sites for vinculin (Roberts and Critchley, 2009), a second integrin-binding site (IBS2) and an actin binding domain at the very C-terminus important for talin homodimer formation and for direct actin binding. The homodimer formation is proposed to promote integrin clustering (Gingras et al., 2008) (see section 2.2) (Figure 4A). Finally, through the ability to interact with the actin-binding protein vinculin, talin forms an anchoring complex that allows integrins to establish a linkage between the extracellular environment and the actin cytoskeleton.

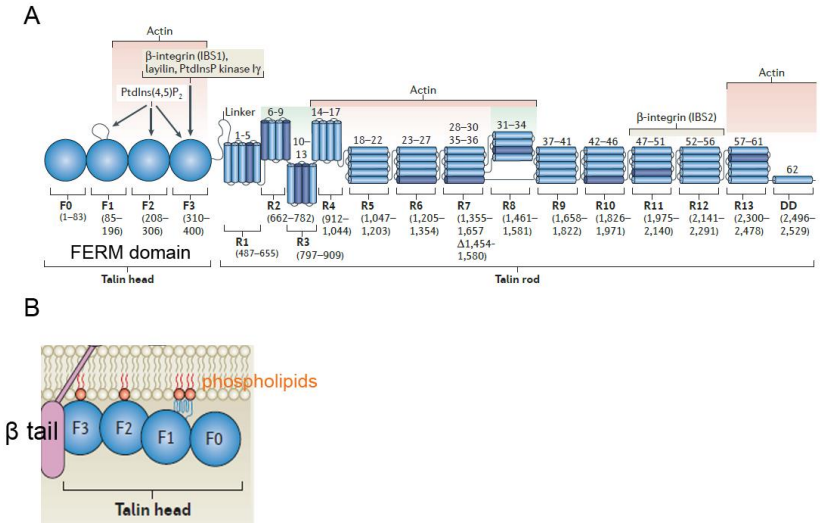

Figure 4 Schematic full-length structure of talin. (A) Talin uses its N-terminal FERM domain and IBS2 domain in C-terminal rod to interact with β integrin tails. Talin can directly bind actin and contains several vinculin binding sites to link to the actin cytoskeleton. Helices that bind vinculin are shown in dark blue. (B) F0/F1, F2, and F3 subdomains within FERM domain interact with phospholipids in the plasma membrane which is crucial to trigger integrin activation (modified from Calderwood et al., 2013).

The role of talin in integrin activation was predominately analyzed in CHO cells that exogenously express the platelet integrin αIIbβ3. In this cell system, the PTB-like F3 domain of talin was sufficient to activate αIIbβ3 integrins (Calderwood et al., 2002; Calderwood et al., 1999) and *in vivo* studies showed that talin is necessary for integrin activation in platelets (Nieswandt et al., 2007; Petrich et al., 2007). Talin1 depletion in neutrophils also shows defects to activate αLβ2 and αMβ2 integrins suggesting talin 1 is essential for integrin activation in leukocyte (Lefort et al., 2012; Watts, 2015).

Recent structural studies using αIIbβ3 integrins revealed the underlying mechanisms of talin-mediated integrin activation (Anthis et al., 2009; Wegener et al., 2007). During integrin activation, the PTB-like F3 domain of talin binds to the proximal NPxY motif of the β subunit and in then forms an interaction with the conserved Asp723 (D) of the β tail. This interaction disrupts the salt bridge (R-995(αIIb) and D-723(β3)) which stabilizes the αβ heterodimer association, and triggers the disassociation of transmembrane and cytoplasmic domains, consequently inducing conformational changes in the extracellular region allowing ligand binding (Anthis et al., 2009). Importantly, binding of other PTB domains to the proximal integrin NPxY motif, such as DOK1 (competes talin binding to integrin; see section 2.1.2) or Numb (regulates integrin trafficking; see section 4), is not sufficient to activate integrins indicating that other features of talin apart from the NPxY interaction are important for integrin activation. Indeed, there is a series of basic residues distributed within the talin FERM domain (Elliott et al., 2010) that bind to the negatively charged phospholipids of the plasma membrane. Negatively charged PtdIns(4,5)P2 increases the affinity of talin FERM domain with for β3 cytoplasmic tail by three orders of magnitude (Moore et al., 2012) and the extensive talin-membrane interactions further orientate the talin FERM domain and induce a tilting of the bound β integrin tail, which promotes integrin tail separation (Figure 4B). Mutations within this basic stretch impair talin membrane binding and integrin activation (Anthis et al., 2009; Elliott et al., 2010; Goult et al., 2010).

Because of its vital role in integrin inside-out signaling, cells tightly control talin localization and activity to prevent unwanted integrin activation. Cytosolic talin resides in an auto-inhibited conformation in which the interaction of the negatively charged surface in rod (R9 domain) with positively charged residues in F3 domain (Figure 4A) block the

PTB-like domain inhibiting membrane localization and integrin binding (Goksoy et al., 2008). The release of talin from this auto-inhibited conformation is a stepwise process that requires different components. 1) PtdIns(4,5)P2 in the plasma membrane impairs the autoinhibitory interaction and releases the integrin binding pocket to facilitate binding to integrin tails (Goksoy et al., 2008). 2) Vinculin binding to the talin rod domain results in talin recruitment to the plasma membrane. Expression of talin-binding domain of vinculin in cells induces talin membrane targeting (Banno et al., 2012). 3) Talin can enhance its own activation and membrane recruitment during early adhesion formation via a positive regulatory loop by recruiting phosphatidylinositol 4-phosphate 5-kinase type Iγ (PIPKIγ). PIPKIγ increases the PtdIns(4,5)P2 concentration locally to activate talin (see point 1). Indeed, depletion PIPKIγ leads to slower recruitment of talin and vinculin to FAs (Legate et al., 2011). 4) The small GTPase, Rap1 and its effector Rap1-GTP-interacting adaptor molecule (RIAM) are involved in talin recruitment to integrin cytoplasmic tails (Figure 5) (Han et al., 2006; Lee et al., 2009). RIAM interacts with the talin rod domains to localize talin to plasma membrane and also binds to the talin F3 domain, which disrupts the intracellular autoinhibitory interaction (Chang et al., 2014; Yang et al., 2014). 5) The interaction of talin with FAK is required to recruit talin to nascent adhesions. However, it is unclear how FAK localization to nascent adhesion is achieved (Lawson et al., 2012).

Next to the release autoinhibitory interaction and the regulation of talin targeting to the plasma membrane, talin-integrin interaction is negatively affected by the phosphorylation levels of the β integrin tail. v-Src family kinases can phosphorylate the tyrosine residue within the proximal and distal NxxY motif of β1 and β3 integrin which directly interferes with talin-integrin binding but promotes DOK1 binding to the same motif. Exchanging Tyr with Phe can rescue the migration and adhesion defects of v-Src transformed cells (Law et al., 1996; Moser et al., 2009b; Oxley et al., 2008; Sakai et al., 2001).

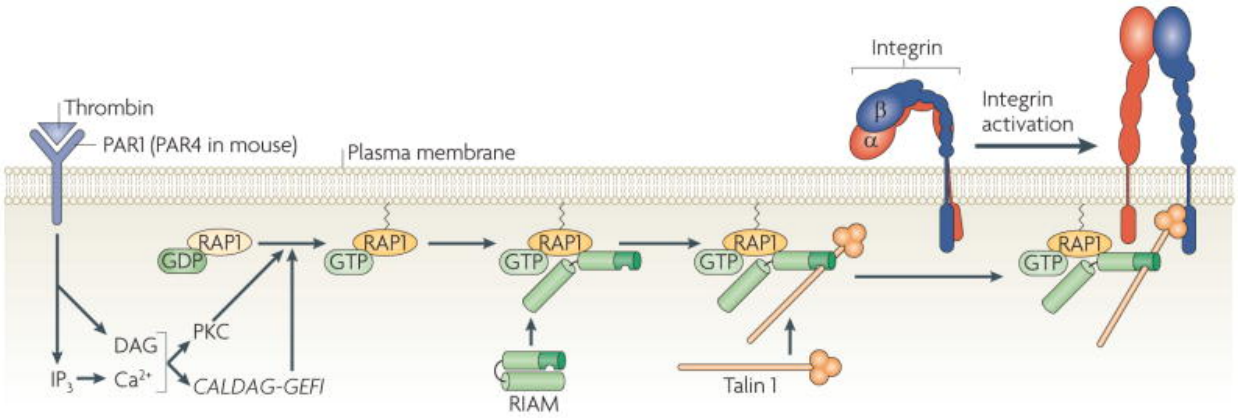

Figure 5. Connection between agonist stimulation and integrin activation. In hematopoietic cells agonist stimulation leads to activation of phospholipase C (PLC) and the generation of the secondary messenger inositol trisphosphate (IP_3) and diacylglycerol (DAG). IP3 stimulates the release of Ca^{2+} into the cytosol, which together with DAG activates protein kinase C and the Ca^{2+} and DAG-dependent guanine nucleotide exchange factor (Cal-DAG-GEF). PKC and Cal-DAG-GEF convert RAP1, from a GDP-bound inactive to an active GTP-bound form which binds to its effector RIAM. The Rap1/RIAM complex interacts with talin leading to the unmasking of the integrin binding site on talin and the recruitment of talin to plasma membrane (taken from (Shattil et al., 2010)).

Kindlin

Although the role of talin in integrin activation is well established, experimental data derived from *in vivo* studies or biochemical approaches questioned if talin is the only key player in integrin activation. Indeed, different studies revealed kindlins as important regulators of integrin activation together with talin. Kindlins were named after the gene (*KIND1*) mutated in Kindler Syndrome, a rare autosomal recessive genodermatosis disorder (Jobard et al., 2003). The kindlin gene family contains three members: kindlin 1, kindlin 2 and kindlin 3, which exhibit different expression patterns in tissue. Kindlin 1 is predominantly expressed in epithelia cells of the skin, intestine, and kidneys while kindlin 2 is ubiquitously expressed with the exception of the hematopoietic system. Kindlin 3 is exclusively expressed in hematopoietic cells (Ussar et al., 2006). Kindlin orthologues can be also found in *C. elegans* (UNC112) and in *D. Melanogaster* (Fermitin-1 and -2) and deletion of kindlin in these two model organisms led to integrin-mediated attachment defects (Bai et al., 2008; Rogalski et al., 2000). Knockout mouse studies firmly established the role of kindlins in integrin activation. Intestinal epithelial cells and embryonic stem cells derived from kindlin 1 and kindlin 2 knock-out mice,

respectively, fail to activate β integrins (Montanez, 2008; Ussar, 2008). Deletion of kindlin 1 in mice leads to defects resembling the phenotypes reported in Kindler Syndrome patients, including abnormal pigmentation (poikiloderma), skin atrophy, skin cancer and intestinal epithelial dysfunction causing perinatal lethality in mice due to a severe ulcerative colitis-like intestinal epithelium detachment (Ussar et al., 2008). Furthermore, kindlin 1 controls epithelial stem cell homeostasis and consequently loss of kindlin1 leads to enlarged and hyperactive stem cell compartments and aberrant stem cell commitment, resulting in severe hair follicle abnormalities. Kindlin1-deleted keratinocytes revealed β1 integrin associated adhesion defect as well as a severe deregulation of the Wnt/β-catenin and TGFβ signaling pathway, both important for skin epithelial stem cell quiescence, self-renewal and differentiation (Rognoni et al., 2014).

Kindlin 2 deleted mice die at peri-implantation stage due to defective integrin activation leading to the detachment of the endoderm and the epiblast from the connecting basement membrane (Dowling et al., 2008; Montanez et al., 2008). Similar to LAD-III patients who bear *KIND3* gene mutations (Kuijpers et al., 2009; Malinin et al., 2009; Svensson et al., 2009; Zimmerman, 2009), mice lacking of kindlin 3 suffer from severe bleeding as well as defective leukocyte adhesion and spreading in the presence of unchanged talin expression levels due to defective β1, β2 and β3 integrin activation on leukocytes and platelets (Moser et al., 2009a; Moser et al., 2008).

All three kindlin members are highly conserved on the amino acid level and in their overall structure. They have a length of around 680 amino acids and a size of ~75 kDa. High-resolution structure of intact kindlins are still not available, but partial domain structures are reported (Goult et al., 2010; Liu et al., 2011; Liu et al., 2012; Perera et al., 2011; Yates et al., 2012). Like talin, kindlins contain a FERM domain, composing of F0, F1, F2, and F3 subdomains, which share high sequence similarity with the talin FERM domain, in particular within the F3 subdomain (Figure 6C). The F3 subdomain forms PTB fold that directly interacts with different β integrin cytoplasmic domains (Bottcher et al., 2009; Meves et al., 2009). However, kindlins carry an additional insertion of a pleckstin homology (PH) domain within the F2 subdomain (Figure 6C). (Kloeker et al., 2004), which is not present in talin and facilitates the translocation of kindlins toward plasma membrane through interaction with PtdIns(4,5)P2 or PtdIns(3,4,5)P3

phospholipids (Goult et al., 2009; Hart et al., 2013; Xu et al., 2013; Yates et al., 2012). PtdIns(4,5)P2 can also be bound by the kindlin F0 domain (Perera et al., 2011). In contrast to talin, kindlin utilizes its F3 subdomain to bind the membrane-distal NxxY and the double Thr (in β1 tails) or Ser-Thr (in β3 tails) located between two NxxY motifs (Figure 6) (Ma et al., 2008; Montanez et al., 2008; Moser et al., 2009a; Moser et al., 2008; Shi et al., 2007; Ussar et al., 2008). Importantly, the different kindlin family members exhibit differential binding affinities to different β integrin tails. Kindlin 1 strongly binds to β1 and β6, whereas kindlin 2 interacts with β1 in high affinity but less with β2 and β3 tails and shows no binding to the β6 integrin tail (Calderwood et al., 2013; Rognoni et al., 2014). While kindlin 3 binds to β1, β2, and β3 tails (Huet-Calderwood et al., 2014; Moser et al., 2009a; Moser et al., 2008). What are the underlying mechanisms that regulate the binding affinities of the kindlin family members to the different integrin tails? Much remains unknown, but a recent publication implicates the charges of the last three C-terminal residues in the β tail as important regulators of kindlin 2 binding affinity (Bledzka et al., 2012).

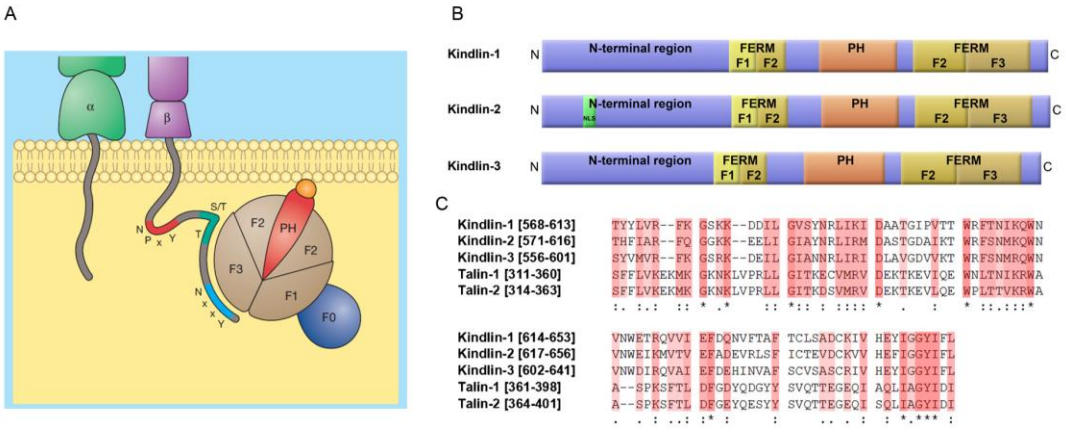

Figure 6 Kindlin domain structure and binding with integrin β tails. (A) Kindlins use F3 domain to interact distal NxxY motif and conserved TT (S/T) within β tails. (B) Domain structure of three kindlins. (C) Sequence alignment of the F3 subdomains of kindlins and talin shows high similarity. (modified from Meves et al., 2009 and Karaköse et al., 2010)

It is still unclear how kindlins contribute to activate integrins mechanistically. Since the binding sites of talin and kindlin in β integrin cytoplasmic tails are in close

proximity it has been proposed that talin and kindlin may bind sequentially to β tails and function consecutively rather than conjointly to control activation and stabilization of integrin ligand binding (Moser et al., 2009b; Ye et al., 2010). Interestingly, recent results indicate that the region linking the PH-domain of kindlin to its F2 subdomain (Fukuda et al., 2014; Huet-Calderwood et al., 2014) mediates interaction with ILK and is required for facilitating kindlin recruitment to focal adhesions, integrin signaling, and integrin activation (only in(Huet-Calderwood et al., 2014)). While this interaction is proposed to regulate the ability of kindlin to interact with β integrin tails in *C. elegans* (Qadota et al., 2014; Qadota et al., 2012), this function cannot be confirmed for mammalian cells (Fukuda et al., 2014; Huet-Calderwood et al., 2014) and that the mechanism for these functions remain unclear. Furthermore, migfilin binds to kindlin and filamin with its Lin11, Isl-1 & Mec-3 (LIM) homology domains (Brahme et al., 2013). The interaction of migfilin to filamin competes with the interaction of filamin to β integrin tails and it was therefore suggested that kindlin-mediated recruitment of migfilin to integrins may contribute to integrin activation by sequestering filamin (Calderwood et al., 2013). However, mice deleted for migfilin show no integrin activation defects, raising the question how relevant this interaction is for integrin activation (Moik et al., 2011).

The most recent studies suggests that both proteins fulfill distinct roles in integrin activation: In this study only talin could regulate monovalent ligand affinity of αIIbβ3 integrin (activation) while kindlin increases the multivalent ligand binding by promoting the clustering of talin-activated integrins (clustering) (Ye et al., 2013). Talin 1 depletion neutrophils are deficient in both slowly rolling and arrest, whilst kindlin 3 deficient neutrophils can still mediate slowly rolling, indicating that these different integrin regulators serve different roles in αLβ2 integrin activation (Lefort et al., 2012). Neither talin 1 nor kindlin 3 deficient neutrophils were able to adopt the high-affinity conformation (extended/open extracellular domain) of the αLβ2 integrin, whilst only talin 1 -/- cells were deficient the first step of integrin activation to the intermediate affinity form (extended/closed extracellular domain) (Lefort et al., 2012). On the other hand, nascent adhesions (see section 3) can form in the absence of talin (Lawson et al., 2012) and fibroblasts lacking talin 1 and talin 2 still show limited adhesion and spreading on FN (Zhang et al., 2008). Taken together, talin and kindlin fulfil essential roles during

integrin activation although the mechanism how they cooperate to regulate integrin activity still remains unclear.

2.1.2 Other integrin binding partners inhibit integrin activation

Integrin activation requires talin and kindlin binding and a lot of effort has been devoted to clarify the underlying mechanisms. In contrast, the transition of integrins from an active to an inactive conformation is much less well understood and studied. The inactive conformation has long been considered as 'default state' but recent studies indicate that the inactive conformation is actively regulated by the binding of intracellular integrin inactivators, including ICAP1, filamin, DOK1, SHARPIN, and MDGI (Figure 7). This suggests that integrin affinity regulation machinery might be even more complex and that integrin activation might not only be regulated by the breaking of the associated TM and cyto domains, extending bent conformation to increase the affinity but also by the maintenance of integrins in the inactive conformation to prevent unwanted activation.

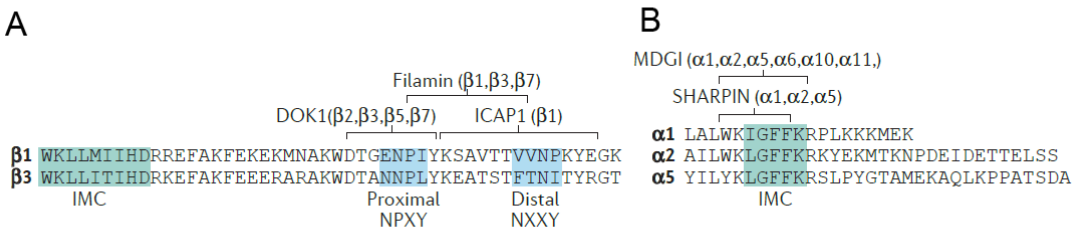

Figure 7 Integrin inhibitors binding sites on α (A) and β (B) integrin cytoplasmic tails. The integrin subunits that bind to each molecule are indicated in brackets. The residues form the inner membrane clasp (IMC) between the α and β subunitsTM domain are shown in green, and the proximal NPXY and distal NXXY motifs are shown in blue (modified from Bouvard et al., 2013).

ICAP1 (integrin cytoplasmic domain-associated protein 1)

ICAP1 is a PTB domain containing protein that specifically binds to the distal NxxY motif of β1 (but not to β2, β3 and β5) (Chang et al., 1997). It localizes with β1 integrins in peripheral ruffles but not in focal adhesions suggesting a role in integrin inactivation

(Fournier et al., 2002). Indeed, it has been shown that ICAP1 inhibits β1 integrin activation through simultaneous competition with talin and kindlin (Bouvard et al., 2003; Brunner et al., 2011). How ICAP1 competes with talin is still not fully understood, as the crystal structure of ICAP1-β1 integrin complex shows that the talin-binding proximal NPxY is not involved in the interaction interface (Liu et al., 2013). This would suggest that ICAP1 prevents talin binding indirectly. In contrast, ICAP1 directly competes with kindlin binding to β1 tails to impair β1 activation (Brunner et al., 2011). ICAP1 binding to integrins is further regulated by its interaction with KRIT1 (Krev interaction trapped 1), which relieves ICAP1 from the distal NxxY motif on β1 integrin, allowing kindlin binding and integrin activation (Liu et al., 2013).

Filamin

Another molecule whose direct interaction with integrin tail inhibits integrin activity is filamin. Filamin is a huge rod-like protein (about 280 kDa) containing an actin binding domain and 24 Ig-like domains to connect various proteins. Dimerization through the 24th Ig-like domain results in a flexible parallel homodimer that can promote high-angle branching of actin filaments and is essential for stabilizing the actin networks (Flanagan et al., 2001). This permits assembly of complex networks linking integrins with signaling proteins and the actin cytoskeleton and that is important for integrin outside-in signaling. There are three isoforms of filamin; filamin A and B are ubiquitously expressed, while filamin C expression is restricted to cardiac and skeletal muscle (Das et al., 2011). The filamin binding interface on the β integrin tail overlaps the talin binding site and thus filamin-binding to β integrins antagonizes talin-mediated integrin activation (Kiema et al., 2006). Indeed, depletion of filamin in cells enhances integrin activity (Kiema et al., 2006) and regulates cell spreading and migration in multiple cell lines (Baldassarre et al., 2009; Das et al., 2011; Kiema et al., 2006; Xu et al., 2010). Similar to KRIT1-ICAP1 interaction, migfilin, a filamin-binding protein, can displace filamin from β1 and β3 tails and thereby enhance integrin activity by promoting talin binding when overexpressed (Ithychanda et al., 2009; Lad et al., 2008). Interestingly, a recent structure of the cytoplasmic domain of human integrin αIIbβ3 and the immunoglobin repeat 21 of filamin A (FLNa-Ig21) revealed an unexpected ternary complex. FLNa-Ig21 not only binds to the C terminus of the integrin β3 cytoplasmic tail but also engages N-terminal helices

from both αIIbβ3 integrin cytoplasmic tails to stabilize an IMC and promote heterodimerization that helps restrain the integrin in a resting state (Liu et al., 2015).

DOK1 (docking protein 1)

The PTB domain-containing protein DOK1 binds to the proximal NPxY motif in β integrin tails and inhibits integrin activity (Calderwood et al., 2003; Wegener et al., 2007). DOK1 binding to the β integrin cytoplasmic tail can be increased by Src kinases-mediated Tyr phosphorylation of the NPxY motif in β1and β3 integrins. As the integrin-binding affinity of talin decreases upon Tyr phosphorylation, this phosphorylation event might provide a switch for integrin inactivation and a transition from talin-dependent to DOK1-dependent integrin signaling (Oxley et al., 2008; Wegener et al., 2007).

SHARPIN (SHANK-associated RH domain-containing protein)

Most integrin inactivators described so far bind to β integrin tails, however, few α integrin interactors have also been shown to inactivate integrins. SHARPIN (SHANK-associated RH-domain containing protein) is a ubiquitously expressed cytosolic protein that forms a linear ubiquitin chain assembly complex (LUBAC) to regulate NF-κB activation in response to stimuli like tumor necrosis factor (TNF) (Wang et al., 2012b). SHARPIN has been identified as an important inhibitor for integrin activation (Rantala et al., 2011). SHARPIN co-localizes with inactive integrin β1 to membrane ruffles but not in focal adhesions and depletion of SHARPIN in PC3 prostate cancer cells increases the active β1 integrin levels on the surface without altering the total integrin surface expression. SHARPIN binds integrin at the highly conserved WKxGFFKR sequence within integrin α subunits. Since this Arginine (R) has been shown to form a salt bridge with a conserved aspartic acid (D) the β integrin tail, SHARPIN is believed to stabilize the salt bridge and thereby keeps integrin heterodimers in the inactive state (Bouvard et al., 2013). However, as the mutation of the salt bridge aspartic acid (D) in β1 integrins does not affect integrin activation (Czuchra et al., 2006), this hypothesis might not be correct for all integrin heterodimers and needs further analysis. Alternatively, SHARPIN might function by inhibiting talin and kindlin recruitment to the β integrin cytoplasmic domains (Rantala et al., 2011). So far, SHARPIN has been established as an inhibitor of

β1 and αLβ2, whether this is also true for other integrins still needs further investigation (Bouvard et al., 2013; Pouwels et al., 2013; Rantala et al., 2011)

MDGI (mammary-derived growth inhibitor)

MDGI is found in lactating bovine mammary glands and has growth inhibitory propertied in human mammary carcinoma cell culture (Bohmer et al., 1987). MDGI is ubiquitously expressed (Haunerland and Spener, 2004). Like SHARPIN, MDGI interacts with several α subunits (α1, α2, α5, α6, α10, α11) via the WKxGFFKR sequence. MDGI overexpression leads to cell adhesion defects on different substrates and impairs migration and invasion specifically in human breast cancer cell lines but not in other cell types (Nevo et al., 2010). These phenotypes are accompanied by the reduction of active integrin β1 on the surface and inhibited kindlin recruitment to active β1 integrin by *in situ* proximity assay upon expression of MDGI in human breast cancer lines (Nevo et al., 2010). However the mechanism of MDGI function requires more studies as it is not clear why MDGI inhibits integrin activity only in mammary epithelium cells.

2.2 Integrin clustering and catch-bond formation

Once integrins are activated, they are ready to bind to their ligands. However, a single integrin-ligand interaction is too weak to maintain the adhesion to ECM. Therefore, integrins associate laterally at the site of adhesion so that multiple weak individual non-covalent linkages to the ECM join in a synergistic manner to generate stronger adhesion force. The relevance of this process, termed integrin clustering, for adhesion strengthening and the transmission of signals from the ECM into the cell has been shown (Roca-Cusachs et al., 2009; Shi and Boettiger, 2003). The underling mechanism of integrin clustering is still unknown but a recent model put forward an inter-relationship between integrin catch bond formation, clustering and signaling (Boettiger, 2012; Paszek et al., 2014). This model is based on the fact that cell surface integrins are surrounded by a dense network of glycosylated proteins, called glycocalyx, which extends from the cell membrane typically between 30-50nm. This distance is longer than the extension of integrins from the plasma membrane (around 20nm) (see Figure 8). The glycocalyx effectively reduces the initial ligand-integrin interaction but after the initial contact is formed it brings the cell surface closer to the ECM (as the

glycocalyx gets compressed) facilitating the association of further integrins (Paszek et al., 2014). Consequently, integrins cluster around the initial contact as soon as the contact is stabilized (Boettiger, 2012). In addition to its role in integrin activation and outside-in signaling it was suggested that talin could also potentially play role in integrin clustering while talin contains two distinct integrin binding sites can also dimerize and thereby act as a scaffold for integrin clustering (Gingras et al., 2008) (see section 2.2.1). In Drosophila, talin stabilizes the integrin adhesion complex by promoting integrin clustering distinct from its ability to support inside-out activation (Ellis et al., 2014). A recent study also suggests that kindlin can regulate integrin clustering through an unknown mechanism (Ye et al., 2013).

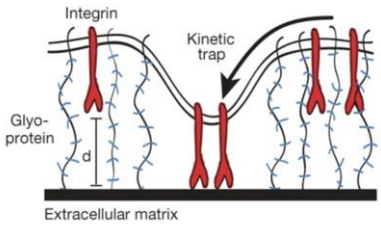

Figure 8. The role of glycocalyx for integrin clustering. The glycocalyx is formed by extracellular, membrane bound glycoproteins (blue/black lines). Integrins (red) cannot reach to the ECM when the glycocalyx is too far away. The local exclusion or compression of glycocalyx and a membrane deformation are required for initial contact formation. Once such a structure forms, other integrin molecules can quickly form further ECM contacts. (adapted from (Paszek et al., 2014))

In addition to integrin clustering, two additional actin-dependent adhesion strengthening mechanisms are described for specific integrin heterodimers: catch-bond formation and cyclic mechanical reinforcement. These mechanisms seem to be integrin subtype specific and have only been demonstrated so far for α5β1 and αLβ2 integrins not for αvβ3 or αIIbβ3 integrins (Chen et al., 2010; Friedland et al., 2009; Kong et al., 2009; Kong et al., 2013; Litvinov et al., 2011; Roca-Cusachs et al., 2009). For most non-covalent bonds the half-life of the binding between molecules decrease when pulling force is applied (slip-bond). In contrast, a catch-bond is a type of non-covalent bond whose dissociation lifetime increases with tensile force applied to the bond before decreasing again with further higher force. In the case of α5β1 integrins, a study from Friedland suggests that engagement of FN synergy site in response to myosin II-generated cytoskeletal force controls the catch bond behavior (Friedland et al., 2009). A distinct mechanism from catch-bond formation suggests applications of cyclic force to a

fibronectin-integrin α5β1 bond switch the bond from a short-lived state with 1 s lifetime to a long-lived state with 100 s lifetime. This observation was named cyclic-mechanical reinforcement (Kong et al., 2013), however, the underlying mechanism is still unclear.

2.3 Outside-in signaling

Integrins activate signaling pathways and connect to the actin cytoskeleton after ligand binding to regulate many cellular processes, such as adhesion, migration, and cytoskeleton organization. However, due to their short cytoplasmic, non-enzymatic tail domains they rely on the recruitment of proteins to transmit signals into the cell, to cross-talk with other signaling pathways and to the dynamically regulate the actin network. Upon integrin activation (section 2.1), ligand binding and clustering (section 2.2) integrins assemble a multi-protein complex around their cytoplasmic domains (termed outside-in signaling). The initial adhesion complexes, also referred to as nascent adhesions, are either quickly disassembled or mature into focal adhesions, fibrillar adhesion or podosomes (see below section 3). The signaling outcome depends on the composition of these signaling complexes, which changes over time and is further influenced by the size, shape and sub-cellular localization of the signaling complex. Literature-based analyses of adhesion complexes and proteomic studies have identified a highly connected network of over 232 proteins directly and indirectly associate with integrins (collectively termed integrin ‘adhesome’) (Winograd-Katz et al., 2014). These proteins can further divide into 148 intrinsic components (reside mainly in the adhesion site) and 84 components that transiently associate with the adhesion (Winograd-Katz et al., 2014). More than 40 molecules bind non-simultaneously with β integrin tails, while much fewer α tails’ interactors were reported (Legate and Fassler, 2009).

Integrin outside-in signaling results in downstream signaling events which can be subdivided in three temporal stages, immediate early (0-10 minutes), short term (10-60 minutes) and long term effects (Figure 9A) (Legate and Fassler, 2009). The immediate consequences of integrin activation and signaling are up-regulation of lipid kinase activity, including Phosphatidylinositol 3-kinase (PI3K) and PIPKIγ that enhance the local concentration of the phosphoinositide second messengers PtdIns(4,5)P2 and

PtdIns(3,4,5)P3 as well as rapid phosphorylation of specific protein substrates. This local enrichment of PtdIns(4,5)P2 also further promotes talin activation and its recruitment to plasma membrane (see section 2.1.1). This subsequently leads to the recruitment of many adhesion proteins such as Numb, Src homology containing protein (Shc), Tensin and in the time range of several minutes, these changes lead to the activation of diverse multiple signaling pathways. Among many cell adhesion-mediated phosphorylation events, the one initiated by focal adhesion kinase (FAK) and Src kinases are the most crucial. Phosphorylation of FAK at the autophosphorylation site Tyr397 enables the interaction with Src family kinases via their SH2 domain. This interaction in turn releases an auto-inhibitory interaction to activate Src. Full Src activation is finally achieved by its auto-phosphorylation at Tyr416. Activated Src in turn further promotes FAK activity by phosphorylation of FAK on several Tyr residues. The activated FAK/Src complex is able to phosphorylate other early focal adhesion proteins such as paxillin and p130Cas, generating highly divers signaling platform (Legate and Fassler, 2009).

As a short term effect, these signals translate into rearrangement of the actin cytoskeleton and myosin mediated force generation induced by the activation of Ras homolog (Rho) family GTPases and other actin regulatory proteins. Consequently, activation of rapidly accelerated fibrosarcoma (Raf) / extracellular signal-regulated kinase (ERK) / mitogen-activated protein kinase (MAPK), Jun N-terminal kinase (JNK) and Akt signaling pathways. Finally, in a long-term scale, integrin-activated signaling pathways coordinately will lead to changes in gene expression to regulate proliferation, survival and to induce genetic programs that control cell fate (Figure 9) (Legate and Fassler, 2009).

An additional level of regulation of integrin-mediated signaling pathways is the cross-talk with different growth factor receptor signaling pathways. The signaling events initiated by the two receptor classes intersect at multiple levels thereby changing the activity of the integrin-associated signaling proteins or downstream effectors (Figure 9B). For example, αVβ3 integrins can induce specific phosphorylation on the Epidermal Growth Factor (EGF)-Receptor (EGFR) required for downstream signaling events in the absence of EGF (Moro et al., 1998). In addition, αVβ3 integrins mediate growth-factor

independent clustering of growth factor receptors, such as the VEGFR2 (Soldi et al., 1999), Platelet Derived Growth Factor Receptor (PDGFR) (Borges et al., 2000; DeMali et al., 1999; Schneller et al., 1997).

In summary, ligand-binding, the formation of a highly complex and dynamic multi-molecular adhesion complex as well as the cross-talk with growth factor receptor pathways regulates the integrin mediated outside-in signaling machinery.

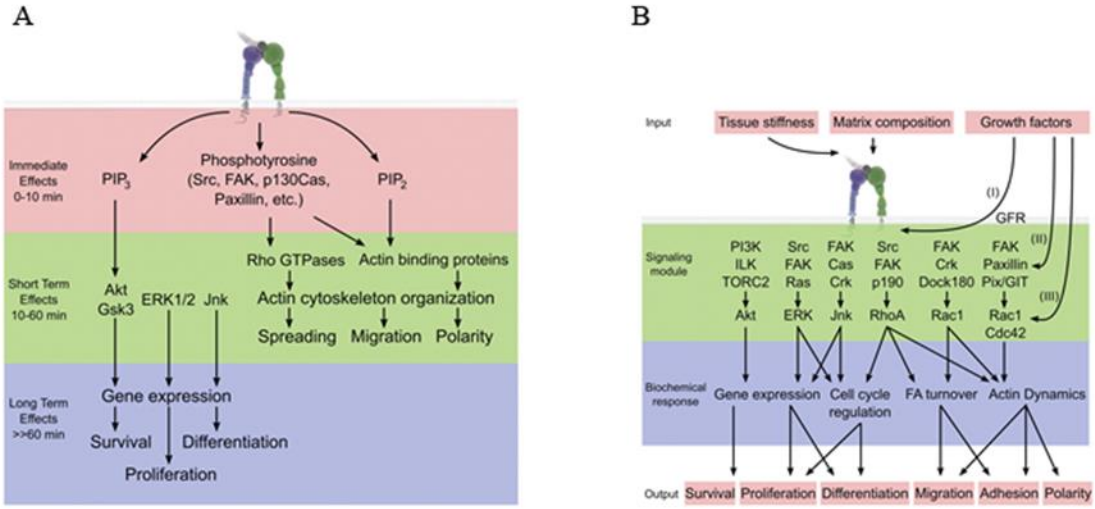

Figure 9. Integrin inside-out activation. (A) The three temporal stages of integrin signaling downstream events. (B) Integrin-mediated signal transduction pathways. The growth factor receptors (GFRs) and the growth factor environment coordinated outside-in signaling of integrins. Integrin-mediated signaling interacts with growth factor signaling on multiple levels: (I) integrin affinity for ligands, (II) the activity of the integrin-associated signaling proteins (FAK, Src, and PI3K), and (III) the activity of the downstream effectors (ERK, Akt, JNK, and the Rho GTPases). The central signaling module downstream of integrins is the Src/FAK complex that activates ERK and JNK to regulate cell survival, proliferation, and differentiation. In addition, the Src/FAK complex regulates Rho GTPase activity through activation of Crk/Dock180 or PIX/GIT pathways, resulting in cytoskeletal reorganization and leading to regulation of cell migration, adhesion, and polarity. Integrins also activate PI3K, which in collaboration with mTOR and possibly ILK regulates cell survival through Akt. The alternative activation pathways and cross-talk between the various depicted pathways are not presented. (GFR) Growth factor receptor; (PI3K) PI-3-kinase; (ILK) integrin linked kinase; (TORC) mammalian target of rapamycin complex; (FAK) FA kinase; (ERK) extracellular signal regulated kinase; (Cas) Crk-associated substrate; (JNK) Janus kinase; (DOCK180) dedicator of cytokinesis 1; (PIX) PAK interactive exchange factor; (GIT) G protein-coupled receptor kinase-interacting protein. (taken from Legate et al., 2008)

3. Assembly of integrin-dependent adhesion structures

Upon activation, integrins increase their affinity toward ligands; however, each individual integrin-ligand interaction is relatively weak. The firm adhesion of a cell to ligand requires the collective binding of multiple integrins, also referred to as clustering (see section 2.1), to establish strong adhesion with ECM. The adhesion structures differ between cell types and are classified by morphology, molecules composition, and dynamics. Moreover, they also localize in different areas in the cells (Figure 10D) (Geiger et al., 2009).

The very initial integrin-based adhesions are termed nascent adhesions. They are dot-shaped with approximately 100 nm in diameter (Geiger and Yamada, 2011) and are mostly assembled along membrane protrusions that promote the activity of Rho-GTPases such as Rac1. Most nascent adhesions disassemble very fast, however, few nascent adhesions subsequently mature by further integrin clustering and recruitment of actin-linker multi-protein complexes to the cytoplasmic platform into a punctate structure (>100 nm in diameter) named focal complexes (FXs). FXs are located close to the edge of the lamellipodium and if further stabilized, they will mature and form focal adhesion (FA) structures (commonly ~1 μm wide, 3–5 μm long) (Figure 10A). The transition from FXs to FAs activates Myosin II which in turn exerts contractile force on the adhesion structures resulting in adhesion reinforcement and recruitment of more molecules to FAs that further increase myosin II activity (Geiger et al., 2009). One marker for maturation of focal adhesions is zyxin, as it is recruited to FAs but does not appear in nascent adhesion and FXs (Zaidel-Bar et al., 2003). Our group (Schiller et al., 2011) and Waterman's lab (Kuo et al., 2011) have further analyzed the changes of myosin II activity-dependent proteins recruitment by treating myosin II inhibitor, blebbistain, and then by quantitative mass spectrometry. This provided the ample data of adhesion site maturation process of fibroblast seeded on FN (Kuo et al., 2011; Schiller et al., 2011). Interestingly, many 'core adhesome' proteins including talin and kindlin do not change their stoichiometry to β1 integrin during the adhesion maturation process (Schiller et al., 2011). Rac specific GEF β-pix stays in nascent adhesion sites and that plays a crucial role in lamellipodial protrusion (Kuo et al., 2011). In contrast, vinculin (Humphries et al., 2007b) and filamin (Ehrlicher et al., 2011) which can stabilize integrin-actin linkage and

thereby increase tension as well as testin which activates RhoA (Magno et al., 2011) leading to increased myosin II activation are relatively increased in the progression of FAs maturation.

In certain cell types (eg. fibroblasts) FAs further mature into centrally localized, elongated fibrillar adhesions (FBs) during adhesion to FN (Figure 10B). The maturation process is characterized by the recruitment of tensin as well as centripetal translocation of α5β1 integrin containing FAs, accompanied by the stretching of FN fibrils (Pankov et al., 2000). Another adhesion structure called podosome is mainly observed in highly migratory and invasive cell lines such as osteoclasts, macrophages and dendritic cells. They are composed of a ring-like assembly of matrix adhesion components surrounding an F-actin core (Gimona et al., 2008) (Figure 10C).

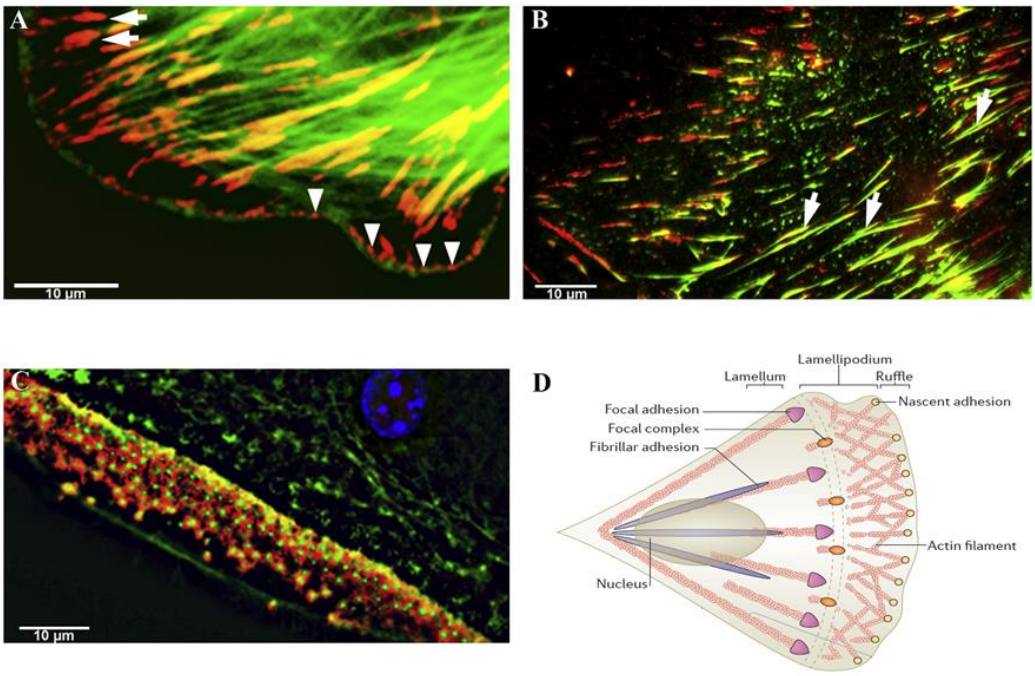

Figure 10. Diversity of integrin-mediated adhesion structures. (A) FA (arrows) and FX (arrowheads) formed in a human foreskin fibroblast stained for paxillin (red) and actin (green). (B) FB (arrows) formed by a WI38 human lung fibroblast, stained for tensin (red) and fibronectin (green). (C) Podosomes in a cultured osteoclast derived from murine bone marrow, stained for paxillin (red) and actin (green). (D) Localization of different adhesion structures in the cell. (modified from Bouvard et al., 2013 and Wolfenson et al., 2013)

Notably, the different adhesion structures have been described in cell culture on rigid 2D surfaces and their existence *in vivo* and in 3D matrices have been controversially discussed. Embedding most of cells in 3D matrices can lead the formation of 3D adhesion structures which resemble FBs as they are α5β1 integrins-rich but on the other hand contain proteins mainly found in FAs such as α-actinin and phosphorylated paxillin (Berrier and Yamada, 2007; Harunaga and Yamada, 2011) (Figure 11). Only few *in vivo* integrin-mediated adhesion structures have been characterized including FAs of endothelial cells at sites of fluid shear stress in blood vessels and in smooth muscle dense plaques (Geiger and Yamada, 2011).

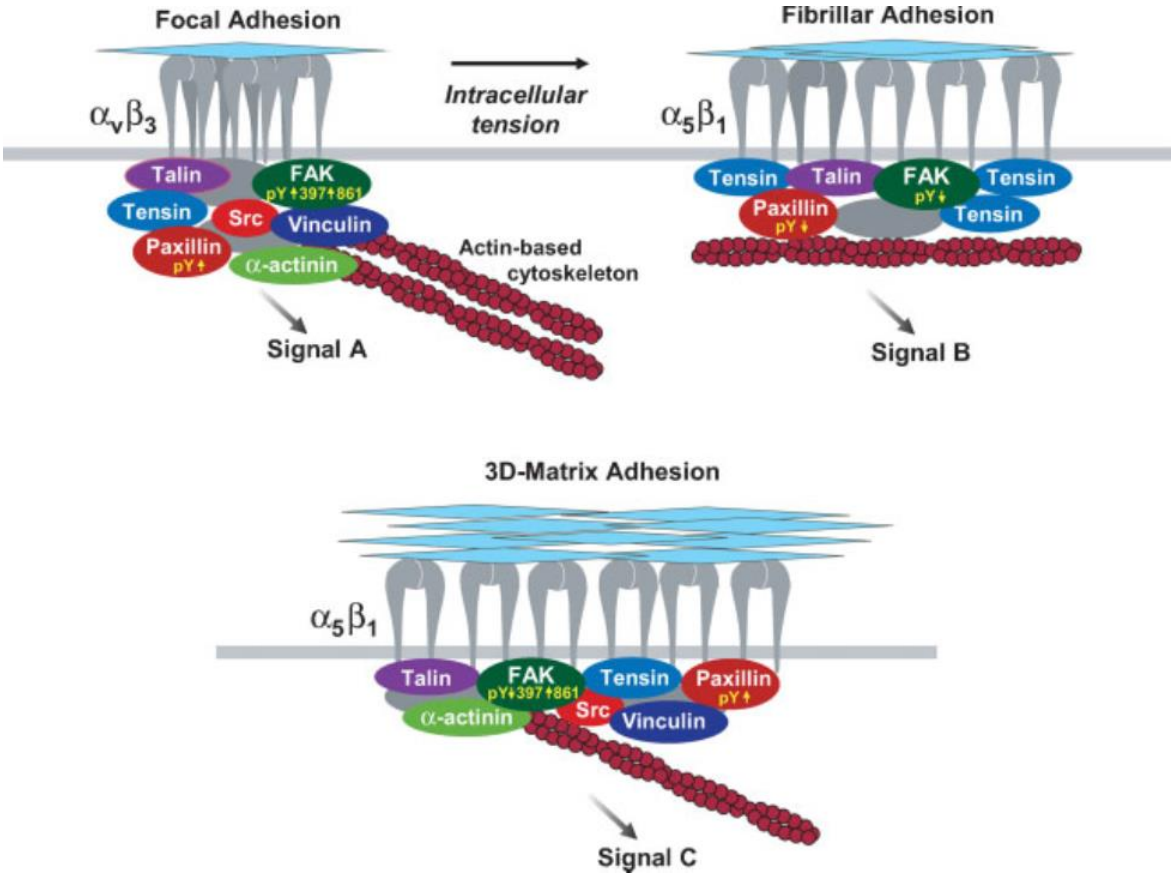

Figure 11. Differences between focal adhesions, fibrillar adhesions, and adhesions in a 3D matrix. Different adhesion structures do not only recruit a distinct set of cytoplasmic proteins but also show difference in the phosphorylation of those proteins. For instance, FAK Tyr-397 is highly phosphorylated in FAs but lower in FB and 3D adhesion structures. In contrast, Paxillin phospho-Tyr 31 and FAK phospho-Tyr 861 levels are high in both FAs and 3D adhesions but are lower in FB. Distinct protein complexes are likely to form within each type of matrix adhesion leading to the activation of specific signaling pathways. (taken from Berrier et al., 2007)

3.1 Integrin-actin connection

One key function of the integrin outside-in signaling is the linkage to and the regulation of the cell actin cytoskeleton to modulate cell morphology, to initiate cell migration but also to convert mechanical stimuli into chemical activity, in a process termed mechanotransduction. FA proteins are divided into four classes based on their involvement in establishing and maintaining the integrin-cytoskeleton linkage: (1) integrin-interacted proteins that directly bind actin, such as talin, α-actinin and filamin; (2) non-integrin-associated actin-binding proteins, such as vinculin; (3) integrin-bound proteins that indirectly associate with/regulate the cytoskeleton, such as kindlin, ILK, and paxillin and (4) scaffolding/signaling molecules that tune integrin signals but are not associated with integrin or actin (Legate and Fassler, 2009)

The initial linkage of integrin to the actin cytoskeleton is mediated through the recruitment of talin to β integrin tails upon ECM binding. Thereby, a talin-dependent 2-pN slip bond is established, providing the initial force from the cytoskeleton to the ECM (Jiang et al., 2003). Several *in vivo* studies corroborate the key role of talin to connect to cytoskeleton. For example, depletion of talin 1 in mice leads to lethal phenotype during gastrulation because of defects in cytoskeletal organization and cell migration (Monkley et al., 2000). Furthermore, deletion of both talin1 and talin2 in skeletal mouse muscles impairs muscle development comparable to a β1 integrin knock-out (Conti et al., 2009). Importantly, functional active β1 integrin are still detectable on skeletal muscle cells and adhesion of isolated cells to ECM is not affected, suggesting that the observed defects are due to disruption of integrin actin connections rather than an inability to activate integrins (Conti et al., 2009). Talins have a cryptic actin binding site (ABS) in the C-terminal region of their rod domain (Figure 4). This Talin/HIP1R/Sla2p actin-tethering C-terminal homology (THATCH) is also required for homodimer formation (Gingras et al., 2008).

After the binding of talin to actin to generate the first connection, vinculin is rapidly recruited to the talin rod region to reinforce the linkage. There are 11 vinculin binding sites within talin rod domain (Figure 4) (Roberts and Critchley, 2009) which are buried in helical bundles if talin is not under tension (termed as cryptic binding site) and mechanical stretching is required to expose these sites allowing vinculin binding

(Papagrigoriou et al., 2004). Vinculin is required to strengthen the linkage by acting as a crosslinker and by stabilizing the talin-actin interaction. Expressing the talin head domain in talin-null cells activates integrins but only full-length talin restores the ECM-cytoskeleton linkage and normal cytoskeleton organization (Zhang et al., 2008). This shows that talin head itself is able to interact with β integrin cytoplasmic domains but it is not sufficient to maintain the actin linkage. Vinculin knockout cells display fewer and smaller FAs and close a wound more rapidly (Coll et al., 1995; Volberg et al., 1995; Xu et al., 1998). Conversely, in vinculin-overexpressing cells, the number and size of FAs are increased and cell motility is reduced (Rodriguez Fernandez et al., 1992). Nevertheless, the observation that vinculin-null cells have focal adhesions suggests that vinculin is required to stabilize FAs once they have formed but not their assembly.

The talin-vinculin axis is a major contributor for the integrin-actin linkage. Vinculin itself can be recruited to β integrin adhesion sites via directly binding to paxillin (Turner et al., 1990). However, several other proteins contribute to the establishment and maintenance of this linkage. As force is generated, the actin binding protein α-actinin is recruited to FAs via vinculin, talin and direct β-integrin interaction as well (Laukaitis et al., 2001). Besides, α-parvin also harbors two actin binding Calponin homology (CH)-domains (Olski et al., 2001). Together with ILK and PINCH, it constitutes a protein complex termed as IPP (ILK/PINCH/parvin) complex. The link to the integrin β tails is made by ILK which also binds to paxillin, a direct integrin interactor. The IPP complex exemplifies the elaborate interactions of FA proteins linking integrins to the actin cytoskeleton. In summary, the integrin-actin connection is established and coordinated on multiple levels and the individual actin-binding components within FAs are highly interconnected (Humphries et al., 2007a; Legate and Fassler, 2009). A topographical study (using super resolution microscopy) revealed the nanoscale architecture of integrin-based adhesions. Integrins and actin are vertically separated by a 40 nm FA core region consisting of a membrane apposed integrin signalling layer (integrin cytoplasmic tails, FAK, paxillin), an intermediate force transduction layer (talin and vinculin), and an uppermost actin-regulatory layer (Zyxin, VASP, α-actinin) (Kanchanawong et al., 2010).

3.2 Dynamic regulation of the actin cytoskeleton

Apart from establishing a physical anchorage of the actin cytoskeleton at the plasma membrane, cell adhesion proteins also regulate actin distribution and dynamics. The spatiotemporal control of actin dynamics is crucial for many processes such as cell morphology, cell polarity, as well as tissue homeostasis, wound healing, and embryonic development (Jaffe and Hall, 2005).

The key regulators of actin dynamics and distribution within cells are members of the Rho family of small GTPases (Rho GTPases). The Rho family comprises more than 22 members in mammals, which cycle between an active GTP-bound state and an inactive GDP-bound state and thereby function as molecular switches (Bustelo et al., 2007). They are controlled by three classes of regulatory proteins: GEFs (guanine nucleotide exchange factors), GAPs (GTPase activating proteins), and GDIs (guanine nucleotide dissociation inhibitors). GEFs activate the GTPases while GAPs promotes inactivation by stimulating the intrinsic GTPase activity of the Rho proteins. GDIs sequester inactive GDP-bound Rho-GTPases into the cytoplasm and thus remove them from their activation cycle by GEFs at the plasma membrane. The best-studied representatives are RhoA (Ras homologous), Rac1 (Ras related C3 botulinum toxin substrate 1) and Cdc42 (cell division cycle 42). When activated by cellular signals these Rho GTPase promote and regulate formation of prominent and morphologically distinct actin-based structures, namely protrusive lamellipodia (Rac1), protrusive actin-rich filopodia (Cdc42) and stress fibers (RhoA). While Rac1 and Cdc42 both promote morphologically distinct actin-based protrusive structures (Rac1 promotes dendritic actin organization in lamellipodia and Cdc42 is thought to be the main mediator of the parallel linear actin filaments constituting filopodia), they both initiate peripheral actin polymerization through the Arp2/3 complex. In contrast, RhoA stimulates actin polymerization through formins (Jaffe and Hall, 2005).

Regulation of myosin-based contraction by RhoA, Rac and Cdc42 is antagonistic and that is related to cell spreading. Initial cell adhesion and spreading occurs in parallel with an inhibition of RhoA activity and the simultaneous activation of Rac and CDC42, which results in suppressed myosin II activity leading to suppression of contractility and enhanced actin-mediated protrusion leading to spreading. At later phases, the activities

of Rac1 and Cdc42 decrease, whereas the activity of RhoA gradually increases, and that activates ROCK (Rho-associated kinase), which phosphorylates and inactivates the MLC phosphatase that dephosphorylates MLC or directly phosphorylates MLC, resulting in increasing the activity of myosin II and contractility. This drives FAs maturation. Besides, the actin stress fiber is mainly regulated by myosin II contraction that pulls antiparallel actin fibers past each other, thus creating the force. (Geiger and Yamada, 2011).

Integrins regulate Rho GTPase activity by recruiting different GEFs and GAPs to the adhesion sites. For instance, integrin outside-in mediated FAK/Src activation recruits a complex composed of Dock180 (180 kDa protein downstream of CRK) and ELMO1 (engulfment and motility 1) serves as unconventional GEF for Rac which is crucial for phagocytosis and cell migration in mammalian cells (Brugnera et al., 2002). In addition, the activated FAK/Src complex can also phosphorylate paxillin which is important to recruit a complex consisting of the ArfGAP PKL(paxillin-kinase linker)/GIT (G-protein-coupled receptor kinase interacting protein) and β-PIX (PAK-interacting exchange factor-beta), which as a GEF for Rac1, which mediates Rac1 targeting to membrane ruffles and to FAs as well as Rac1 activation and Rac1-mediated cell spreading (ten Klooster et al., 2006). As spreading ends, RhoA activity gradually increases leading to stress fiber formation and FA maturation. The GEFs p115RhoGEF (also known as Lsc and Gef1), LARG (also known as Gef12) (Dubash et al., 2007), and p190RhoGEF (Lim et al., 2008) are involved in these processes.

In summary, integrin-mediated adhesion provides the linkage from ECM to actin cytoskeleton and profoundly regulates the spatiotemporal coordination of actin cytoskeleton dynamics through Rho GTPase. Indeed, the adhesion structures formation as well as protrusion and contractility mediated via Rho GTPases need the delicate balance for appropriate cell spreading and migration.

4. Integrin trafficking

It is known that integrins reside only for a short time on the cell surface because they constantly undergo exo-endocytic cycle, a process also referred as integrin trafficking. The intracellular trafficking not only regulates integrin availability and

distribution on the cell surface, but also affects integrin stability and signaling of integrin-associated growth factor receptors. Thereby integrin trafficking profoundly influences integrin-dependent cell adhesion, spreading, and migration in adherent cells as well as cancer cell invasion (Bridgewater et al., 2012). It includes several separated processes of targeted protein transport such as the cell surface delivery of newly synthesized integrins by **biosynthetic-secretory pathways**, **integrin internalization**, **recycling of internalized integrins** as well as **regulation of their degradation**.

Biosynthetic-secretory pathways

In the late 80s it was shown that β1 integrin precursor form α-β heterodimers in the ER and that only heterodimeric integrin can exit the ER to be transported via the Golgi apparatus to the plasma membrane (Heino et al., 1989). Excess single α or β integrin subunits in the ER will be degraded through the ERAD pathway (Darom et al., 2010). During the synthesis and transport through the ER and Golgi, integrins undergo glycosylation in a series of tightly controlled, step-wise processes that starts in the case of β1 integrin with the synthesis of a 88 kDa polypeptide that undergoes sequential glycosylation in the ER and in the Golgi (Akiyama and Yamada, 1987) giving rise to incompletely glycosylated β1 integrin subunit of 105 kDa and a complete or 'mature' β1 subunit of around 125 kDa that moves to plasma membrane together with α subunits (Gu et al., 2009). However incomplete glycosylated integrins also appear on cell surface. In human fibroblasts culture in the presence of N-linked oligosaccharide processing inhibitor, immature integrin α5β1 appeared at the cell surface but adhesion on FN is greatly reduced (Akiyama et al., 1989; Janik et al., 2010). Experiments using conformation-specific antibodies suggested that the newly synthesized and assembled αxβ1 integrin heterodimer adopts the inactive conformation in ER and maintains the bent conformation on the way until it reaches membrane by binding Ca^{2+} (Tiwari et al., 2011b). We still know surprisingly little about the process of integrin maturation on a molecular level. However, several protein-protein interactions are required to shuttle integrins to the cell surface that include ER-resident chaperons such as calnexin, the transmembrane protein LRP-1 but also cytosolic proteins binding to the integrin tails (Hotchin et al., 1995; Martel et al., 2000; Salicioni et al., 2004). An early study suggests

that talin-integrin interaction in ER might regulate delivery of newly synthesized integrin to plasma membrane along actin filament. Talin binding in the β1 tail exposes a GFFKR motif in α subunit, which was proposed to function as ER-export signal of integrins (Martel et al., 2000). Indeed, mutations within this sequence in αIIb integrin lead to redcued integrin surface level in some Glanzmann thrombosthenia (GT) patients (reviewed in (Margadant et al., 2011)).

Although integrin biosynthesis and exocytosis are fundamental to integrin function, the underlying molecular mechanisms regulating these processes are only incompletely understood. However, integrin conformation and protein binding to the integrin ecto- and cytosolic domains regulate these steps.

Integrin internalization

Once integrins reach the cell surface they reside in their inactive conformation or become activated, bind to their ligands and cluster to form cell adhesion sites. However, independent of their conformation the resident time of integrins on the cell surface is short because they are constantly internalized into the endosomal system. Integrin internalization occurs both through clathrin-independent and clathrin-dependent pathways or by macropinocytosis from dorsal ruffles. Integrins can follow more than one route to internalize (Figure 12A). For example, α5β1 integrins internalization is caveolin-dependent during FN assembly (Shi and Sottile, 2008), but is clathrin-dependent in migrating cells (Nishimura and Kaibuchi, 2007). Besides, α5β1 integrins also have been shown to internalize through macropinocytosis during stimulated cell migration (Gu et al., 2011).

Clathrin-dependent integrin internalization is thought to be the predominant form of integrin endocytosis in most cell types. It often requires clathrin-associated sorting proteins [CLASPs; for instance, Dab2, Numb or ARH (also known as LDLRAP1)] to interact with the integrin cytoplasmic domains (Ezratty et al., 2009; Nishimura and Kaibuchi, 2007; Teckchandani et al., 2009). The PTB-domain containing protein Numb has been shown to localize at FAs and can directly interact with the proximal NPxY motif of β1, β3, and β5 integrins via its PTB domain to regulate α5β1 and αVβ3 integrin internalization (Calderwood et al., 2003; Nishimura and Kaibuchi, 2007). Although Dab-

2 uses PTB domain binds to the distal NxxY motif in β integrin tails knockdown of Dab-2 predominantly affects β1 integrins surface levels as determined in proteomics approaches (Teckchandani et al., 2009) Additionally, Dab-2 localizes at or near FAs together with clathrin shortly before their disassembly (Chao and Kunz, 2009) and interacts with Eps15 and Itsn which also regulate integrin internalization (Teckchandani et al., 2012). While the role of Dab-2 in integrin clathrin-dependent endocytosis is undisputed there are conflicting observations on the role of Dab-2 for the internalization of specific α5β1 integrin conformations. Using antibodies against the active α5β1 conformation (12G10) Chao and Kunz showed that active integrins (FN occupied) are preferentially internalized via Dab-2/clathrin mediated integrin internalization during disassembly of focal adhesions (Chao and Kunz, 2009) while another study shows Dab-2-mediated-clathrin-dependent endocytosis of non-occupied (inactive) β1 integrins that are not engaged with the actin cytoskeleton or the ECM and lie outside of adhesion sites (Teckchandani et al., 2009). While this needs further clarification, the importance of the proximal NPxY and distal NxxY in β integrin tails for associated sorting protein binding is highlighted in cells expressing mutant β1 integrin with Tyrosine to Phenylalanine substitutions in both proximal NPxY and distal NxxY motives which show reduced clathrin-dependent endocytosis of β1 integrins (Pellinen et al., 2008).

While clathrin-mediated integrin internalization is important in migrating ECV304 and HeLa cells (Nishimura and Kaibuchi, 2007), integrins can also be internalized by the clathrin-independent pathways such as caveolin-dependent or using clathrin-independent carriers (CLICs). Rab21 directly binds to α integrin cytoplasmic tails to induce β1 endocytosis via caveolin-dependent routes and that overexpression of Rab21 rescues the impaired β1 endocytosis in $\beta1^{YY/FF}$ cells probably through increasing clathrin-independent endocytosis to compensate for the block of Dab-2 and Numb induced clathrin-dependent internalization. (Pellinen et al., 2008). β1 integrins can follow clathrin-independent endocytic routes that depends on caveolin (Shi and Sottile, 2008) macropinocytosis (Gu et al., 2011), and clathrin-independent carriers (Howes et al., 2010; Lakshminarayan et al., 2014) (Figure 13A). Several studies support the role caveolae in integrin endocytosis pathway such as for α5β1 internalization in myofibroblasts (Shi and Sottile, 2008) and for α2β1 whose endocytosis is mediated by

direct interaction of protein kinase Cα (PKCα) with the cytoplasmic tail of β1 integrin (Ng et al., 1999). In addition, αVβ3 can internalize by macropinocytosis, from PDGF (Platelet Derived Growth Factor)-induced dorsal ruffles to recycle back the basal side to form new focal adhesions (Gu et al., 2011). Finally, the carbonhydrate-binding protein galectin-3 can interact with glycosylated extracellular domain of β1 integrin to promote clathrin-independent endocytosis through CLICs by mechanical deformation of plasma membrane (Lakshminarayan et al., 2014)

Integrin recycling

Once internalized, integrins are delivered to early endosomes (EE), which are the key organelle to route integrins in different recycling or degradation pathways. Most internalized integrins are not degraded but recycled back to cell surface in different routes. In comparison to the long protein half-life of integrins (estimated >18 h) (Lobert et al., 2010), integrin recycling is fast (about every 15-30 minutes dependent on the cell type) (Roberts et al., 2004). This highly efficient spatiotemporally regulated integrin recycling does not only save energy, which would otherwise be necessary for synthesis, but also allows a continuous redistribution of integrins being an essential prerequisite for cell migration.

The molecular mechanisms underlying integrin trafficking have been the topic of multiple studies and several cytosolic integrin interactors have been shown to regulate the processes; many of those however in a cell type-dependent manner. For example, αVβ3 but not α5β1 integrins recycle via the Rab4-dependent short loop after PDGF stimulation. This short loop requires direct protein kinase D1 (PKD1) binding to β3 tails to C-terminal 14 amino acids of the integrin to recycle rapidly αVβ3 integrins from EEs to the plasma membrane into newly forming focal adhesions during cell spreading and migration (Woods et al., 2004). Integrins can also be routed in the so-called long loop from EE to the cell surface via a perinuclear recycling compartments (PNRC) in a process involving Rab11 and Arf6. α5β1 integrins take the Rab11-dependent loop in non-stimulated and serum stimulated fibroblast while αVβ3 integrin only in the absence of growth factors. This trafficking route requires the inactivation of glycogen 3 kinase 3 beta (GSK3β) by phosphorylation through Akt/PKB (Roberts et al., 2004). Akt also

phosphorylates ArfGAP With Coiled-Coil, Ankyrin Repeat And PH Domains 1 (ACAP1), which then associates directly with the β1 integrin tail for α5β1 integrin recycling (Li et al., 2005).

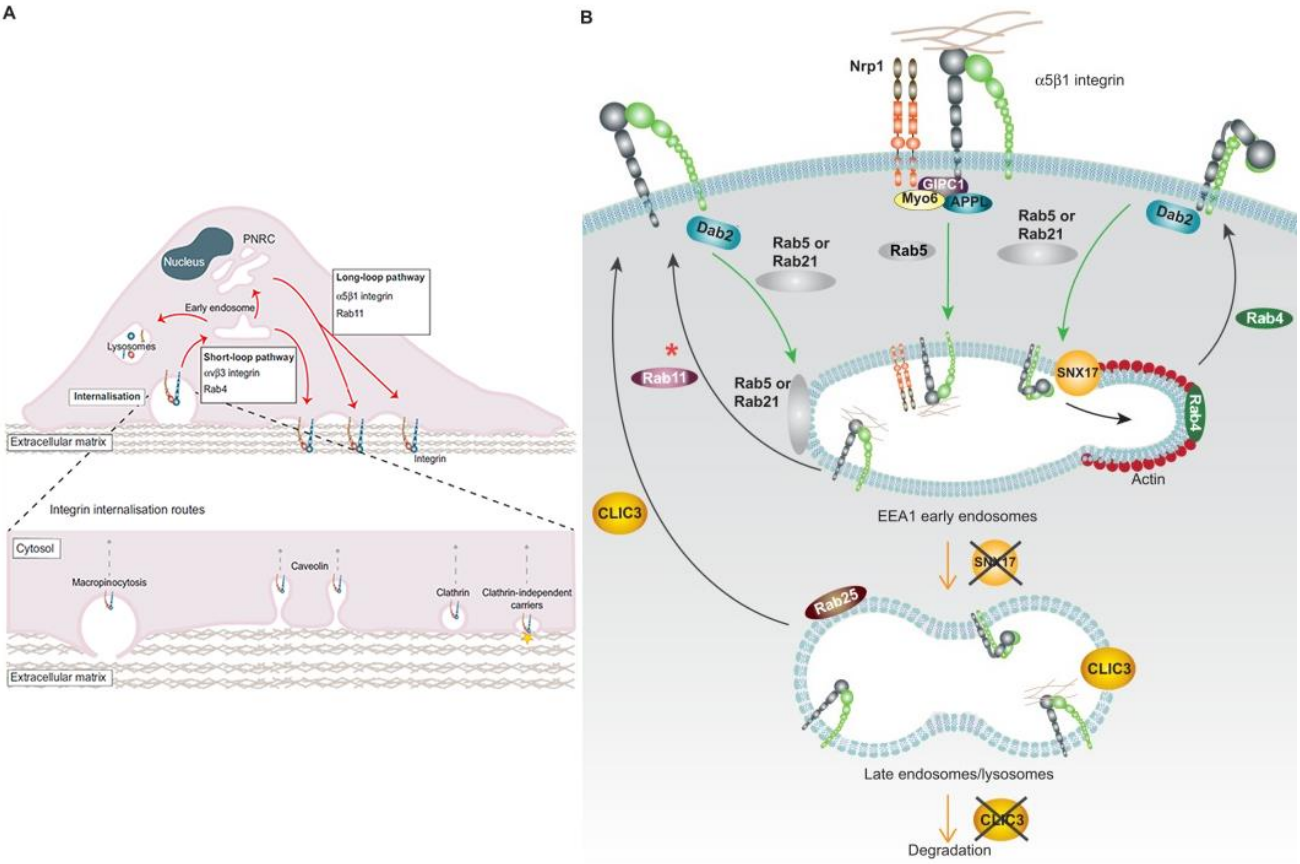

Figure 12. Integrin trafficking. (A) Canonical integrin trafficking. Integrins can be internalized in several functional distinct ways: Macropinocytosis from dorsal ruffles, clathrin-dependent internalization, caveolin-dependent, and via CLICs induced by galectin-3 binding to the extracellular domain of integrins (indicated in yellow star). Once integrins are internalized and reach early endosomes, α5β1 integrins mainly recycles through a Rab11-positive perinuclear recycling component (PNRC) long-loop αVβ3 integrin is mainly recycled via a Rab4-dependent short loop. **(B)** Representation of the trafficking routes of active and inactive α5β1 integrins. Endocytosis: Both active and inactive internalize in Dab-2/clathrin dependent pathways depending on the cell type. Active α5β1 integrins are also internalized from FBs in the complex with Nrp1-GIPC1-Myo6-APPL in endothelia cells. Recycling: Inactive integins are rapidly recycled back to plasma membrane in Rab4-dependent manner. Degradation: Upon binding of SNX17 (or SNX31, not shown) to β integrins tails in early endosome α5β1integrins are routed back to plasma membrane while in the absence of SNX17 binding α5β1 integrins are sent for lysosomal degradation. In late endosomes/ lysosomes, active α5β1 integrins traffic back to plasma membrane in present of CLIC3. (modified from De Franceschi et al., 2015)

While most cytosolic proteins interact with the β integrin subunits to regulate integrin recycling few proteins bind to the α integrin subunit. Rab21 and p120RasGAP bind to the same motif present in different integrin α subunits and their knockdowns affect integrin recycling. Rab21 regulates the trafficking from the cell surface through EE and PNRC. In the PNRC p120RasGAP replaces Rab21 at the α integrin subunits to promote the recycling back to the plasma membrane (Mai et al., 2011). It is becoming evident that integrin engagement affects the trafficking of receptor tyrosine kinases, which in turn affects cancer cell invasion. For example, mutant p53 or disruption αVβ3 function by cilengitide weakens the Rab-coupling protein (RCP), a Rab11 effector, and β3 tail association but conversely strengthens to β1 binding. α5β1 integrin and RCP coordinately recruits receptor tyrosine kinase, such as EGFR1, and both recycle back to plasma membrane where activates EGFR1 downstream signaling to promote tumor cell invasion through Akt activation (Caswell et al., 2008; Muller et al., 2009).

As integrins reside in an active and inactive conformation on the cell surface the question arose whether the integrin conformation affects the way integrins are trafficked within cells. In endothelia cells a complex consisting of Neuropilin1 (Nrp1) and GAIP interaction protein-C-terminus membrane 1 (GIPC1) promotes endocytosis and fast recycling of active integrin α5β1 from FBs while inactive α5β1 integrins traffic in a Neuropilin1-independent mechanisms (Valdembri et al., 2009) (Figure 12B). A recent study from the Ivaska lab made use of conformation-specific α5β1 integrin antibodies to follow the trafficking routes of active and inactive β1 integrins in NCI-H460, PC-3 and MDA-MB-231 cells (Arjonen et al., 2012). They show that active and inactive β1 integrins can be internalized to Rab5 or Rab21 positive early endosomes. While inactive α5β1 integrins predominantly recycle rapidly via the Rab4-dependent loop active β1 integrin is seen in Rab4a- and Rab11-positive compartments, but more careful studies in respect to active β1 integrin recycling are needed (Arjonen et al., 2012) (Figure 12B). This study also shows that only active β1 integrins (not inactive) are observed in Rab7 positive late endosomes, suggesting the existence of additional recycling pathways. Indeed, ligand bound active α5β1 integrins are sorted to late endosomes/lysosomes in Rab25-expressing A2780 ovarian carcinoma cells, from where they are recycled back to

the plasma membrane in a CLIC3 (Chloride intracellular channel protein 3) -dependent manner (Dozynkiewicz et al., 2012). A recent paper by the same lab shows the internalization of active α5β1 integrins from FBs directly to late endosomes without prior trafficking through EEs (Rainero et al., 2015). These examples indicate that integrin internalization and recycling is tightly and spatially regulated in the cell and is dependent on different factors such as the specific integrin heterodimer, the integrin conformation and cell-type specific factors.

Integrin degradation

Compared to integrin recycling the mechanisms underlying degradation of integrins is less studied. The Parker lab was the first to show the delivery of integrins to late endosomes (LE) (Ng et al., 1999). The half-life of integrins is long (>20 h for α5β1 integrin) and therefore researchers did not pay much attention towards the sorting of integrins into a degradation pathway. Nevertheless, it is becoming more evident that integrin internalization might be more than just a start point of integrin recycling, but part of a quality control mechanism for integrins. Functional integrins enter the recycling process, while defect molecules are routed to lysosomal degradation.

Proteins such as syntaxin-6 or CLIC3 were shown in cell depletion studies to regulate lysosomal β1 integrin degradation (Dozynkiewicz et al., 2012; Riggs et al., 2012; Tiwari et al., 2011a). However their loss likely affects more general aspects of endosome function such as vesicle fusion or maintenance of intracellular membranes rather than specific functions of integrins. In contrast, two factors have been shown to specifically regulate integrin protein stability: Ligand-binding to the integrin ectodomain (Dozynkiewicz et al., 2012; Lobert et al., 2010) and the interaction of the endosomal proteins SNX17 and SNX31 to the integrin cytoplasmic tail (Bottcher et al., 2012; Steinberg et al., 2012; Tseng et al., 2014). After internalization into EEs, unligated/inactive integrins are rapidly recycled back to plasma membrane while ligand-bound/active α5β1 integrins are ubiquitinylated and subsequently sorted into LEs/lysosomes for degradation in the absence of CLIC3 (Dozynkiewicz et al., 2012; Lobert et al., 2010) (Figure 12B). The molecular mechanism underlying CLIC3 function and the E3 ligases mediating integrin ubiquitination are unknown. It is also still unclear

why cells degrade active integrins over integrins in their inactive conformation. One explanation for the degradation of active integrins could be the need to recycle ligand-free integrins to the plasma membrane (Lobert et al., 2010). On the other hand, it is reported that the endocytosis of active integrins to the lysosome in tensin-dependent manner is necessary to maintain a population of centrally located late endosomes/lysosomes capable of recruiting and activating mTOR in response to nutrient. This spatially restricted trafficking of a particular subpopulation of integrins between FBs and lysosomes provides evidence for mechanistic links between ECM internalization and nutrient signaling. (Rainero et al., 2015).

Conversely, inactive α5β1 integrins are routed to EEs where the endosomal protein SNX17 utilizes its FERM domain to bind to the membrane distal NPxY motif within β1 integrin to save inactive β1 integrins from lysosomal degradation (Bottcher et al., 2012; Steinberg et al., 2012) (Paper II). The SNX17-integrin interaction prevents integrin degradation and enables integrins to recycle back to the plasma membrane by an unknown mechanism, while integrins are degraded rapidly in SNX17 knockdown cells. SNX31, another member of the FERM-domain containing subfamily of SNX proteins, also binds different β integrin tails and can rescue β1 integrin surface levels and stability in SNX17-depleted mouse fibroblasts (Tseng et al., 2014) (Paper III). This indicates that SNX17 and SNX31 play a similar role to regulate integrin β1 degradation. The SNX proteins will be further discussed in the following part.

In summary, there is accumulated evidence for the importance of integrin trafficking to modulate integrin function. From these studies it is also clear that the mechanisms underlying integrin trafficking and degradation differ between different integrin conformations, amidst distinct integrins, even between cell types. Since proteins binding to the cytoplasmic domains of the integrin α and β subunits are key to understand the different trafficking routes and mechanisms it merits to search and identify new proteins interacting with integrins in a conformation-specific and spatially defined manner.

4.1 Sortin nexins

Sorting nexins (SNXs) are a family of proteins that contain a Phox homology (PX) domain which serves as phosphoinositide-binding motif to guide the SNX proteins to phosphatidylinositol-3-monophsphate (PI3P)-enriched membranes found in endosomes. Members of this protein family have been identified from yeast (10 SNXs) to mammals (33 SNXs) (Seet and Hong, 2006) and are mainly implicated in endocytosis and endosomal sorting (Cullen, 2008). The name SNX was introduced by Kurten *et al.* to highlight the sequence similarity within their PX domains (Kurten et al., 1996). Besides the PX-domain SNXs carry different protein-protein and protein-lipid interaction domains and are divided into subfamilies according to their additional protein domains (Teasdale and Collins, 2012). The best studied SNX family members are those that are part of the retromer complex, which associates with endosomes and mediates the retrograde transport of transmembrane cargo from endosomes to the trans-Golgi network (Hierro et al., 2007; Wassmer et al., 2009).

The SNX-FERM subfamily contains three members: SNX17, SNX27, and SNX31, which are conserved in metazoans, but not in yeast (Gallon and Cullen, 2015). All members of this subfamily are characterized by an atypical FERM domain right after the SNX-PX domain (Ghai et al., 2013) and are involved in cargo trafficking. Importantly, the FERM domain interacts with NxxY motives in transmembrane proteins, including β integrins (Bottcher et al., 2012; Steinberg et al., 2012). SNX27 contains an additional PDZ domain that can engage PDZ binding motifs at the C-terminus of transmembrane proteins (Balana et al., 2011).

Most of SNX17 interactors are transmembrane proteins that rely on SNX17 to regulate their trafficking between endosome and plasma membrane by a yet unidentified mechanism. The cargo proteins of SNX17 include integrins (Paper II) (Bottcher et al., 2012; Steinberg et al., 2012), low density lipoprotein receptor (LDLR) (Stockinger et al., 2002), low density lipoprotein receptor related protein 1 (LRP) (Stockinger et al., 2002; van Kerkhof et al., 2005), and P-selectin (Knauth et al., 2005). SNX17 also interacts with some cytosolic proteins such as krev 1 interaction trapped 1 (KRIT1) (Stiegler et al., 2014) and kinesin microtubule-motor (KIF1B) (Seog and Han, 2008); however, the functional impact of these interactions for SNX17 function are still

unknown. SNX31 is the least-characterized member in this subfamily but seems functionally very similar to SNX17 as it binds integrins and regulates integrin surface level similarly to SNX17 (Paper III)(Tseng et al., 2014). SNX31 also functions in lysosomal degradation of uroplakins, a transmembrane protein group in urothelial cells (Vieira et al., 2014). In contrast to SNX17 and SNX31, SNX27 is not involved in the regulation of integrin protein stability and surface levels (Steinberg et al., 2013; Tseng et al., 2014). Instead, SNX27 prevents lysosomal routing of β2 adrenergic receptors and transmembrane proteins required for maintaining cellular nutrient homeostasis through binding to the SNX-BAR retromer (Steinberg et al., 2013; Temkin et al., 2011), a protein complex that transports transmembrane proteins from endosomes to the trans-Golgi network (Hierro et al., 2007). In line with its role in trafficking, loss of SNX27 is also shown to contribute to excitatory synaptic dysfunction in Down's syndrome patients by affecting glutamate receptor recycling (Wang et al., 2013).

5. Membrane mimicking systems

The typical biological membrane is a complex structure primarily composed of lipids and proteins. Such membranes surround every living cell and form stable barriers between two compartments. These compartments can be either the inside or the outside of the cell in case of the plasma membrane or different compartments within the cell such as cytosol and endoplasmic reticulum or Golgi lumen.

The fundamental structure of the plasma membrane is the phospholipid bilayer with a hydrophilic exterior and a hydrophobic core. Phosphatidylcholine (PC) is the most prevalent phospholipid and accounts for 40%–50% of the total phospholipid content; Phosphatidylethanolamine (PE) ranges from 20% to 45%, and Phosphatidylinositol (PI), Phosphatidylserine (PS), and Phosphatidic Acid (PA) are present in lesser amounts. The lipid composition of different membranes varies throughout the cell. (Leventis and Grinstein, 2010; van Meer et al., 2008). In addition to be a hydrophobic barrier, plasma membranes also serve other functions such as import and export of nutrients and for cell-cell communication. These functions are mainly carried out by transmembrane proteins embedded within the plasma membrane or by proteins linked to the membranes via lipid anchors. Indeed, transmembrane proteins play crucial roles in many processes such as connection between extracellular matrices and intracellular

molecules like actin, transmit signals and transport molecules. It is therefore not surprising that mutations in membrane proteins are the underlying cause of many diseases (Sanders and Myers, 2004). However, structural studies of transmembrane proteins are challenging as the correct structure and function of transmembrane proteins depend on their membrane embedding (review in (Kim et al., 2009b)). Transmembrane proteins are naturally embedded in a native lipid bilayer to maintain proper conformation and function. For most studies, the transmembrane protein has to be extracted from its native environment. Therefore the researchers need proper systems to study these proteins. As the generation of native membranes is difficult several minimal artificial membrane systems have been established over the past decades that mimic certain properties of native membranes thereby preserving the integrity, stability, and native structure of transmembrane proteins once extracted from their native environment (Sachs and Engelman, 2006). In case of integrins studies have used micelles, bicelles and nanodiscs (see below) that allowed studying in αIIbβ3 integrins transmembrane structure (Lau et al., 2009; Yang et al., 2009) and integrin αIIbβ3 activation process (Ye et al., 2010) (also see section 1.3.2).

Membrane mimicking systems have a second advantage in interacting/proteomics studies of transmembrane proteins: proteins binding to the cytoplasmic domain of transmembrane proteins frequently interact with lipid components of membranes. The lipid interaction either strengthens the protein-protein interacting and/or allows the proper orientation of the proteins. Because of the short integrin cytoplasmic domains it is even more likely that proteins directly binding to integrin tails are affected by the plasma membrane. Indeed, it has been shown that the interaction of talin (Anthis et al., 2009; Goult et al., 2010), kindlin (Goult et al., 2009; Liu et al., 2011; Perera et al., 2011), and ILK (Widmaier et al., 2012) with integrins and their functions also rely on the interaction with phospholipids in the plasma membrane.

The membrane mimicking systems used in the integrin field, namely micelles, bicelles, and nanodiscs, will be discussed briefly.

5.1 Detergent micelles

One of the most common approaches to solubilize membrane proteins is the use of detergent-micelles. Micelles consist of detergent molecules that aggregate above a defined threshold concentration called the critical micelle concentration (CMC), while detergent stays as monomer in aqueous solution when they are below the CMC. The increase in the detergent concentration above the CMC results in the assembly of more micelles in a highly dynamic equilibrium with detergent monomers. The classical micelles characterize with a hydrophilic head oriented to solution and hydrophobic single tail in the core (Figure 13A). In general, micelles have a relatively small diameter (ranging from 2 nm to 20 nm depending on the detergent (Garavito and Ferguson-Miller, 2001)) and the membrane curvature (Lipfert et al., 2007; Prive, 2007). Micelles are still used because of their ease to prepare. Still, they are generally not optimal to preserve the integrity and stability of transmembrane proteins for two reasons (Tate, 2010). First, micelles are highly dynamic in solution and this intrinsic instability can trigger proteins aggregation and degradation. Second, the differences of lateral forces and curvature of micelles compared to planar plasma membrane can affect the protein conformation and even lead to protein unfolding (Lu et al., 2012).

Dodecylphosphocholine (DPC) micelles have been used to investigate the interaction between αIIbβ3 TM/cyto interactions but failed to detect associations between the two integrin subunits (Li et al., 2001). It was suggested that under micelle condition the relatively weak interaction between α and β TM/cyto was weakened to the point that no specific interaction was detectable by NMR anymore (Li et al., 2001).

5.2 Bicelles

Bilayered phospholipid micelles (bicelles) represent a new category of biological model membrane characterized by their liquid-crystalline phase behavior which was established as a membrane model system for structural NMR studies (Sanders and Landis, 1995). Classical bicelles are discoidal zwitterionic phospholipids mixture structures: long-chain phospholipids (dimyristoylphosphatidylcholine, DMPC) retrain the bilayer feature to better imitate plasma membrane and short-chain phospholipids (dihexanoylphosphatidylcholine DHPC or 6-cyclohexyl-1-hexylphosphocholine,

Cyclofos-6) coat the rim of the bilayer and isolate the hydrophobic core from the water phase (Figure 13B). The bicelles size can be varied and is defined by the total concentration and the molar ratio of long-chain and short-chain phospholipids (q value). Bicelles have disc-like shape at low q values that are edge-stabilized at the rim by short-chain phospholipids while the bilayer-ordered long-chain phospholipid are in the center. At higher q value (q>3), bicelles show a “Swiss cheese”-like morphology, in which the holes are edge-stabilized by short-chain phospholipid (Figure 13B).

Bicelles share the advantages of detergent micelles, such as water solubility, optically transparency and easy generation. On the other hand, they overcome the disadvantages of micelles especially the high global curve tension and bicelles also better represent plasma membrane features as they are lipid-rich (Andersson and Maler, 2006; Chou et al., 2004; Kim et al., 2009a; Lu et al., 2012; Whiles et al., 2002; Wu et al., 2010). In many studies, bicelles have also been proved to have several advantages over the use of micelles. For instance, diacylglycerol kinase retains its activity in bicelles, but not in micelles (Sanders and Landis, 1995) and bacteriorhodopsin refolds into native conformation in bicelles (Booth and Farooq, 1997; Booth et al., 1996). Furthermore, incorporation of the HIV-1 envelope peptide into micelles induces a strong curvature, which is not observed in bicelles (Chou et al., 2002). Bicelles have also successfully been used in NMR studies aimed to determine the structure of TM domains of integrins. While earlier studies utilizing DPC micelles for NMR and other biophysical methods failed to detect the interaction between the TMcyto domains of αIIbβ3 integrin (Li et al., 2001), incorporation of the TM domains of αIIbβ3 integrin into bicelles allowed to determine the first TM α/β regions complex structure (Lau et al., 2009). Additionally, β1 integrin TMcyto domains embedded in bicelles also have been shown in NMR (Lu et al., 2012). This suggests the environment provided by bicelles allow the integrin α-β heterodimer TM segment to retain native-like interactions.

5.3 Nanodiscs

Nanodiscs contain phospholipids assembled noncovalently as bilayer, which are surrounded by amphipathic apolipoproteins (Figure 13C). They were developed by Sligar and colleagues to solubilize transmembrane proteins (Bayburt and Sligar, 2002).

They made use of natural structures, which are used to assemble high-density lipoproteins (HDLs) into bilayered, spherical shapes surrounded by the scaffold protein apolipoprotein A1 and to transport HDLs to the liver for degradation (Schmitz and Grandl, 2009). The size of nanodiscs is determined by the length of apolipoprotein A1, also called Membrane Scaffold Protein (MSP), which can be modified *in vitro* to generate nanodiscs with various diameters (Borch et al., 2008). Nanodiscs can generate a native-like bilayered plasma membrane and allow access on both sides of membranes similar to bicelles. However, unlike bicelles, nanodiscs require the MSP ring around the lipid core to stabilize the lipid bilayers. This increases the membrane stability and minimizes size variations within a specific population of membrane particles when transmembrane proteins are incorporated but hampers a fast variation of the particle size compared to bicelles.

The structures of several transmembrane proteins have successfully been determined using nanodiscs as membrane-mimicking models including a potassium channel (KcsA) (Shenkarev et al., 2009) or the voltage-dependent anion channel (VDAC-1) (Raschle et al., 2009). Others used nanodiscs in functional assay for example to determine ligand binding to the β2-Adrenergic receptor (β2AR) (Leitz et al., 2006). An EM study used full length αIIbβ3 integrins embedded into nanodiscs to show that talin head binding could induce conformational changes of integrin extracellular domain (Ye et al., 2010).

For our proteomics study we have chosen to incorporate integrins into bicelles as membrane system for several reasons. (1) Structural studies have shown that incorporation of the αIIbβ3 integrin transmembrane domains does not interfere with its native, inactive conformation. (2) The Sanders' lab developed bicelles systems that can still preserve the bicelles properties when diluted below 1% in solution (Lu et al., 2012) which is favorable for pull-down experiment. (3) Bicelles can be supplemented with extra lipids such as negatively charged lipids (MOPS) or phospholipids to closer mirror the endogenous plasma membrane composition (Struppe et al., 2000). This is important as many protein-lipid interactions rely in the negative membrane charge (Anthis et al., 2009; Goult et al., 2010; Goult et al., 2009; Liu et al., 2011; Perera et al., 2011; Widmaier et al., 2012) (4) In contrast to nanodiscs, bicelles do not contain an additional

protein, which reduces the risk of non-specific protein-protein interaction in the biochemical and proteomic analysis.

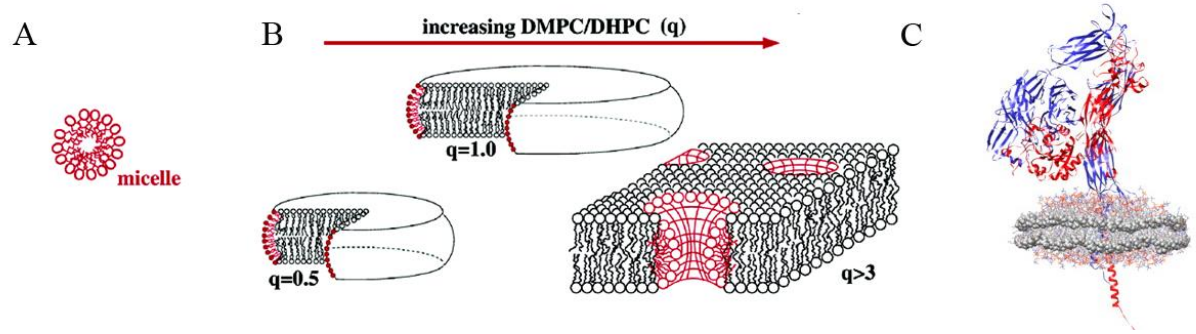

Figure 13. The structure of detergent micelles, bicelles, and nanodisc. (A) Detergent micelles are small, global structures. Their size can be varied by changing the detergent. (B) Bicelles are discoidal zwitterionic phospholipids mixture structures that display bilayer features. Their size can be controlled by modulating the ratio of long-chain phospholipids/short-chain phospholipids (q). In low q values, bicelles have disc-like shape. When q > 3, bicelles are “Swiss cheese”-like structures. (C) Nanodisc-embedded integrin heterodimer. Nanodiscs are protein−lipid particles which size is regulated by Membrane Scaffold Proteins (MSP) (indicated in grey). Integrins are shown in blue (α subunit) and red (β subunit). (modified from Prosser et al., 2006, Ye et al., 2010)

Aim of the thesis

Integrins are a family of heterodimeric transmembrane proteins consisting of a large ectodomain and a short cytoplasmic tail. Proteins binding to the cytoplasmatic tails of integrins are fundamental for integrin function. They regulate the integrin affinity for ligands, allow integrins to connect to the actin cytoskeleton and to initiate intracellular signaling pathways, and regulate intracellular integrin trafficking and protein stability.
Like other cell surface receptors integrins signal in response to ligand binding, however they can also regulate their affinity for ligand. The shift between low and high conformations for ligand during integrin activation requires the binding of the cytosolic proteins kindlin and talin to the β integrin tail. In the inactive, low affinity conformation the transmembrane and cytoplasmic domains associate with each other while they become separated in the active, high affinity state. While integrin activation is studied extensively, the inactive conformation has long been considered as ‘default state’ but growing evidences indicate that the inactive conformation might also be actively regulated by the binding of intracellular integrin interactors. We speculate that cells have protein(s), which bind clasped α/β tails to keep them in a low affinity conformation. Such proteins could serve to strengthen the association, which might be particularly important for leukocytes, or to regulate other processes important for integrin function such as internalization, recycling, degradation, etc. Integrin trafficking and stability control is coupled and is believed to determine their cell surface distribution and the signaling crosstalk with growth factor receptors. However, the mechanisms controlling integrin trafficking and stability are poorly understood.

The aim of my PhD project was to identify and characterize integrin tail binding proteins that bind to specific integrin conformations. I focused on cytoplasmic interactors that (i) only bind α/β heterodimeric and not to the isolated tails and might prevent unwanted signaling as well as (ii) proteins may play a critical role for the recycling and/or degradation of integrins.

Therefore the aims of the thesis were:

1. **To establish a biochemical/proteomics method that allows screening for cytoplasmic conformation-specific integrin and supports protein-lipid interactions.**
2. **To systemically identify and compare cytoplasmic interactors of the single α- and β integrin subunits as well as of associated αMβ2 integrin tails.**
3. **To characterize these new candidates for their roles in integrin-mediated functions.**

Short summaries of publications

Paper I: A proteomic approach reveals conformation specific cytoplasmic integrin interactors

Integrins exist in at least two distinct conformations; a high ('active') and a low affinity ('inactive') state for ligands. In their inactive state the transmembrane and cytoplasmic (TMcyto) domains of the two integrin subunits are associated while they become separated upon activation. Although several cytoplasmic integrin interactors have been identified only filamin A has been shown to bind to associated α-β integrin TM-cyto domains. We hypothesize that more such proteins exist that only bind α/β heterodimeric tails and might serve as regulators of integrin activation or allow cells to distinguish between active and inactive integrins in other processes, such as integrin trafficking. In order to identify such conformation-specific integrin interactors by mass spectrometry we generated recombinant proteins for pull-down experiments that mimic associated integrin TM-cyto domains by fusion the αMβ2 TMcyto domains to the Fos-Jun hetero-dimerization domains as "velcro". Furthermore, we incorporated the αMβ2 TM-cyto complex into bicelles to sustain the native protein conformation and to support protein-lipid interactions. In a first set of experiments we used the single α5, αM and αIIb as well as β1, β2 and β3 integrin incorporated into bicelles to pull-down interactors from bone marrow derived macrophages lysates. Subsequent identification of the cytosolic binding proteins by liquid chromatography–tandem mass spectrometry (LCMS/MS) allowed us to determine the compositional differences between binding proteins associated with different integrins. Using the Jun-Fos-mediated associated αMβ2 TMcyto baits we we identified several conformation-specific integrin interactors including L-plastin (LCP1). Further experiments implicated LCP1 in the regulation of αMβ2 surface levels in leukocyte cell lines. LCP1 knock-down increases integrin αMβ2 surface level and enhances cell attachment to fibrinogen and ICAM in unstimulated cells. Our proteomics data provide a resource for the global view on cytoplasmic proteins interacting with different integrin classes and provides evidence for the presence of several conformation-specific integrin interactors.

Paper II: Sorting nexin 17 prevents lysosomal degradation of β1 integrins by binding to the β1-integrin tail

Integrin function is controlled by the interaction of proteins to their cytoplasmic tails which regulate integrin affinity for ligands, intracellular signaling as well as integrin trafficking through the endosomal system.

Here we demonstrate that the kindlin-binding site in the β1 integrin cytoplasmic domain serve as a molecular switch enabling the sequential binding of two FERM-domain-containing proteins in different cellular compartments. Kindlins occupy the membrane distal NPxY and adjacent Thr residues on β1 integrin at the plasma membrane. During integrin internalization kindlins dissociated and the FERM-domain containing protein SNX17 directly binds to the free binding site in early endosomes. The interaction of SNX17 with β1 integrin prevents integrins routing into the lysosomal, degradative pathway and promotes sorting of the integrins into recycling pathways back to plasma membrane. In the absence of SNX17, β1 integrin is sent to lysosomes and rapidly degraded leading to reduced surface availability of β1 integrin and slower cell migration velocities when cells were plated on fibronectin. Our results identify SNX17 as a novel β1 integrin tail binding protein in early endosomes to prevent integrin degradation.

Paper III: Sorting nexin 31 binds multiple β integrin cytoplasmic domains and regulates β1 integrin surface levels and stability

In paper II, we showed that the trafficking of α5β1 integrin to lysosomes and its subsequent degradation is regulated by direct binding of SNX17 to the cytoplasmic domain of β1 integrin in early endosomes. This interaction requires the SNX17-FERM domain and an intact membrane-distal NxxY motif in the β1 integrin tail. Two other SNX family members, SNX27 and SNX31, also contain a FERM domain next to a phox domain, which could potentially enable them to bind β integrin tails. We therefore investigated the SNX-FERM subfamily members for their ability to bind integrins and to control integrin recycling and stability.

Here we demonstrate that the SNX-FERM family members SNX17 and SNX31 but not SNX27 are able to bind several β integrin tails in early endosomes in a PI3-kinase-dependent manner. While SNX17 is ubiquitously expressed, SNX31 expression is restricted to predominantly bladder and melanoma cells. SNX31 needs intact FERM domain to directly interact with β tails in early endosomes and to rescue β1 integrin surface levels and stability in SNX17 depleted cells. All together, these results demonstrate that SNX31 is tissue-specific endosomal regulator of β1 integrin protein stability.

Paper IV: Kank family proteins comprise a novel type of talin activator

In this paper, we demonstrate the evolutionarily conserved Kank family as a novel focal adhesion molecules and is concentrated at the border of FAs (termed FA belt) and FBs but not in nascent adhesions. The conserved KN motif is essential to localize Kank to FAs belt and central FBs. We demonstrated that Kank2 and talin was co-recruited to integrin β tails in a talin-dependent manner. Unlike kindlin2 and c-Src,which profoundly binds to β1 and β3 tails respectively, Kank2 binds equally with β1 and β3 tails. The recruitment induces and/or maintaines the formation of active integrins at sites uncoupling with actomyosin. The further analysis reveales Kank2 directly binds to talin R7 domain via KN motif and that promotes talin activation to induce and/or maintain integrin β tails binding in a force and actin-independent manner. Subsequently, Kank2 destabilized talin-actin connection. Altogether, we have identified Kank family as a new FA proteins, a novel talin activator, which specifically stabilized integrin-talin complex that are uncoupled from actomyosin system.

Paper V: Integrin α3β1 regulates kidney collecting duct development via TRAF6-dependent K63-linked polyubiquitination of Akt

Integrin-mediated signaling plays vital roles during various developmental processes including branching morphogenesis during kidney development. Laminin-binding integrins are highly expressed in the ureteric bud (UB) and α3β1 integrins was shown to be crucial for UB branching to form the collecting duct system of the kidney. However, the laminin type and the signaling pathways initiated though laminin-integrin α3β1 are not well characterized. In this study, we show that integrin α3β1 interactions with α3 chain-containing laminins are important for Akt activation in collecting duct cells. Mechanistically, we identified TRAF6 as novel binding partner of β1 integrin cytoplasmic tails required to induce K63-linked polyubiquitination of Akt and to promote Akt recruitment to the plasms membrane. Furthermore, laminin-integrin α3β1 inactivates Phosphatase and tensin homolog (PTEN), thereby increasing PtdIns (3,4,5)P3 levels which further enhances Akt translocation and then full Akt activation. The importance of TRAF6 for kidney development is underlined by developmental defects of TRAF6- and integrin α3-depleted mouse kidneys.

Reference

Adair, B.D., and M. Yeager. 2002. Three-dimensional model of the human platelet integrin alpha IIbbeta 3 based on electron cryomicroscopy and x-ray crystallography. *Proc Natl Acad Sci U S A*. 99:14059-14064.

Akiyama, S.K., and K.M. Yamada. 1987. Biosynthesis and acquisition of biological activity of the fibronectin receptor. *J Biol Chem*. 262:17536-17542.

Akiyama, S.K., S.S. Yamada, and K.M. Yamada. 1989. Analysis of the role of glycosylation of the human fibronectin receptor. *J Biol Chem*. 264:18011-18018.

Andersson, A., and L. Maler. 2006. Size and shape of fast-tumbling bicelles as determined by translational diffusion. *Langmuir*. 22:2447-2449.

Anthis, N.J., K.L. Wegener, F. Ye, C. Kim, B.T. Goult, E.D. Lowe, I. Vakonakis, N. Bate, D.R. Critchley, M.H. Ginsberg, and I.D. Campbell. 2009. The structure of an integrin/talin complex reveals the basis of inside-out signal transduction. *Embo J*. 28:3623-3632.

Arjonen, A., J. Alanko, S. Veltel, and J. Ivaska. 2012. Distinct recycling of active and inactive beta1 integrins. *Traffic*. 13:610-625.

Arnaout, M.A., B. Mahalingam, and J.P. Xiong. 2005. Integrin structure, allostery, and bidirectional signaling. *Annu Rev Cell Dev Biol*. 21:381-410.

Askari, J.A., P.A. Buckley, A.P. Mould, and M.J. Humphries. 2009. Linking integrin conformation to function. *J Cell Sci*. 122:165-170.

Bader, B.L., H. Rayburn, D. Crowley, and R.O. Hynes. 1998. Extensive vasculogenesis, angiogenesis, and organogenesis precede lethality in mice lacking all alpha v integrins. *Cell*. 95:507-519.

Bai, J., R. Binari, J.Q. Ni, M. Vijayakanthan, H.S. Li, and N. Perrimon. 2008. RNA interference screening in Drosophila primary cells for genes involved in muscle assembly and maintenance. *Development*. 135:1439-1449.

Balana, B., I. Maslennikov, W. Kwiatkowski, K.M. Stern, L. Bahima, S. Choe, and P.A. Slesinger. 2011. Mechanism underlying selective regulation of G protein-gated inwardly rectifying potassium channels by the psychostimulant-sensitive sorting nexin 27. *Proc Natl Acad Sci U S A*. 108:5831-5836.

Baldassarre, M., Z. Razinia, C.F. Burande, I. Lamsoul, P.G. Lutz, and D.A. Calderwood. 2009. Filamins regulate cell spreading and initiation of cell migration. *PLoS One*. 4:e7830.

Banno, A., B.T. Goult, H. Lee, N. Bate, D.R. Critchley, and M.H. Ginsberg. 2012. Subcellular localization of talin is regulated by inter-domain interactions. *J Biol Chem*. 287:13799-13812.

Baudoin, C., M.J. Goumans, C. Mummery, and A. Sonnenberg. 1998. Knockout and knockin of the beta1 exon D define distinct roles for integrin splice variants in heart function and embryonic development. *Genes Dev*. 12:1202-1216.

Bayburt, T.H., and S.G. Sligar. 2002. Single-molecule height measurements on microsomal cytochrome P450 in nanometer-scale phospholipid bilayer disks. *Proc Natl Acad Sci U S A*. 99:6725-6730.

Berrier, A.L., and K.M. Yamada. 2007. Cell-matrix adhesion. *J Cell Physiol*. 213:565-573.

Bix, G., and R.V. Iozzo. 2005. Matrix revolutions: "tails" of basement-membrane components with angiostatic functions. *Trends Cell Biol*. 15:52-60.

Bledzka, K., J. Liu, Z. Xu, H.D. Perera, S.P. Yadav, K. Bialkowska, J. Qin, Y.Q. Ma, and E.F. Plow. 2012. Spatial coordination of kindlin-2 with talin head domain in interaction with integrin beta cytoplasmic tails. *J Biol Chem*. 287:24585-24594.

Boettiger, D. 2012. Mechanical control of integrin-mediated adhesion and signaling. *Curr Opin Cell Biol*. 24:592-599.

Bohmer, F.D., Q. Sun, M. Pepperle, T. Muller, U. Eriksson, J.L. Wang, and R. Grosse. 1987. Antibodies against mammary derived growth inhibitor (MDGI) react with a fibroblast growth inhibitor and with heart fatty acid binding protein. *Biochem Biophys Res Commun*. 148:1425-1431.

Booth, P.J., and A. Farooq. 1997. Intermediates in the assembly of bacteriorhodopsin investigated by time-resolved absorption spectroscopy. *Eur J Biochem*. 246:674-680.

Booth, P.J., A. Farooq, and S.L. Flitsch. 1996. Retinal binding during folding and assembly of the membrane protein bacteriorhodopsin. *Biochemistry*. 35:5902-5909.

Borch, J., F. Torta, S.G. Sligar, and P. Roepstorff. 2008. Nanodiscs for immobilization of lipid bilayers and membrane receptors: kinetic analysis of cholera toxin binding to a glycolipid receptor. *Anal Chem*. 80:6245-6252.

Borges, E., Y. Jan, and E. Ruoslahti. 2000. Platelet-derived growth factor receptor beta and vascular endothelial growth factor receptor 2 bind to the beta 3 integrin through its extracellular domain. *J Biol Chem*. 275:39867-39873.

Bottcher, R.T., A. Lange, and R. Fassler. 2009. How ILK and kindlins cooperate to orchestrate integrin signaling. *Curr Opin Cell Biol*. 21:670-675.

Bottcher, R.T., C. Stremmel, A. Meves, H. Meyer, M. Widmaier, H.Y. Tseng, and R. Fassler. 2012. Sorting nexin 17 prevents lysosomal degradation of beta1 integrins by binding to the beta1-integrin tail. *Nat Cell Biol*. 14:584-592.

Bouvard, D., J. Pouwels, N. De Franceschi, and J. Ivaska. 2013. Integrin inactivators: balancing cellular functions in vitro and in vivo. *Nat Rev Mol Cell Biol*. 14:430-442.

Bouvard, D., L. Vignoud, S. Dupe-Manet, N. Abed, H.N. Fournier, C. Vincent-Monegat, S.F. Retta, R. Fassler, and M.R. Block. 2003. Disruption of focal adhesions by integrin cytoplasmic domain-associated protein-1 alpha. *J Biol Chem*. 278:6567-6574.

Brahme, N.N., D.S. Harburger, K. Kemp-O'Brien, R. Stewart, S. Raghavan, M. Parsons, and D.A. Calderwood. 2013. Kindlin binds migfilin tandem LIM domains and regulates migfilin focal adhesion localization and recruitment dynamics. *J Biol Chem*. 288:35604-35616.

Bridgewater, R.E., J.C. Norman, and P.T. Caswell. 2012. Integrin trafficking at a glance. *J Cell Sci*. 125:3695-3701.

Brugnera, E., L. Haney, C. Grimsley, M. Lu, S.F. Walk, A.C. Tosello-Trampont, I.G. Macara, H. Madhani, G.R. Fink, and K.S. Ravichandran. 2002. Unconventional Rac-GEF activity is mediated through the Dock180-ELMO complex. *Nat Cell Biol*. 4:574-582.

Brunner, M., A. Millon-Fremillon, G. Chevalier, I.A. Nakchbandi, D. Mosher, M.R. Block, C. Albiges-Rizo, and D. Bouvard. 2011. Osteoblast mineralization requires beta1 integrin/ICAP-1-dependent fibronectin deposition. *J Cell Biol*. 194:307-322.

Burke, R.D. 1999. Invertebrate integrins: structure, function, and evolution. *Int Rev Cytol*. 191:257-284.

Burridge, K., and L. Connell. 1983. A new protein of adhesion plaques and ruffling membranes. *J Cell Biol*. 97:359-367.

Bustelo, X.R., V. Sauzeau, and I.M. Berenjeno. 2007. GTP-binding proteins of the Rho/Rac family: regulation, effectors and functions in vivo. *Bioessays*. 29:356-370.

Calderwood, D.A., I.D. Campbell, and D.R. Critchley. 2013. Talins and kindlins: partners in integrin-mediated adhesion. *Nat Rev Mol Cell Biol*. 14:503-517.

Calderwood, D.A., Y. Fujioka, J.M. de Pereda, B. Garcia-Alvarez, T. Nakamoto, B. Margolis, C.J. McGlade, R.C. Liddington, and M.H. Ginsberg. 2003. Integrin beta cytoplasmic domain interactions with phosphotyrosine-binding domains: a structural prototype for diversity in integrin signaling. *Proc Natl Acad Sci U S A*. 100:2272-2277.

Calderwood, D.A., B. Yan, J.M. de Pereda, B.G. Alvarez, Y. Fujioka, R.C. Liddington, and M.H. Ginsberg. 2002. The phosphotyrosine binding-like domain of talin activates integrins. *J Biol Chem*. 277:21749-21758.

Calderwood, D.A., R. Zent, R. Grant, D.J. Rees, R.O. Hynes, and M.H. Ginsberg. 1999. The Talin head domain binds to integrin beta subunit cytoplasmic tails and regulates integrin activation. *J Biol Chem*. 274:28071-28074.

Campbell, I.D., and M.J. Humphries. 2011. Integrin structure, activation, and interactions. *Cold Spring Harb Perspect Biol*. 3.

Carman, C.V., and T.A. Springer. 2003. Integrin avidity regulation: are changes in affinity and conformation underemphasized? *Curr Opin Cell Biol*. 15:547-556.

Caswell, P.T., M. Chan, A.J. Lindsay, M.W. McCaffrey, D. Boettiger, and J.C. Norman. 2008. Rab-coupling protein coordinates recycling of alpha5beta1 integrin and EGFR1 to promote cell migration in 3D microenvironments. *J Cell Biol*. 183:143-155.

Chang, D.D., C. Wong, H. Smith, and J. Liu. 1997. ICAP-1, a novel beta1 integrin cytoplasmic domain-associated protein, binds to a conserved and functionally important NPXY sequence motif of beta1 integrin. *J Cell Biol*. 138:1149-1157.

Chang, Y.C., H. Zhang, J. Franco-Barraza, M.L. Brennan, T. Patel, E. Cukierman, and J. Wu. 2014. Structural and mechanistic insights into the recruitment of talin by RIAM in integrin signaling. *Structure*. 22:1810-1820.

Chao, W.T., and J. Kunz. 2009. Focal adhesion disassembly requires clathrin-dependent endocytosis of integrins. *FEBS Lett*. 583:1337-1343.

Chen, W., J. Lou, and C. Zhu. 2010. Forcing switch from short- to intermediate- and long-lived states of the alphaA domain generates LFA-1/ICAM-1 catch bonds. *J Biol Chem*. 285:35967-35978.

Chou, J.J., J.L. Baber, and A. Bax. 2004. Characterization of phospholipid mixed micelles by translational diffusion. *J Biomol NMR*. 29:299-308.

Chou, J.J., J.D. Kaufman, S.J. Stahl, P.T. Wingfield, and A. Bax. 2002. Micelle-induced curvature in a water-insoluble HIV-1 Env peptide revealed by NMR dipolar coupling measurement in stretched polyacrylamide gel. *J Am Chem Soc*. 124:2450-2451.

Coll, J.L., A. Ben-Ze'ev, R.M. Ezzell, J.L. Rodriguez Fernandez, H. Baribault, R.G. Oshima, and E.D. Adamson. 1995. Targeted disruption of vinculin genes in F9 and embryonic stem cells changes cell morphology, adhesion, and locomotion. *Proc Natl Acad Sci U S A*. 92:9161-9165.

Conti, F.J., S.J. Monkley, M.R. Wood, D.R. Critchley, and U. Muller. 2009. Talin 1 and 2 are required for myoblast fusion, sarcomere assembly and the maintenance of myotendinous junctions. *Development*. 136:3597-3606.

Cullen, P.J. 2008. Endosomal sorting and signalling: an emerging role for sorting nexins. *Nat Rev Mol Cell Biol*. 9:574-582.

Czuchra, A., H. Meyer, K.R. Legate, C. Brakebusch, and R. Fassler. 2006. Genetic analysis of beta1 integrin "activation motifs" in mice. *J Cell Biol*. 174:889-899.

Darom, A., U. Bening-Abu-Shach, and L. Broday. 2010. RNF-121 is an endoplasmic reticulum-membrane E3 ubiquitin ligase involved in the regulation of beta-integrin. *Mol Biol Cell*. 21:1788-1798.

Das, M., S.S. Ithychanda, J. Qin, and E.F. Plow. 2011. Migfilin and filamin as regulators of integrin activation in endothelial cells and neutrophils. *PLoS One*. 6:e26355.

de Melker, A.A., and A. Sonnenberg. 1999. Integrins: alternative splicing as a mechanism to regulate ligand binding and integrin signaling events. *Bioessays*. 21:499-509.

de Pereda, J.M., K.L. Wegener, E. Santelli, N. Bate, M.H. Ginsberg, D.R. Critchley, I.D. Campbell, and R.C. Liddington. 2005. Structural basis for phosphatidylinositol phosphate kinase type Igamma binding to talin at focal adhesions. *J Biol Chem*. 280:8381-8386.

Debrand, E., Y. El Jai, L. Spence, N. Bate, U. Praekelt, C.A. Pritchard, S.J. Monkley, and D.R. Critchley. 2009. Talin 2 is a large and complex gene encoding multiple transcripts and protein isoforms. *Febs J*. 276:1610-1628.

DeMali, K.A., E. Balciunaite, and A. Kazlauskas. 1999. Integrins enhance platelet-derived growth factor (PDGF)-dependent responses by altering the signal relay enzymes that are recruited to the PDGF beta receptor. *J Biol Chem*. 274:19551-19558.

Dowling, J.J., E. Gibbs, M. Russell, D. Goldman, J. Minarcik, J.A. Golden, and E.L. Feldman. 2008. Kindlin-2 is an essential component of intercalated discs and is required for vertebrate cardiac structure and function. *Circ Res*. 102:423-431.

Dozynkiewicz, M.A., N.B. Jamieson, I. Macpherson, J. Grindlay, P.V. van den Berghe, A. von Thun, J.P. Morton, C. Gourley, P. Timpson, C. Nixon, C.J. McKay, R. Carter, D. Strachan, K. Anderson, O.J. Sansom, P.T. Caswell, and J.C. Norman. 2012. Rab25 and CLIC3 collaborate to promote integrin recycling from late endosomes/lysosomes and drive cancer progression. *Dev Cell*. 22:131-145.

Dubash, A.D., K. Wennerberg, R. Garcia-Mata, M.M. Menold, W.T. Arthur, and K. Burridge. 2007. A novel role for Lsc/p115 RhoGEF and LARG in regulating RhoA activity downstream of adhesion to fibronectin. *J Cell Sci*. 120:3989-3998.

Ehrlicher, A.J., F. Nakamura, J.H. Hartwig, D.A. Weitz, and T.P. Stossel. 2011. Mechanical strain in actin networks regulates FilGAP and integrin binding to filamin A. *Nature*. 478:260-263.

Elliott, P.R., B.T. Goult, P.M. Kopp, N. Bate, J.G. Grossmann, G.C. Roberts, D.R. Critchley, and I.L. Barsukov. 2010. The Structure of the talin head reveals a novel extended conformation of the FERM domain. *Structure*. 18:1289-1299.

Ellis, S.J., E. Lostchuck, B.T. Goult, M. Bouaouina, M.J. Fairchild, P. Lopez-Ceballos, D.A. Calderwood, and G. Tanentzapf. 2014. The talin head domain reinforces integrin-mediated adhesion by promoting adhesion complex stability and clustering. *PLoS Genet*. 10:e1004756.

Ezratty, E.J., C. Bertaux, E.E. Marcantonio, and G.G. Gundersen. 2009. Clathrin mediates integrin endocytosis for focal adhesion disassembly in migrating cells. *J Cell Biol*. 187:733-747.

Fassler, R., M. Pfaff, J. Murphy, A.A. Noegel, S. Johansson, R. Timpl, and R. Albrecht. 1995. Lack of beta 1 integrin gene in embryonic stem cells affects morphology, adhesion, and migration but not integration into the inner cell mass of blastocysts. *J Cell Biol*. 128:979-988.

Flanagan, L.A., J. Chou, H. Falet, R. Neujahr, J.H. Hartwig, and T.P. Stossel. 2001. Filamin A, the Arp2/3 complex, and the morphology and function of cortical actin filaments in human melanoma cells. *J Cell Biol*. 155:511-517.

Fournier, H.N., S. Dupe-Manet, D. Bouvard, M.L. Lacombe, C. Marie, M.R. Block, and C. Albiges-Rizo. 2002. Integrin cytoplasmic domain-associated protein 1alpha (ICAP-1alpha) interacts directly with the metastasis suppressor nm23-H2, and both proteins are targeted to newly formed cell adhesion sites upon integrin engagement. *J Biol Chem*. 277:20895-20902.

Friedland, J.C., M.H. Lee, and D. Boettiger. 2009. Mechanically activated integrin switch controls alpha5beta1 function. *Science*. 323:642-644.

Fukuda, K., K. Bledzka, J. Yang, H.D. Perera, E.F. Plow, and J. Qin. 2014. Molecular basis of kindlin-2 binding to integrin-linked kinase pseudokinase for regulating cell adhesion. *J Biol Chem*. 289:28363-28375.

Gallon, M., and P.J. Cullen. 2015. Retromer and sorting nexins in endosomal sorting. *Biochem Soc Trans*. 43:33-47.

Garavito, R.M., and S. Ferguson-Miller. 2001. Detergents as tools in membrane biochemistry. *J Biol Chem*. 276:32403-32406.

Geiger, B., J.P. Spatz, and A.D. Bershadsky. 2009. Environmental sensing through focal adhesions. *Nat Rev Mol Cell Biol*. 10:21-33.

Geiger, B., and K.M. Yamada. 2011. Molecular architecture and function of matrix adhesions. *Cold Spring Harb Perspect Biol*. 3.

Georges-Labouesse, E., N. Messaddeq, G. Yehia, L. Cadalbert, A. Dierich, and M. Le Meur. 1996. Absence of integrin alpha 6 leads to epidermolysis bullosa and neonatal death in mice. *Nat Genet*. 13:370-373.

Ghai, R., A. Bugarcic, H. Liu, S.J. Norwood, S. Skeldal, E.J. Coulson, S.S. Li, R.D. Teasdale, and B.M. Collins. 2013. Structural basis for endosomal trafficking of diverse transmembrane cargos by PX-FERM proteins. *Proc Natl Acad Sci U S A*. 110:E643-652.

Giancotti, F.G., and E. Ruoslahti. 1999. Integrin signaling. *Science*. 285:1028-1032.

Gimona, M., R. Buccione, S.A. Courtneidge, and S. Linder. 2008. Assembly and biological role of podosomes and invadopodia. *Curr Opin Cell Biol*. 20:235-241.

Gingras, A.R., N. Bate, B.T. Goult, L. Hazelwood, I. Canestrelli, J.G. Grossmann, H. Liu, N.S. Putz, G.C. Roberts, N. Volkmann, D. Hanein, I.L. Barsukov, and D.R. Critchley. 2008. The structure of the C-terminal actin-binding domain of talin. *Embo J*. 27:458-469.

Goksoy, E., Y.Q. Ma, X. Wang, X. Kong, D. Perera, E.F. Plow, and J. Qin. 2008. Structural basis for the autoinhibition of talin in regulating integrin activation. *Mol Cell*. 31:124-133.

Goult, B.T., M. Bouaouina, P.R. Elliott, N. Bate, B. Patel, A.R. Gingras, J.G. Grossmann, G.C. Roberts, D.A. Calderwood, D.R. Critchley, and I.L. Barsukov. 2010. Structure of a double ubiquitin-like domain in the talin head: a role in integrin activation. *Embo J*. 29:1069-1080.

Goult, B.T., M. Bouaouina, D.S. Harburger, N. Bate, B. Patel, N.J. Anthis, I.D. Campbell, D.A. Calderwood, I.L. Barsukov, G.C. Roberts, and D.R. Critchley. 2009. The structure of the N-terminus of kindlin-1: a domain important for alphaiibbeta3 integrin activation. *J Mol Biol*. 394:944-956.

Gu, J., T. Isaji, Y. Sato, Y. Kariya, and T. Fukuda. 2009. Importance of N-glycosylation on alpha5beta1 integrin for its biological functions. *Biol Pharm Bull*. 32:780-785.

Gu, Z., E.H. Noss, V.W. Hsu, and M.B. Brenner. 2011. Integrins traffic rapidly via circular dorsal ruffles and macropinocytosis during stimulated cell migration. *J Cell Biol*. 193:61-70.

Han, J., C.J. Lim, N. Watanabe, A. Soriani, B. Ratnikov, D.A. Calderwood, W. Puzon-McLaughlin, E.M. Lafuente, V.A. Boussiotis, S.J. Shattil, and M.H. Ginsberg. 2006. Reconstructing and deconstructing agonist-induced activation of integrin alphaIIbbeta3. *Curr Biol*. 16:1796-1806.

Hart, R., P. Stanley, P. Chakravarty, and N. Hogg. 2013. The kindlin 3 pleckstrin homology domain has an essential role in lymphocyte function-associated antigen 1 (LFA-1) integrin-mediated B cell adhesion and migration. *J Biol Chem*. 288:14852-14862.

Harunaga, J.S., and K.M. Yamada. 2011. Cell-matrix adhesions in 3D. *Matrix Biol*. 30:363-368.

Haunerland, N.H., and F. Spener. 2004. Fatty acid-binding proteins--insights from genetic manipulations. *Prog Lipid Res*. 43:328-349.

Heino, J., R.A. Ignotz, M.E. Hemler, C. Crouse, and J. Massague. 1989. Regulation of cell adhesion receptors by transforming growth factor-beta. Concomitant regulation of integrins that share a common beta 1 subunit. *J Biol Chem*. 264:380-388.

Hierro, A., A.L. Rojas, R. Rojas, N. Murthy, G. Effantin, A.V. Kajava, A.C. Steven, J.S. Bonifacino, and J.H. Hurley. 2007. Functional architecture of the retromer cargo-recognition complex. *Nature*. 449:1063-1067.

Hodivala-Dilke, K.M., K.P. McHugh, D.A. Tsakiris, H. Rayburn, D. Crowley, M. Ullman-Cullere, F.P. Ross, B.S. Coller, S. Teitelbaum, and R.O. Hynes. 1999. Beta3-integrin-deficient mice are a model for Glanzmann thrombasthenia showing placental defects and reduced survival. *J Clin Invest*. 103:229-238.

Hogg, N., and P.A. Bates. 2000. Genetic analysis of integrin function in man: LAD-1 and other syndromes. *Matrix Biol*. 19:211-222.

Hotchin, N.A., A. Gandarillas, and F.M. Watt. 1995. Regulation of cell surface beta 1 integrin levels during keratinocyte terminal differentiation. *J Cell Biol*. 128:1209-1219.

Howes, M.T., M. Kirkham, J. Riches, K. Cortese, P.J. Walser, F. Simpson, M.M. Hill, A. Jones, R. Lundmark, M.R. Lindsay, D.J. Hernandez-Deviez, G. Hadzic, A. McCluskey, R. Bashir, L. Liu, P. Pilch, H. McMahon, P.J. Robinson, J.F. Hancock, S. Mayor, and R.G. Parton. 2010. Clathrin-independent carriers form a high capacity endocytic sorting system at the leading edge of migrating cells. *J Cell Biol*. 190:675-691.

Huet-Calderwood, C., N.N. Brahme, N. Kumar, A.L. Stiegler, S. Raghavan, T.J. Boggon, and D.A. Calderwood. 2014. Differences in binding to the ILK complex determines kindlin isoform adhesion localization and integrin activation. *J Cell Sci*. 127:4308-4321.

Hughes, P.E., F. Diaz-Gonzalez, L. Leong, C. Wu, J.A. McDonald, S.J. Shattil, and M.H. Ginsberg. 1996. Breaking the integrin hinge. A defined structural constraint regulates integrin signaling. *J Biol Chem*. 271:6571-6574.

Humphries, J.D., A. Byron, and M.J. Humphries. 2006. Integrin ligands at a glance. *J Cell Sci*. 119:3901-3903.

Humphries, J.D., P. Wang, C. Streuli, B. Geiger, M.J. Humphries, and C. Ballestrem. 2007a. Vinculin controls focal adhesion formation by direct interactions with talin and actin. *J Cell Biol*. 179:1043-1057.

Humphries, J.D., P. Wang, C. Streuli, B. Geiger, M.J. Humphries, and C. Ballestrem. 2007b. Vinculin controls focal adhesion formation by direct interactions with talin and actin. *J Cell Biol*. 179:1043-1057.

Humphries, M.J., P.A. McEwan, S.J. Barton, P.A. Buckley, J. Bella, and A.P. Mould. 2003. Integrin structure: heady advances in ligand binding, but activation still makes the knees wobble. *Trends Biochem Sci*. 28:313-320.

Hynes, R.O. 2002. Integrins: bidirectional, allosteric signaling machines. *Cell*. 110:673-687.

Ithychanda, S.S., M. Das, Y.Q. Ma, K. Ding, X. Wang, S. Gupta, C. Wu, E.F. Plow, and J. Qin. 2009. Migfilin, a molecular switch in regulation of integrin activation. *J Biol Chem*. 284:4713-4722.

Jaffe, A.B., and A. Hall. 2005. Rho GTPases: biochemistry and biology. *Annu Rev Cell Dev Biol*. 21:247-269.

Janik, M.E., A. Litynska, and P. Vereecken. 2010. Cell migration-the role of integrin glycosylation. *Biochim Biophys Acta*. 1800:545-555.

Jiang, G., G. Giannone, D.R. Critchley, E. Fukumoto, and M.P. Sheetz. 2003. Two-piconewton slip bond between fibronectin and the cytoskeleton depends on talin. *Nature*. 424:334-337.

Jobard, F., B. Bouadjar, F. Caux, S. Hadj-Rabia, C. Has, F. Matsuda, J. Weissenbach, M. Lathrop, J.F. Prud'homme, and J. Fischer. 2003. Identification of mutations in a new gene encoding a FERM family protein with a pleckstrin homology domain in Kindler syndrome. *Hum Mol Genet*. 12:925-935.

Kanchanawong, P., G. Shtengel, A.M. Pasapera, E.B. Ramko, M.W. Davidson, H.F. Hess, and C.M. Waterman. 2010. Nanoscale architecture of integrin-based cell adhesions. *Nature*. 468:580-584.

Kiema, T., Y. Lad, P. Jiang, C.L. Oxley, M. Baldassarre, K.L. Wegener, I.D. Campbell, J. Ylanne, and D.A. Calderwood. 2006. The molecular basis of filamin binding to integrins and competition with talin. *Mol Cell*. 21:337-347.

Kim, H.J., S.C. Howell, W.D. Van Horn, Y.H. Jeon, and C.R. Sanders. 2009a. Recent Advances in the Application of Solution NMR Spectroscopy to Multi-Span Integral Membrane Proteins. *Prog Nucl Magn Reson Spectrosc*. 55:335-360.

Kim, H.J., S.C. Howell, W.D. Van Horn, Y.H. Jeon, and C.R. Sanders. 2009b. Recent Advances in the Application of Solution NMR Spectroscopy to Multi-Span Integral Membrane Proteins. *Prog Nucl Magn Reson Spectrosc*. 55:335-360.

Kishimoto, T.K., N. Hollander, T.M. Roberts, D.C. Anderson, and T.A. Springer. 1987. Heterogeneous mutations in the beta subunit common to the LFA-1, Mac-1, and p150,95 glycoproteins cause leukocyte adhesion deficiency. *Cell*. 50:193-202.

Kloeker, S., M.B. Major, D.A. Calderwood, M.H. Ginsberg, D.A. Jones, and M.C. Beckerle. 2004. The Kindler syndrome protein is regulated by transforming growth factor-beta and involved in integrin-mediated adhesion. *J Biol Chem*. 279:6824-6833.

Knauth, P., T. Schluter, M. Czubayko, C. Kirsch, V. Florian, S. Schreckenberger, H. Hahn, and R. Bohnensack. 2005. Functions of sorting nexin 17 domains and recognition motif for P-selectin trafficking. *J Mol Biol*. 347:813-825.

Kong, F., A.J. Garcia, A.P. Mould, M.J. Humphries, and C. Zhu. 2009. Demonstration of catch bonds between an integrin and its ligand. *J Cell Biol*. 185:1275-1284.

Kong, F., Z. Li, W.M. Parks, D.W. Dumbauld, A.J. Garcia, A.P. Mould, M.J. Humphries, and C. Zhu. 2013. Cyclic mechanical reinforcement of integrin-ligand interactions. *Mol Cell*. 49:1060-1068.

Kuijpers, T.W., E. van de Vijver, M.A. Weterman, M. de Boer, A.T. Tool, T.K. van den Berg, M. Moser, M.E. Jakobs, K. Seeger, O. Sanal, S. Unal, M. Cetin, D. Roos, A.J. Verhoeven, and F. Baas. 2009. LAD-1/variant syndrome is caused by mutations in FERMT3. *Blood*. 113:4740-4746.

Kuo, J.C., X. Han, C.T. Hsiao, J.R. Yates, 3rd, and C.M. Waterman. 2011. Analysis of the myosin-II-responsive focal adhesion proteome reveals a role for beta-Pix in negative regulation of focal adhesion maturation. *Nat Cell Biol*. 13:383-393.

Kurten, R.C., D.L. Cadena, and G.N. Gill. 1996. Enhanced degradation of EGF receptors by a sorting nexin, SNX1. *Science*. 272:1008-1010.

Lad, Y., P. Jiang, S. Ruskamo, D.S. Harburger, J. Ylanne, I.D. Campbell, and D.A. Calderwood. 2008. Structural basis of the migfilin-filamin interaction and competition with integrin beta tails. *J Biol Chem*. 283:35154-35163.

Lakshminarayan, R., C. Wunder, U. Becken, M.T. Howes, C. Benzing, S. Arumugam, S. Sales, N. Ariotti, V. Chambon, C. Lamaze, D. Loew, A. Shevchenko, K. Gaus, R.G. Parton, and L. Johannes. 2014. Galectin-3 drives glycosphingolipid-dependent biogenesis of clathrin-independent carriers. *Nat Cell Biol*. 16:595-606.

Lau, T.L., V. Dua, and T.S. Ulmer. 2008a. Structure of the integrin alphaIIb transmembrane segment. *J Biol Chem*. 283:16162-16168.

Lau, T.L., C. Kim, M.H. Ginsberg, and T.S. Ulmer. 2009. The structure of the integrin alphaIIbbeta3 transmembrane complex explains integrin transmembrane signalling. *Embo J*. 28:1351-1361.

Lau, T.L., A.W. Partridge, M.H. Ginsberg, and T.S. Ulmer. 2008b. Structure of the integrin beta3 transmembrane segment in phospholipid bicelles and detergent micelles. *Biochemistry*. 47:4008-4016.

Laukaitis, C.M., D.J. Webb, K. Donais, and A.F. Horwitz. 2001. Differential dynamics of alpha 5 integrin, paxillin, and alpha-actinin during formation and disassembly of adhesions in migrating cells. *J Cell Biol*. 153:1427-1440.

Law, D.A., L. Nannizzi-Alaimo, and D.R. Phillips. 1996. Outside-in integrin signal transduction. Alpha IIb beta 3-(GP IIb IIIa) tyrosine phosphorylation induced by platelet aggregation. *J Biol Chem*. 271:10811-10815.

Lawson, C., S.T. Lim, S. Uryu, X.L. Chen, D.A. Calderwood, and D.D. Schlaepfer. 2012. FAK promotes recruitment of talin to nascent adhesions to control cell motility. *J Cell Biol*. 196:223-232.

Lee, H.S., C.J. Lim, W. Puzon-McLaughlin, S.J. Shattil, and M.H. Ginsberg. 2009. RIAM activates integrins by linking talin to ras GTPase membrane-targeting sequences. *J Biol Chem*. 284:5119-5127.

Lefort, C.T., J. Rossaint, M. Moser, B.G. Petrich, A. Zarbock, S.J. Monkley, D.R. Critchley, M.H. Ginsberg, R. Fassler, and K. Ley. 2012. Distinct roles for talin-1 and kindlin-3 in LFA-1 extension and affinity regulation. *Blood*. 119:4275-4282.

Legate, K.R., and R. Fassler. 2009. Mechanisms that regulate adaptor binding to beta-integrin cytoplasmic tails. *J Cell Sci*. 122:187-198.

Legate, K.R., S. Takahashi, N. Bonakdar, B. Fabry, D. Boettiger, R. Zent, and R. Fassler. 2011. Integrin adhesion and force coupling are independently regulated by localized PtdIns(4,5)2 synthesis. *Embo J*. 30:4539-4553.

Leitz, A.J., T.H. Bayburt, A.N. Barnakov, B.A. Springer, and S.G. Sligar. 2006. Functional reconstitution of Beta2-adrenergic receptors utilizing self-assembling Nanodisc technology. *Biotechniques*. 40:601-602, 604, 606, passim.

Leventis, P.A., and S. Grinstein. 2010. The distribution and function of phosphatidylserine in cellular membranes. *Annu Rev Biophys*. 39:407-427.

Ley, K., C. Laudanna, M.I. Cybulsky, and S. Nourshargh. 2007. Getting to the site of inflammation: the leukocyte adhesion cascade updated. *Nat Rev Immunol*. 7:678-689.

Li, J., B.A. Ballif, A.M. Powelka, J. Dai, S.P. Gygi, and V.W. Hsu. 2005. Phosphorylation of ACAP1 by Akt regulates the stimulation-dependent recycling of integrin beta1 to control cell migration. *Dev Cell*. 9:663-673.

Li, R., C.R. Babu, J.D. Lear, A.J. Wand, J.S. Bennett, and W.F. DeGrado. 2001. Oligomerization of the integrin alphaIIbbeta3: roles of the transmembrane and cytoplasmic domains. *Proc Natl Acad Sci U S A*. 98:12462-12467.

Li, R., N. Mitra, H. Gratkowski, G. Vilaire, R. Litvinov, C. Nagasami, J.W. Weisel, J.D. Lear, W.F. DeGrado, and J.S. Bennett. 2003. Activation of integrin alphaIIbbeta3 by modulation of transmembrane helix associations. *Science*. 300:795-798.

Lim, Y., S.T. Lim, A. Tomar, M. Gardel, J.A. Bernard-Trifilo, X.L. Chen, S.A. Uryu, R. Canete-Soler, J. Zhai, H. Lin, W.W. Schlaepfer, P. Nalbant, G. Bokoch, D. Ilic, C. Waterman-Storer, and D.D. Schlaepfer. 2008. PyK2 and FAK connections to p190Rho guanine nucleotide exchange factor regulate RhoA activity, focal adhesion formation, and cell motility. *J Cell Biol*. 180:187-203.

Lipfert, J., L. Columbus, V.B. Chu, S.A. Lesley, and S. Doniach. 2007. Size and shape of detergent micelles determined by small-angle X-ray scattering. *J Phys Chem B*. 111:12427-12438.

Litvinov, R.I., V. Barsegov, A.J. Schissler, A.R. Fisher, J.S. Bennett, J.W. Weisel, and H. Shuman. 2011. Dissociation of bimolecular alphaIIbbeta3-fibrinogen complex under a constant tensile force. *Biophys J*. 100:165-173.

Liu, J., M. Das, J. Yang, S.S. Ithychanda, V.P. Yakubenko, E.F. Plow, and J. Qin. 2015. Structural mechanism of integrin inactivation by filamin. *Nat Struct Mol Biol*.

Liu, J., K. Fukuda, Z. Xu, Y.Q. Ma, J. Hirbawi, X. Mao, C. Wu, E.F. Plow, and J. Qin. 2011. Structural basis of phosphoinositide binding to kindlin-2 protein pleckstrin homology domain in regulating integrin activation. *J Biol Chem*. 286:43334-43342.

Liu, W., K.M. Draheim, R. Zhang, D.A. Calderwood, and T.J. Boggon. 2013. Mechanism for KRIT1 release of ICAP1-mediated suppression of integrin activation. *Mol Cell*. 49:719-729.

Liu, Y., Y. Zhu, S. Ye, and R. Zhang. 2012. Crystal structure of kindlin-2 PH domain reveals a conformational transition for its membrane anchoring and regulation of integrin activation. *Protein Cell*. 3:434-440.

Lobert, V.H., A. Brech, N.M. Pedersen, J. Wesche, A. Oppelt, L. Malerod, and H. Stenmark. 2010. Ubiquitination of alpha 5 beta 1 integrin controls fibroblast migration through lysosomal degradation of fibronectin-integrin complexes. *Dev Cell*. 19:148-159.

Lu, Z., W.D. Van Horn, J. Chen, S. Mathew, R. Zent, and C.R. Sanders. 2012. Bicelles at low concentrations. *Mol Pharm*. 9:752-761.

Luo, B.H., C.V. Carman, J. Takagi, and T.A. Springer. 2005. Disrupting integrin transmembrane domain heterodimerization increases ligand binding affinity, not valency or clustering. *Proc Natl Acad Sci U S A*. 102:3679-3684.

Luo, B.H., T.A. Springer, and J. Takagi. 2004. A specific interface between integrin transmembrane helices and affinity for ligand. *PLoS Biol*. 2:e153.

Ma, Y.Q., J. Qin, C. Wu, and E.F. Plow. 2008. Kindlin-2 (Mig-2): a co-activator of beta3 integrins. *J Cell Biol*. 181:439-446.

Magno, A.L., E. Ingley, S.J. Brown, A.D. Conigrave, T. Ratajczak, and B.K. Ward. 2011. Testin, a novel binding partner of the calcium-sensing receptor, enhances receptor-mediated Rho-kinase signalling. *Biochemical and biophysical research communications*. 412:584-589.

Mai, A., S. Veltel, T. Pellinen, A. Padzik, E. Coffey, V. Marjomaki, and J. Ivaska. 2011. Competitive binding of Rab21 and p120RasGAP to integrins regulates receptor traffic and migration. *J Cell Biol*. 194:291-306.

Malinin, N.L., L. Zhang, J. Choi, A. Ciocea, O. Razorenova, Y.Q. Ma, E.A. Podrez, M. Tosi, D.P. Lennon, A.I. Caplan, S.B. Shurin, E.F. Plow, and T.V. Byzova. 2009. A point mutation in KINDLIN3 ablates activation of three integrin subfamilies in humans. *Nat Med*. 15:313-318.

Margadant, C., H.N. Monsuur, J.C. Norman, and A. Sonnenberg. 2011. Mechanisms of integrin activation and trafficking. *Curr Opin Cell Biol*. 23:607-614.

Martel, V., L. Vignoud, S. Dupe, P. Frachet, M.R. Block, and C. Albiges-Rizo. 2000. Talin controls the exit of the integrin alpha 5 beta 1 from an early compartment of the secretory pathway. *J Cell Sci*. 113 (Pt 11):1951-1961.

Meves, A., C. Stremmel, K. Gottschalk, and R. Fassler. 2009. The Kindlin protein family: new members to the club of focal adhesion proteins. *Trends Cell Biol*. 19:504-513.

Moik, D.V., V.C. Janbandhu, and R. Fassler. 2011. Loss of migfilin expression has no overt consequences on murine development and homeostasis. *J Cell Sci*. 124:414-421.

Monkley, S.J., X.H. Zhou, S.J. Kinston, S.M. Giblett, L. Hemmings, H. Priddle, J.E. Brown, C.A. Pritchard, D.R. Critchley, and R. Fassler. 2000. Disruption of the talin gene arrests mouse development at the gastrulation stage. *Dev Dyn*. 219:560-574.

Montanez, E., S. Ussar, M. Schifferer, M. Bosl, R. Zent, M. Moser, and R. Fassler. 2008. Kindlin-2 controls bidirectional signaling of integrins. *Genes Dev*. 22:1325-1330.

Moore, D.T., P. Nygren, H. Jo, K. Boesze-Battaglia, J.S. Bennett, and W.F. DeGrado. 2012. Affinity of talin-1 for the beta3-integrin cytosolic domain is modulated by its phospholipid bilayer environment. *Proc Natl Acad Sci U S A*. 109:793-798.

Moro, L., M. Venturino, C. Bozzo, L. Silengo, F. Altruda, L. Beguinot, G. Tarone, and P. Defilippi. 1998. Integrins induce activation of EGF receptor: role in MAP kinase induction and adhesion-dependent cell survival. *Embo J*. 17:6622-6632.

Moser, M., M. Bauer, S. Schmid, R. Ruppert, S. Schmidt, M. Sixt, H.V. Wang, M. Sperandio, and R. Fassler. 2009a. Kindlin-3 is required for beta2 integrin-mediated leukocyte adhesion to endothelial cells. *Nat Med*. 15:300-305.

Moser, M., K.R. Legate, R. Zent, and R. Fassler. 2009b. The tail of integrins, talin, and kindlins. *Science*. 324:895-899.

Moser, M., B. Nieswandt, S. Ussar, M. Pozgajova, and R. Fassler. 2008. Kindlin-3 is essential for integrin activation and platelet aggregation. *Nat Med*. 14:325-330.

Muller, P.A., P.T. Caswell, B. Doyle, M.P. Iwanicki, E.H. Tan, S. Karim, N. Lukashchuk, D.A. Gillespie, R.L. Ludwig, P. Gosselin, A. Cromer, J.S. Brugge, O.J. Sansom, J.C. Norman, and K.H. Vousden. 2009. Mutant p53 drives invasion by promoting integrin recycling. *Cell*. 139:1327-1341.

Nevo, J., A. Mai, S. Tuomi, T. Pellinen, O.T. Pentikainen, P. Heikkila, J. Lundin, H. Joensuu, P. Bono, and J. Ivaska. 2010. Mammary-derived growth inhibitor (MDGI) interacts with integrin alpha-subunits and suppresses integrin activity and invasion. *Oncogene*. 29:6452-6463.

Ng, T., D. Shima, A. Squire, P.I. Bastiaens, S. Gschmeissner, M.J. Humphries, and P.J. Parker. 1999. PKCalpha regulates beta1 integrin-dependent cell motility through association and control of integrin traffic. *Embo J*. 18:3909-3923.

Nieswandt, B., M. Moser, I. Pleines, D. Varga-Szabo, S. Monkley, D. Critchley, and R. Fassler. 2007. Loss of talin1 in platelets abrogates integrin activation, platelet aggregation, and thrombus formation in vitro and in vivo. *J Exp Med*. 204:3113-3118.

Nishida, N., C. Xie, M. Shimaoka, Y. Cheng, T. Walz, and T.A. Springer. 2006. Activation of leukocyte beta2 integrins by conversion from bent to extended conformations. *Immunity*. 25:583-594.

Nishimura, T., and K. Kaibuchi. 2007. Numb controls integrin endocytosis for directional cell migration with aPKC and PAR-3. *Dev Cell*. 13:15-28.

Olski, T.M., A.A. Noegel, and E. Korenbaum. 2001. Parvin, a 42 kDa focal adhesion protein, related to the alpha-actinin superfamily. *J Cell Sci*. 114:525-538.

Oxley, C.L., N.J. Anthis, E.D. Lowe, I. Vakonakis, I.D. Campbell, and K.L. Wegener. 2008. An integrin phosphorylation switch: the effect of beta3 integrin tail phosphorylation on Dok1 and talin binding. *J Biol Chem*. 283:5420-5426.

Pankov, R., E. Cukierman, B.Z. Katz, K. Matsumoto, D.C. Lin, S. Lin, C. Hahn, and K.M. Yamada. 2000. Integrin dynamics and matrix assembly: tensin-dependent translocation of alpha(5)beta(1) integrins promotes early fibronectin fibrillogenesis. *J Cell Biol*. 148:1075-1090.

Partridge, A.W., S. Liu, S. Kim, J.U. Bowie, and M.H. Ginsberg. 2005. Transmembrane domain helix packing stabilizes integrin alphaIIbbeta3 in the low affinity state. *J Biol Chem*. 280:7294-7300.

Paszek, M.J., C.C. DuFort, O. Rossier, R. Bainer, J.K. Mouw, K. Godula, J.E. Hudak, J.N. Lakins, A.C. Wijekoon, L. Cassereau, M.G. Rubashkin, M.J. Magbanua, K.S. Thorn, M.W. Davidson, H.S. Rugo, J.W. Park, D.A. Hammer, G. Giannone, C.R. Bertozzi, and V.M. Weaver. 2014. The cancer glycocalyx mechanically primes integrin-mediated growth and survival. *Nature*. 511:319-325.

Pellinen, T., S. Tuomi, A. Arjonen, M. Wolf, H. Edgren, H. Meyer, R. Grosse, T. Kitzing, J.K. Rantala, O. Kallioniemi, R. Fassler, M. Kallio, and J. Ivaska. 2008. Integrin trafficking regulated by Rab21 is necessary for cytokinesis. *Dev Cell*. 15:371-385.

Perera, H.D., Y.Q. Ma, J. Yang, J. Hirbawi, E.F. Plow, and J. Qin. 2011. Membrane binding of the N-terminal ubiquitin-like domain of kindlin-2 is crucial for its regulation of integrin activation. *Structure*. 19:1664-1671.

Petrich, B.G., P. Marchese, Z.M. Ruggeri, S. Spiess, R.A. Weichert, F. Ye, R. Tiedt, R.C. Skoda, S.J. Monkley, D.R. Critchley, and M.H. Ginsberg. 2007. Talin is required for integrin-mediated platelet function in hemostasis and thrombosis. *J Exp Med*. 204:3103-3111.

Plow, E.F., T.A. Haas, L. Zhang, J. Loftus, and J.W. Smith. 2000. Ligand binding to integrins. *J Biol Chem*. 275:21785-21788.

Pouwels, J., N. De Franceschi, P. Rantakari, K. Auvinen, M. Karikoski, E. Mattila, C. Potter, J.P. Sundberg, N. Hogg, C.G. Gahmberg, M. Salmi, and J. Ivaska. 2013. SHARPIN regulates uropod detachment in migrating lymphocytes. *Cell Rep*. 5:619-628.

Prive, G.G. 2007. Detergents for the stabilization and crystallization of membrane proteins. *Methods*. 41:388-397.

Qadota, H., Y. Luo, Y. Matsunaga, A.S. Park, K.M. Gernert, and G.M. Benian. 2014. Suppressor mutations suggest a surface on PAT-4 (Integrin-linked Kinase) that interacts with UNC-112 (Kindlin). *J Biol Chem*. 289:14252-14262.

Qadota, H., D.G. Moerman, and G.M. Benian. 2012. A molecular mechanism for the requirement of PAT-4 (integrin-linked kinase (ILK)) for the localization of UNC-112 (Kindlin) to integrin adhesion sites. *J Biol Chem*. 287:28537-28551.

Rainero, E., J.D. Howe, P.T. Caswell, N.B. Jamieson, K. Anderson, D.R. Critchley, L. Machesky, and J.C. Norman. 2015. Ligand-Occupied Integrin Internalization Links Nutrient Signaling to Invasive Migration. *Cell Rep*.

Rantala, J.K., J. Pouwels, T. Pellinen, S. Veltel, P. Laasola, E. Mattila, C.S. Potter, T. Duffy, J.P. Sundberg, O. Kallioniemi, J.A. Askari, M.J. Humphries, M. Parsons, M. Salmi, and J. Ivaska. 2011. SHARPIN is an endogenous inhibitor of beta1-integrin activation. *Nat Cell Biol*. 13:1315-1324.

Raschle, T., S. Hiller, T.Y. Yu, A.J. Rice, T. Walz, and G. Wagner. 2009. Structural and functional characterization of the integral membrane protein VDAC-1 in lipid bilayer nanodiscs. *J Am Chem Soc*. 131:17777-17779.

Riggs, K.A., N. Hasan, D. Humphrey, C. Raleigh, C. Nevitt, D. Corbin, and C. Hu. 2012. Regulation of integrin endocytic recycling and chemotactic cell migration by syntaxin 6 and VAMP3 interaction. *J Cell Sci*. 125:3827-3839.

Roberts, G.C., and D.R. Critchley. 2009. Structural and biophysical properties of the integrin-associated cytoskeletal protein talin. *Biophys Rev*. 1:61-69.

Roberts, M.S., A.J. Woods, T.C. Dale, P. Van Der Sluijs, and J.C. Norman. 2004. Protein kinase B/Akt acts via glycogen synthase kinase 3 to regulate recycling of alpha v beta 3 and alpha 5 beta 1 integrins. *Mol Cell Biol*. 24:1505-1515.

Roca-Cusachs, P., N.C. Gauthier, A. Del Rio, and M.P. Sheetz. 2009. Clustering of alpha(5)beta(1) integrins determines adhesion strength whereas alpha(v)beta(3) and talin enable mechanotransduction. *Proc Natl Acad Sci U S A*. 106:16245-16250.

Rodriguez Fernandez, J.L., B. Geiger, D. Salomon, I. Sabanay, M. Zoller, and A. Ben-Ze'ev. 1992. Suppression of tumorigenicity in transformed cells after transfection with vinculin cDNA. *J Cell Biol*. 119:427-438.

Rogalski, T.M., G.P. Mullen, M.M. Gilbert, B.D. Williams, and D.G. Moerman. 2000. The UNC-112 gene in Caenorhabditis elegans encodes a novel component of cell-matrix adhesion structures required for integrin localization in the muscle cell membrane. *J Cell Biol*. 150:253-264.

Rognoni, E., M. Widmaier, M. Jakobson, R. Ruppert, S. Ussar, D. Katsougkri, R.T. Bottcher, J.E. Lai-Cheong, D.B. Rifkin, J.A. McGrath, and R. Fassler. 2014. Kindlin-1 controls Wnt and TGF-beta availability to regulate cutaneous stem cell proliferation. *Nat Med*. 20:350-359.

Rosa, J.P., and R.P. McEver. 1989. Processing and assembly of the integrin, glycoprotein IIb-IIIa, in HEL cells. *J Biol Chem*. 264:12596-12603.

Sachs, J.N., and D.M. Engelman. 2006. Introduction to the membrane protein reviews: the interplay of structure, dynamics, and environment in membrane protein function. *Annu Rev Biochem*. 75:707-712.

Sakai, T., R. Jove, R. Fassler, and D.F. Mosher. 2001. Role of the cytoplasmic tyrosines of beta 1A integrins in transformation by v-src. *Proc Natl Acad Sci U S A*. 98:3808-3813.

Salicioni, A.M., A. Gaultier, C. Brownlee, M.K. Cheezum, and S.L. Gonias. 2004. Low density lipoprotein receptor-related protein-1 promotes beta1 integrin maturation and transport to the cell surface. *J Biol Chem*. 279:10005-10012.

Sanders, C.R., 2nd, and G.C. Landis. 1995. Reconstitution of membrane proteins into lipid-rich bilayered mixed micelles for NMR studies. *Biochemistry*. 34:4030-4040.

Sanders, C.R., and J.K. Myers. 2004. Disease-related misassembly of membrane proteins. *Annu Rev Biophys Biomol Struct*. 33:25-51.

Scharffetter-Kochanek, K., H. Lu, K. Norman, N. van Nood, F. Munoz, S. Grabbe, M. McArthur, I. Lorenzo, S. Kaplan, K. Ley, C.W. Smith, C.A. Montgomery, S. Rich, and A.L. Beaudet. 1998. Spontaneous skin ulceration and defective T cell function in CD18 null mice. *J Exp Med*. 188:119-131.

Schiller, H.B., C.C. Friedel, C. Boulegue, and R. Fassler. 2011. Quantitative proteomics of the integrin adhesome show a myosin II-dependent recruitment of LIM domain proteins. *EMBO Rep*. 12:259-266.

Schmidt, S., M. Moser, and M. Sperandio. 2013. The molecular basis of leukocyte recruitment and its deficiencies. *Mol Immunol*. 55:49-58.

Schmitz, G., and M. Grandl. 2009. The molecular mechanisms of HDL and associated vesicular trafficking mechanisms to mediate cellular lipid homeostasis. *Arterioscler Thromb Vasc Biol*. 29:1718-1722.

Schneller, M., K. Vuori, and E. Ruoslahti. 1997. Alphavbeta3 integrin associates with activated insulin and PDGFbeta receptors and potentiates the biological activity of PDGF. *Embo J*. 16:5600-5607.

Seet, L.F., and W. Hong. 2006. The Phox (PX) domain proteins and membrane traffic. *Biochim Biophys Acta*. 1761:878-896.

Seog, D.H., and J. Han. 2008. Sorting Nexin 17 Interacts Directly with Kinesin Superfamily KIF1Bbeta Protein. *The Korean journal of physiology & pharmacology : official journal of the Korean Physiological Society and the Korean Society of Pharmacology*. 12:199-204.

Shattil, S.J., C. Kim, and M.H. Ginsberg. 2010. The final steps of integrin activation: the end game. *Nat Rev Mol Cell Biol*. 11:288-300.

Shenkarev, Z.O., E.N. Lyukmanova, O.I. Solozhenkin, I.E. Gagnidze, O.V. Nekrasova, V.V. Chupin, A.A. Tagaev, Z.A. Yakimenko, T.V. Ovchinnikova, M.P. Kirpichnikov, and A.S. Arseniev. 2009. Lipid-protein nanodiscs: possible application in high-resolution NMR investigations of membrane proteins and membrane-active peptides. *Biochemistry. Biokhimiia*. 74:756-765.

Shi, F., and J. Sottile. 2008. Caveolin-1-dependent beta1 integrin endocytosis is a critical regulator of fibronectin turnover. *J Cell Sci*. 121:2360-2371.

Shi, Q., and D. Boettiger. 2003. A novel mode for integrin-mediated signaling: tethering is required for phosphorylation of FAK Y397. *Mol Biol Cell*. 14:4306-4315.

Shi, X., Y.Q. Ma, Y. Tu, K. Chen, S. Wu, K. Fukuda, J. Qin, E.F. Plow, and C. Wu. 2007. The MIG-2/integrin interaction strengthens cell-matrix adhesion and modulates cell motility. *J Biol Chem*. 282:20455-20466.

Soldi, R., S. Mitola, M. Strasly, P. Defilippi, G. Tarone, and F. Bussolino. 1999. Role of alphavbeta3 integrin in the activation of vascular endothelial growth factor receptor-2. *Embo J*. 18:882-892.

Springer, T.A., J. Zhu, and T. Xiao. 2008. Structural basis for distinctive recognition of fibrinogen gammaC peptide by the platelet integrin alphaIIbbeta3. *J Cell Biol*. 182:791-800.

Steinberg, F., M. Gallon, M. Winfield, E.C. Thomas, A.J. Bell, K.J. Heesom, J.M. Tavare, and P.J. Cullen. 2013. A global analysis of SNX27-retromer assembly

and cargo specificity reveals a function in glucose and metal ion transport. *Nat Cell Biol*. 15:461-471.

Steinberg, F., K.J. Heesom, M.D. Bass, and P.J. Cullen. 2012. SNX17 protects integrins from degradation by sorting between lysosomal and recycling pathways. *J Cell Biol*. 197:219-230.

Stephens, L.E., A.E. Sutherland, I.V. Klimanskaya, A. Andrieux, J. Meneses, R.A. Pedersen, and C.H. Damsky. 1995. Deletion of beta 1 integrins in mice results in inner cell mass failure and peri-implantation lethality. *Genes Dev*. 9:1883-1895.

Stiegler, A.L., R. Zhang, W. Liu, and T.J. Boggon. 2014. Structural determinants for binding of sorting nexin 17 (SNX17) to the cytoplasmic adaptor protein Krev interaction trapped 1 (KRIT1). *J Biol Chem*. 289:25362-25373.

Stockinger, W., B. Sailler, V. Strasser, B. Recheis, D. Fasching, L. Kahr, W.J. Schneider, and J. Nimpf. 2002. The PX-domain protein SNX17 interacts with members of the LDL receptor family and modulates endocytosis of the LDL receptor. *Embo J*. 21:4259-4267.

Struppe, J., J.A. Whiles, and R.R. Vold. 2000. Acidic phospholipid bicelles: a versatile model membrane system. *Biophys J*. 78:281-289.

Svensson, L., K. Howarth, A. McDowall, I. Patzak, R. Evans, S. Ussar, M. Moser, A. Metin, M. Fried, I. Tomlinson, and N. Hogg. 2009. Leukocyte adhesion deficiency-III is caused by mutations in KINDLIN3 affecting integrin activation. *Nat Med*. 15:306-312.

Takagi, J., H.P. Erickson, and T.A. Springer. 2001. C-terminal opening mimics 'inside-out' activation of integrin alpha5beta1. *Nat Struct Biol*. 8:412-416.

Takagi, J., B.M. Petre, T. Walz, and T.A. Springer. 2002. Global conformational rearrangements in integrin extracellular domains in outside-in and inside-out signaling. *Cell*. 110:599-511.

Takizawa, Y., H. Shimizu, T. Nishikawa, N. Hatta, L. Pulkkinen, and J. Uitto. 1997. Novel ITGB4 mutations in a patient with junctional epidermolysis bullosa-pyloric atresia syndrome and altered basement membrane zone immunofluorescence for the alpha6beta4 integrin. *J Invest Dermatol*. 108:943-946.

Tamkun, J.W., D.W. DeSimone, D. Fonda, R.S. Patel, C. Buck, A.F. Horwitz, and R.O. Hynes. 1986. Structure of integrin, a glycoprotein involved in the transmembrane linkage between fibronectin and actin. *Cell*. 46:271-282.

Tate, C.G. 2010. Practical considerations of membrane protein instability during purification and crystallisation. *Methods Mol Biol*. 601:187-203.

Teasdale, R.D., and B.M. Collins. 2012. Insights into the PX (phox-homology) domain and SNX (sorting nexin) protein families: structures, functions and roles in disease. *Biochem J*. 441:39-59.

Teckchandani, A., E.E. Mulkearns, T.W. Randolph, N. Toida, and J.A. Cooper. 2012. The clathrin adaptor Dab2 recruits EH domain scaffold proteins to regulate integrin beta1 endocytosis. *Mol Biol Cell*. 23:2905-2916.

Teckchandani, A., N. Toida, J. Goodchild, C. Henderson, J. Watts, B. Wollscheid, and J.A. Cooper. 2009. Quantitative proteomics identifies a Dab2/integrin module regulating cell migration. *J Cell Biol*. 186:99-111.

Temkin, P., B. Lauffer, S. Jager, P. Cimermancic, N.J. Krogan, and M. von Zastrow. 2011. SNX27 mediates retromer tubule entry and endosome-to-plasma membrane trafficking of signalling receptors. *Nat Cell Biol*. 13:715-721.

ten Klooster, J.P., Z.M. Jaffer, J. Chernoff, and P.L. Hordijk. 2006. Targeting and activation of Rac1 are mediated by the exchange factor beta-Pix. *J Cell Biol*. 172:759-769.

Tiwari, A., J.J. Jung, S.M. Inamdar, C.O. Brown, A. Goel, and A. Choudhury. 2011a. Endothelial cell migration on fibronectin is regulated by syntaxin 6-mediated alpha5beta1 integrin recycling. *J Biol Chem*. 286:36749-36761.

Tiwari, S., J.A. Askari, M.J. Humphries, and N.J. Bulleid. 2011b. Divalent cations regulate the folding and activation status of integrins during their intracellular trafficking. *J Cell Sci*. 124:1672-1680.

Tronik-Le Roux, D., V. Roullot, C. Poujol, T. Kortulewski, P. Nurden, and G. Marguerie. 2000. Thrombasthenic mice generated by replacement of the integrin alpha(IIb) gene: demonstration that transcriptional activation of this megakaryocytic locus precedes lineage commitment. *Blood*. 96:1399-1408.

Tseng, H.Y., N. Thorausch, T. Ziegler, A. Meves, R. Fassler, and R.T. Bottcher. 2014. Sorting nexin 31 binds multiple beta integrin cytoplasmic domains and regulates beta1 integrin surface levels and stability. *J Mol Biol*. 426:3180-3194.

Turner, C.E., J.R. Glenney, Jr., and K. Burridge. 1990. Paxillin: a new vinculin-binding protein present in focal adhesions. *J Cell Biol*. 111:1059-1068.

Ulmer, T.S., B. Yaspan, M.H. Ginsberg, and I.D. Campbell. 2001. NMR analysis of structure and dynamics of the cytosolic tails of integrin alpha IIb beta 3 in aqueous solution. *Biochemistry*. 40:7498-7508.

Ussar, S., M. Moser, M. Widmaier, E. Rognoni, C. Harrer, O. Genzel-Boroviczeny, and R. Fassler. 2008. Loss of Kindlin-1 Causes Skin Atrophy and Lethal Neonatal Intestinal Epithelial Dysfunction. *PLoS Genet*. 4.

Ussar, S., H.V. Wang, S. Linder, R. Fassler, and M. Moser. 2006. The Kindlins: subcellular localization and expression during murine development. *Exp Cell Res*. 312:3142-3151.

Valdembri, D., P.T. Caswell, K.I. Anderson, J.P. Schwarz, I. Konig, E. Astanina, F. Caccavari, J.C. Norman, M.J. Humphries, F. Bussolino, and G. Serini. 2009. Neuropilin-1/GIPC1 signaling regulates alpha5beta1 integrin traffic and function in endothelial cells. *PLoS Biol*. 7:e25.

van der Flier, A., and A. Sonnenberg. 2001. Function and interactions of integrins. *Cell Tissue Res*. 305:285-298.

van der Neut, R., P. Krimpenfort, J. Calafat, C.M. Niessen, and A. Sonnenberg. 1996. Epithelial detachment due to absence of hemidesmosomes in integrin beta 4 null mice. *Nat Genet*. 13:366-369.

van Kerkhof, P., J. Lee, L. McCormick, E. Tetrault, W. Lu, M. Schoenfish, V. Oorschot, G.J. Strous, J. Klumperman, and G. Bu. 2005. Sorting nexin 17 facilitates LRP recycling in the early endosome. *Embo J*. 24:2851-2861.

van Meer, G., D.R. Voelker, and G.W. Feigenson. 2008. Membrane lipids: where they are and how they behave. *Nat Rev Mol Cell Biol*. 9:112-124.

Vidal, F., D. Aberdam, C. Miquel, A.M. Christiano, L. Pulkkinen, J. Uitto, J.P. Ortonne, and G. Meneguzzi. 1995. Integrin beta 4 mutations associated with junctional epidermolysis bullosa with pyloric atresia. *Nat Genet*. 10:229-234.

Vieira, N., F.M. Deng, F.X. Liang, Y. Liao, J. Chang, G. Zhou, W. Zheng, J.P. Simon, M. Ding, X.R. Wu, R. Romih, G. Kreibich, and T.T. Sun. 2014. SNX31: a novel sorting nexin associated with the uroplakin-degrading multivesicular bodies in terminally differentiated urothelial cells. *PLoS One*. 9:e99644.

Vinogradova, O., A. Velyvis, A. Velyviene, B. Hu, T. Haas, E. Plow, and J. Qin. 2002. A structural mechanism of integrin alpha(IIb)beta(3) "inside-out" activation as regulated by its cytoplasmic face. *Cell*. 110:587-597.

Volberg, T., B. Geiger, Z. Kam, R. Pankov, I. Simcha, H. Sabanay, J.L. Coll, E. Adamson, and A. Ben-Ze'ev. 1995. Focal adhesion formation by F9 embryonal carcinoma cells after vinculin gene disruption. *J Cell Sci*. 108 (Pt 6):2253-2260.

Wang, S., T. Watanabe, K. Matsuzawa, A. Katsumi, M. Kakeno, T. Matsui, F. Ye, K. Sato, K. Murase, I. Sugiyama, K. Kimura, A. Mizoguchi, M.H. Ginsberg, J.G. Collard, and K. Kaibuchi. 2012a. Tiam1 interaction with the PAR complex promotes talin-mediated Rac1 activation during polarized cell migration. *J Cell Biol*. 199:331-345.

Wang, X., Y. Zhao, X. Zhang, H. Badie, Y. Zhou, Y. Mu, L.S. Loo, L. Cai, R.C. Thompson, B. Yang, Y. Chen, P.F. Johnson, C. Wu, G. Bu, W.C. Mobley, D. Zhang, F.H. Gage, B. Ranscht, Y.W. Zhang, S.A. Lipton, W. Hong, and H. Xu. 2013. Loss of sorting nexin 27 contributes to excitatory synaptic dysfunction by modulating glutamate receptor recycling in Down's syndrome. *Nat Med*. 19:473-480.

Wang, Z., C.S. Potter, J.P. Sundberg, and H. Hogenesch. 2012b. SHARPIN is a key regulator of immune and inflammatory responses. *J Cell Mol Med*. 16:2271-2279.

Wassmer, T., N. Attar, M. Harterink, J.R. van Weering, C.J. Traer, J. Oakley, B. Goud, D.J. Stephens, P. Verkade, H.C. Korswagen, and P.J. Cullen. 2009. The retromer coat complex coordinates endosomal sorting and dynein-mediated transport, with carrier recognition by the trans-Golgi network. *Dev Cell*. 17:110-122.

Watts, L., and Craig, L 2015. The Role of Talin-1 and Kindlin-3 in Neutrophilic Mac-1 Activation *Faseb J*. 29.

Wegener, K.L., J. Basran, C.R. Bagshaw, I.D. Campbell, G.C. Roberts, D.R. Critchley, and I.L. Barsukov. 2008. Structural basis for the interaction between the cytoplasmic domain of the hyaluronate receptor layilin and the talin F3 subdomain. *J Mol Biol*. 382:112-126.

Wegener, K.L., and I.D. Campbell. 2008. Transmembrane and cytoplasmic domains in integrin activation and protein-protein interactions (review). *Mol Membr Biol*. 25:376-387.

Wegener, K.L., A.W. Partridge, J. Han, A.R. Pickford, R.C. Liddington, M.H. Ginsberg, and I.D. Campbell. 2007. Structural basis of integrin activation by talin. *Cell*. 128:171-182.

Whiles, J.A., R. Deems, R.R. Vold, and E.A. Dennis. 2002. Bicelles in structure-function studies of membrane-associated proteins. *Bioorg Chem*. 30:431-442.

Wickstrom, S.A., and J. Keski-Oja. 2005. [Degradation products of endothelial basement membranes: their role as tumor suppressor]. *Duodecim; laaketieteellinen aikakauskirja*. 121:1829-1837.

Widmaier, M., E. Rognoni, K. Radovanac, S.B. Azimifar, and R. Fassler. 2012. Integrin-linked kinase at a glance. *J Cell Sci*. 125:1839-1843.

Winograd-Katz, S.E., R. Fassler, B. Geiger, and K.R. Legate. 2014. The integrin adhesome: from genes and proteins to human disease. *Nat Rev Mol Cell Biol*. 15:273-288.

Woods, A.J., D.P. White, P.T. Caswell, and J.C. Norman. 2004. PKD1/PKCmu promotes alphavbeta3 integrin recycling and delivery to nascent focal adhesions. *Embo J*. 23:2531-2543.

Wu, H., K. Su, X. Guan, M.E. Sublette, and R.E. Stark. 2010. Assessing the size, stability, and utility of isotropically tumbling bicelle systems for structural biology. *Biochim Biophys Acta*. 1798:482-488.

Xia, W., and T.A. Springer. 2014. Metal ion and ligand binding of integrin alpha5beta1. *Proc Natl Acad Sci U S A*. 111:17863-17868.

Xie, C., J. Zhu, X. Chen, L. Mi, N. Nishida, and T.A. Springer. 2010. Structure of an integrin with an alphaI domain, complement receptor type 4. *Embo J*. 29:666-679.

Xiong, J.P., T. Stehle, B. Diefenbach, R. Zhang, R. Dunker, D.L. Scott, A. Joachimiak, S.L. Goodman, and M.A. Arnaout. 2001. Crystal structure of the extracellular segment of integrin alpha Vbeta3. *Science*. 294:339-345.

Xiong, J.P., T. Stehle, R. Zhang, A. Joachimiak, M. Frech, S.L. Goodman, and M.A. Arnaout. 2002. Crystal structure of the extracellular segment of integrin alpha Vbeta3 in complex with an Arg-Gly-Asp ligand. *Science*. 296:151-155.

Xu, W., J.L. Coll, and E.D. Adamson. 1998. Rescue of the mutant phenotype by reexpression of full-length vinculin in null F9 cells; effects on cell locomotion by domain deleted vinculin. *J Cell Sci*. 111 (Pt 11):1535-1544.

Xu, Y., T.A. Bismar, J. Su, B. Xu, G. Kristiansen, Z. Varga, L. Teng, D.E. Ingber, A. Mammoto, R. Kumar, and M.A. Alaoui-Jamali. 2010. Filamin A regulates focal adhesion disassembly and suppresses breast cancer cell migration and invasion. *J Exp Med*. 207:2421-2437.

Xu, Z., J. Gao, J. Hong, and Y.Q. Ma. 2013. Integrity of kindlin-2 FERM subdomains is required for supporting integrin activation. *Biochemical and biophysical research communications*. 434:382-387.

Yang, J., Y.Q. Ma, R.C. Page, S. Misra, E.F. Plow, and J. Qin. 2009. Structure of an integrin alphaIIb beta3 transmembrane-cytoplasmic heterocomplex provides insight into integrin activation. *Proc Natl Acad Sci U S A*. 106:17729-17734.

Yang, J., L. Zhu, H. Zhang, J. Hirbawi, K. Fukuda, P. Dwivedi, J. Liu, T. Byzova, E.F. Plow, J. Wu, and J. Qin. 2014. Conformational activation of talin by RIAM triggers integrin-mediated cell adhesion. *Nat Commun*. 5:5880.

Yang, J.T., H. Rayburn, and R.O. Hynes. 1993. Embryonic mesodermal defects in alpha 5 integrin-deficient mice. *Development*. 119:1093-1105.

Yang, J.T., H. Rayburn, and R.O. Hynes. 1995. Cell adhesion events mediated by alpha 4 integrins are essential in placental and cardiac development. *Development*. 121:549-560.

Yates, L.A., C.N. Lumb, N.N. Brahme, R. Zalyte, L.E. Bird, L. De Colibus, R.J. Owens, D.A. Calderwood, M.S. Sansom, and R.J. Gilbert. 2012. Structural and functional characterization of the kindlin-1 pleckstrin homology domain. *J Biol Chem*. 287:43246-43261.

Ye, F., G. Hu, D. Taylor, B. Ratnikov, A.A. Bobkov, M.A. McLean, S.G. Sligar, K.A. Taylor, and M.H. Ginsberg. 2010. Recreation of the terminal events in physiological integrin activation. *J Cell Biol*. 188:157-173.

Ye, F., J. Liu, H. Winkler, and K.A. Taylor. 2008. Integrin alpha IIb beta 3 in a membrane environment remains the same height after Mn2+ activation when observed by cryoelectron tomography. *J Mol Biol*. 378:976-986.

Ye, F., B.G. Petrich, P. Anekal, C.T. Lefort, A. Kasirer-Friede, S.J. Shattil, R. Ruppert, M. Moser, R. Fassler, and M.H. Ginsberg. 2013. The mechanism of kindlin-mediated activation of integrin alphaIIbbeta3. *Curr Biol*. 23:2288-2295.

Zaidel-Bar, R., C. Ballestrem, Z. Kam, and B. Geiger. 2003. Early molecular events in the assembly of matrix adhesions at the leading edge of migrating cells. *J Cell Sci*. 116:4605-4613.

Zhang, X., G. Jiang, Y. Cai, S.J. Monkley, D.R. Critchley, and M.P. Sheetz. 2008. Talin depletion reveals independence of initial cell spreading from integrin activation and traction. *Nat Cell Biol*. 10:1062-1068.

Zhu, J., B.H. Luo, P. Barth, J. Schonbrun, D. Baker, and T.A. Springer. 2009. The structure of a receptor with two associating transmembrane domains on the cell surface: integrin alphaIIbbeta3. *Mol Cell*. 34:234-249.

Zhu, J., B.H. Luo, T. Xiao, C. Zhang, N. Nishida, and T.A. Springer. 2008. Structure of a complete integrin ectodomain in a physiologic resting state and activation and deactivation by applied forces. *Mol Cell*. 32:849-861.

Zhu, J., J. Zhu, and T.A. Springer. 2013. Complete integrin headpiece opening in eight steps. *J Cell Biol*. 201:1053-1068.

Zimmerman, G.A. 2009. LAD syndromes: FERMT3 kindles the signal. *Blood*. 113:4485-4486.

Acknowledgement

During the years of my PhD study, I have benefited from the knowledge, support, help and advices of so many excellent people around me in Max-Planck-Institute of Biochemistry. This thesis would not be possible without help and support by all of you. I would like to express my sincere gratitude here:

First of all, I am greatly thankful to my supervisor Prof. Reinhard Fässler for giving me the great opportunity to study the extremely interesting subject in his laboratory. I would like to thank him for all the encouragement and the continuous support throughout the entire period of my study. Importantly, he created such an amazing scientific atmosphere in the lab with many gifted scientists, which inspired us for the excellent research.

Second, I want to thank Prof. Christian Wahl-Schott, who agreed to be the second referee of my thesis as well as Prof. Markus Sperandio, Prof. Martin Biel, Prof. Stefan Zahler, and Prof. Karl-Peter Hopfner for their willingness and time to evaluate my work. I am also grateful to Dr. Thomas Wollert and Prof. Christian Wahl-Schott to be my thesis committee member to discuss and give suggestions to my project all the time.

Third, I am specially, truly thankful to Dr. Ralph Böttcher for his invaluable supervision, endless support and patiently discussing about everything throughout my entire doctoral work. I really learned a lot from him in all respects. I especially have to thank Prof. Roy Zent to always bring up so many good ideas and suggestions in the bicelles project and the excellent collaboration in TRAF6 paper to make it come true. Moreover, to Prof. Ambra Pozzi for nice discussions and suggestions all the time.

Fourth, I have to thank the people in our ‘Böttcher group’: Dr. Ralph Böttcher, Dr. Tilman Ziegler, Dr. Valeria Samaralli, and Hildegard Reiter (Mischa) for not only all the support in all difficult moments in the lab but also great time we have in and out of the lab.

Furthermore, I would also like to thank for my all my former labmates in department of Molecular Medicine, Anika, Korana, Esra, Johannes, Eloi, Sara, Ondrej, Rosi, Moritz, Emanuel, Alex (Meves), Johannes, Kyle, Josie, and so many more people. You really help a lot and cheer me up in the lab all the time. Of course, I have to thank to all the

current labmates. Especially Raphael for the great help for FACS and great time, Sarah and Prof. Karim Dib for the help of the cells, Madis and Maili for the nice discussion and suggestions, Verawan, Marina, Despina, Manndoph, Maik, Patricia, Maria, Gerogina, Zhiqi, Anita, Julien, Franzi, Julia, Markus and Armin for all the great time. Besides, certainly I have to thank Prof. Marc Schmidt-Supprian and his people who are current in TUM, especially Klaus, Yuanyuan, and Valeria S. for the great help in FACS and discussion.

I would also like to thank to Dr. Nagarjuna Nagaraj and Dr. Cyril Boulègue from core facility for the help of Mass spectrometry and data analysis. Dr. Stephan Uebel for the help of the Dynamic Light Scattering experiment. Elisabeth Weyher-Stingl (Lissy) for the great help in LC-MS of my lipid samples.

I also want to thank Dr. Walter Göhring and Klaus Weber for constant technical and administrative support, Ursula Kuhn for help in experiments in the lab. Carmen Schmitz, Ines Lach-Kusevic, and Lidia Wimmer for help with administrative work and also the life in Germany.

Last, I want to thank my family for their continuous support although they more than 9000km away, on the other side of the earth, they are always the strength for me to stand in all these years.

Curriculum Vitae

Personal Data

Full name: Hui-yuan Tseng

Born: in Tainan, Taiwan, on August 6th, 1983

Nationality: Taiwan

Email: huiyuan@biochem.mpg.de

Education:

- **Max Planck Institute of Biochemistry, Department of Molecular Medicine PhD (5/2009-present)**
- **National Taiwan University, Department of Plant Pathology and Microbiology, Taiwan**
  Master degree of science (9/2005 – 6/2007)
  Cell Biology Laboratory (Mentor: Dr. Tang-Long Shen)
  "The interaction between focal adhesion kinase (FAK) and integrin β4 in carcinoma cells."
- **National Taiwan University, Taiwan**
  Bachelor degree of science (9/2001 – 6/2005)
- **National Tainan First Senior High School (9/1998-6/2001)**

Publications:

1. **Hui-yuan Tseng,** Ralph T. Böttcher, Charles R. Sanders, Roy Zent, and Reinhard Fässler. A proteomic approach reveals conformation specific cytoplasmic integrin interactors. (*Manuscript in progress*)
2. Ralph Thomas Böttcher, Christopher Stremmel, Alexander Meves, Hannelore Meyer, Moritz Widmaier, **Hui-Yuan Tseng** and Reinhard Fässler. Sorting nexin 17 prevents lysosomal degradation of β1integrins by binding to the β 1-integrin tail. Nat Cell Biol. 2012 14(6):584-92

3. **Hui-Yuan Tseng**, Niko Thorausch, Tilman Ziegler, Alexander Meves, Reinhard Fässler, and Ralph T. Böttcher. Sorting nexin 31 binds multiple β integrin cytoplasmic domains and regulates β1 integrin surface levels and stability. J Mol Biol. 2014 Sep 9;426(18):3180-94
4. Eugenia M. Yazlovitskaya , **Hui-yuan Tseng**, Olga Viquez, Tianxiang Tu, Glenda Mernaugh, Karen Riggins, Vito Quaranta, Peter Yurchenco, Arnoud Sonnenberg, Ralph T. Böttcher, Ambra Pozzi, Roy Zent. Integrin α3β1 regulates kidney collecting duct development via TRAF6-dependent K63-linked polyubiquitination of Akt. Mol. Biol. Cell May 15, 2015 vol. 26 no. 10 1857-1874
5. Zhiqi Sun, **Hui-Yuan Tseng**, Sally J. Deeb, Dirk Dedden, Maik Veelders, Naoko Mizuno, Matthias Mann, Reinhard Fässler. **Kank family proteins comprise a novel type of talin activator.** (*Manuscript in progress*)

Appendix

In the following, papers I to V are reprinted.

I. **Hui-yuan Tseng,** Ralph T. Böttcher, Charles R. Sanders, Roy Zent, and Reinhard Fässler. **A proteomic approach reveals conformation specific cytoplasmic integrin interactors.** (*Manuscript in progress*)

II. Ralph Thomas Böttcher, Christopher Stremmel, Alexander Meves, Hannelore Meyer, Moritz Widmaier, **Hui-Yuan Tseng** and Reinhard Fässler. **Sorting nexin 17 prevents lysosomal degradation of β1integrins by binding to the β 1-integrin tail.** Nat Cell Biol. 2012 14(6):584-92

III. **Hui-Yuan Tseng**, Niko Thorausch, Tilman Ziegler, Alexander Meves, Reinhard Fässler, and Ralph T. Böttcher. **Sorting nexin 31 binds multiple β integrin cytoplasmic domains and regulates β1 integrin surface levels and stability.** J Mol Biol. 2014 Sep 9;426(18):3180-94

IV. Zhiqi Sun, **Hui-Yuan Tseng**, Sally J. Deeb, Dirk Dedden, Maik Veelders, Naoko Mizuno, Matthias Mann, Reinhard Fässler. **Kank family proteins comprise a novel type of talin activator.** (*Manuscript in progress*)

V. Eugenia M. Yazlovitskaya , **Hui-yuan Tseng**, Olga Viquez, Tianxiang Tu, Glenda Mernaugh, Karen Riggins, Vito Quaranta, Peter Yurchenco, Arnoud Sonnenberg, Ralph T. Böttcher, Ambra Pozzi, Roy Zent. **Integrin α3β1 regulates kidney collecting duct development via TRAF6-dependent K63-linked polyubiquitination of Akt.** Mol. Biol. Cell May 15, 2015 vol. 26 no. 10 1857-1874

A proteomic approach reveals conformation specific cytoplasmic integrin interactors

Hui-yuan Tseng[1], Ralph T. Böttcher[1], Anna V. Samarelli[1], Tilman Ziegler[1], Nagarjuna Nagaraj[1], Charles R. Sanders[2], Roy Zent[3], and Reinhard Fässler[1]

[1]Department of Molecular Medicine, Max Planck Institute for Biochemistry, 82152 Martinsried, Germany

[2] Department of Biochemistry, Center for Structural Biology, and Institute of Chemical Biology, Vanderbilt University School of Medicine, Nashville, Tennessee USA

[3][1] Division of Nephrology and Hypertension, Department of Medicine, Vanderbilt University, Nashville, Tennessee, USA [2] Department of Medicine, Veterans Affairs Hospitals, Nashville, Tennessee, USA

Abstract

Integrins rely on the interaction with cytosolic proteins to induce a conformational shift, which is required for their activation, to initiate intracellular signaling, to establish a connection to the actin cytoskeleton and for their trafficking through the endosomal system. They exist in at least two distinct conformations: a high affinity (‘active’) and a low affinity (‘inactive’) state for ligands. In their inactive state the transmembrane and cytoplasmic (TMcyto) domains of the two integrin subunits are associated while they become separated upon activation. In this study we developed a screening approach for the isolation and identification of cytoplasmic integrin interactors, which combines the expression of conformation-specific integrin TMcyto domains, their incorporation into bicelles as membrane mimicking system, pull-downs and high resolution mass spectrometry. We compared binding proteins of distinct integrin α or β subunits and identified proteins that interacted specifically with associated α/β TMcyto, including L-plastin (LCP1). Knockdown of LCP1 in macrophages increased αMβ2 integrin surface level and led to increased adhesion on fibrinogen and ICAM under non-stimulatory conditions. Our proteomics data offers a global view on cytoplasmic proteins interacting with different integrin classes and provides evidence for the existence and functional relevance of conformation-specific integrin interactors.

Introduction

Integrins are α/β heterodimeric cell surface receptors that function throughout development and adult life to establish cell-cell and cell-extracellular matrix (ECM) interactions and thereby control migration, proliferation, differentiation and survival. α and β integrin subunits are composed of a large extracellular domain, a single transmembrane segment (approx. 25 amino acids) and a short cytoplasmic tail (10-70 amino acids). The consequence of integrin-ligand binding is the assembly of a large protein complex at the short cytoplasmic tails of integrins, which themselves lack enzymatic and actin-binding activity, to initiate signal transduction and to establish a connection to the actin cytoskeleton (Hynes, 2002; Wegener and Campbell, 2008).

Like other cell surface receptors integrins signal in response to ligand binding (outside-in signaling), however they can also regulate their affinity for ligand (also called integrin activation or inside-out signaling). The allosteric affinity switch is characterized by converting the unbound form of integrins from the inactive (low affinity) via an intermediate ligand binding affinity (or primed state) to the ligand-bound (high affinity) state. In their inactive state, the transmembrane and cytoplasmic domains of the two integrin subunits are associated and the extracellular domain is bent. Upon binding of the two adaptor proteins, Talin and Kindlin, to the β integrin cytoplasmic domain, the proximal leg domains, transmembrane domains and cytoplasmic tails of the α and β subunits become unclasped, leading to a "swing-out" of the hybrid domain and full opening of the ligand binding pocket (Campbell and Humphries, 2011; Kim et al., 2011; Shattil et al., 2010). The association of integrin α-β TMcyto subunits in the inactive conformation is stabilized by interaction between GxxxG dimerization motifs in the outer half of the plasma membrane and by hydrophobic and electrostatic bridges together with a salt bridge in the inner half of the plasma membrane (Lau et al., 2009; Yang et al., 2009). Recently, there is growing evidence that integrin inactivation might not be the default state but is actively regulated by the binding of intracellular integrin inactivators, such as Sharpin or Filamin (Bouvard et al., 2013). Integrin inactivators may deactivate integrins or lock integrins in an inactive state thereby establishing a regulatory mechanism to efficiently prevent unwanted integrin activation which is particularly important for cells of hematopoietic origin (Schmidt et al., 2013). Furthermore, interactors of inactive integrins would also allow cells to distinguish between active and inactive integrins in other processes including integrin

biosynthesis and intracellular integrin trafficking, which affect the integrin surface levels and modulate signaling pathways (Bouvard et al., 2013; De Franceschi et al., 2015).

Plastins are a family of three actin-bundling proteins with distinct expression patterns: T-plastin (plastin 3) is broadly expressed, including all cells with replicative potential (Lin et al., 1993), I-plastin (plastin 1) is restricted to intestine and kidney, while L-plastin (plasin 2, LCP1) expression occurs in leukocytes and in many types of malignant human cells of non-hematopoietic origin (Lin et al., 1988). Plastins consist of two aminoterminal EF-hands, implicated in Ca^{2+}-binding, and two tandem actin-binding domains each divided into two calponin homology (CH) domains. Although plastins are primarily involved in regulation of the actin cytoskeleton, they possess additional properties and are involved in several cellular functions such as cell migration, neutrophil function, DNA repair, and endocytosis (Delanote et al., 2005). LCP1 has been linked to integrins, yet the precise mechanism how LCP1 binds integrins and regulates integrin function is unclear. LCP1 has been shown to interact with β integrin subunits (Le Goff et al., 2010) and to activate αMβ2 integrin in polymorphonuclear neutrophils (PMNs) (Jones et al., 1998) and αVβ3 integrins in K562 cells (Wang et al., 2001). In contrast, $LCP1^{-/-}$ neutrophils exhibit no integrin activation defect but fail to mount an efficient integrin adhesion-dependent respiratory burst (Chen et al., 2003).

Since integrin activity, signaling, and trafficking rely on the interaction of proteins with their cytoplasmic tails (Legate and Fassler, 2009) we aimed to identify cytoplasmic integrin interactors by quantitative proteomics. For this, we established a screening assay which combined the generation of conformation-specific integrin tail constructs incorporated into bicelles, pull-downs and high resolution mass spectrometry to isolate and identify novel α and β intgrin tail interacting proteins. We identified LCP1 as interactor of associated integrin TMcyto, and further analyzed its role in the regulation of integrin functions.

Results

Bicelle-incorporation of recombinant integrin bait proteins for pull-down experiments

Due to the short cytoplasmic domains of integrin α and β subunits direct integrin interactors such as Talin, Kindlins and ILK are in close vicinity to plasma membrane and frequently require the plasma membrane interaction to fulfill their function (Anthis et al., 2009; Goult et al., 2010; Goult et al., 2009; Liu et al., 2011; Perera et al., 2011; Widmaier et al., 2012). Previous studies employed two-hybrid or pull-down experiments with either single α or β integrin cytoplasmic domains to identify specific interacting partners (Legate and Fassler, 2009; Morse et al., 2014; Raab et al., 2010). However, these approaches fail to detect binding partners that require interaction with the plasma membrane for integrin binding. We therefore reasoned that the incorporation of recombinant integrin TMcyto into a membrane-mimicking system may strengthen the interaction of binding partners with the integrin tails and support the integrin TMcyto structure. We used bicelles as mimetic membrane model as they form discoidal nanostructures that have been successfully used to study the structure of different integrins by NMR (Lau et al., 2008a; Lau et al., 2009; Lau et al., 2008b; Lu et al., 2012; Surya et al., 2013). The bicelles were composed of the long-chain phospholipid 1,2-dimyristoyl-sn-glycero-3-phosphocholine (DMPC) and 6-cyclohexyl-1-hexylphosphocholine (Cyclofos-6) as short-chain phospholipid that compose flanking rims (Figure 1A). As biological membranes contain negatively charged lipids (Leventis and Grinstein, 2010) we replaced 10% of DMPC with phosphatidylserine (POPS) to provide a negative charge (Figure 1A) and confirmed the correct ratio of the individual phospholipids by LC-MS (Supplemental Figure 1). By changing the ratio of DMPC and Cyclofos-6, referred to as q-value, we obtained bicelles with hydrodynamic radii ranging from 3.16±0.08 nm (q=0.25) to 19.95±0.64 nm (q=4), which was in line with a previous study (Lu et al., 2012; van Dam et al., 2004) (Figure 1B).

In a next step, we determined the incorporation of integrin TMcyto domains into bicelles by Dynamic Light Scattering (DLS) measurements. α5 and β1 integrin TMcyto domains were successfully incorporated into bicelles with a 0.25 q-value however their direct integration into bigger bicelles (q>2; > ~9 nm radius) failed (data not shown). As *in silico* modeling Kindlin Talin recommends a bicelles radius of >8 nm to support membrane interactions of Kindlin and Talin in a complex with β3 integrin (data not shown) we tested the possibility of increasing the radius of small bicelles by incubation with bigger bicelles. Indeed, incubation of q=0.25 bicelles with 5.2 times volume of q=4 bicelles resulted in a homogenous solution of bicelles

with a hydrodynamic radius of 8.88±0.51 nm (q=2*) (Figure 1B and Supplemental Figure 2B). Using this approach we incorporated α5 or β1 integrins TMcyto into q=0.25 bicelles and added 5.2 times volume q=4 bicelles resulting in q=2* bicelles containing our protein of interest with a hydrodynamic radius of ~10 nm (Supplemental Figure 2A, B).

To investigate if the presence of a negatively charged membrane increases the affinity of proteins to integrin cytoplasmic tails, we analyzed the pull-down efficiency of Talin and Kindlin-2, which require plasma membrane interactions for optimal integrin binding (Anthis et al., 2009; Goult et al., 2010; Goult et al., 2009; Liu et al., 2011; Moore et al., 2012; Perera et al., 2011). For this, we used his-tagged TMcyto domains of α5 and β1 integrin either incorporated into bicelles or left without bicelles to pull-down Talin and Kindlin-2 from whole cell lysate. As expected no interaction of the two proteins was detected to α5 integrin TMcyto or empty beads but Western blot analysis revealed that bicelles incorporation increased the interaction of Talin (48%) and Kindlin-2 (38%) with the β1 integrin TMcyto domain (Figure 1C). This indicates that the presence of negatively charged membranes increases the affinity of proteins for the integrin cytoplasmic domains and thereby could promote the identification of novel cytosolic integrin interactors in pull-down assays.

Proteomic analysis of cytoplasmic α and β integrin interactors using bicelle-incorporated TMcyto domains

To identify interacting partners of α and β subunits of different integrin heterodimers and to determine compositional differences between binding proteins associated with different integrins, we determined and compared the interactome of α5, αM and αIIb as well as β1, β2 and β3 integrin cytoplasmic domains using our bicelles pull-down approach (Figure 2). Integrin α and β TMcyto constructs were expressed in and purified from *E. coli* and incorporated into q=0.25 bicelles. The bicelle diameter was increased by incubation with q=4 bicelles before incubation of the integrin TMcyto incorporated bicelles with cell lysates derived from mouse bone marrow derived macrophages (BMDM). To avoid incorporation of transmembrane proteins into bicelles, the BMDM were lysed by hypotonic shock and only the soluble fraction was incubated with the bait proteins. After pull-down, the interacting proteins were resolved by SDS-PAGE and identified by LC-MS/MS.

Proteomic analysis identified about 1000 proteins (Table 1). Label-free quantification demonstrated good reproducibility and consistency between data from replicates (Supplemental Figure 3). 5, 56 and 161 proteins significantly bound to α5, αM, and αIIb

cytoplasmic tails, respectively (Figure 3A, B, C and Table 2). This number is in line with a previous proteomic study comparing interacting proteins of α5 integrin and αIIb integrin in peptide pull-down experiments (Raab et al., 2010). Compared to α integrin subunits, 74, 60 and 111 proteins were identified in β1, β2 and β3 pull-downs, respectively (Figure 3A, B, C and Table 2). Interestingly, no common interactors were identified for all three integrin α cytoplasmic tails while all tested β subunit had 16 common interactors, including Talin and Filamin-A (Figure 3D and Table 2). This is in line with the presence of conserved motives within the β integrin cytoplasmic domains while the α integrin tails are highly divergent (Figure 3E). In summary, these data demonstrate that we have successfully established a bicelle-incorporated integrin TMcyto screening method to identify cytoplasmic integrin interactors.

Identification of conformation-specific αMβ2 integrin interactors

Various proteins bind to α or β cytoplasmic tails to regulate integrin-mediated functions (Legate and Fassler, 2009). Yet, only recently Filamin A was shown to simultaneously bind α and β cytoplasmic tails of inactive associated αIIbβ3 integrin to maintain its inactive state (Liu et al., 2015). Besides their role in integrin inactivation, proteins that specifically interact with inactive integrin might also allow cells to distinguish between active and inactive integrins in other processes such as integrin biosynthesis and intracellular integrin trafficking (De Franceschi et al., 2015). A shortcoming of earlier screening approaches is the use of single α or β integrin cytoplasmic domains which fail to detect interactors that require both integrin tails for binding. We hypothesized that cytoplasmic integrin interactors exist that bind predominantly or exclusively to associated α-β cytoplasmic domains of integrins and therefore we modified our pull-down to identify conformation-specific integrin interactors. To this end we developed a strategy to mimic the heterodimeric integrin cytoplasmic tail conformation in its inactive, associated state based on the Jun-Fos dimerization domains as a ‘velcro‘ to mediate heterodimer formation, which have been used to recombinantly express heterodimeric integrin ectodomains (Eble et al., 1998; Raynal et al., 2006) and related coiled coil domains were used to dimerize the cytoplasmic domains of αIIbβ3 integrin (Pfaff et al., 1998; Ulmer et al., 2001). We chose αMβ2 because previous fluorescence resonance energy transfer (FRET) study has shown that the spatial separation of the αM and β2 subunit cytoplasmic tails activates integrin and transmits signal across plasma membrane (Kim et al., 2003; Lefort et al., 2009). We expressed recombinant proteins consisting an N-terminal tag sequence (His or Flag for purification and pull-down) followed by a Cys-Gly linker, the Jun-Fos dimerization domains, a glycine linker and the αM or β2 integrin TMcyto domains (Figure 4A, B). The cystine bridge

ensures stability, a parallel orientation and a correct stagger of the coiled coil sequences within the dimer, while the glycine linker provides flexibility of the integrin tails. These proteins could be expressed and purified from bacteria (Figure 4B, lanes 2-4) and when incubated together His-Fos-αM and Flag-Jun-β2 formed heterodimers in a one-to-one ratio (Figure 4B, lane 1). Similar to single α and β integrin subunits the incorporation of αMβ2 TMcyto heterodimers into bicelles was measured by DLS. The bicelles size increased from 8.88 nm to 10.05 nm and 10.25 nm after αM or β2 incorporation, while αMβ2 integrin TMcyto incorporation further increased the hydrodynamic radius to 11.17 nm confirming the successful incorporation of the αMβ2 TMcyto heterodimers into bicelles (Figure 4C and Supplementary Figure 2B).

We used the αMβ2 TMcyto domains incorporated into bicelles to pull-down proteins from BMDM lysates as before, identified interacting proteins by LC-MS/MS and compared them to the interactome of single αM and β2 TMcyto domains. Isolated proteins were quantified using the label-free quantification algorithm of the MaxQuant software. 1561 proteins were identified and t-test between β2 and αMβ2 interactors revealed 293 proteins that increase binding to associated αMβ2 integrins (Figure 5A, 5B and Table 3), among them Filamin A as reported previously (Liu et al., 2015). In contrast, 183 proteins only interacted with associated αMβ2 integrin tails and 62 proteins that interact with single αM or β2 integrin tails were lost after heterodimerization of the αMβ2 cytoplasmic domains (Table 4). Together these results indicate that proteins exists that interact predominantly or exclusively with different conformations of αMβ2 integrin.

L-plastin (LCP1) controls αMβ2 integrin surface levels by binding to inactive αMβ2 integrin

We observed a highly specific interaction of the hematopoietic-specific α-actinin family member L-plastin (LCP1) with inactive, associated αMβ2 integrin cytoplasmic domains. LCP1 is an actin-bundling that has been implicated in the formation or maintenance of integrin-associated adhesion structures (Jones et al., 1998; Morley, 2012; Wang et al., 2001). As LCP1 has been shown to interact to the cytoplasmic domain of β1 and β2 integrins (Le Goff et al., 2010) we first validated the stronger interaction with associated αMβ2 integrin tails than single β2 integrin tails in pull-down experiments. As expected from the proteomics data LCP1 was predominantly pulled-down with the Fos-Jun-induced αMβ2 heterodimer in compare with single β2 integrin tail while Talin interacted most efficiently with the single β2 integrin tail (Figure 5C). To demonstrate the interactions of the endogenous proteins, we performed co-

immunoprecipitation experiments of β2 integrin and LCP1 after protein crosslinking (Figure 5D). Importantly, LCP1 was strongly co-immunoprecipitated with β2 integrin in cell lysate from EDTA-treated cells (resting) macrophages while PMA-induced αMβ2 integrin activation reduced LCP1 interaction with αMβ2 integrin (Figure 5D) confirming our mass spectrometry data.

To assess the role of LCP1 for αMβ2 integrin function we depleted LCP1 by short hairpin RNAs (shRNA) retroviral expression in the macrophage cell line Raw 264.7 (Figure 5E) and the differentiated-neutrophils cell line PLB985 (Supplemental Figure 4A). The two independent shRNAs reduced the LCP1 protein levels to ~30% and ~15% in Raw 264.7 and PLB985 cells, respectively (Figure 5E, Supplemental Figure 4A). LCP1 depletion increased surface levels of αMβ2 integrin in both Raw264.7 cells (Figure 5F) and differentiated-PLB985 cells (Supplemental Figure 4B) without significantly changing the levels of active αMβ2 in differentiated-PLB985 cells (Supplemental Figure 4C). Cell surface biotinylation labeling followed by streptavidin pull-down confirmed the upregulation of β2 integrin on the plasma membrane of LCP1 knockdown Raw264.7 cells while unrelated transmembrane proteins such as transferrin receptor were unaffected (Figure 5G). Importantly, re-expression of shRNA-resistant wild type LCP1 restored αMβ2 integrin surface levels in LCP1-depleted cells (Figure 5H, I). Thus, the level of LCP1 determines the amount of αMβ2 integrin presented on the cell surface.

To determine whether LCP1 influences integrin-mediated functions we analyzed cell adhesion of LCP1-depleted Raw264.7 cells to fibrinogen or ICAM. Without prior stimulation, LCP1 depletion leads to stronger adhesion to fibrinogen or ICAM (Figure 6 A, B) suggesting that LCP1 might function to prevent unwanted integrin activation. This difference in adhesion was lost on fibrinogen upon PMA-stimulated integrin activation (Figure 6 A, B). In summary, LCP1 modulates several αMβ2 integrin-mediated functions in leukocytes in part by changing the surface level of αMβ2 integrin.

Discussion

Integrins heavily rely on the recruitment of proteins to their cytoplasmic tails for integrin activation and inactivation, to establish a connection to the actin cytoskeleton, to initiate intracellular signaling and to regulate their intracellular trafficking (Legate and Fassler, 2009; Margadant et al., 2011). Here, we identified and characterized cytosolic proteins that interact

with active integrins as well as inactive, associated integrins using a combination of pull-downs and high resolution mass spectrometry. We determined the interactome of distinct α and β integrin subunits and could show that several integrin interactors have a preference to bind either to the active or inactive integrin conformation.

Integrin contain only short cytoplasmic domains and recruit their intracellular interactors in close proximity or even in directly contact with plasma membrane. Many intracellular integrin interactors, including Talin, Kindlin and ILK, contain membrane binding sites which are important for their ability to bind integrin tails with high affinity (Anthis et al., 2009; Goult et al., 2010; Goult et al., 2009; Liu et al., 2011; Perera et al., 2011; Widmaier et al., 2012). To stabilize such interactions we recombinantly expressed the transmembrane and cytoplasmic domains of several α and β integrin subunits and incorporated them into bicelles as membrane mimicking system. Three artificial membrane systems have been used to study integrin structure which are detergent micelles (Li et al., 2001), nanodiscs (Ye et al., 2010), and bicelles (Lau et al., 2008a; Lau et al., 2009; Lau et al., 2008b; Lu et al., 2012). Detergent micelles became less popular mainly due to the differences of lateral forces and curvature compared to native planar plasma membrane that can affect the protein conformation and even lead to protein unfolding (Lu et al., 2012). In contrast, bicelles and nanodiscs form membranes with planar lipid bilayer features and were successfully used to study integrin structure (Lau et al., 2008a; Lau et al., 2009; Lau et al., 2008b; Lu et al., 2012; Surya et al., 2013) and activation (Ye et al., 2010). Using integrin bait proteins incorporated into bicelles, we identified 5, 56 and 161 proteins that were pulled-down with α5, αM, and αIIb cytoplasmic tails, respectively, and between 60 and 111 proteins with the different β integrin subunits. The number of potential interactors is slightly higher but in the range previous proteomics interaction studies with α or β peptides (Raab et al., 2010; Schiller et al., 2013). The increased interactor number could be the result of our less stringent washing conditions since the bicelles prevented us from washing with detergent containing solutions or the presence of a membrane to facilitate and stabilize potential interactions. Indeed, we could show a stronger interaction of Talin and Kindlin-2 to the β1 TMcyto domain after incorporation of the β1 bait protein into bicelles (Figure 1C). The charged membrane either presents an additional binding motif that adds to the overall affinity or favors optimal alignment of the two interactors for high affinity binding as this has been shown between talin FERM domain and β3 cytoplasmic tail in the present of Negatively charged PtdIns(4,5)P2 (Moore et al., 2012). Despite the different pull-down approaches we observe the similar trend in the number of interactors to the individual α or β cytoplasmic

domains such as only few proteins bind to α5 tails compared to αIIb (Raab et al., 2010) or the higher numbers of β3 integrin interactors compared to β1 integrins (Schiller et al., 2013). A large number of potential interactors differ between our analysis and previously published proteomics studies which in part reflects differences in the approaches (bicelle-incorporated recombinant proteins vs peptides; different washing conditions) and also the use of different cell lysates (platelet and BMDM).

The cell has to distinguish between the inactive integrin conformation with associated α or β transmembrane and cytoplasmic domains and the active conformation characterized by the separation of the α or β TMcyto domains during integrin activation but also for the conformation-specific trafficking of integrins through the endosomal system. Growing evidence suggests that the inactive integrin conformation is not a default state but is dynamically regulated by the binding of intracellular proteins, referred to as integrin inactivators (Bouvard et al., 2013). Intracellular integrin inactivators could inactivate integrins or retain integrins in an inactive state thereby establishing a regulatory mechanism to efficiently prevent unwanted integrin activation. This tight regulation is particularly important for β2 integrins and αIIbβ3 expressed on cells of hematopoietic system to prevent blood clotting or unwanted attachment of leukocytes to the vessel wall with dramatic consequences for the immune functions (Schmidt et al., 2013). Active and inactive integrins are also internalized and trafficked in different pathways (reviewed in (De Franceschi et al., 2015)). Studies using conformation-specific antibodies show that both active and inactive β1 integrins can be internalized to early endosomes and inactive α5β1 integrins predominantly recycle rapidly via the Rab4-dependent loop (Arjonen et al., 2012). In contrast, the ligand bound (active) α5β1 integrins are ubiquitinylated and sorted to lysosomes in the absence of CLIC3 (Dozynkiewicz et al., 2012; Lobert and Stenmark, 2010). Although the underlying molecular mechanisms are still unclear it is suggested that the conformation-specific interaction of cytosolic proteins is crucial for the distinct trafficking events.

To mimic the heterodimeric integrin cytoplasmic tail conformation in its inactive state we developed a pull-down approach based on the Jun-Fos dimerization domains, which have been used to recombinantly express heterodimeric integrin ectodomains (Eble et al., 1998; Raynal et al., 2006). A somewhat unexpected observation was the large number of proteins that were pulled-down with associated αMβ2 TMcyto tails compared to the single subunits. We speculate that due to the low stringency binding and washing conditions we pull-down low affinity binding proteins and complexes as well as unspecific interactors. Among the dimer-specific

interactors are filamin and moesin, which have been shown to inactivate integrins. Filamin has been established as negative regulator of integrin activation by competing with Talin for integrin β tails binding (Das et al., 2011; Ithychanda et al., 2009; Kiema et al., 2006). A recent NMR structure shows that filamin forms ternary complex with both αIIb and β3 cytoplasmic tails rather than only with β integrin cytoplasmic domain, stabilizes the integrin inner membrane clasp and restrains the integrin in a resting state (Liu et al., 2015). Filamin is the first molecule shown to bind to both α and β tail and that also preferentially interacted with associated αMβ2 TMcyto tails in our screen. Mosein a member of ERM protein family (ERMs) is activated upon phosphorylation by MAP4K4 and displaces Talin from integrin β tails leading to integrin inactivation (Baumgartner et al., 2006; Vitorino et al., 2015). Our proteomics data suggest that moesin has binding sites for α and β tails and therefore binds associated αMβ2 integrins. However, further structural and biochemical analyses are necessary to support this hypothesis.

Our proteomic screen identified LCP1 as interactor of associated αMβ2 TMcyto tails. LCP1 is a member of the α-actinin family of actin crosslinking proteins, with a restricted expression pattern in hematopoietic cells and cancer tissue (reviewed in (Delanote et al., 2005; Morley, 2012)). Several members of the α-actinin family of proteins, particularly α-actinin-1 and Filamin or the related plectin, link the actin cytoskeleton to the plasma membrane via interaction with integrins (Garcia-Alvarez et al., 2003; Geerts et al., 1999; Otey et al., 1990; Pavalko and LaRoche, 1993; Sharma et al., 1995). Previous studies have shown that LCP1 binds to the cytoplasmic domains of β integrin via its actin binding domain (Le Goff et al., 2010). However, a structural characterization of how LCP1 engages the complete integrin cytoplasmic face has not been reported. Our pull-down experiments suggest that LCP1 predominantly binds to associated αMβ2 TMcyto tails and exhibits a low affinity for the single αM cytoplasmic domain which increases once αM cytoplasmic domain is in proximity to the β2 tail. A similar increased affinity has been observed for the ternary binding of Filamin A to the cytoplasmic domains of αIIb and β3 integrin (Liu et al., 2015). Site-directed mutagenesis combined with structural studies will provide further insight into the LCP1 binding sites within the αMβ2 integrin tail domains.

We found that depletion of LCP1 increased αMβ2 integrin surface levels on macrophage and differentiated neutrophils cells without changing αMβ2 mRNA levels (data not shown) suggesting a role of LCP1 in the trafficking of inactive αMβ2 integrin. Actin dynamics is important for vesicle biogenesis, and for propelling vesicles and larger endosomal

compartments through the cytoplasm to reach their destination. As a result actin-regulatory proteins, such as LCP1 or actinin, are frequently involved in transmembrane protein trafficking (Burgueno et al., 2003; Foran et al., 2006; Schulz et al., 2004). Serval studies provide evidence for a role of LCP1 in the recycling of transmembrane proteins including the co-localization and direct binding of LCP1 with Rab5, a critical GTPase for the endocytic pathway(Hagiwara et al., 2011). Furthermore, deletion of Sac6P, the yeast LCP homolog, leads to in morphologic disorganization of the actin cytoskeleton and inhibits maltose transporter endocytosis (Adams et al., 1995; Penalver et al., 1997; Skau et al., 2011) and LCP1 participates in E-cadeherin endocytosis in colon cancer cells (Foran et al., 2006). We observed small but significant changes of αMβ2 integrin surface level in LCP1 depletion differentiated neutrophils while the increase in αMβ2 surface level was more profound in macrophage cell lines indicating that the effect of LCP1 on integrin surface levels might be cell type or integrin heterodimer dependent. Indeed, in the LCP1-depleted PMNs β2 integrin surface level did not change (Chen et al., 2003) and β1 integrin levels were unaffected in colon cancer cells after LPC1 knockdown (Foran et al., 2006).

Finally, a remaining question is whether LCP1 is involved in the regulation of integrin inside-out activation. Previous work has implicated LCP1 in the regulation of integrin activation since introduction of peptides containing the N-terminal 19 amino acids LCP1 into cells leads to rapid integrin activation (Jones et al., 1998; Wang et al., 2001). However this is challenged because neutrophils derived from LCP1 knockout mice were defective in generating the respiratory burst but LCP1-deficient neutrophils adhered and spread without significant defects in integrin activation (Chen et al., 2003). A closer look at the adhesion assays in this study showed that LCP1-deficient neutrophils adhered slightly stronger to a polyRGD substrate in the absence of stimulation agents (Chen et al., 2003). Importantly, we also measured increased adhesion to fibrinogen and ICAM in LCP1-depleted macrophages before but not after the activation of integrins by PMA. While this might be due to higher surface integrin αMβ2 level it can also be explained by the inability of macrophages to properly inactivate αMβ2 integrin in the absence of LCP1. Additional work such as the overexpression of LCP1 will be necessary to understand the role of LCP1 in integrin activation.

Taken together, proteomics data from our modified screening approach provide a resource for the global view on cytoplasmic proteins interacting with different integrin subunits and provides evidence for the presence of several conformation-specific integrin interactors.

Material and Methods

Antibodies

The following antibodies were used: Talin (8d4, Sigma; 1: 1000 for WB), Kindlin-2 (MAB2617, Millipore; 1:1000 for WB), His (2365, Cell signaling; 1:1000 for WB), PAK4 (3242, Cell signaling; 1:1000 for WB), Flag-M2-HRP (A8592, Sigma; 1:10000 for WB), GAPDH (CB1001, Calbiochem; 1:2000 for WB), LCP1 (GTX 114524, Genetex; 1:1000 for WB), GFP (A11122, Invitrogen; 1:1000 for WB), β2 integrin (gift from Dr. Melanie Laschinger, IP and 1:200 for WB), activated αM integrin (301402, Biolegend; 1:100 for FACs), αM integrin (301302, Biolegend; 1:100 for FACs), MAC1-PE (12-0112, eBioscience; 1:200 for FACs), MAC1-biotin (557395, PharMingen; 1:200 for FACs). Recombinant Human ICAM-1/CD54 (R & D systems ADP4-200)
The following secondary antibodies were used: streptavidin-Cy5 (016170084; Dianova 1:200 for FACs); streptavidin-Cy5 (016160084; Dianova 1:200 for FACs); goat anti-mouse Alexa546 (A-11003; Life Technologies, 1:200 for FACs), goat anti–mouse Alexa488 (A-11029; Life Technologies, 1:200 for FACs), Donkey anti-mouse-Alexa 647(A-31571, Life Technologies, 1:200 for FACs), goat anti–rat horseradish peroxidase (HRP) (712035150, Dianova; 1:10000 for WB), goat anti–mouse HRP (172-1011; 1:10000 for WB) and goat anti–rabbit HRP (172-1019; 1:10000 for WB) (all from Biorad).

Plasmids

For recombinant bacterial expression, integrin-β1-TMcyto (residues from 719 to 799 of the full length mouse protein), integrin β2-TMCyto (residues from 698 to 771 of the full length mouse protein), β3-TMCyto (residues from 714 to 787 of the full length mouse protein), α5-TMCyto (residues from 993 to 1054 of the full length mouse protein), αIIb-TMCyto (residues from 986 to 1033 of the full length mouse protein), αM-TMCyto (residues from 1106 to 1153 of the full length mouse protein), Fos dimerization domain (residues from161-200 of full length mouse protein), and Jun dimerization domain (residues from277-318 of full length mouse protein) were cloned in frame with the Fos dimerization domain (αIIb, αM, and α5 TMcyto) or Jun dimerization domain (β1, β2, and β3 TMcyto) and subcloned into pET15b vector (Clonetech) to generate His-fos-α5, TMCyto, His-Fos-αIIb TMCyto, His-Fos-αM TMCyto, His-Jun-β1 TMCyto, His-Jun-β2 TMCyto, and His-Jun-β3 TMCyto constructs. The 6xHis tag sequence was replaced with a 3xflag tag within pET16b vector to generate Flag-Jun-β2.

For generate a stable LCP1 knockdown in PLB985 cells, shRNA sequences targeting the human LCP1 sequences were introduced into the pSuper-Retro vector (OligoEngine) to produce retroviral particles: 5'-AGTAGCCTCTCCTGTATTT-3' (shLCP-1), 5'-AGAAGCTGCAGTGGTATTA-3' (shLCP1-2). In Raw 264.7 cells, shRNA target sequences directed against the mouse LCP1 sequences were introduced into the pSuper.Retro vector to produce retroviral particles: 5'-GATGGCATAGTTCTTTGTA-3' (shLCP-1), 5'-CAAGTAGCTTCTGCTATAA-3' (shLCP1-2). LCP1 were PCR from OCAA human library (imaGenes GmbH) clone OCAAo5051D1183D and clone into pJET1.2 cloning vector (Life technologies). LCP1 was cloned into pEGFP-N1 and rrl-cPPT-CMV-eGFP-WPRE lentiviral vector.

Cell culture

Raw 264.7 cells were cultured in DMEM supplemented with 10% (v/v) FBS and PLB985 cells in RPMI supplemented with 10% (v/v) FBS at 37°C and 10% CO_2. Differentiation of PLB985 cells into neutrophils-like cells has been described (Pivot-Pajot et al., 2010). Briefly, PLB985 cell differentiation was induced by incubation in RPMI medium supplemented with 5% (v/v) FBS and 1.25% DMSO for five days. The medium was changed once on day three of the differentiation period.

Bone marrow was isolated from C57BL/6 mice and passed through a 70-µm cell strainer (BD) to obtain single cell suspensions. $4x10^6$ cells were seeded in 15 cm petri dishes (non-treated) and cultivated at 37°C and 5% CO_2 in RPMI medium supplemented with 10% (v/v) FBS and 10% macrophage-colony stimulating factor (M-CSF). Non-adherent cells were removed after 24 h and cultured for additional six days. The cells were lysed in hypotonic lysis buffer (10 mM Tris-HCl pH 7.6, 5 mM KCl, 1.5 mM $MgCl_2$, 1 mM (dithiothreitol) DTT, protease inhibitor cocktail (Roche), phosphatase inhibitor cocktail 2 and 3 (Sigma)) and cleared by centrifugation.

Transient and stable transfection/transduction

Cells were transiently transfected with Lipofectamine 2000 or Lipofectamine LTX (Life technology) according to the manufacturer's protocol. To generate stable cell lines, VSV-G (vesicular stomatitis virus G glycoprotein) pseudotyped retroviral vectors were produced by transient transfection of 293T (human embryonic kidney) cells. Viral particles were

concentrated from cell culture supernatant as previously described (Pfeiffer et al, 2000) and used for infection.

Adhesion assay

For cell adhesion and migration assays, the Raw 264.7 cells were washed and resuspended in FBS-free growth medium. Adhesion assays were performed in 96-well plates coated for 2 hours at room temperature with 10µg/ml fibrinogen (Sigma) or 4µg/ml ICAM (R&D systems). Unspecific binding was blocked by incubating the wells with 1% BSA/PBS, washed once with PBS, and then incubated with the cells ($1x10^5$ cells/well). After indicated time incubation at 37°C, the wells were washed by immersion in a plastic tray containing PBS. Adhered cells were fixed with methanol and stained with crystal violet overnight (20% Methanol, 0.1% Crystal violet in H_2O). After intense washings, cells were solubilized in 0.5% Triton X-100, and the number of cells was determined by measuring the absorbance at 595 nm using an ELISA reader (Schiller et al., 2013).

Bicelles preparation

6-cyclohexyl-1-hexylphosphocholine (Cyclofos-6) was purchased from Anatrace. 1-palmitoyl-2-oleoyl-sn-glycero-3-phospho-L-serine (PS) was purchased from Avanti Polar Lipids 1, 2-Dimyristoyl-sn-Glycero-3-Phosphocholine (DMPC) were purchase from Genezyme pharmaceuticals. Bicelles stock solutions were prepared by weighing out 500 mg of DMPC in 5 mL of cyto buffer (139 mM K2HPO4, 8.8 mM NaH2PO4, 0.4 mM MgCl2, 3.2 mM NaCl, pH 7.0), 200 mg of DMPC in 4 mL of cyto buffer and 75 mg of PS in 3.75 mL of cyto buffer. For 1 mL 3%, q=4 bicelles, 236 µl DMPC stock, 152 µl PS stock, and 68µl Cyclofos-6 stock plus 544 µl cyto buffer were mixed and subjected to a temperature cycle: 45°C for 2 minutes, 5°C (or ice water) for 5 minutes. In-between the solution was carefully mixed to avoid foaming. The temperature cycle was repeated 10 times until solution becomes clear. For 1 mL 3% q=0.25 bicelles, 72 µl DMPC stock, 56 PS stock, and 400 µl Cyclofos-6 stock plus 472 µl of cyto buffer were mixed and incubated as described above. The stocks were snap frozen in liquid Nitrogen and stored at -80°C.

Expression and purification and incorporation recombinant proteins into bicelles.

Plasmids encoding His-Fos-αIIb TMCyto, His-Fos-αIIb TMCyto, His-Fos-αM TMCyto, Flag-Jun-β2 TMCyto, His-Jun-β1 TMCyto, His-Jun-β2 TMCyto, and His-Jun-β3 TMCyto were transformed into BL21(DE3) Arctic Express *Escherichia coli*, and protein expression was induced with 1 mM IPTG (30°C 3 h for α tails and 18°C 24h for β tails). Afterwards, bacteria were pelleted by centrifugation, resuspended in TBS buffer (50 mM Tris pH 7.4, 150 mM NaCl) containing Lysozyme 100µg/ml and DNAse 50 µg/ml and rotated at 4°C for 2 hours. After the addition of Empigen (30% solution) (1 ml per 10 ml of lysate) the bacterial lysates were rotated at 4°C for 1 hour and centrifuged 4000 rpm 4°C for 1 hour. To purify His-tagged proteins supernatants were incubated with Ni-NTA magnetic agarose beads (Qiagen, 36113) and ANTI-FLAG M2 Affinity Gel (Sigma, A2220)hours at 4°C followed by extensive washing of the beads three times with TBS buffer and twice with pre-equilibration buffer (20 mM imidazole, 50 mM, Tris, 150 mM NaCl, pH 6.5 in 1% bicelles, q=0.25, as described (Lu et al., 2012)). The 6xHis tagged proteins were eluted with elution buffer (250 mM imidazole, 50 mM Tris (pH 7.4), 150 mM NaCl in 1% bicelles). The proteins were concentrated using Amicon Ultra Centrifugal filters (10 kDa molecular weight cutoff, Millipore) by a factor of 10 to obtain a final bicelles concentration of 10%.

For pull-down experiments, 9 times volume of cyto buffer (139 mM K2HPO4, 8.8 mM NaH2PO4, 0.4 mM MgCl2, 3.2 mM NaCl, pH 7.0) was added to bring it back to 1% bicelles. To bring the incorporated q=0.25 bicelles into q=2 bicelles, 5.2 x volume of 1%, q=4 bicelles was added. Thereby, integrin TMcyto incorporated q=(0.25+4) bicelles incubated with soluble fraction BMDM lysate isolated by hypotonic buffer (10 mM Tris, 5 mM KCl, 1.5 mM $MgCl_2$, 1 mM DTT, protease inhibitor cocktail (Roche)) overnight at 4°C. Afterwards, the bicelles-lysate mixture was incubated with Ni-NTA magnetic agarose beads for 2 hours at 4°C. After three washes with q=(0.25+4) bicelle solution in cyto buffer, proteins were eluted from the beads by boiling with 80µl laemmli buffer for 5 min, separated by SDS PAGE and analyzed by LCMS/MS or western blotting.

LC-MS to determine lipid composition of bicelles

Bicelles samples (1%) were diluted 1:100 for identification by Liquid chromatography-mass spectrometry (LC-MS) using a Bruker Daltonik micrOTOF connected to an Agilent 1100 HPLC. Analyses were performed on a YMC-Pack Butyl 30 mm column with water: acetonitrile

(0.05% trifluoroacetic acid) gradient from 30%-80% in 15 minute at a mass range from 200-2000 m/z in positive mode. Extracted ion chromatogram at 350.2, 678.5 and 762.5 m/z were used to compare the relative ratio of the individual lipids.

Mass spectrometry analysis of the pull down samples

The samples were eluted from the Ni-NTA magnetic agarose beads using 1X final concentration of laemmli buffer and separated by SDS-PAGE. The gel was fixed with 50% methanol and 10% acetic acid and stained with GelCode Blue Safe Protein Stain reagent (Thermo Scientific). Each sample/lane was cut into three bands and digested by the standard in-gel digestion protocol (Shevchenko et al., 2006). Briefly, the gel bands were cut into roughly 1 mm cubes and de-stained in ethanol solution before incubation with 20 mM dithiothreitol (DTT) and 40 mM chloroacetamide (CAA) sequentially to reduce and alkylate the proteins. The gel pieces were then rehydrated in Trypsin solution (12.5 ng/µl in 50 mM ammonium bicarbonate) incubated overnight at 37˚C. After overnight digestion, the peptides were extracted in 30% acetonitrile and 3% trifluoroacetic acid solution followed by 100% acetonitrile solution. The extracted peptides were then desalted and concentrated using C_{18} StageTips (Rappsilber et al., 2003) prior to LC-MSMS analysis. The peptides were separated by a 120 minute gradient in a 15 cm reversed phase column, 75 µm inner diameter columns (New Objective) packed in-house with 3 µm Reprosil C_{18} beads (Dr Maisch GmbH) using EASY-nLC II (Thermo Scientific) and sprayed directly into a LTQ Orbitrap XL mass spectrometer via nano-electrospray ion source (Thermo scientific).

Peptides were analyzed using a top 5 data dependent acquisition method. Survey scans were acquired in the Orbitrap at resolution of 60,000 (m/z=400) after accumulating a target of 1E6 ions within a maximum injection time of 1000 ms. From the survey scan up to top 5 most abundant precursors were selected and fragmented in the linear ion trap by collisional induced dissociation (CID) with automatic gain control AGC target value of 10000 within a maximum injection time of 150 ms and the fragmentation spectra were recorded in the ion trap. The peptide precursors selected for fragmentation were dynamically excluded for 90 s after a repeat count of 1 in order to minimize the repeat sequencing.

For each set of integrin heterodimer pull downs, the raw files were processed using MaxQuant computational platform (Cox and Mann, 2008) version 1.5.1.8. The peak lists generated were searched against the Mouse Uniprot proteome sequence database (59375 entries) using the Andromeda search engine (Cox et al., 2011). The peptide precursors were searched with an

initial mass tolerance of 7 ppm and the fragment ions were searched with a tolerance of 0.5 Da. Carbamidomethlylation of cysteine was used as a fixed modification and oxidation of methionine and N terminal protein acetylation were set as variable modification for the database search. Minimum peptide length was set to six amino acids and the identification were filtered at 1% for the peptide level and 5% for the protein level and the q value was used for assessing the confidence in the identification of individual proteins (Cox, 2015). Match between the runs feature was enabled and label-free protein quantitation was performed using the MaxLFQ algorithm (Cox et al., 2014).

All statistical analysis were performed using Perseus bioinformatics. Student t-tests were used to compare two samples with permutation based FDR (5%) for multiple hypothesis testing.

Dynamic light scattering

Bicelles samples with different ratios of DMPC, POPS, and Cyclofos-6 were freshly prepared, with or without integrin TMcyto incorporation. The samples were measured by DLS (DynaPro® NanoStar™ from WYATT Technology corp.). Each sample was measured at 4°C, acquisition time was set to 5 seconds for 10 times and in each measurement contained three repeats. All samples were measured in three independent experiments. Hydrodynamic radius was calculated with DYNAMICS V7.1.7.16 (WYATT Technology corp.).

Surface biotinylation

3x 10^6 cells were seeded into 10 cm dishes and incubated overnight at 37°C. After washing 3 times with ice-cold PBS 3mL of Sulfo-NHS-LC-Biotin (0.2mg/mL in PBS, Thermo) was added to each plate and incubated for 60 minutes in the cold room. Cells were wash twice with ice-cold PBS and lysed with 1 mL lysis buffer (50mM Tris-HCl (pH 7.5), 150mM NaCl, 1% Triton X-100, 0.1% sodium deoxycholate, 1mM EDTA and protease inhibitors (Roche)) for 10 minutes on ice. After clearing the lysates by centrifugation, biotinylated proteins were pulled down with streptavidin-Sepharose beads (GE Healthcare) for 3 hours at 4°C. After washes with lysis buffer, samples were analyzed by SDS-PAGE and western blotting.

Immunoprecipitation

For crosslink IP, Raw 264.7 cells were trypsinized and treated with EDTA or PMA (phorbol 12-myristate 13-acetate, Calbiochem 524400) in suspension for 30 mins at 37°C. Cells were

washed with PBS and then incubated with DSP (1mM in PBS) Dithiobis[succinimidyl propionate], Life technology 22585) at room temperature for 30 minutes followed by quenching of non-reacted crosslinker with 50mM Tris for 30 minutes at room temperature. Cells were then washed twice with PBS, lysed in lysis buffer and cleared by centrifugation. β2 integrin antibody was incubated with lysate at 4°C overnight and incubated with protein A/G Sepharose (Santa Cruz sc-2003) for 2 hours at 4°C with gentle agitation. After several washes with lysis buffer, proteins were subjected to SDS-PAGE and western blotting.

Reference

Adams, A.E., W. Shen, C.S. Lin, J. Leavitt, and P. Matsudaira. 1995. Isoform-specific complementation of the yeast sac6 null mutation by human fimbrin. *Mol Cell Biol*. 15:69-75.

Anthis, N.J., K.L. Wegener, F. Ye, C. Kim, B.T. Goult, E.D. Lowe, I. Vakonakis, N. Bate, D.R. Critchley, M.H. Ginsberg, and I.D. Campbell. 2009. The structure of an integrin/talin complex reveals the basis of inside-out signal transduction. *Embo J*. 28:3623-3632.

Arjonen, A., J. Alanko, S. Veltel, and J. Ivaska. 2012. Distinct recycling of active and inactive beta1 integrins. *Traffic*. 13:610-625.

Baumgartner, M., A.L. Sillman, E.M. Blackwood, J. Srivastava, N. Madson, J.W. Schilling, J.H. Wright, and D.L. Barber. 2006. The Nck-interacting kinase phosphorylates ERM proteins for formation of lamellipodium by growth factors. *Proc Natl Acad Sci U S A*. 103:13391-13396.

Bouvard, D., J. Pouwels, N. De Franceschi, and J. Ivaska. 2013. Integrin inactivators: balancing cellular functions in vitro and in vivo. *Nat Rev Mol Cell Biol*. 14:430-442.

Burgueno, J., D.J. Blake, M.A. Benson, C.L. Tinsley, C.T. Esapa, E.I. Canela, P. Penela, J. Mallol, F. Mayor, Jr., C. Lluis, R. Franco, and F. Ciruela. 2003. The adenosine A2A receptor interacts with the actin-binding protein alpha-actinin. *J Biol Chem*. 278:37545-37552.

Campbell, I.D., and M.J. Humphries. 2011. Integrin structure, activation, and interactions. *Cold Spring Harb Perspect Biol*. 3.

Chen, H., A. Mocsai, H. Zhang, R.X. Ding, J.H. Morisaki, M. White, J.M. Rothfork, P. Heiser, E. Colucci-Guyon, C.A. Lowell, H.D. Gresham, P.M. Allen, and E.J. Brown. 2003. Role for plastin in host defense distinguishes integrin signaling from cell adhesion and spreading. *Immunity*. 19:95-104.

Cox, J. 2015. Controlling false discovery rates (FDRs) in genome-wide proteomics datasets. *WOB informatics ASMS conference*.

Cox, J., M.Y. Hein, C.A. Luber, I. Paron, N. Nagaraj, and M. Mann. 2014. Accurate proteome-wide label-free quantification by delayed normalization and maximal peptide ratio extraction, termed MaxLFQ. *Mol Cell Proteomics*. 13:2513-2526.

Cox, J., and M. Mann. 2008. MaxQuant enables high peptide identification rates, individualized p.p.b.-range mass accuracies and proteome-wide protein quantification. *Nature biotechnology*. 26:1367-1372.

Cox, J., N. Neuhauser, A. Michalski, R.A. Scheltema, J.V. Olsen, and M. Mann. 2011. Andromeda: a peptide search engine integrated into the MaxQuant environment. *J Proteome Res*. 10:1794-1805.

Das, M., S.S. Ithychanda, J. Qin, and E.F. Plow. 2011. Migfilin and filamin as regulators of integrin activation in endothelial cells and neutrophils. *PLoS One*. 6:e26355.

De Franceschi, N., H. Hamidi, J. Alanko, P. Sahgal, and J. Ivaska. 2015. Integrin traffic - the update. *J Cell Sci*. 128:839-852.

Delanote, V., J. Vandekerckhove, and J. Gettemans. 2005. Plastins: versatile modulators of actin organization in (patho)physiological cellular processes. *Acta Pharmacol Sin*. 26:769-779.

Dozynkiewicz, M.A., N.B. Jamieson, I. Macpherson, J. Grindlay, P.V. van den Berghe, A. von Thun, J.P. Morton, C. Gourley, P. Timpson, C. Nixon, C.J. McKay, R. Carter, D. Strachan, K. Anderson, O.J. Sansom, P.T. Caswell, and J.C. Norman. 2012. Rab25 and CLIC3 collaborate to promote integrin recycling from late endosomes/lysosomes and drive cancer progression. *Dev Cell*. 22:131-145.

Eble, J.A., K.W. Wucherpfennig, L. Gauthier, P. Dersch, E. Krukonis, R.R. Isberg, and M.E. Hemler. 1998. Recombinant soluble human alpha 3 beta 1 integrin: purification, processing, regulation, and specific binding to laminin-5 and invasin in a mutually exclusive manner. *Biochemistry*. 37:10945-10955.

Foran, E., P. McWilliam, D. Kelleher, D.T. Croke, and A. Long. 2006. The leukocyte protein L-plastin induces proliferation, invasion and loss of E-cadherin expression in colon cancer cells. *Int J Cancer*. 118:2098-2104.

Garcia-Alvarez, B., A. Bobkov, A. Sonnenberg, and J.M. de Pereda. 2003. Structural and functional analysis of the actin binding domain of plectin suggests alternative mechanisms for binding to F-actin and integrin beta4. *Structure*. 11:615-625.

Geerts, D., L. Fontao, M.G. Nievers, R.Q. Schaapveld, P.E. Purkis, G.N. Wheeler, E.B. Lane, I.M. Leigh, and A. Sonnenberg. 1999. Binding of integrin alpha6beta4 to plectin prevents plectin association with F-actin but does not interfere with intermediate filament binding. *J Cell Biol*. 147:417-434.

Goult, B.T., M. Bouaouina, P.R. Elliott, N. Bate, B. Patel, A.R. Gingras, J.G. Grossmann, G.C. Roberts, D.A. Calderwood, D.R. Critchley, and I.L. Barsukov. 2010. Structure of a double ubiquitin-like domain in the talin head: a role in integrin activation. *Embo J*. 29:1069-1080.

Goult, B.T., M. Bouaouina, D.S. Harburger, N. Bate, B. Patel, N.J. Anthis, I.D. Campbell, D.A. Calderwood, I.L. Barsukov, G.C. Roberts, and D.R. Critchley. 2009. The structure of the N-terminus of kindlin-1: a domain important for alphaiibbeta3 integrin activation. *J Mol Biol*. 394:944-956.

Hagiwara, M., H. Shinomiya, M. Kashihara, K. Kobayashi, T. Tadokoro, and Y. Yamamoto. 2011. Interaction of activated Rab5 with actin-bundling proteins, L- and T-plastin and its relevance to endocytic functions in mammalian cells. *Biochemical and biophysical research communications*. 407:615-619.

Hynes, R.O. 2002. Integrins: bidirectional, allosteric signaling machines. *Cell*. 110:673-687.

Ithychanda, S.S., M. Das, Y.Q. Ma, K. Ding, X. Wang, S. Gupta, C. Wu, E.F. Plow, and J. Qin. 2009. Migfilin, a molecular switch in regulation of integrin activation. *J Biol Chem*. 284:4713-4722.

Jones, S.L., J. Wang, C.W. Turck, and E.J. Brown. 1998. A role for the actin-bundling protein L-plastin in the regulation of leukocyte integrin function. *Proc Natl Acad Sci U S A*. 95:9331-9336.

Kiema, T., Y. Lad, P. Jiang, C.L. Oxley, M. Baldassarre, K.L. Wegener, I.D. Campbell, J. Ylanne, and D.A. Calderwood. 2006. The molecular basis of filamin binding to integrins and competition with talin. *Mol Cell*. 21:337-347.

Kim, C., F. Ye, and M.H. Ginsberg. 2011. Regulation of integrin activation. *Annu Rev Cell Dev Biol*. 27:321-345.

Kim, M., C.V. Carman, and T.A. Springer. 2003. Bidirectional transmembrane signaling by cytoplasmic domain separation in integrins. *Science*. 301:1720-1725.

Lau, T.L., V. Dua, and T.S. Ulmer. 2008a. Structure of the integrin alphaIIb transmembrane segment. *J Biol Chem*. 283:16162-16168.

Lau, T.L., C. Kim, M.H. Ginsberg, and T.S. Ulmer. 2009. The structure of the integrin alphaIIbbeta3 transmembrane complex explains integrin transmembrane signalling. *Embo J*. 28:1351-1361.

Lau, T.L., A.W. Partridge, M.H. Ginsberg, and T.S. Ulmer. 2008b. Structure of the integrin beta3 transmembrane segment in phospholipid bicelles and detergent micelles. *Biochemistry*. 47:4008-4016.

Le Goff, E., A. Vallentin, P.O. Harmand, G. Aldrian-Herrada, B. Rebiere, C. Roy, Y. Benyamin, and M.C. Lebart. 2010. Characterization of L-plastin interaction with beta integrin and its regulation by micro-calpain. *Cytoskeleton*. 67:286-296.

Lefort, C.T., Y.M. Hyun, J.B. Schultz, F.Y. Law, R.E. Waugh, P.A. Knauf, and M. Kim. 2009. Outside-in signal transmission by conformational changes in integrin Mac-1. *J Immunol*. 183:6460-6468.

Legate, K.R., and R. Fassler. 2009. Mechanisms that regulate adaptor binding to beta-integrin cytoplasmic tails. *J Cell Sci*. 122:187-198.

Leventis, P.A., and S. Grinstein. 2010. The distribution and function of phosphatidylserine in cellular membranes. *Annu Rev Biophys*. 39:407-427.

Li, R., C.R. Babu, J.D. Lear, A.J. Wand, J.S. Bennett, and W.F. DeGrado. 2001. Oligomerization of the integrin alphaIIbbeta3: roles of the transmembrane and cytoplasmic domains. *Proc Natl Acad Sci U S A*. 98:12462-12467.

Lin, C.S., T. Park, Z.P. Chen, and J. Leavitt. 1993. Human plastin genes. Comparative gene structure, chromosome location, and differential expression in normal and neoplastic cells. *J Biol Chem*. 268:2781-2792.

Liu, J., M. Das, J. Yang, S.S. Ithychanda, V.P. Yakubenko, E.F. Plow, and J. Qin. 2015. Structural mechanism of integrin inactivation by filamin. *Nat Struct Mol Biol*.

Liu, J., K. Fukuda, Z. Xu, Y.Q. Ma, J. Hirbawi, X. Mao, C. Wu, E.F. Plow, and J. Qin. 2011. Structural basis of phosphoinositide binding to kindlin-2 protein pleckstrin homology domain in regulating integrin activation. *J Biol Chem*. 286:43334-43342.

Lobert, V.H., and H. Stenmark. 2010. Ubiquitination of alpha-integrin cytoplasmic tails. *Commun Integr Biol*. 3:583-585.

Lu, Z., W.D. Van Horn, J. Chen, S. Mathew, R. Zent, and C.R. Sanders. 2012. Bicelles at low concentrations. *Mol Pharm*. 9:752-761.

Margadant, C., H.N. Monsuur, J.C. Norman, and A. Sonnenberg. 2011. Mechanisms of integrin activation and trafficking. *Curr Opin Cell Biol*. 23:607-614.

Moore, D.T., P. Nygren, H. Jo, K. Boesze-Battaglia, J.S. Bennett, and W.F. DeGrado. 2012. Affinity of talin-1 for the beta3-integrin cytosolic domain is modulated by its phospholipid bilayer environment. *Proc Natl Acad Sci U S A*. 109:793-798.

Morley, S.C. 2012. The actin-bundling protein L-plastin: a critical regulator of immune cell function. *Int J Cell Biol*. 2012:935173.

Morse, E.M., N.N. Brahme, and D.A. Calderwood. 2014. Integrin cytoplasmic tail interactions. *Biochemistry*. 53:810-820.

Otey, C.A., F.M. Pavalko, and K. Burridge. 1990. An interaction between alpha-actinin and the beta 1 integrin subunit in vitro. *J Cell Biol*. 111:721-729.

Pavalko, F.M., and S.M. LaRoche. 1993. Activation of human neutrophils induces an interaction between the integrin beta 2-subunit (CD18) and the actin binding protein alpha-actinin. *J Immunol*. 151:3795-3807.

Penalver, E., L. Ojeda, E. Moreno, and R. Lagunas. 1997. Role of the cytoskeleton in endocytosis of the yeast maltose transporter. *Yeast*. 13:541-549.

Perera, H.D., Y.Q. Ma, J. Yang, J. Hirbawi, E.F. Plow, and J. Qin. 2011. Membrane binding of the N-terminal ubiquitin-like domain of kindlin-2 is crucial for its regulation of integrin activation. *Structure*. 19:1664-1671.

Pfaff, M., S. Liu, D.J. Erle, and M.H. Ginsberg. 1998. Integrin beta cytoplasmic domains differentially bind to cytoskeletal proteins. *J Biol Chem*. 273:6104-6109.

Pivot-Pajot, C., F.C. Chouinard, M.A. El Azreq, D. Harbour, and S.G. Bourgoin. 2010. Characterisation of degranulation and phagocytic capacity of a human neutrophilic cellular model, PLB-985 cells. *Immunobiology*. 215:38-52.

Raab, M., H. Daxecker, R.J. Edwards, A. Treumann, D. Murphy, and N. Moran. 2010. Protein interactions with the platelet integrin alpha(IIb) regulatory motif. *Proteomics*. 10:2790-2800.

Rappsilber, J., Y. Ishihama, and M. Mann. 2003. Stop and go extraction tips for matrix-assisted laser desorption/ionization, nanoelectrospray, and LC/MS sample pretreatment in proteomics. *Anal Chem*. 75:663-670.

Raynal, N., S.W. Hamaia, P.R. Siljander, B. Maddox, A.R. Peachey, R. Fernandez, L.J. Foley, D.A. Slatter, G.E. Jarvis, and R.W. Farndale. 2006. Use of synthetic peptides to locate novel integrin alpha2beta1-binding motifs in human collagen III. *J Biol Chem*. 281:3821-3831.

Schiller, H.B., M.R. Hermann, J. Polleux, T. Vignaud, S. Zanivan, C.C. Friedel, Z. Sun, A. Raducanu, K.E. Gottschalk, M. Thery, M. Mann, and R. Fassler. 2013. beta1- and alphav-class integrins cooperate to regulate myosin II during rigidity sensing of fibronectin-based microenvironments. *Nat Cell Biol*. 15:625-636.

Schmidt, S., M. Moser, and M. Sperandio. 2013. The molecular basis of leukocyte recruitment and its deficiencies. *Mol Immunol*. 55:49-58.

Schulz, T.W., T. Nakagawa, P. Licznerski, V. Pawlak, A. Kolleker, A. Rozov, J. Kim, T. Dittgen, G. Kohr, M. Sheng, P.H. Seeburg, and P. Osten. 2004. Actin/alpha-actinin-dependent transport of AMPA receptors in dendritic spines: role of the PDZ-LIM protein RIL. *The Journal of neuroscience : the official journal of the Society for Neuroscience*. 24:8584-8594.

Sharma, C.P., R.M. Ezzell, and M.A. Arnaout. 1995. Direct interaction of filamin (ABP-280) with the beta 2-integrin subunit CD18. *J Immunol*. 154:3461-3470.

Shattil, S.J., C. Kim, and M.H. Ginsberg. 2010. The final steps of integrin activation: the end game. *Nat Rev Mol Cell Biol*. 11:288-300.

Shevchenko, A., H. Tomas, J. Havlis, J.V. Olsen, and M. Mann. 2006. In-gel digestion for mass spectrometric characterization of proteins and proteomes. *Nat Protoc*. 1:2856-2860.

Skau, C.T., D.S. Courson, A.J. Bestul, J.D. Winkelman, R.S. Rock, V. Sirotkin, and D.R. Kovar. 2011. Actin filament bundling by fimbrin is important for endocytosis, cytokinesis, and polarization in fission yeast. *J Biol Chem*. 286:26964-26977.

Surya, W., Y. Li, O. Millet, T. Diercks, and J. Torres. 2013. Transmembrane and Juxtamembrane Structure of alphaL Integrin in Bicelles. *PLoS One*. 8:e74281.

Ulmer, T.S., B. Yaspan, M.H. Ginsberg, and I.D. Campbell. 2001. NMR analysis of structure and dynamics of the cytosolic tails of integrin alpha IIb beta 3 in aqueous solution. *Biochemistry*. 40:7498-7508.

van Dam, L., G. Karlsson, and K. Edwards. 2004. Direct observation and characterization of DMPC/DHPC aggregates under conditions relevant for biological solution NMR. *Biochim Biophys Acta*. 1664:241-256.

Vitorino, P., S. Yeung, A. Crow, J. Bakke, T. Smyczek, K. West, E. McNamara, J. Eastham-Anderson, S. Gould, S.F. Harris, C. Ndubaku, and W. Ye. 2015. MAP4K4 regulates integrin-FERM binding to control endothelial cell motility. *Nature*. 519:425-430.

Wang, J., H. Chen, and E.J. Brown. 2001. L-plastin peptide activation of alpha(v)beta(3)-mediated adhesion requires integrin conformational change and actin filament disassembly. *J Biol Chem*. 276:14474-14481.

Wegener, K.L., and I.D. Campbell. 2008. Transmembrane and cytoplasmic domains in integrin activation and protein-protein interactions (review). *Mol Membr Biol*. 25:376-387.

Widmaier, M., E. Rognoni, K. Radovanac, S.B. Azimifar, and R. Fassler. 2012. Integrin-linked kinase at a glance. *J Cell Sci*. 125:1839-1843.

Yang, J., Y.Q. Ma, R.C. Page, S. Misra, E.F. Plow, and J. Qin. 2009. Structure of an integrin alphaIIb beta3 transmembrane-cytoplasmic heterocomplex provides insight into integrin activation. *Proc Natl Acad Sci U S A*. 106:17729-17734.

Ye, F., G. Hu, D. Taylor, B. Ratnikov, A.A. Bobkov, M.A. McLean, S.G. Sligar, K.A. Taylor, and M.H. Ginsberg. 2010. Recreation of the terminal events in physiological integrin activation. *J Cell Biol*. 188:157-173.

Figure legends

Figure 1 Integrin transmembrane-cytoplasmic (TMcyto) tail incorporated into bicelles. **(A)** The chemical structures of selected phospholipids used and cartoons of the lipid distribution within bicelles are shown. **(B)** Translational hydrodynamic radius (nm) represented the size of different bicelles (q=0.25: 3.53±0.16nm; q=4: 19.93±0.16nm; q=2*: 8.44±0.72nm, mean±s.e.m., *n*=3) measured by dynamic light scattering (DLS). **(C)** Western blot analysis of pull-downs with recombinant His-tagged integrin TMcyto-α5 or -β1 proteins with or without bicelle incorporation with antibodies against Talin and Kindlin-2. Western blots were quantified by Image J (mean±s.e.m., *n*=3, * $P < 0.05$,).

Figure 2 Workflow for the bicelle incorporation of recombinant integrin TMcyto proteins followed by pull-down and proteomic analysis. Purified heterodimeric or monomeric integrin TMcyto were immobilized to Ni-NTA beads, and incorporated into bicelles solution (q=0.25). The bicelles size was increased by adding 5.2 times volume of q=4 bicelles followed by the pull-down of proteins from with hypotonic BMDM lysate. Interactors were identified by LC-MS/MS and analyzed by MaxQuant LFQ based intensity.

Figure 3 Interactome analysis of single α and β integrin subunits. **(A, B)** Number of proteins binding significantly to α **(A)** and β tails **(B)**. **(C)** Volcano plots of t-test difference vs p value; statistically significant interactors are labelled in red. **(D)** Overlap of proteins identified with the different α and β tails subunits illustrated as a Venn diagram. **(E)** Alignment of mouse integrin α and β TMcyto segments used in pull-down experiment.

Figure 4 Integrin TMcyto constructs used to mimic the associated integrin conformation. **(A)** Schematic representation of the integrin TMcyto constructs used. CG (Cysteine-Glycine) stabilize the dimer formation; GGGG (Glycine-Glycine-Glycine-Glycine) increase the flexibility of the integrin TMcyto. **(B)** Recombinant His-FosαM, His-Junβ2, and Flag-Junβ2 were expressed and purified with Ni-NTA or flag-M2 beads as monomer (lane 2, 3, 4). His-FosαM and Flag-Junβ2 were co-incubated and purified by Ni-NTA. Note, His-FosαIIb pulled-

down Flag-Junβ2 indicating heterodimer formation in the optimal one-to-one ratio (lane 1). **(C)** Hydrodynamic radii of the indicated bicelles determined by DLS. Note the size differences of q=0.25, q=4, q=2* bicelles and the size increase after integrin TMcyto incorporation (mean±s.e.m. *n*=3).

Figure 5 LCP1 interacted with inactive αMβ2 integrins to regulate integrin-mediated functions. **(A)** Volcano plot showing P values (-log10) versus protein ratio (log2 fold change) of αM vs αMβ2 interacting proteins. Proteins with significantly increased binding to either αM or αMβ2 are labelled in red. **(B)** Number of identified proteins which bind to dimeric αMβ2, only bind to dimeric αMβ2, and do not interact with αMβ2 TMcyto tail proteins. **(C)** Western blot analysis of proteins pulled-down with either single αM and β2 integrin TMcyto or associated αMβ2 TMcyto proteins embedded in bicells. **(D)** β2 immunoprecipitation from Raw 264.7 cells treated with EDTA (resting state) or PMA (activated state) after protein crosslinking. Immunoprecipitated proteins were analyzed by western blotting with antibodies against integrin β2 and LCP1. Note the reduced LCP1 binding to β2 integrin when integrins were activated with PMA. **(E)** Western blot analysis of control (shCtr) or two shLCP1-infected (shLCP1-1 and shLCP1-2) Raw 264.7 cells. **(F, G)** Mac1 (αMβ2 integrin) surface expression level was analyzed by FACS **(F)** or by surface biotinylation and pull-down of biotinylated proteins with streptavidin agarose beads **(G)** (mean±s.e.m., *n*=3, * $P < 0.05$). **(H)** Western blot analysis of cell lysates derived from shCtrl or LCP1-depleted PLB-985 cells. LCP1 levels were restored in the LCP1-depleted cell lines (shLCP1-1, shLCP1-2) by re-expressing shRNA-resistent LCP1-GFP or GFP alone. **(I)** αMβ2 integrin surface levels in the indicated LCP1-depleted and rescued differentiated- PLB-985 cell lines determined by FACS (mean±s.e.m., *n*=2, n.s. not significant, * $P < 0.05$, ** $P < 0.01$).

Figure 6 LCP1 depletion cells increased adhesion on fibrinogen and ICAM. **(A, B)** Increased adhesion of LCP1-depleted Raw264.7 cells on fibrinogen (A) (10µg/ml) and ICAM (B) (4µg/ml). Cells were seeded for 30 minutes without or with PMA treatment and the number of adherent cells was determined by crystal violet staining. Relative values compared to control cells (shCtr) are shown (mean±s.e.m., *n*=3, * $P < 0.05$, n.s. not significant).

Supplementary figure legends

Figure S1 Bicelles characterization by LC-MS. (A, B) The relative molar ratio of lipids and detergent in q=0.25 **(A)**, q=4 **(B)** bicelles was determined by LC-MS. Cyclofos-6 (blue), POPS (green), DMPC (red).

Figure S2 DLS measurements of bicelles samples. (A) Hydrodynamic radii of bicelles after incorporation of the indicated integrin α and β subunits determined by DLS. **(B)** DLS measurement curves.

Figure S3 Reproducibility of LC MSMS pull down data. Multi-scatter plot of the protein LFQ intensities showing the reproducibility within the triplicate measurements of different pulldowns. The indicated values correspond to Pearson correlation.

Figure S4 LCP1 depletion in PLB985 cells. **(A)** shRNA-mediated knock-down of LCP1 in differentiated and undifferentiated PLB985 cells. Cell lysates were analyzed by Western blot with antibodies against LCP1 and GAPDH. Cells were infected with shCtrl or two different LCP1 targeted shRNA (shLCP1-1 and shLCP1-2). **(B, C)** FACS analysis of LCP1-depleted or control infected, differentiation PLB985 cells for αMβ2 surface expression level **(B)** and activated αMβ2 levels **(C)**. The bar graph shows mean±s.e.m. (n=3, * $P < 0.05$, ** $P < 0.01$ n.s. not significant).

Table1: List of all identified proteins (α5 β1 αIIb β3 αM β2)

Table2: List of proteins significantly binding to α or β tails. Overlap of proteins significantly binding to α or β tail across the three different combinations (α5 vs β1; αIIb vs β3; αM vs β2)

Table3: List of proteins selectively binding to αMβ2 vs β2 tail

Table4: Proteins identified at least in 1 replicates of each α or β and αMβ2 indicating proteins identified exclusively in each α, β or in the αMβ2 heterodimer

Figure 1

A

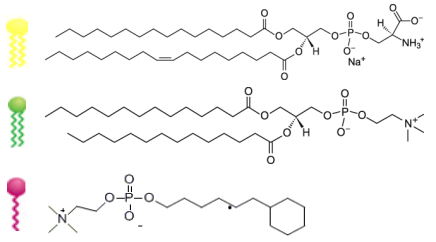

POPS
1-palmitoyl-2-oleoyl-sn-glycero-3-phospho-L-serine

DMPC
1,2-dimyristoyl-sn-glycero-3-phosphocholine

Cyclofos-6
6-cyclohexyl-1-hexylphosphocholine

B

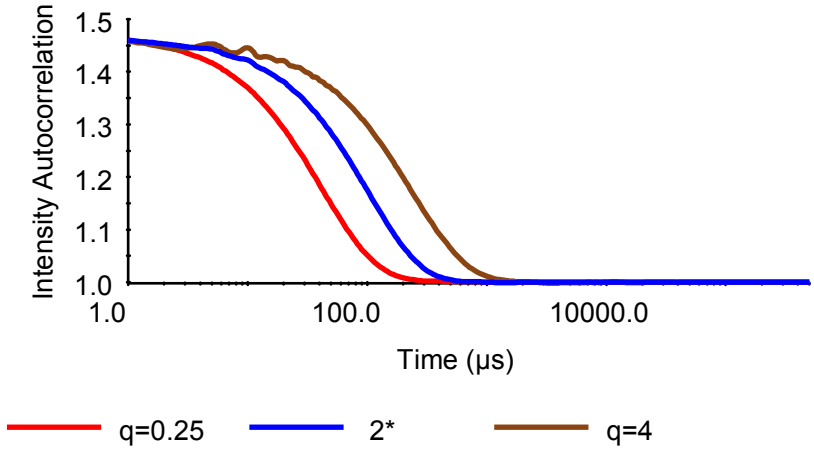

Bicelles	Hydrodynamic Radius (nm)
0.25	3.16±0.08
4	19.95±0.64
2*	8.88±0.51

C

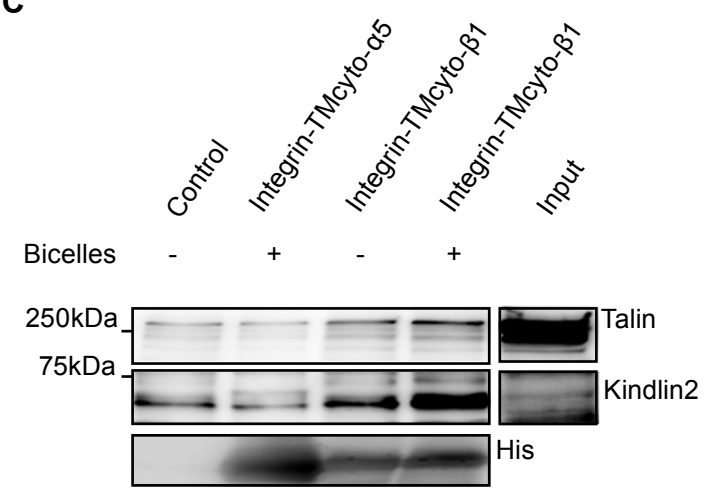

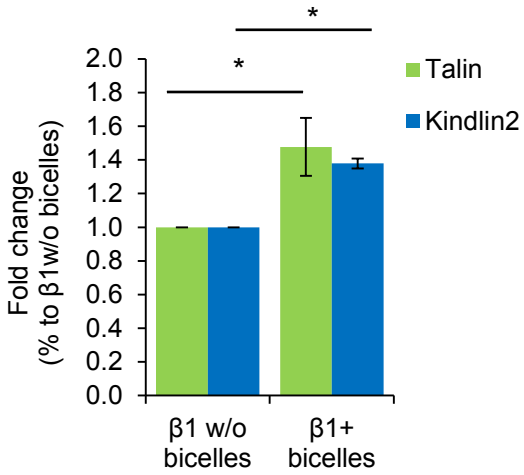

Figure 2

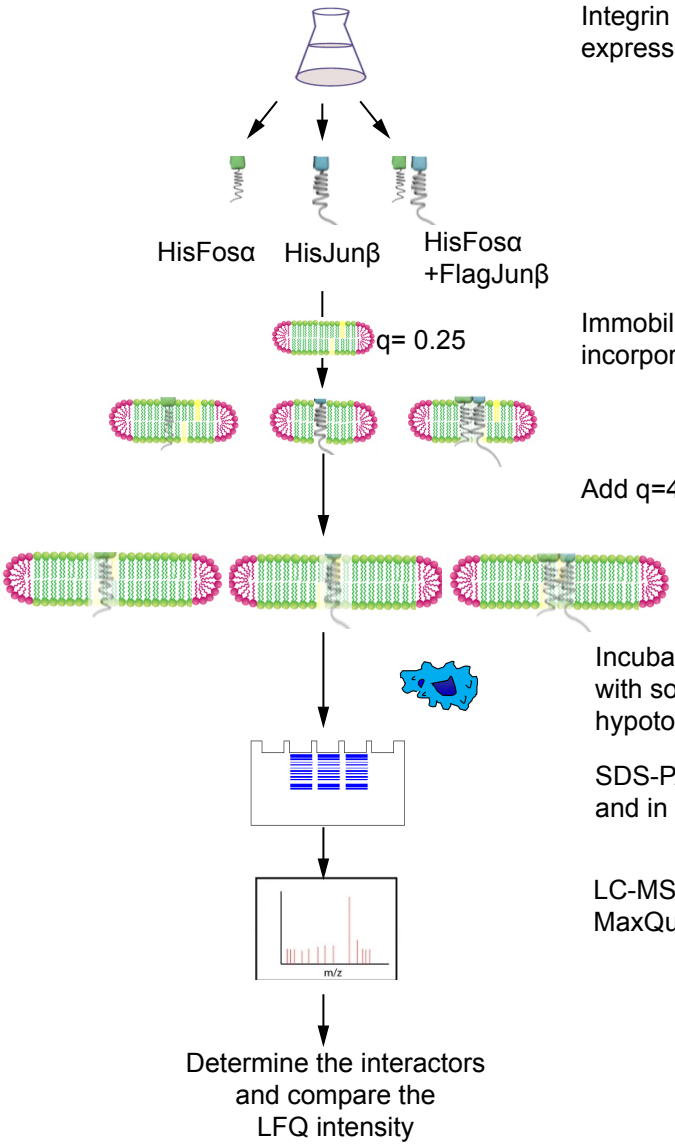

Integrin TM-cyto proteins
expressed in E. coli

Immobilize to Ni-NTA beads and
incorporate into q=0.25 bicelles

Add q=4 bicelles brings to q= 2* bicells

Incubate bicelles incorporated Integrin TM-cyto
with soluble fraction of BMDM lysate from
hypotonic buffer

SDS-PAGE separation
and in gel digestion

LC-MS/MS Orbitrap
MaxQuant- LFQ based

Determine the interactors
and compare the
LFQ intensity

Figure 3

A

α interactors	
Integrin	Protein no.
α5	5
αIIb	161
αM	56

B

β interactors	
Integrin	Protein no.
β1	74
β3	111
β2	60

C

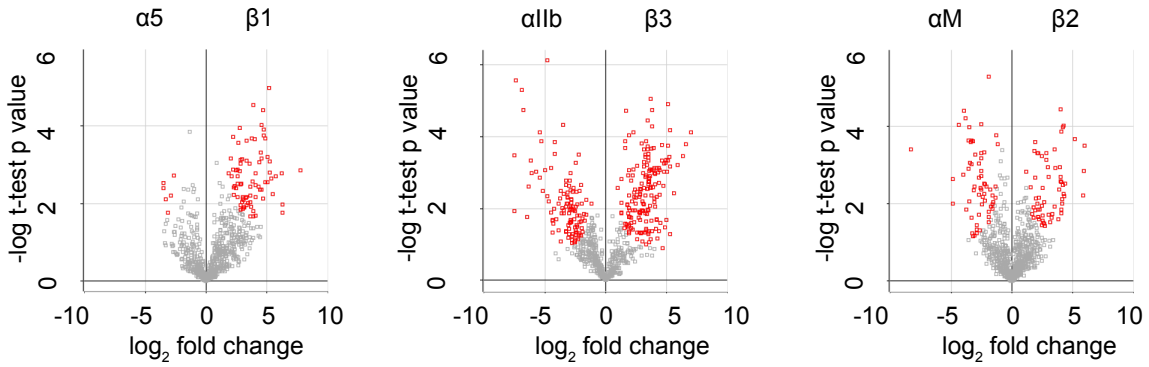

D

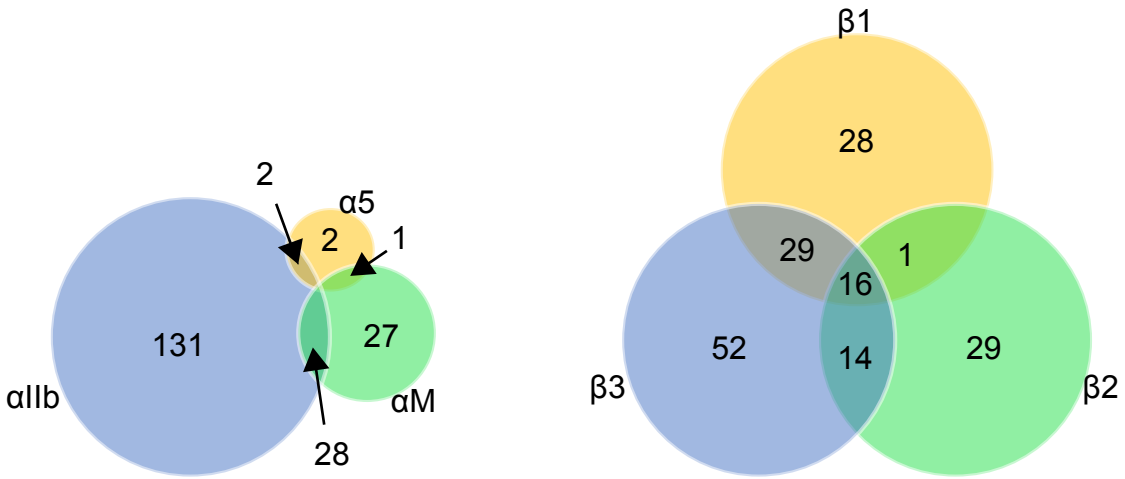

E

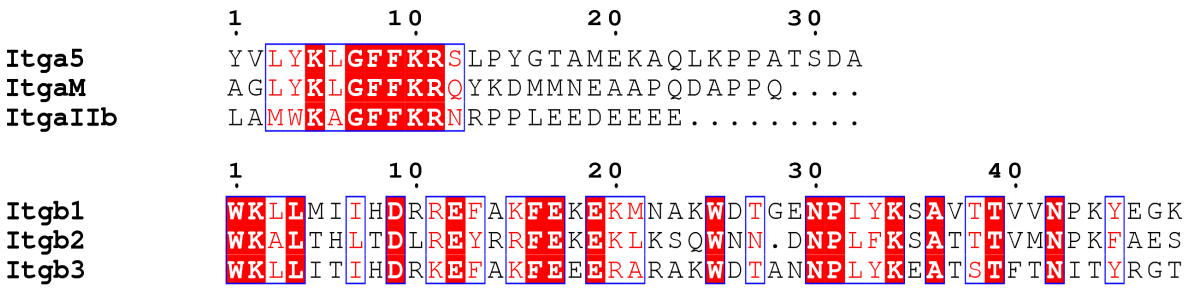

Figure 4

A

B

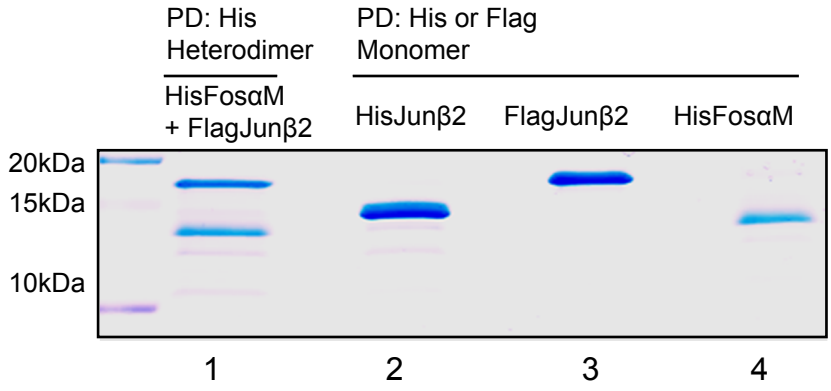

C

Bicelles integrin TMcyto	Hydrodynamic Radius (nm)
0.25-αM	4.41±0.20
0.25-β2	4.93±0.42
0.25-αMβ2	5.15±0.31
2*-αM	10.05±0.26
2*-β2	10.25±0.31
2*-αMβ2	11.17±0.49

Figure 5

A

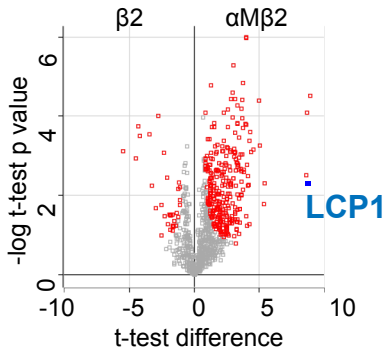

B

Category	Protein no.
Increase binding in αMβ2	293
Only in αMβ2	183
Not in αMβ2	62

C

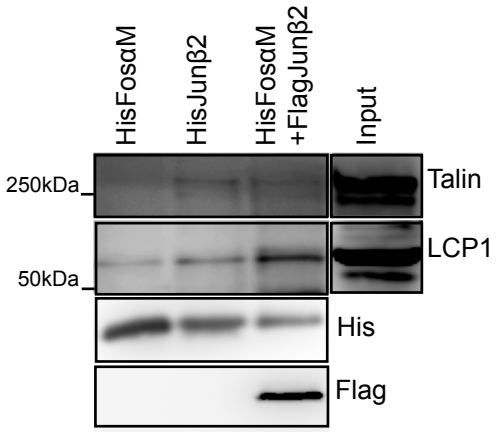

D

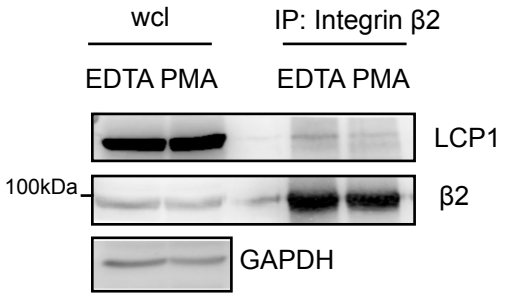

E

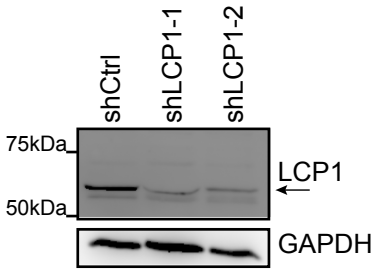

F

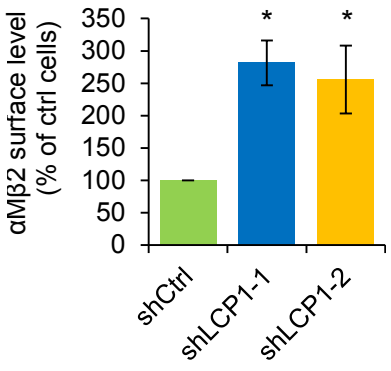

G

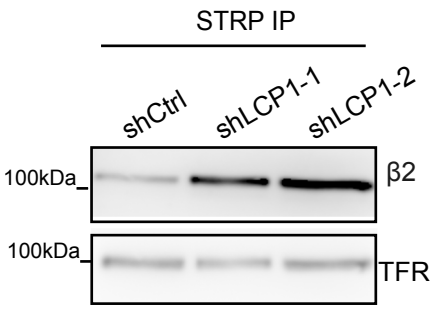

H

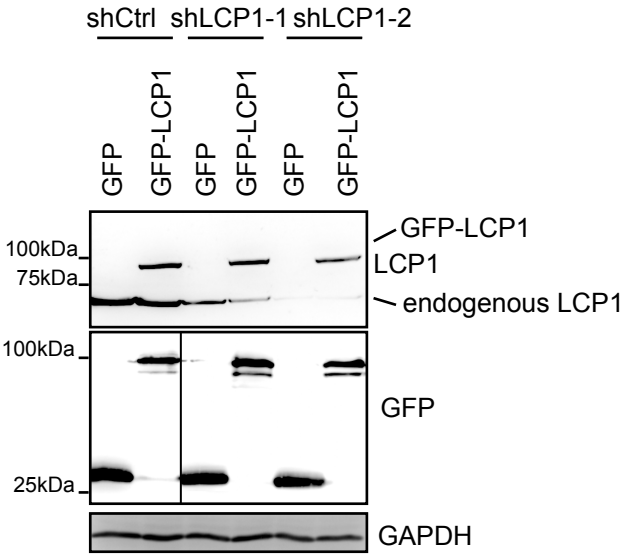

I

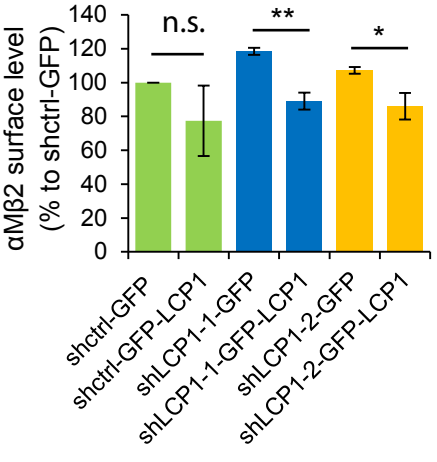

Figure 6

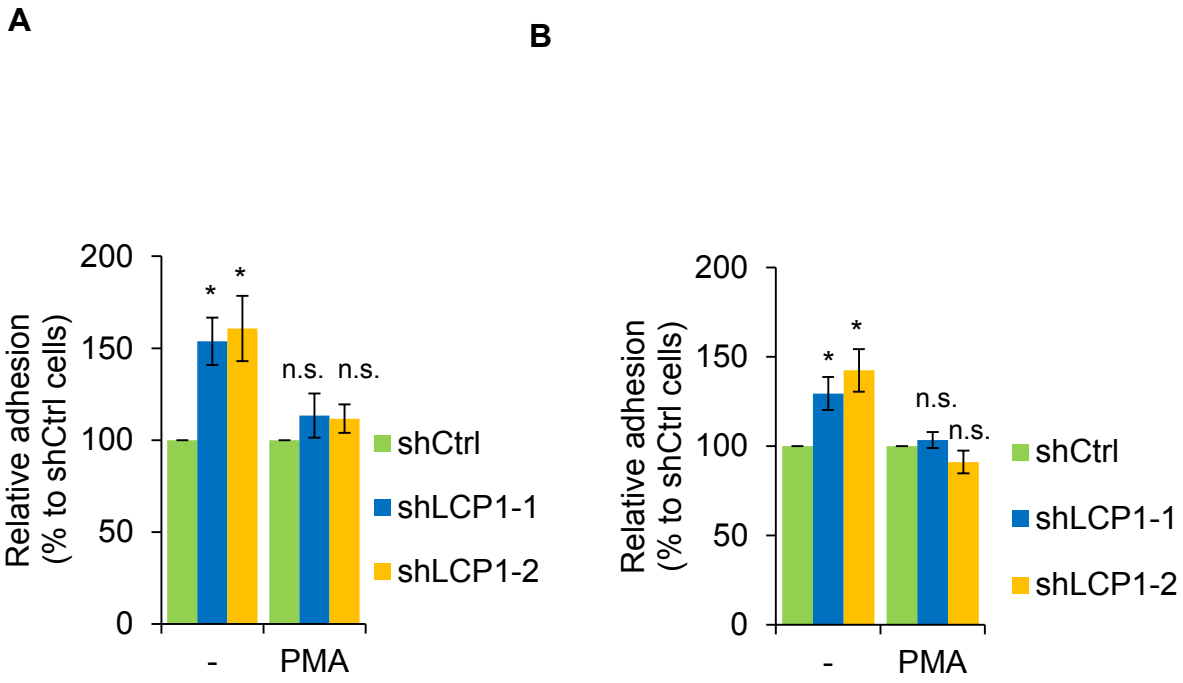
A
B
Relative adhesion (% to shCtrl cells)
200
150
100
50
0
*
*
n.s.
n.s.
-
PMA
shCtrl
shLCP1-1
shLCP1-2

Figure S1

A

q= 0.25
Cyclo-fos: POPS: DMPC
= 4: 0.2: 0.97

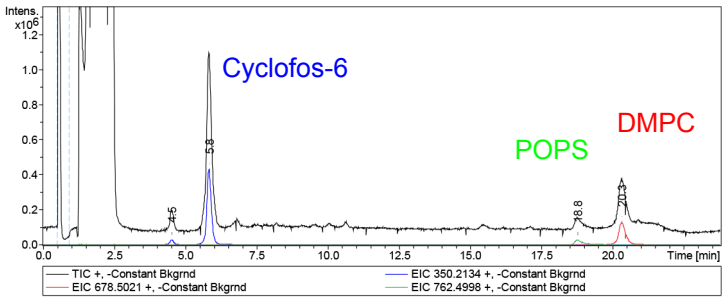

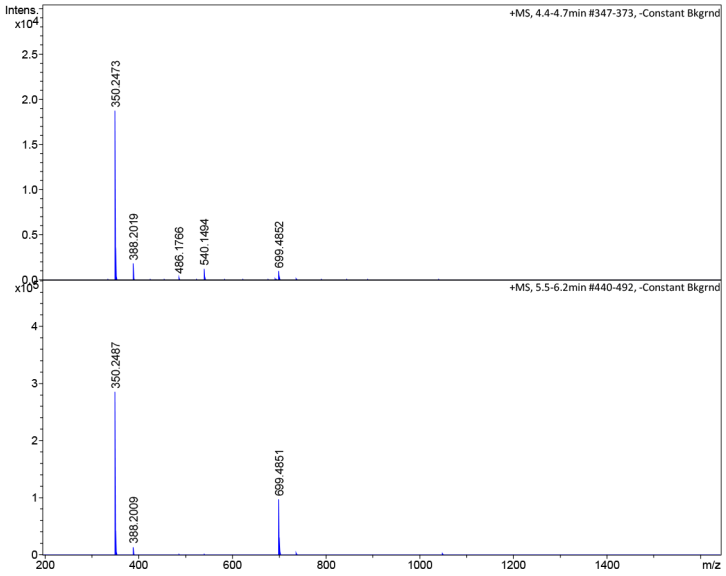

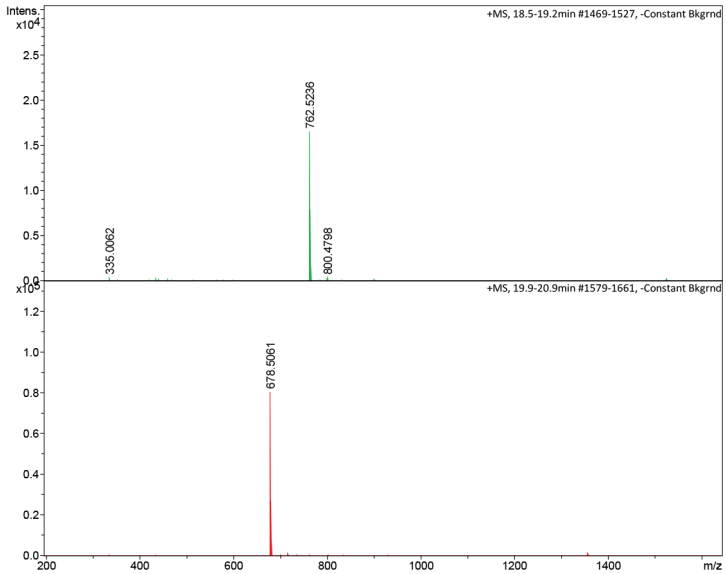

B

q= 4
Cyclo-fos: POPS: DMPC
= 1: 1.66: 3.87

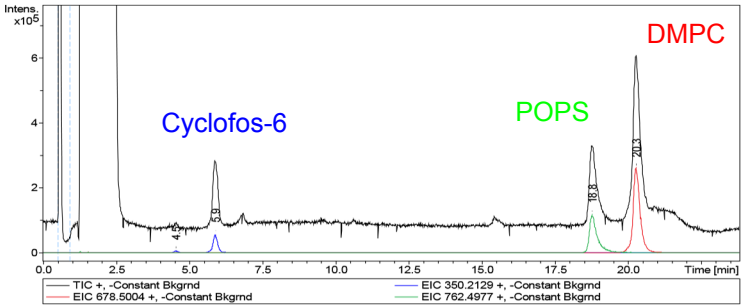

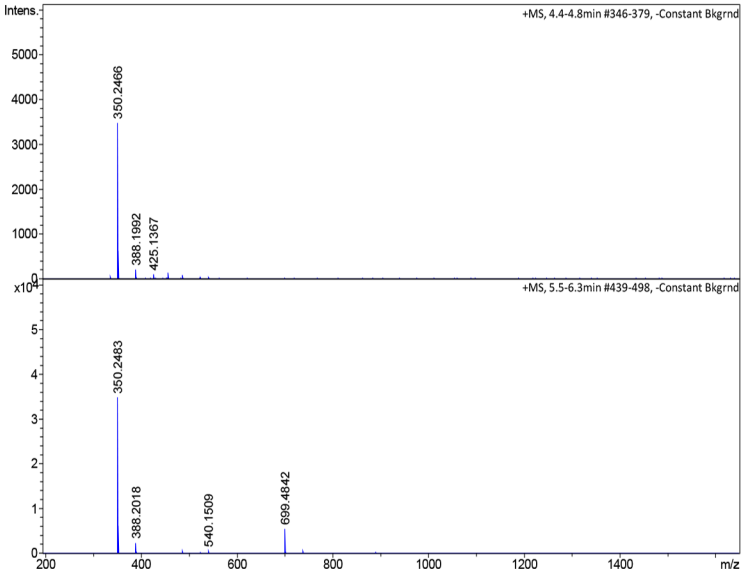

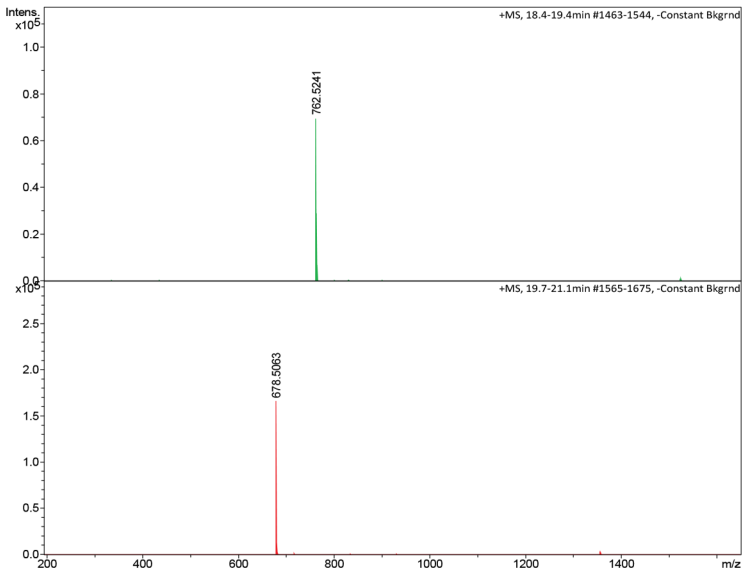

Figure S2

A

Bicelles integrin TMCT	Hydrodynamic Radius (nm)
0.25-α5	4.54±0.22
0.25-β1	4.58±0.15
0.25-α5β1	6.15±0.28
2*-α5	10.47±0.65
2*-β1	11.32±1.29
0.25-αIIb	4.45±0.25
0.25-β3	6.00±0.54
0.25-αIIβ3	6.98±0.42
2*-αIIb	10.29±0.44
2*-β3	11.30±0.77

B

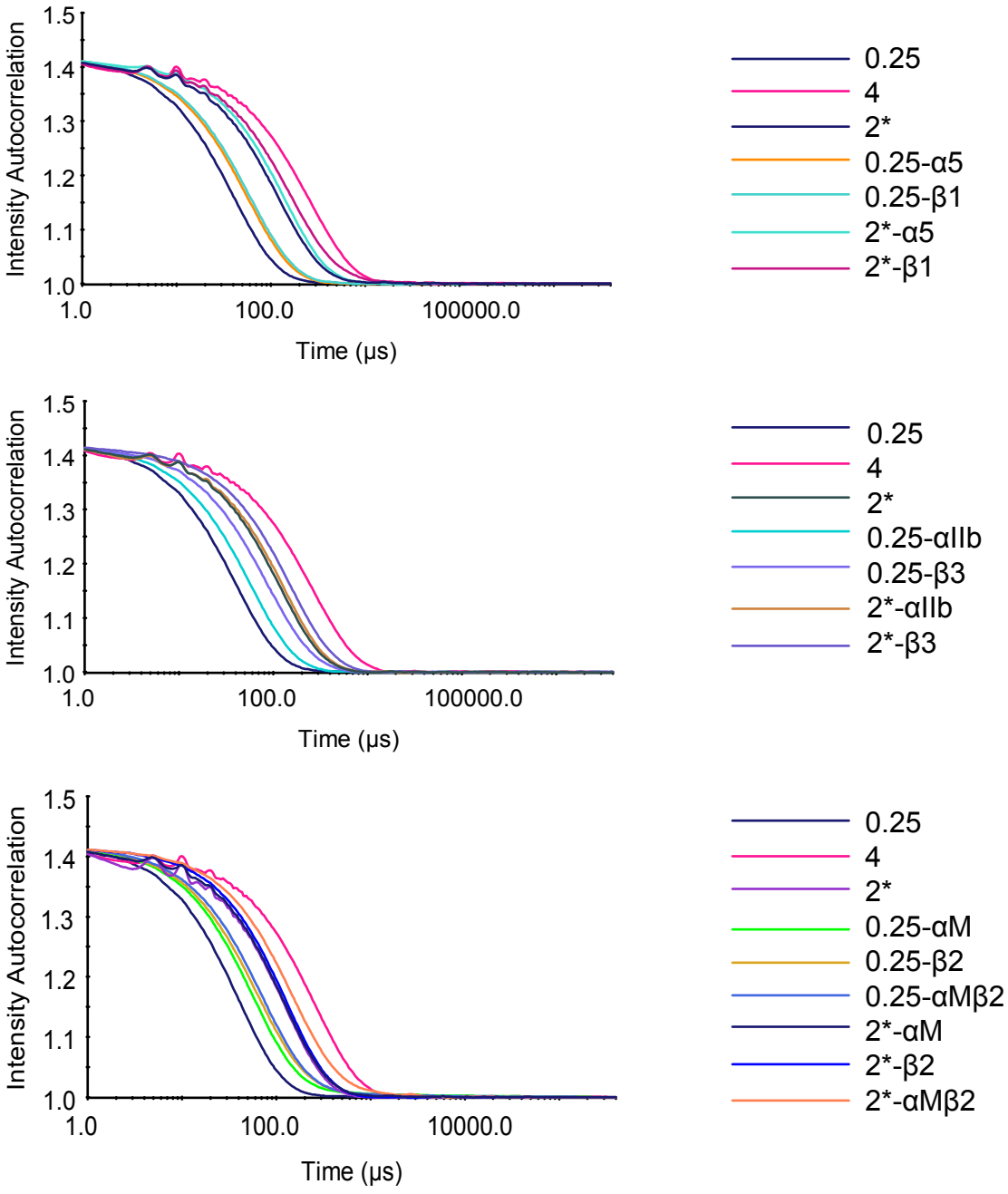

Figure S3

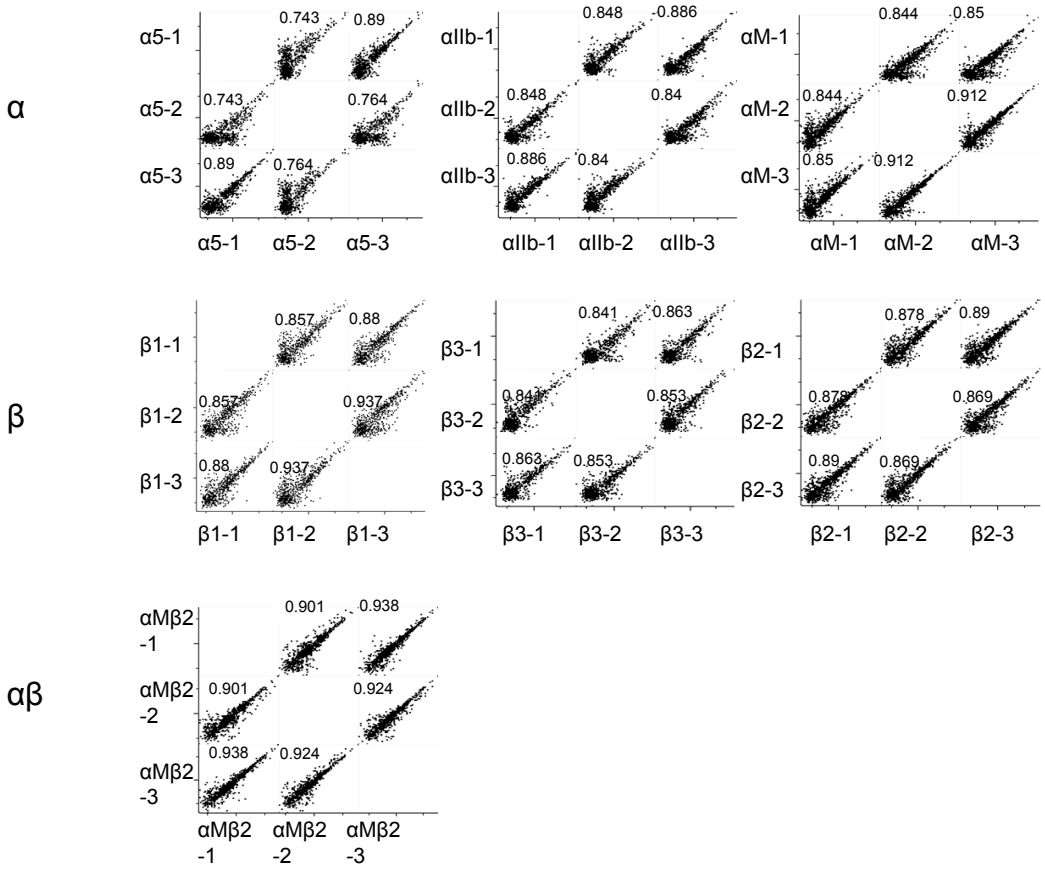
α
α5-1
α5-2
α5-3
0.743
0.89
0.743
0.764
0.89
0.764
α5-1
α5-2
α5-3
αIIb-1
αIIb-2
αIIb-3
0.848
0.886
0.848
0.84
0.886
0.84
αIIb-1
αIIb-2
αIIb-3
αM-1
αM-2
αM-3
0.844
0.85
0.844
0.912
0.85
0.912
αM-1
αM-2
αM-3
β
β1-1
β1-2
β1-3
0.857
0.88
0.857
0.937
0.88
0.937
β1-1
β1-2
β1-3
β3-1
β3-2
β3-3
0.841
0.863
0.841
0.853
0.863
0.853
β3-1
β3-2
β3-3
β2-1
β2-2
β2-3
0.878
0.89
0.878
0.869
0.89
0.869
β2-1
β2-2
β2-3
αβ
αMβ2-1
αMβ2-2
αMβ2-3
0.901
0.938
0.901
0.924
0.938
0.924
αMβ2-1
αMβ2-2
αMβ2-3

Figure S4

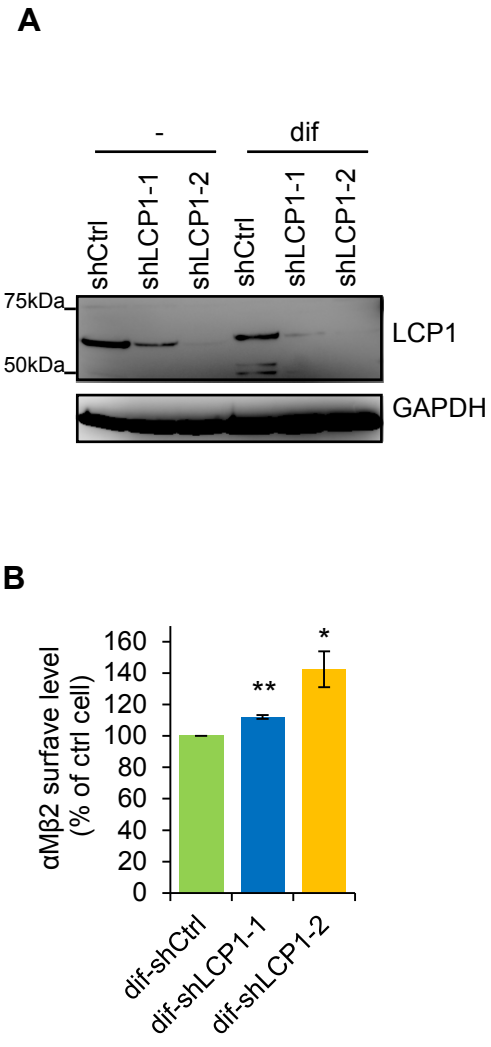
A
-
dif
shCtrl
shLCP1-1
shLCP1-2
shCtrl
shLCP1-1
shLCP1-2
75kDa
50kDa
LCP1
GAPDH
B
αMβ2 surfave level
(% of ctrl cell)
160
140
120
100
80
60
40
20
0
**
*
dif-shCtrl
dif-shLCP1-1
dif-shLCP1-2
C
activeαMβ2 / αMβ2 surface level
(% of ctrl cell)
140
120
100
80
60
40
20
0
n.s.
n.s.
dif-shCtrl
dif-shLCP1-1
dif-shLCP1-2

nature cell biology

Sorting nexin 17 prevents lysosomal degradation of β_1 integrins by binding to the β_1-integrin tail

Ralph Thomas Böttcher[1,2], Christopher Stremmel[1,2], Alexander Meves[1,3], Hannelore Meyer[1,3], Moritz Widmaier[1], Hui-Yuan Tseng[1] and Reinhard Fässler[1,4]

Integrin functions are controlled by regulating their affinity for ligand, and by the efficient recycling of intact integrins through endosomes. Here we demonstrate that the Kindlin-binding site in the β_1-integrin cytoplasmic domain serves as a molecular switch enabling the sequential binding of two FERM-domain-containing proteins in different cellular compartments. When β_1 integrins are at the plasma membrane, Kindlins control ligand-binding affinity. However, when they are internalized, Kindlins dissociate from integrins and sorting nexin 17 (SNX17) is recruited to free β_1-integrin tails in early endosomes to prevent β_1-integrin degradation, leading to their recycling back to the cell surface. Our results identify SNX17 as a β_1-integrin-tail-binding protein that interacts with the free Kindlin-binding site in endosomes to stabilize β_1 integrins, resulting in their recycling to the cell surface where they can be reused.

Integrins are the main family of adhesion molecules mediating cell interactions with the extracellular matrix[1] (ECM). A hallmark of integrins is their ability to tune their affinity for ligand by shifting their extracellular domain between different conformations. Key molecules that increase ligand-binding affinity are the FERM (4.1, ezrin, radixin, moesin)-domain-containing proteins Talins and Kindlins[2,3]. Talins bind the membrane-proximal NPxY motif of β-integrin cytoplasmic tails and Kindlins the membrane-distal NxxY motif and the adjacent threonine residues[4–9].

Increasing evidence indicates that integrin trafficking through the endosomal pathway affects their function, cell surface distribution, signalling through integrin-associated growth factor receptors and the turnover of ECM proteins such as fibronectin[10,11]. In contrast to the well-established mechanisms for integrin recycling[10,12–14], the mechanisms for integrin degradation are not well understood. Fibronectin-bound $\alpha_5\beta_1$ integrin was recently shown to be internalized, sorted into multivesicular endosomes and degraded in lysosomes in a ubiquitin- and endosomal sorting complex required for transport (ESCRT)-dependent manner[15].

Here, we identified the FERM-domain-containing protein SNX17 as a β_1-tail-binding protein that, following β_1-integrin internalization and Kindlin dislodgement, is recruited to the free β_1 tails in early endosomes to prevent β_1-integrin degradation by lysosomes.

RESULTS

β_1-integrin TT788/789AA and Y795A substitutions cause peri-implantation lethality in mice

Thr 788 and 789 and Tyr 795 in the β_1-integrin tail are required for binding Kindlins[6,9,16]. To investigate their significance *in vivo* they were substituted with alanines in mice. Although mice heterozygous for the mutation were normal, their intercross failed to produce live homozygous offspring (TT/AA: +/+: 35%, (TT/AA)/+: 65%, (TT/AA)/(TT/AA): 0%, $N = 100$; Y795A: +/+: 33%, (Y795A)/+: 67%, (Y795A)/(Y795A): 0%, $N = 100$). Timed mating revealed severely malformed or resorbed embryos (Fig. 1a,b and Supplementary Fig. S1a) at embryonic day (E) 7.5 (+/+: 25%, (TT/AA)/+: 53%, (TT/AA)/(TT/AA): 17%, resorbed: 5%, $N = 36$) characterized by defects in cell polarity, laminin111 deposition and cavitation (Fig. 1b). As the defects of the β_1 TT/AA and β_1 Y795A were identical, we mainly show results for β_1 TT/AA mice and cells.

Embryoid bodies generated from embryonic stem (ES) cells derived from littermate wild-type (β_1 wt) and homozygous TT/AA (β_1 TT/AA) blastocysts confirmed the *in vivo* findings. After 2–4 days in suspension culture, β_1 wt ES cells developed embryoid bodies consisting of an outer primitive endoderm layer, a basement membrane and an undifferentiated core, which converted into a layer of pseudo-stratified primitive ectoderm and a central cavity

[1]Department of Molecular Medicine, Max Planck Institute for Biochemistry, 82152 Martinsried, Germany. [2]These authors contributed equally to this work. [3]Present addresses: Department of Dermatology, Mayo Clinic, Rochester, Minnesota 55905, USA (A.M.); Institute of Medical Microbiology, Immunology and Hygiene, Technical University Munich, 81675 Munich, Germany (H.M.).
[4]Correspondence should be addressed to R.F. (e-mail: Faessler@biochem.mpg.de)

Received 22 December 2011; accepted 10 April 2012; published online 6 May 2012; DOI: 10.1038/ncb2501

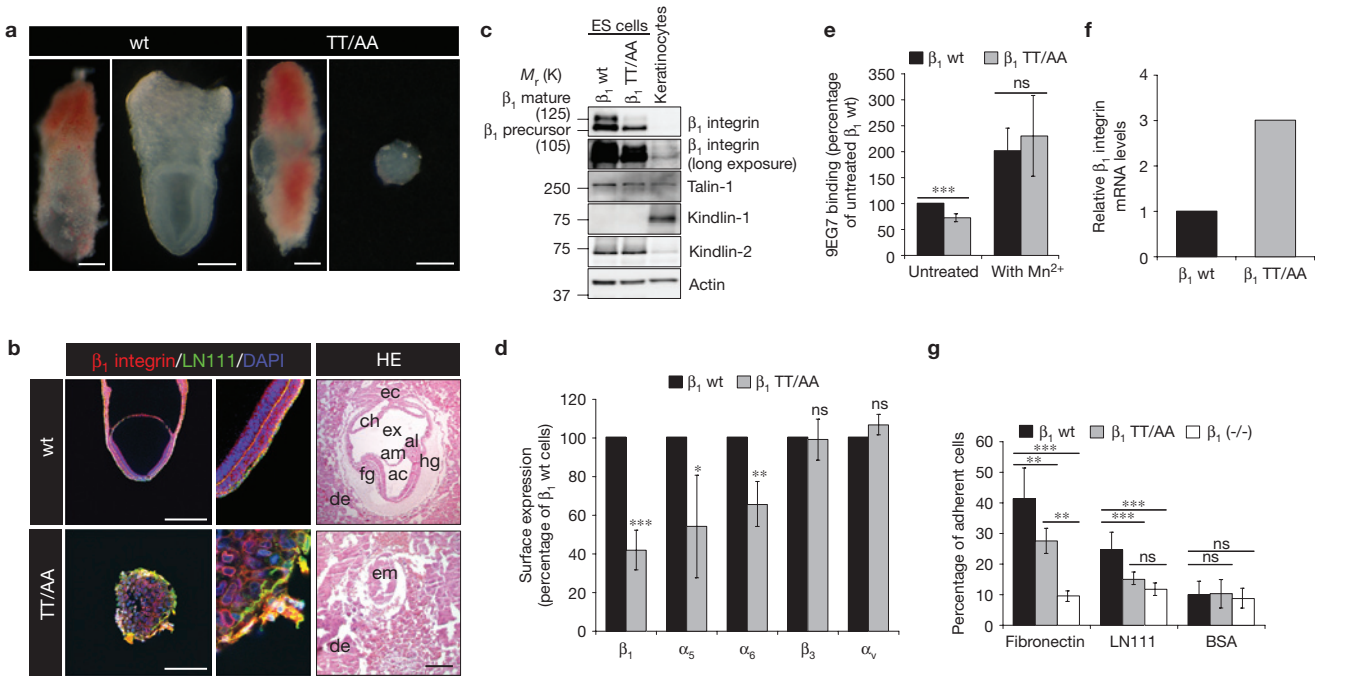

Figure 1 The β_1-TT/AA-integrin tail mutation leads to severe defects. (**a**) Bright-field images of E7.5 embryos with and without implantation chamber. Wild type, wt. (**b**) Left and central panels show whole-mount pictures of E7.5 embryos stained for β_1 integrin (red) and laminin111 (green). Nuclei were counterstained with DAPI (blue). Right panels show haematoxilin and eosin (HE) staining of E7.5 embryo sections. em, embryo; de, decidua; ac, amniotic cavity; am, amnion; al, allantois; ch, chorion; ec, ectoplacental cone; fg, foregut; hg, hindgut; ex, exocoelomic cavity. (**c**) Western blot for β_1 integrin, Talin-1, Kindlin-1, Kindlin-2 and actin of embryonic stem (ES) cell lysates, including a control lane for Kindlin-1 from a wt keratinocyte lysate. (**d**) Expression of integrin subunits on ES cells determined by FACS (mean ± s.d.; $n = 4$; $^{*}P = 0.0134$, $^{**}P = 0.0011$, $^{***}P < 0.0001$). (**e**) Integrin activation on ES cells measured by 9EG7 binding and corrected for total β_1-integrin expression (mean ± s.d.; $n = 4$; $^{***}P = 0.0003$). (**f**) Expression of β_1-integrin mRNA in ES cells measured by quantitative real-time PCR ($n = 2$). (**g**) Adhesion assay of ES cells on different substrates (mean ± s.d.; $n = 3$; $^{**}P < 0.01$ and $^{***}P < 0.005$). *P* values, Student's *t*-test; ns, not significant. Scale bars, 100 μm. Uncropped images of blots are shown in Supplementary Fig. S6.

on day 4–6 (Supplementary Fig. S1b). In contrast, β_1 TT/AA ES cells formed compact aggregates covered by a discontinuous basement membrane and few endoderm cells, which lost their polarized β-catenin, E-cadherin and F-actin distribution, and lacked a central cavity (Supplementary Fig. S1b,c).

β_1 TT/AA ES cells adhered less to feeder cells (Supplementary Fig. S1d) and had reduced levels of the mature (relative molecular mass, 125,000; M_r125K) β_1 integrin, whereas Kindlin-2 and Talin-1 expression were normal (Fig. 1c). Fluorescence-activated cell sorting (FACS) analysis confirmed reduced β_1-integrin surface levels to about 40% in β_1 TT/AA ES cells and revealed decreased levels of α_5 and α_6 integrins, whereas β_3 and α_v levels were unaffected (Fig. 1d). Kindlin-2 binding to the β_1-integrin tail is required for activating the 9EG7 epitope in ES cells[7]. The level of 9EG7 antibody binding to β_1 TT/AA was reduced after adjusting to total β_1 levels but could be normalized to wt levels with manganese (Fig. 1e). The reduced β_1-TT/AA-integrin levels were not due to insufficient messenger RNA transcription, as we detected increased β_1-integrin mRNA transcript levels in β_1 TT/AA ES cells (Fig. 1f). 'Plate-and-wash' adhesion assays revealed a significantly diminished level of attachment of β_1 TT/AA ES cells to ECM substrates (Fig. 1g). Similar results were observed in β_1 Y795A ES cells (Supplementary Fig. S1e–g).

To determine whether the reduced level of β_1 TT/AA and β_1 Y795A surface expression occurs in other cell types, we characterized fibroblasts expressing β_1 wt, β_1 TT/AA or β_1 Y795A integrins. We generated β_1-null fibroblasts from floxed β_1 parental cells re-expressing either β_1 wt, β_1 TT/AA or β_1 Y795A complementary DNAs. We also isolated fibroblasts from β_1 flox/wt and β_1 flox/TT/AA littermates and deleted the floxed alleles by adenoviral Cre transduction (Supplementary Fig. S2a,b). Fibroblasts from both cell systems behaved similarly in all assays. Fibroblasts expressing β_1 TT/AA or β_1 Y795A integrins showed a reduced level of β_1 surface expression despite increased mRNA levels (Supplementary Fig. S2c–f and data not shown). Immunoblotting showed a reduced expression level of the mature (M_r125K) β_1-TT/AA-integrin polypeptide, whereas the level of immature form (M_r105K) was increased when compared with cells expressing β_1 wt (Supplementary Fig. S2g). In line with our ES cell results, we observed significantly less 9EG7 antibody binding to β_1-TT/AA-expressing fibroblasts (Supplementary Fig. S2h).

These findings show that the TT/AA or Y795A β_1 tail substitutions reduce β_1 cell-surface levels and suggest defects in integrin processing or turnover.

The distal NxxY motif and the adjacent TT788/789 control β_1-integrin turnover

Surface levels of transmembrane proteins are controlled by the synthesis rate, maturation and export of the polypeptide to the cell surface, internalization, recycling and degradation. To determine whether the TT/AA substitutions alter β_1-integrin maturation in the secretory pathway, β_1-wt- and β_1-TT/AA-expressing fibroblasts were

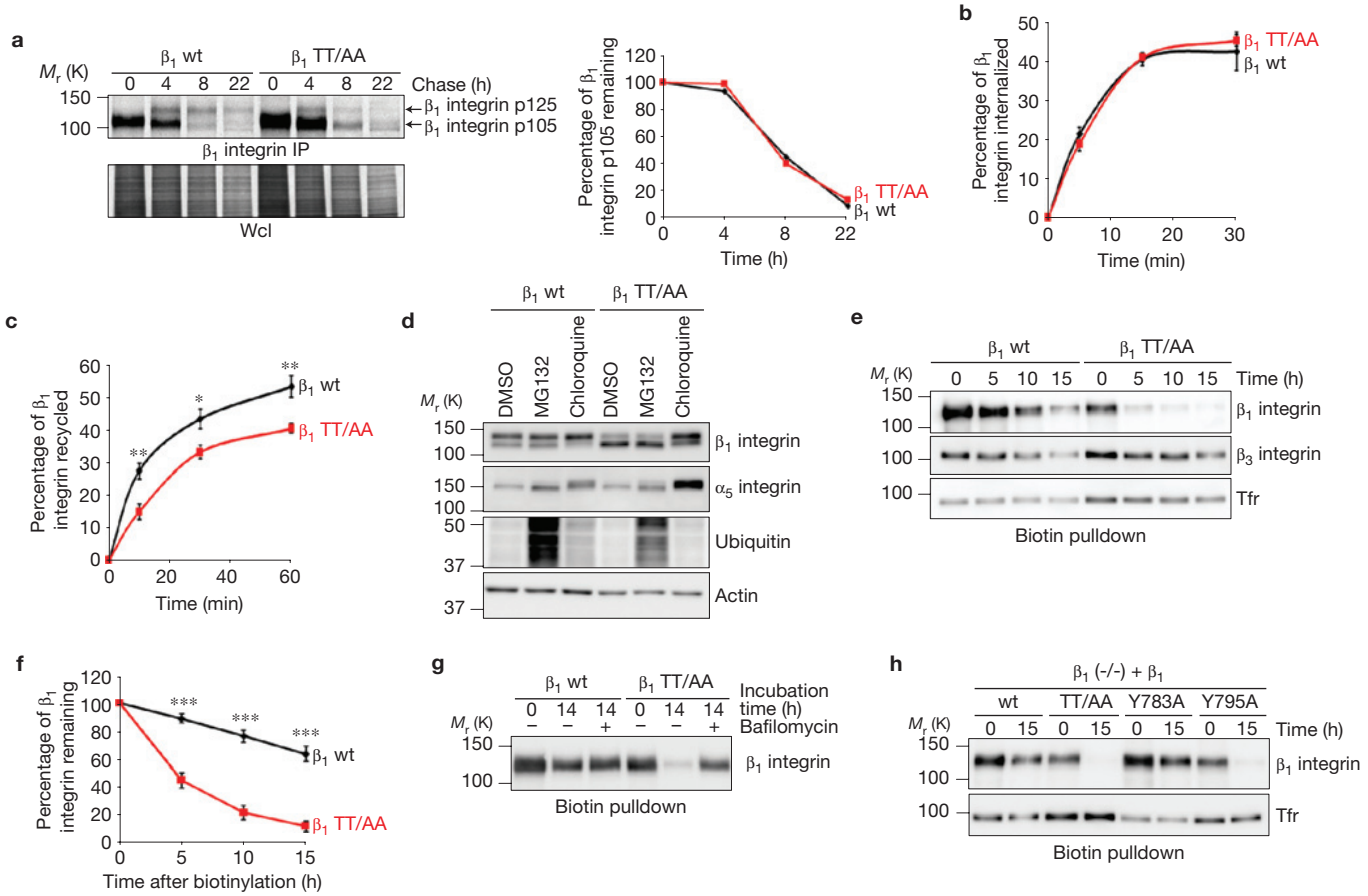

Figure 2 TT788/789 regulate β_1 recycling and degradation. (**a**) Pulse-chase analyses of β_1-integrin maturation in cells expressing wt or β_1 TT/AA integrins. Cells were collected and analysed by immunoprecipitation after metabolic labelling with [^{35}S]methionine/cysteine and chased for the indicated time points. Maturation curves show immature β_1 integrin as a percentage of the total β_1 integrin (right) and were drawn from densitometric scans of the autoradiograms (left). (**b**) Quantification of β_1-integrin internalization in β_1-wt- and β_1-TT/AA-expressing cells by capture-ELISA (mean ± s.d.; $n = 4$). (**c**) Quantification of β_1-integrin recycling in β_1-wt- and β_1-TT/AA-expressing fibroblasts by capture-ELISA (mean ± s.d.; $n = 5$; $^{*}P < 0.05$ and $^{**}P < 0.01$). (**d**) Western blot analysis of β_1-wt- and β_1-TT/AA-expressing cells treated with either proteasome (MG132) or lysosome inhibitor (chloroquine) for 20 h. Actin served as a loading control. (**e**,**f**) Degradation of cell-surface integrins was determined by biotinylating cell-surface proteins and incubating for the indicated time points, followed by biotin pulldown and western blot analysis (**e**) or quantification by capture-ELISA (**f**) (mean ± s.d.; $n = 4$; $^{***}P < 0.0001$). (**g**) Lysosomal inhibition by bafilomycin prevents degradation of β_1 TT/AA integrin. Degradation was measured by surface biotinylation and incubation of the cells for 14 h in the presence or absence of bafilomycin. (**h**) Degradation of β_1-integrin mutants (wt, TT/AA, Y783A and Y795A) was determined by biotinylating cell-surface proteins and incubating for 0 h and 15 h, followed by biotin pulldown and western blot analysis. All P values, Student's t-test. Uncropped images of blots are shown in Supplementary Fig. S6.

pulse labelled with [^{35}S]methionine/cysteine. Owing to the higher β_1-TT/AA-integrin mRNA levels, β_1 TT/AA cells expressed more immature β_1 integrin in the initial pulse-labelling phase; however, the immature, M_r105K-sized β_1-integrin polypeptide disappeared in both cell types with the same kinetics, indicating that the TT/AA mutation does not affect the initial processing of the β_1 polypeptide (Fig. 2a). The increased ratio between the M_r105K- and the M_r125K-sized β_1 polypeptides in β_1 TT/AA fibroblasts and the increased persistence of the M_r125K β_1 wt polypeptide indicated marked differences in β_1 TT/AA turnover. As integrin turnover is affected by intracellular trafficking, we compared β_1 wt and β_1 TT/AA internalization and recycling by surface labelling with cleavable biotin. Whereas β_1 wt and β_1 TT/AA integrins internalized with the same kinetics, the TT/AA substitutions showed a decreased recycling rate back to the plasma membrane (Fig. 2b,c). The similar time constant at the start of recycling together with the significantly different plateaux of recycled β_1 wt and β_1 TT/AA integrins indicates that the recycling machinery is normal whereas the number of recycling integrins (reflected by the different plateaux) is lower in β_1-TT/AA-expressing cells.

To determine whether reduced recycling of β_1 TT/AA to the cell surface results from increased degradation, we treated β_1 wt and β_1 TT/AA fibroblasts with the lysosomal inhibitor chloroquine or the proteasomal inhibitor MG132. Lysosome inhibition rescued the mature β_1 TT/AA to wt levels and stabilized the corresponding α_5 subunit, whereas proteasome inhibition had no effect on β_1 TT/AA and α_5 stability (Fig. 2d). We also determined the degradation kinetics of the surface β_1 integrins by surface labelling of β_1 wt and β_1 TT/AA cells with biotin, followed by the measurement of biotinylated proteins after pulldown with streptavidin beads and immunoblotting or capture enzyme-linked immunosorbent assay (ELISA). Whereas β_1 wt was slowly degraded with an estimated half-life of over 20 h, degradation of β_1 TT/AA occurred quickly with a 4–5 h

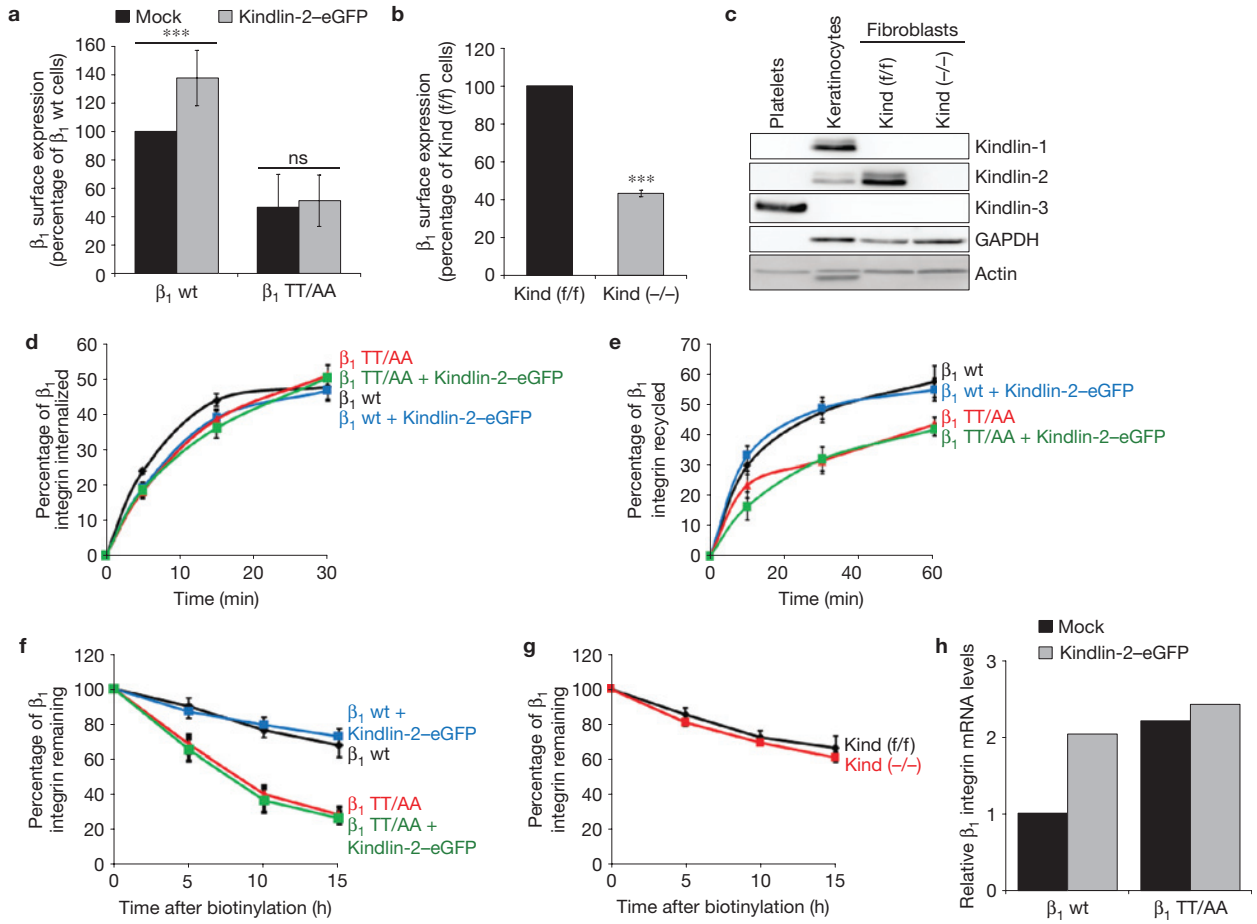

Figure 3 Kindlin-2-dependent regulation of β_1-integrin surface levels. (**a**) β_1 surface expression in β_1-wt- and β_1-TT/AA-expressing fibroblasts after overexpression of Kindlin-2–eGFP determined by FACS (mean ± s.d.; $n = 11$; $^{***}P < 0.0001$; ns, not significant). (**b**) β_1 surface levels in control (Kind (f/f)) and Kindlin-1 and -2 double null (Kind(−/−)) fibroblasts determined by FACS (mean ± s.d.; $n = 3$; $^{***}P < 0.0001$). (**c**) Western blot analysis of cell lysates from platelets, keratinocytes and Kind (−/−) fibroblasts with antibodies against the three Kindlin family members. Actin and GAPDH served as loading control. (**d**,**e**) Quantification of β_1-integrin internalization (**d**) and recycling (**e**) in β_1 wt and β_1 TT/AA cells with and without Kindlin-2–eGFP overexpression by capture-ELISA (mean ± s.e.m.; $n = 8$ (**d**) and $n = 10$ (**e**)). (**f**,**g**) Quantification of surface β_1-integrin stability in Kindlin-2–eGFP-overexpressing (**f**) and Kind(−/−) cells (**g**). Degradation of cell-surface β_1 integrin was determined by biotinylating cell-surface proteins and incubating for the indicated time points, followed by capture-ELISA (mean ± s.d.; $n = 4$ (**f**); $n = 3$ (**g**); ns, not significant). (**h**) β_1-integrin mRNA expression in Kindlin-2–eGFP-overexpressing fibroblasts measured by quantitative real-time PCR ($n = 2$). All P values, Student's t-test. Uncropped images of blots are shown in Supplementary Fig. S6

half-life (Fig. 2e,f). This was specific to β_1 integrin as the degradation rates of β_3 integrin and the transferrin receptor (Tfr) were similar in both cell types (Fig. 2e). Furthermore, bafilomycin rescued the degradation of biotinylated β_1 TT/AA, confirming that the instability of β_1 TT/AA results from lysosomal degradation (Fig. 2g). To determine whether the β_1-tail NxxY motifs are also required for β_1-integrin stability, we expressed β_1 Y783A and β_1 Y795A integrins in β_1-null cells. Biotinylated β_1 protein was detectable after 15 h in β_1-wt- and β_1-Y783A-expressing cells, but was almost completely degraded in β_1-TT/AA- and β_1-Y795A-expressing cells (Fig. 2h).

These experiments indicate that the TT788/789 and distal NxxY sequence control turnover of surface β_1 integrins.

Kindlin-2 regulates β_1 surface levels by controlling β_1-integrin mRNA levels

As the TT788/789 and the membrane-distal NxxY motif in β_1 integrin tails are required for Kindlin binding[6,9,16], we investigated whether disrupting this interaction was responsible for the reduced β_1 TT/AA surface levels, recycling and stability. As reported, overexpression of Kindlin-2–eGFP in β_1 wt cells significantly increased β_1-integrin surface levels[17], but not in β_1-TT/AA-expressing fibroblasts, probably because their mRNA levels are already upregulated (Fig. 3a). Conversely, β_1-integrin surface levels were significantly diminished in fibroblasts lacking the *kindlin-1* and *-2* genes (Fig. 3b,c). Despite increased β_1 surface levels in Kindlin-2-overexpressing cells, internalization, recycling (Fig. 3d,e) and stability of surface β_1 integrins were normal (Fig. 3f). Furthermore, the degradation of surface β_1 integrins was unchanged in fibroblasts lacking Kindlin-1 and -2 (Fig. 3g). Instead, the β_1-integrin mRNA levels were increased in Kindlin-2–eGFP-overexpressing cells (Fig. 3h). Internalization and recycling assays could not be performed with cells lacking Kindlin-1 and -2, as their adhesion to ECM substrates was very weak and cells were lost during the assays. Collectively, these data show that Kindlin-2 increases β_1-integrin surface expression primarily by upregulating β_1-integrin mRNA levels.

SNX17 interacts with the TT788/789–Y795 motif of the β_1 cytoplasmic domain

To understand how TT788/789 and the membrane-distal NxxY motif regulate recycling, stability and surface expression of β_1 integrins, we screened for new β_1-tail-interacting protein(s) using stable isotope labelling by amino acids in cell culture[18] (SILAC) followed by pulldown experiments with synthesized full-length β_1 wt, β_1 TT/AA cytoplasmic domain or scrambled peptides (to identify nonspecific interactors) and mass-spectrometry-based proteomics[19]. Among proteins with high light-to-heavy isotope ratios indicative for specific binding, were known β_1-tail-interacting proteins such as Talin-1, Talin-2, Kindlin-2, Dab2 and ILK, and also SNX17 (Fig. 4a and Supplementary Table S1). Only four of these proteins failed to bind when compared with a β_1-TT/AA-integrin tail, and of those Kindlin-2 and SNX17 showed the highest ratios (Fig. 4a). SNX17 belongs to the sorting nexin (SNX) family of adaptor proteins whose hallmark is a phox-homology (PX) domain known to mediate association with phosphatidylinositol-3-monophosphate (PtdIns(3)P)-enriched endosomes[20]. Similarly to Talin and Kindlin, SNX17 contains a FERM domain with a QW motif in the F3 subdomain required in Talin and Kindlin for binding the β_1 tail[7,20,21]. SNX17 has been implicated in endocytic trafficking of transmembrane proteins including low-density lipoprotein receptor family members LDLR and LRP1 (refs 22–24), P-selectin[25] and APP (ref. 26).

Consistent with the proteomic data, SNX17 and Kindlin-2 were readily detected in peptide pulldowns with β_1 wt but not with β_1 TT/AA, β_1 Y795A, α_5 or scrambled peptides (Fig. 4b). To determine whether SNX17 directly interacts with the β_1-integrin tail, we performed integrin-tail-peptide-pulldown experiments with recombinant wt GST–SNX17 or GST–SNX17 with a mutated QW motif (GST–SNX17QW/AA). These experiments revealed that SNX17 binds directly to β_1 wt but not β_1 TT/AA, β_1 Y795A or scrambled peptides and showed that the interaction is specific because a QW mutation in the F3 subdomain of SNX17 abolished binding (Fig. 4c). SNX17 and Kindlin-2 share the binding site on the β_1-integrin tail and compete for β_1-integrin-tail binding *in vitro* (Supplementary Fig. S3a). However they do not co-localize in living cells, indicating that they interact with the β_1 tail in different subcellular compartments (Fig. 4d). Co-localization studies in living cells revealed that SNX17 partially overlapped with the early endosomal antigen-1 (EEA1), an early endosome marker, as well as with the Tfr, a recycling endosome marker (Fig. 4e, and Supplementary Fig. S3b). No significant co-localization was observed with the lysosomal acid membrane protein 1 (Lamp1) and Rab7 (Fig. 4f and Supplementary Fig. S3c,d). Owing to the lack of suitable antibodies, we employed live-cell microscopy to show co-localization of eGFP-tagged SNX17 with antibody-labelled internalized β_1 integrins (Fig. 4g) and with α_5 integrin–eGFP (Supplementary Fig. S3e). We also observed co-localization of SNX17–eGFP with β_1 TT/AA-positive endosomes (Supplementary Fig. S3f), which is probably due to the binding of the PX domain to endosomal lipids. 9EG7 antibody labelling revealed the presence of active β_1 wt integrins in focal adhesions but not in SNX17–eGFP-positive endosomes (Supplementary Fig. S3g), suggesting that SNX17-bound β_1 integrins are in a low-affinity state. To demonstrate interactions of the endogenous proteins, we surface labelled β_1 integrins, enriched the endosomal β_1-integrin pool by inhibiting recycling with primaquine[27] and co-precipitated labelled β_1 wt integrins with endogenous SNX17 (Fig. 4h). The interaction was lost in cells expressing β_1 TT/AA integrins (Fig. 4h). These findings show that SNX17 is a β_1-integrin-tail-binding protein, that the interaction occurs in endosomes and that the SNX17 and Kindlin-binding site overlap.

SNX17 is required for β_1-integrin recycling and stabilization

To determine whether SNX17 regulates β_1-integrin trafficking and/or degradation we depleted SNX17 by short interfering RNA (siRNA) transfection or by short hairpin RNA (shRNA) retroviral expression (shSNX17-1 and shSNX17-2). SNX17 depletion decreased the mature β_1-integrin pool in whole-cell lysates (Fig. 5a) and reduced the β_1 wt surface levels by 40% (Fig. 5b). Bafilomycin treatment rescued the mature β_1-wt-integrin pool, indicating enhanced lysosomal degradation in SNX17-depleted cells (Fig. 5a). Immunoblotting and capture ELISA of surface-biotinylated β_1 integrins from control (shCtr) and SNX17-depleted fibroblasts confirmed that β_1 wt integrins were degraded in the absence of SNX17 (Fig. 5c,d and Supplementary Fig. S4a). The increased β_1-integrin degradation was specific, as the stability of the Tfr and of the SNX17-binding-deficient β_1 TT/AA integrin were unaffected by SNX17 downregulation (Fig. 5c and Supplementary Fig. S4b). Expression of shRNA-resistant wt SNX17 restored stability and β_1-integrin surface levels in SNX17-depleted cells, whereas SNX17QW/AA did not (Fig. 5d–f and Supplementary Fig. S4a). Similarly to β_1 TT/AA cells, β_1-wt-integrin internalization was normal in SNX17-depleted cells (data not shown), whereas recycling to the cell surface was significantly impaired (Fig. 5g). Thus, SNX17 promotes recycling of β_1 integrins and prevents their degradation.

To monitor β_1 wt trafficking in control and SNX17-depleted cells and β_1 TT/AA trafficking along the endocytic pathway, we labelled surface β_1 integrins with an antibody before internalization. At 10 min after internalization, β_1 wt- and β_1 TT/AA-positive puncta were evenly distributed in the cytoplasm and localized to the early endosomal compartment (Supplementary Fig. S4c). At 30 min, the internalized β_1 wt signal level in control cells was reduced, indicating that β_1 wt efficiently recycled to the cell surface. In contrast, β_1 TT/AA and β_1 wt in SNX17-depleted cells co-localized with Lamp1-positive lysosomes (Supplementary Fig. S4c), supporting the observation that the β_1-tail/SNX17 interaction prevents routing of β_1 integrin into the lysosome.

To investigate whether SNX17 controls recycling or degradation of β_1 integrins, we performed recycling assays of β_1 wt in SNX17-depleted cells and of β_1 TT/AA in the presence and absence of bafilomycin. Bafilomycin treatment rescued the recycling rates and the surface levels of β_1 TT/AA and β_1 wt in SNX17-depleted cells (Fig. 5h and Supplementary Fig. S4d,e). Moreover, internalized β_1 TT/AA and β_1 wt in SNX17-depleted cells no longer accumulated in the late endosome/lysosome compartments 30 min after internalization (Supplementary Fig. S4c). These findings were corroborated by substituting all lysine residues of the α_5 and β_1 tails with arginines (β_1 8xKR±TT/AA; α_5 4xKR) to inhibit ubiquitylation and ESCRT-mediated lysosomal degradation. The lysine to arginine substitutions did not affect integrin internalization (data not shown). However, expression of the β_1 8xKR+TT/AA

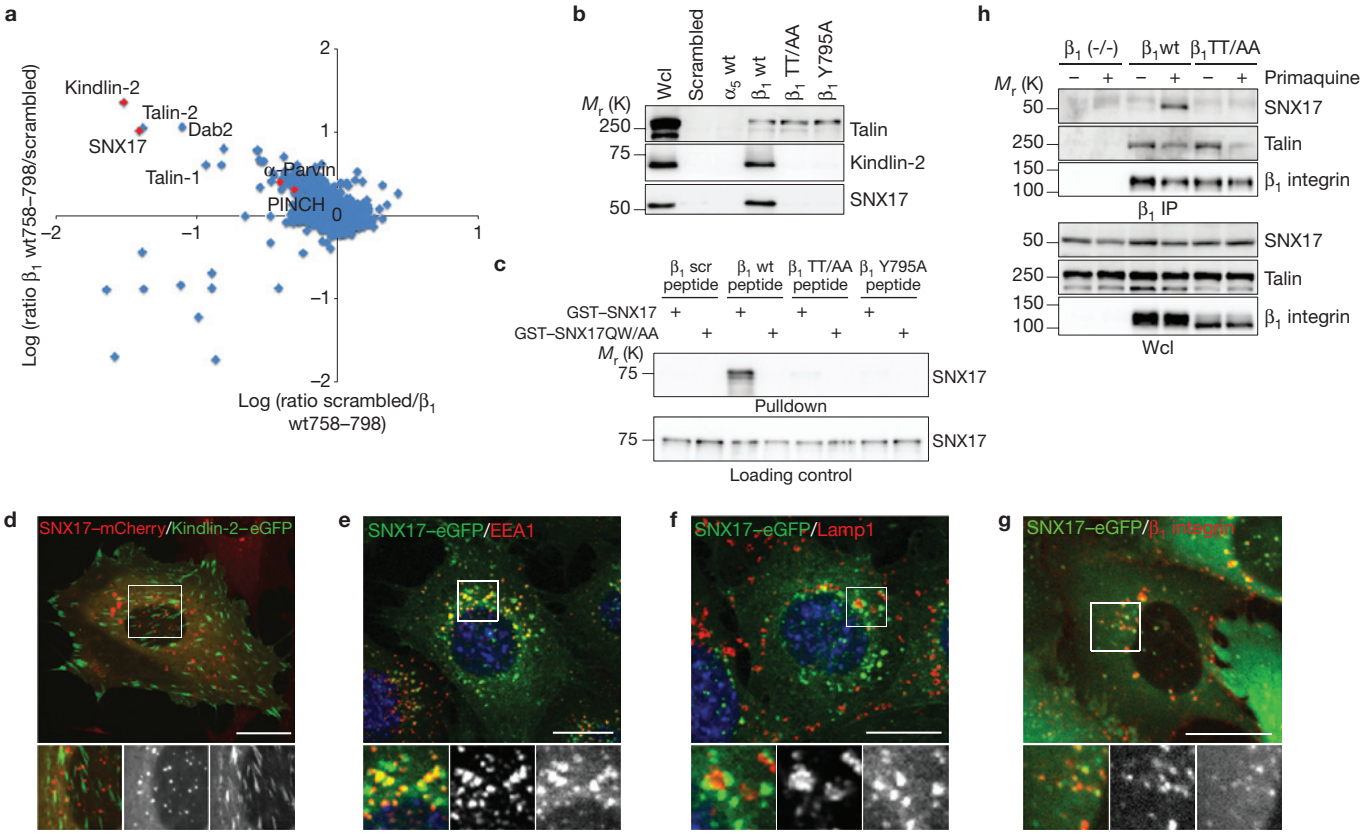

Figure 4 SNX17 requires TT788/789 for β_1-integrin-tail binding. (**a**) Scatter plot of β_1-wt-tail peptide versus scrambled-peptide pulldown results. The $\log_2$ SILAC ratio of proteins identified with at least 2 unique peptides in each mass spectrometry run is plotted as the forward pulldown (*x* axis) against the reverse labelling pulldown (*y* axis). Specific interaction partners show inverse ratios between forward and reverse experiment, grouping them into the upper left quadrant. Red dots indicate those proteins that failed to bind to the β_1-TT/AA-tail peptide in a separate experiment. (**b**) Western blot showing Talin-1, Kindlin-2 and SNX17 binding to the biotinylated peptides indicated. Wcl, whole-cell lysate. (**c**) Streptavidin-bead pulldown assay with the indicated biotinylated β_1-integrin cytoplasmic tail peptides and recombinant GST-tagged SNX17 or a GST-tagged SNX17QW/AA. (**d**) SNX17–mCherry-expressing cells were transfected with Kindlin-2–eGFP and fluorescence distribution was determined in living cells by spinning-disc confocal microscopy. Stills of movies are shown. (**e**,**f**) Immunostaining of SNX17–eGFP-expressing cells with EEA1 (**e**) and Lamp1 (**f**) antibodies. Nuclei were counterstained with DAPI (blue). Correlation coefficient 0.300 ± 0.116 (EEA1), −0.457 ± 0.141 (Lamp1); mean ± s.d.; $n = 44$ (**e**); $n = 25$ (**f**). (**g**) Localization of endogenous β_1 integrin after surface labelling with an anti-β_1-integrin antibody and internalization for 15 min in SNX17–eGFP-expressing cells. The fluorescence intensity was determined in living cells by spinning-disc confocal microscopy. A still of a movie is shown. (**h**) Co-immunoprecipitation of endogenous β_1 integrin and SNX17 from β_1-wt- and β_1-TT/AA-expressing cells pre-treated with or without primaquine. Wcl, whole-cell lysate. Scale bars, 20 μm. In **d**–**g**, lower panels show an enlargement of the area indicated by the white rectangle. Uncropped images of blots are shown in Supplementary Fig. S6.

together with α_5 4xKR rescued the instability and recycling rates induced by the TT/AA mutation (Fig. 5i,j). Expression of the β_1 8xKR+TT/AA along with the α_5 wt was not sufficient to fully stabilize the TT/AA mutation, indicating that ubiquitylation of either the α_5 or the β_1 subunit can mediate $\alpha_5\beta_1$ degradation (Fig. 5i). Thus, SNX17 primarily functions to prevent β_1-integrin degradation and not β_1-integrin recycling.

SNX17 is an important regulator of integrin-mediated cell functions

As Kindlin and SNX17 share the β_1-tail-binding site, mutations in this site affect Kindlin- and SNX17-mediated functions. To determine whether SNX17 influences integrin-mediated functions, we analysed cell spreading and migration in SNX17-depleted cells. Indeed, β_1-TT/AA- and β_1-Y795A-expressing cells and SNX17-depleted fibroblasts did not spread to the same extent as β_1 wt cells (Fig. 6a and Supplementary Movie S1) and were less motile in single-cell migration assays (Fig. 6b and Supplementary Movie S2). Scratch-wound assays confirmed the decreased cell velocity of β_1-TT/AA-expressing and SNX17-depleted cells and indicated a higher persistence when compared with β_1 wt fibroblasts (Fig. 6c). Fibroblasts lacking β_1 integrins barely migrated under these conditions (Fig. 6b,c). Expression of shRNA-resistant wt SNX17 in SNX17-depleted cells rescued the spreading and migration defects, whereas SNX17QW/AA did not (Fig. 6a,b). Despite these differences, focal adhesion size and F-actin distribution were not significantly altered in cells expressing β_1 TT/AA integrins or lacking SNX17 (Supplementary Fig. S5). Interestingly, expression of β_1 8xKR±TT/AA + $\alpha_5$4xKR restored cell spreading but not cell migration (Fig. 6d,e). Thus, SNX17 modulates several integrin-mediated functions in fibroblasts.

DISCUSSION

The present study identified a spatiotemporally controlled series of β_1-integrin/protein interactions in which the TT788/789 and the

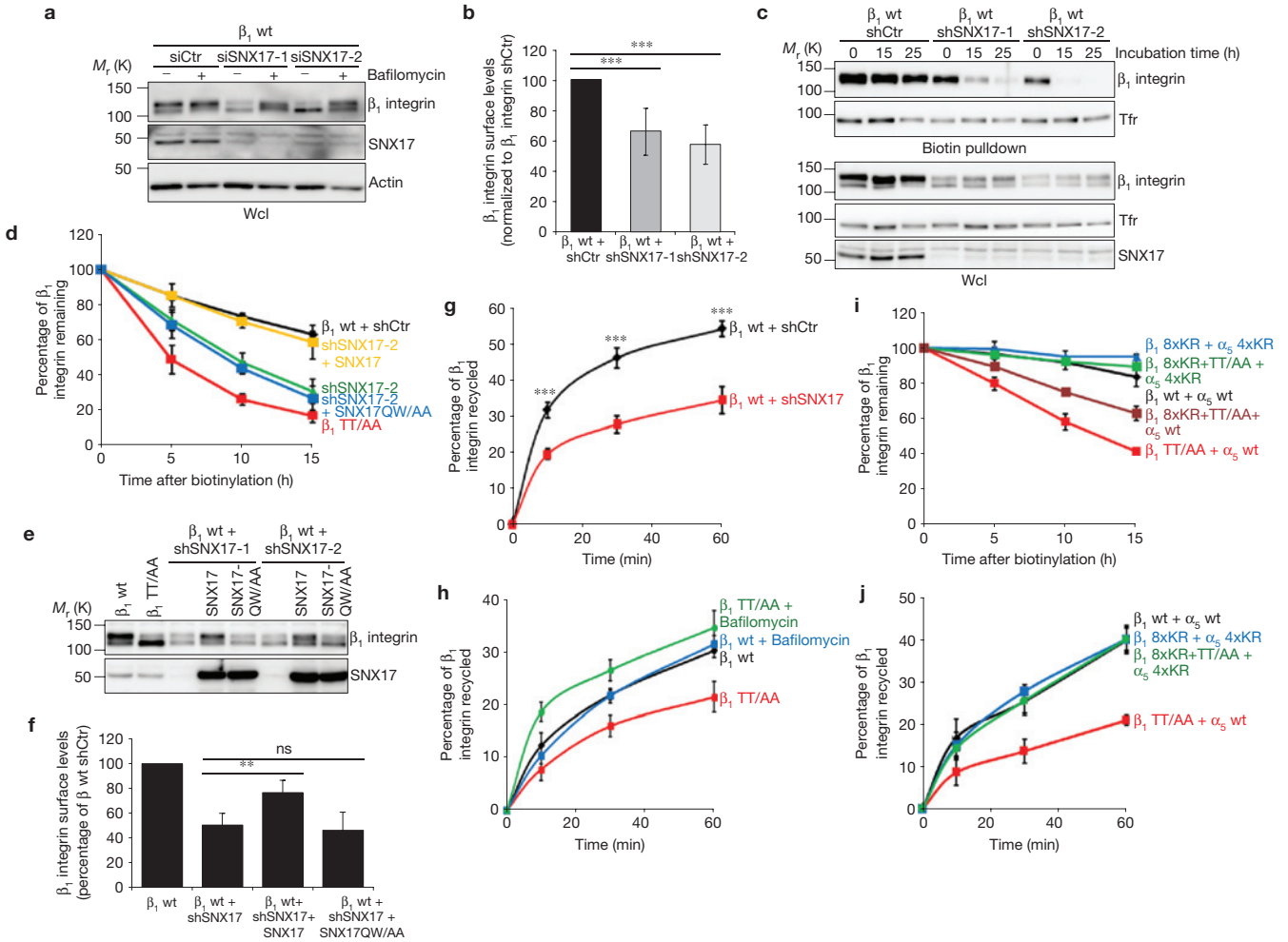

Figure 5 Depletion of SNX17 reduces surface levels of β_1 integrins. (**a**) Western blot analysis of control (siCtr) or two siSNX17-transfected cells (siSNX17-1 and siSNX17-2) treated with or without bafilomycin for 20 h. Actin served as loading control. (**b**) Quantification of β_1 surface levels in control and SNX17-depleted cells determined by FACS (mean ± s.d.; $n = 9$; $^{***}P < 0.0001$). (**c**,**d**) Degradation of cell-surface integrins was determined by biotin pulldown and western blot analysis (**c**) or capture-ELISA (**d**) (mean ± s.d.; $n = 5$). SNX17 levels in the shSNX17-2 knockdown cell line were restored by re-expressing either siRNA-insensitive wt SNX17 or SNX17QW/AA. (**e**) Western blot analysis of cell lysates derived from the indicated β_1-integrin-expressing and SNX17-depleted cells. SNX17 levels were restored in the SNX17-depleted cell lines by re-expressing either siRNA-insensitive wt SNX17 or SNX17QW/AA. (**f**) β_1-integrin surface levels in SNX17-depleted cells were restored by re-expressing siRNA-insensitive wt SNX17 but not with SNX17QW/AA (mean ± s.d.; $n = 3$; $^{**}P = 0.0079$; ns, not significant). (**g**) Quantification of β_1-integrin recycling in SNX17-depleted cells by capture-ELISA (mean ± s.e.m.; $n = 7$; $^{***}P < 0.0008$). Note the strong reduction in the level of β_1-integrin recycling after SNX17 depletion. (**h**) β_1-integrin recycling is restored to wt levels in β_1 TT/AA cells treated with bafilomycin. The quantity of biotinylated β_1 integrin remaining within the cells was determined by capture-ELISA using β_1-integrin-specific antibodies (mean ± s.e.m.; $n = 3$). (**i**) Quantification of the stability of cell-surface β_1 integrins by capture-ELISA. The indicated cell lines were surface biotinylated and incubated under starving conditions (mean ± s.d.; $n = 3$). (**j**) Quantification of β_1-integrin recycling determined by capture-ELISA. Cells express either α_5 wt and β_1 wt or $\alpha_5\beta_1$ with K > R-mutant tails (mean ± s.e.m.; $n = 4$). All P values, Student's t-test. Uncropped images of blots are shown in Supplementary Fig. S6.

membrane-distal NxxY motif of the β_1-integrin tail control the functions of β_1 integrins at the plasma membrane and subsequently their sorting from early endosomes back to the plasma membrane. Kindlins bind these motifs with the F3-FERM subdomain and the plasma membrane with the PH domain and promote β_1-integrin activity and linkage to actin dynamics[28,29]. Following internalization, β_1 integrins release Kindlins from their tails and are transferred into early endosomes where the free Kindlin-binding site recruits SNX17, which prevents β_1-integrin routing to lysosomes (Fig. 6f). Thus, the consecutive usage of the Kindlin-binding site first by Kindlins at the plasma membrane and then by SNX17 at early endosomes could couple integrin function with integrin quality control. If so, one would predict that a major role of integrin internalization and recycling is to sort functional integrins for re-use and non-functional integrins (for example, damaged by actomyosin-mediated tension) for degradation.

SNX17 is a member of the SNX family of proteins, which contain a PX domain that serves as a phosphoinositide-binding motif to aid SNX recruitment to phosphoinositide-enriched endosomal membranes[30]. SNX17 harbours the characteristic PX domain at the amino terminus and a FERM domain at the carboxy terminus, which binds NPxY motifs with its phosphotyrosine (PTB)-related F3 subdomain[20]. The

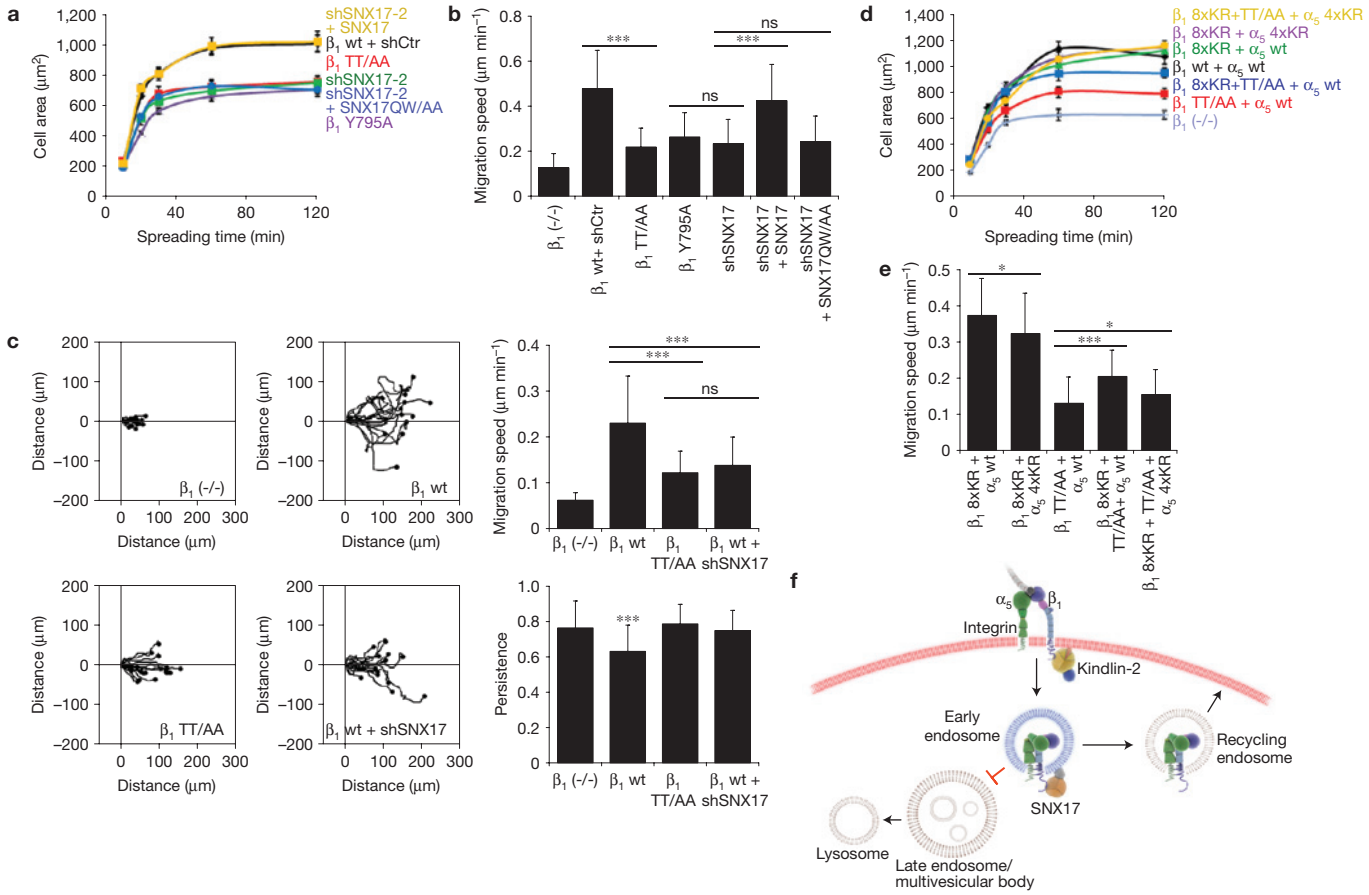

Figure 6 SNX17 is required for β_1-integrin function. (**a**) Quantification of spreading area of the indicated cell lines (mean ± s.e.m. of two independent experiments, $n = 40$ cells). (**b**) Quantification of single-cell migration velocity of the indicated cell lines extracted from time-lapse microscopy recordings by single-cell tracking (mean ± s.d. of three independent experiments, $n = 82$ cells; $^{***}P < 0.0001$; ns, not significant). (**c**) Migration analysis of β_1 wt, β_1 (−/−), β_1 TT/AA and SNX17-depleted cells in a scratch assay by time-lapse video microscopy. The movement of individual cells into the wound was followed using cell-tracking software and representative trajectories are shown (left panels). The speed (distance migrated per minute; upper right) and persistence of migration of cells (lower right) were quantified from the track plots (means ± s.d. of 52 cells analysed in six individual wounds of two independent experiments; $^{***}P < 0.0001$; ns, not significant). (**d**) Quantification of spreading area of the indicated cell lines (mean ± s.e.m. of two independent experiments, $n = 40$ cells). (**e**) Quantification of single-cell migration velocity of the indicated cell lines extracted from time-lapse microscopy recordings by single-cell tracking (mean ± s.d. of three independent experiments, $n = 60$ cells; $^{***}P < 0.0001$; $^{*}P < 0.0325$). All P values, Mann–Whitney U-test. (**f**) Model of serial Kindlin and SNX17 binding to the β_1-integrin cytoplasmic domain to regulate integrin affinity and trafficking. Kindlins bind the β_1-integrin tail with their FERM domain and to PIP2/PIP3 in the plasma membrane (red) with their PH domain to regulate the ligand affinity of integrins. Following integrin internalization, Kindlins are dislodged and SNX17 is recruited to the unoccupied Kindlin-binding site in the β_1 tail in endosomes to prevent β_1-integrin degradation and to promote their recycling back to the cell surface. The β_1-tail/SNX17 interaction in endosomes is supported by the interaction of the SNX17 PX domain with PtdIns(3)P enriched in endosomal membranes (blue).

recruitment of SNX17 to NPxY motifs was shown to be required for turnover of several transmembrane proteins including the low-density lipoprotein receptor[22,23] (LDLR), LDLR-related protein 1 (LRP1; refs 24,31), P-selectin[25,32] and the amyloid precursor protein (APP; ref. 26). However, whether SNX17 promotes their trafficking to the plasma membrane or prevents their degradation is still unclear. We found that inhibition of lysosomal degradation restored β_1 TT/AA recycling rates, indicating that the primary function of SNX17 binding to β_1-integrin tails is to prevent their degradation rather than to promote recycling (Fig. 6f). How SNX17 inhibits lysosomal degradation of β_1 integrin is unclear and needs to be addressed in future. One possibility is that SNX17 prevents integrin sorting into inner vesicles of multi-vesicular bodies, a pre-requisite for degradation by the lysosome, for example by recruiting a deubquitinase that removes ubiquitin moieties from integrin tails required to interact with components of the ESCRT machinery[33]. Alternatively, it is possible that SNX17 prevents access of the ESCRT machinery to β_1 integrins.

The lethality of the β_1 TT/AA and distal Y795A mice results from a combination of functional impairments including defective integrin activation, abnormal actin dynamics and decreased integrin recycling. The reduced adhesion, spreading and migration of SNX17-depleted cells indicate that β_1 functions are severely impaired when their degradation rate is not controlled by SNX17. The reduced β_1-TT/AA-integrin surface levels may also affect other functions including surface expression and signalling of growth factor receptors, co-internalization and re-secretion of fibronectin, and maybe other ECM proteins[11,34]. □

METHODS

Methods and any associated references are available in the online version of the paper at www.nature.com/naturecellbiology

Note: Supplementary Information is available on the Nature Cell Biology website

ACKNOWLEDGEMENTS

We thank J. Norman and R. Ruppert for help with recycling assays and cell sorting, C. Boulegue for mass spectrometry analysis, M. Iglesias for artwork, C. Franke for His–Kindlin-2 purification and R. Zent, A. Pozzi and D. Teis for discussions and critically reading the manuscript. This work was supported by the Deutsche Forschungsgemeinschaft (SFB-914), the Tiroler Zukunftsstiftung and the Max Planck Society.

AUTHOR CONTRIBUTIONS

R.T.B. and C.S. designed and carried out the experiments; A.M. and R.T.B. carried out the proteomics screen; H.M. generated the knock-in mice; M.W. generated Kindlin-null fibroblasts; H-Y.T. carried out the GST-pulldown experiments and contributed to the immunostainings; R.T.B., C.S. and R.F. wrote the manuscript; R.F. initiated and supervised the studies, and designed the experiments.

COMPETING FINANCIAL INTERESTS

The authors declare no competing financial interests.

Published online at www.nature.com/naturecellbiology
Reprints and permissions information is available online at www.nature.com/reprints

1. Hynes, R. O. Integrins: bidirectional, allosteric signaling machines. *Cell* **110,** 673–687 (2002).
2. Moser, M., Legate, K. R., Zent, R. & Fässler, R. The tail of integrins, talin, and kindlins. *Science* **324,** 895–899 (2009).
3. Shattil, S. J., Kim, C. & Ginsberg, M. H. The final steps of integrin activation: the end game. *Nat. Rev. Mol. Cell Biol.* **11,** 288–300 (2010).
4. Calderwood, D. A. *et al.* The phosphotyrosine binding-like domain of talin activates integrins. *J. Biol. Chem.* **277,** 21749–21758 (2002).
5. Calderwood, D. A. *et al.* The Talin head domain binds to integrin β subunit cytoplasmic tails and regulates integrin activation. *J. Biol. Chem.* **274,** 28071–28074 (1999).
6. Ma, Y. Q., Qin, J., Wu, C. & Plow, E. F. Kindlin-2 (Mig-2): a co-activator of β_3 integrins. *J. Cell Biol.* **181,** 439–446 (2008).
7. Montanez, E. *et al.* Kindlin-2 controls bidirectional signaling of integrins. *Genes Dev.* **22,** 1325–1330 (2008).
8. Moser, M. *et al.* Kindlin-3 is required for β_2 integrin-mediated leukocyte adhesion to endothelial cells. *Nat. Med.* **15,** 300–305 (2009).
9. Moser, M., Nieswandt, B., Ussar, S., Pozgajova, M. & Fässler, R. Kindlin-3 is essential for integrin activation and platelet aggregation. *Nat. Med.* **14,** 325–330 (2008).
10. Caswell, P. T., Vadrevu, S. & Norman, J. C. Integrins: masters and slaves of endocytic transport. *Nat. Rev. Mol. Cell Biol.* **10,** 843–853 (2009).
11. Sung, B. H., Zhu, X., Kaverina, I. & Weaver, A. M. Cortactin controls cell motility and lamellipodial dynamics by regulating ECM secretion. *Curr. Biol.* **21,** 1460–1469 (2011).
12. Roberts, M. S., Woods, A. J., Dale, T. C., Van Der Sluijs, P. & Norman, J. C. Protein kinase B/Akt acts via glycogen synthase kinase 3 to regulate recycling of α_v β_3 and $\alpha_5\beta_1$ integrins. *Mol. Cell. Biol.* **24,** 1505–1515 (2004).
13. Woods, A. J., White, D. P., Caswell, P. T. & Norman, J. C. PKD1/PKCmu promotes $\alpha_v\beta_3$ integrin recycling and delivery to nascent focal adhesions. *EMBO J.* **23,** 2531–2543 (2004).
14. Margadant, C., Monsuur, H. N., Norman, J. C. & Sonnenberg, A. Mechanisms of integrin activation and trafficking. *Curr. Opin. Cell Biol.* **23,** 607–614 (2011).
15. Lobert, V. H. *et al.* Ubiquitination of $\alpha_5\beta_1$ integrin controls fibroblast migration through lysosomal degradation of fibronectin-integrin complexes. *Dev. Cell* **19,** 148–159 (2010).
16. Ussar, S. *et al.* Loss of Kindlin-1 causes skin atrophy and lethal neonatal intestinal epithelial dysfunction. *PLoS Genet.* **4,** e1000289 (2008).
17. Harburger, D. S., Bouaouina, M. & Calderwood, D. A. Kindlin-1 and -2 directly bind the C-terminal region of β integrin cytoplasmic tails and exert integrin-specific activation effects. *J. Biol. Chem.* **284,** 11485–11497 (2009).
18. Ong, S. E. *et al.* Stable isotope labeling by amino acids in cell culture, SILAC, as a simple and accurate approach to expression proteomics. *Mol. Cell Proteomics* **1,** 376–386 (2002).
19. Mann, M. Functional and quantitative proteomics using SILAC. *Nat Rev. Mol. Cell Biol.* **7,** 952–958 (2006).
20. Ghai, R. *et al.* Phox homology band 4.1/ezrin/radixin/moesin-like proteins function as molecular scaffolds that interact with cargo receptors and Ras GTPases. *Proc. Natl Acad. Sci. USA* **108,** 7763–7768 (2011).
21. Tadokoro, S. *et al.* Talin binding to integrin β tails: a final common step in integrin activation. *Science* **302,** 103–106 (2003).
22. Burden, J. J., Sun, X. M., Garcia, A. B. & Soutar, A. K. Sorting motifs in the intracellular domain of the low density lipoprotein receptor interact with a novel domain of sorting nexin-17. *J. Biol. Chem.* **279,** 16237–16245 (2004).
23. Stockinger, W. *et al.* The PX-domain protein SNX17 interacts with members of the LDL receptor family and modulates endocytosis of the LDL receptor. *EMBO J.* **21,** 4259–4267 (2002).
24. Van Kerkhof, P. *et al.* Sorting nexin 17 facilitates LRP recycling in the early endosome. *EMBO J.* **24,** 2851–2861 (2005).
25. Knauth, P. *et al.* Functions of sorting nexin 17 domains and recognition motif for P-selectin trafficking. *J. Mol. Biol.* **347,** 813–825 (2005).
26. Lee, J. *et al.* Adaptor protein sorting nexin 17 regulates amyloid precursor protein trafficking and processing in the early endosomes. *J. Biol. Chem.* **283,** 11501–11508 (2008).
27. Van Weert, A. W., Geuze, H. J., Groothuis, B. & Stoorvogel, W. Primaquine interferes with membrane recycling from endosomes to the plasma membrane through a direct interaction with endosomes which does not involve neutralisation of endosomal pH nor osmotic swelling of endosomes. *Eur. J. Cell Biol.* **79,** 394–399 (2000).
28. Meves, A., Stremmel, C., Gottschalk, K. & Fassler, R. The Kindlin protein family: new members to the club of focal adhesion proteins. *Trends Cell Biol.* **19,** 504–513 (2009).
29. Liu, J. *et al.* Structural basis of phosphoinositide binding to kindlin-2 protein pleckstrin homology domain in regulating integrin activation. *J. Biol. Chem.* **286,** 43334–43342 (2011).
30. Cullen, P. J. Endosomal sorting and signalling: an emerging role for sorting nexins. *Nat. Rev. Mol. Cell Biol.* **9,** 574–582 (2008).
31. Donoso, M. *et al.* Polarized traffic of LRP1 involves AP1B and SNX17 operating on Y-dependent sorting motifs in different pathways. *Mol. Biol. Cell* **20,** 481–497 (2009).
32. Williams, R. *et al.* Sorting nexin 17 accelerates internalization yet retards degradation of P-selectin. *Mol. Biol. Cell* **15,** 3095–3105 (2004).
33. Raiborg, C. & Stenmark, H. The ESCRT machinery in endosomal sorting of ubiquitylated membrane proteins. *Nature* **458,** 445–452 (2009).
34. Caswell, P. T. *et al.* Rab-coupling protein coordinates recycling of $\alpha_5\beta_1$ integrin and EGFR1 to promote cell migration in 3D microenvironments. *J. Cell Biol.* **183,** 143–155 (2008).

METHODS

Mouse strains. The targeting constructs with the β_1-integrin threonine-to-alanine mutation in positions 788 and 789 (β_1 TT/AA) and the tyrosine-to-alanine mutation in position 795 (β_1 Y795A) were generated as previously described[35]. All animal studies were approved by the Regierung von Oberbayern.

Antibodies. The following antibodies were used for western blotting (WB) and immunofluorescence (IF): actin (A-2066, Sigma; 1:3,000 for WB), β_1 integrin (MAB1997, MB1.2, Chemicon; 1:400 for IF), β_3 integrin (04-1060, EP2417Y, Millipore; 1:1,000 for WB), β-catenin (C2206, Sigma; 1:800 for IF), E-cadherin (13-1900, ECCD-2, Zymed; 1:200 for IF), laminin111 (ab30320, Abcam: 1:400 for IF), EEA1 (610457, BD Transduction Laboratories; 1:100 for IF), GAPDH (CB1001, 6C5, Calbiochem; 1:5,000 for WB), Kindlin-2 (K3269, Sigma; 1:1,000 for WB), Lamp1 (provided by L. Huber, Medical University Innsbruck, Austria; 1:100 for staining), paxillin (610051, 349, BD Transduction Laboratories), SNX17 (10275-1-AP, Proteintech; 1:1,000 for WB), Talin-1 (T3287, 8d4, Sigma; 1:1,000 for WB), Tfr (13-6,800, H68.4, Invitrogen, 1:1,000 for WB) and ubiquitin (3936, P4D1, Cell Signaling; 1:1,000 for WB). Kindlin-1 (1:5,000 for WB), Kindlin-3 (1:5,000 for WB) and β_1-integrin (1:10,000 for WB) antibodies used for western blotting are home-made[36,37]. Phalloidin (A12379 and A22287, Molecular Probes; 1:400 for IF) was used to stain F-actin. DAPI (Sigma) was used to stain nuclei.

The following antibodies were used for flow cytometry: β_1-integrin PE (102207, HMβ1-1, BioLegend; 1:400), β_1-integrin biotin (555004, Ha2/5, BD Pharmingen; 1:400), β_1-integrin 9EG7 (550531, 9EG7, BD Pharmingen; 1:100), β_3-integrin PE (12-0611, 2C9.G3, eBioscience; 1:400), β_4-integrin PE (MCA2369, 346-11A, Serotec; 1:400), α_2-integrin FITC (554999, Ha1/29, BD Pharmingen; 1:400), α_5-integrin PE (557447, 5H10-27, BD Pharmingen; 1:400), α_5-integrin biotin (557446, 5H10-27, BD Pharmingen), α_6-integrin PE (555736, GoH3, BD Pharmingen) and α_v-integrin PE (551187, RMV-7, BD; 1:400).

Plasmids and constructs. Point mutations into the β_1-integrin (TT788/789AA, Y783A, Y795A, 8xKR (K752R, K765R, K768R, K770R, K774R, K784R, K794R, K798R), 8xKR+TT788/789AA), α_5-integrin (4xKR (K1022R, K1027R, K1038R, K1042R)) and SNX17 (QW360/361AA) cDNA were introduced by site-directed mutagenesis. For stably expressing the β_1-integrin cDNAs (wt, TT788/789AA, Y783A, Y795A, 8xKR, 8xKR+TT/AA), the human α_5 integrin (wt, 4xKR, α_5–eGFP) and the mouse SNX17 (wt, Flag-tagged, eGFP-tagged and mCherry-tagged), we used the retroviral expression vector pCLMFG or pLZRS. For recombinant expression of GST-tagged SNX17, wt SNX17 and SNX17QW360/361AA, cDNA was cloned into the pGEX-6P-1 vector (GE Healthcare). Lamp1–mRFP and Rab7–mRFP vectors were obtained from J. Norman (Beatson Institute, Glasgow, UK), and Rab5a–GFP was provided by L. Huber (Medical University Innsbruck, Austria) and transiently expressed by transfection with Lipofectamine 2000 (Invitrogen).

For stably depleting SNX17 expression, shRNA target sequences were introduced into the pSuper.Retro vector (OligoEngine) to produce retroviral particles: 5′-GTACATGCAAGCTGTTCGG-3′ (shSNX17-1), 5′-GATTGTGCTCAGAAAGAGT-3′ (shSNX17-2).

To obtain a GFP-tagged Kindlin-2, the Kindlin-2 cDNA (ref. 36) was ligated in frame with the GFP using sequence- and ligation-independent cloning[38]. The CAG promoter, GFP fusion and SV40 polyA were flanked by ITR elements; thus, co-transfection of this construct with a sleeping beauty SB100x expression vector[39] resulted in transposase-mediated genomic integration of this DNA sequence.

Cell lines. Heterozygous β_1 TT/AA mice were intercrossed with homozygous β_1-floxed mice and mouse embryonic fibroblasts were isolated from E9.5 embryos, immortalized with the SV40 large T antigen and cloned before deletion of the floxed β_1-integrin allele by adenoviral Cre transduction. Disruption of the β_1 allele and expression of the β_1 TT/AA were checked by PCR. To generate β_1-null rescue cell lines, β_1 wt or β_1 mutant variants were virally re-expressed in β_1-null fibroblasts derived from floxed β_1 parental cells.

Fibroblasts homozygous for floxed *kindlin-1* and *-2* genes were isolated from kidneys of 21-day-old double-floxed mice (whose generation will be described elsewhere), immortalized as described above and cloned. To obtain Kindlin-1 and -2 double-null cells, the floxed *kindlin* alleles were removed by adenoviral Cre transduction.

Transient and stable transfection/transduction. Cells were transiently transfected with Lipofectamine 2000 (Invitrogen) according to the manufacturer's protocol. To generate stable cell lines, VSV-G pseudotyped retroviral vectors were produced by transient transfection of HEK293T (human embryonic kidney) cells. Viral particles were concentrated from cell culture supernatant as described previously[40] and used for infection.

Embryo isolation and histological analysis. For whole-mount analysis, staged embryos (E6.5 to E9.5) were dissected in ice-cold PBS. For histological analysis, decidua swellings were isolated, fixed in 4% paraformaldehyde (PFA) and embedded in paraffin. Sections were stained with haematoxilin and eosin or antibodies as indicated.

Whole-mount immunohistochemistry. Embryos were dissected in cold PBS and fixed in 4% PFA for 2 h at 4 °C. Samples were incubated in 0.5% NP-40/PBS for 20 min and in PBSST (0.1% Triton X-100 and 5% BSA in PBS) for 2 h at 4 °C and then incubated with the primary and secondary antibody, both overnight at 4 °C. Nuclei were stained with DAPI solution for 30 min. Finally, embryos were dehydrated by increasing methanol concentrations, cleared in benzyl alcohol/benzyl benzoate (1:2) and imaged with a confocal microscope (DMIRE2; Leica) using Leica Confocal Software (version 2.5 Build 1227). After imaging, embryos were rehydrated for genotyping.

ES cells and embryoid bodies. ES cells were isolated and cultured as previously described[41]. Embryoid bodies were generated as described previously[41].

Metabolic labelling. Cells were grown overnight to 80% confluency and incubated for 30 min at 37 °C in methionine/cysteine-free labelling media containing 10% dialysed FBS. For pulse labelling, the cells were incubated for 30 min at 37 °C in labelling medium containing [^{35}S]methionine/cysteine (200 µCi/10 cm plate, EasyTag Express ^{35}S Protein Labeling Mix, PerkinElmer). After labelling, the cells were either immediately collected (time 0) or chased for 4 h, 8 h and 22 h in regular growth medium containing 10% FBS. Cells were lysed in immunoprecipitation buffer (50 mM Tris–HCl (pH 7.5), 150 mM NaCl, 1% Triton X-100, 0.1% sodium deoxycholate, 1 mM EDTA and protease inhibitors) and cleared by centrifugation. For β_1 immunoprecipitation, lysates were first incubated with β_1 antibodies for 1 h on ice followed by incubation with protein G Sepharose (Sigma) for 2 h at 4 °C with gentle agitation. After several washes with lysis buffer, proteins were eluted from the beads by boiling with Laemmli sample buffer and subjected to SDS–PAGE. The gels were fixed, dried and exposed to film.

Turnover of surface integrins. The half-life of surface proteins was determined by biotinylation. Briefly, fibroblasts were grown to 80% confluence, washed twice in cold PBS and surface biotinylated with 0.2 mg ml^{-1} sulpho-NHS-LC-biotin (Thermo Scientific) in PBS for 45 min at 4 °C. Following washes with cold PBS, the cells were incubated in regular growth medium for 0, 5, 10 and 15 h at 37 °C. Cells were lysed in immunoprecipitation buffer and biotinylated proteins were pulled down with streptavidin–Sepharose (GE Healthcare). After three washes with lysis buffer, samples were analysed by SDS–PAGE and western blotting. For capture-ELISA, cells were lysed in a low volume of lysis buffer (75 mM Tris, 200 mM NaCl, 7.5 mM EDTA and 7.5 mM EGTA, 1.5% Triton X-100, 0.75% Igepal CA-630 and protease inhibitors).

Integrin-trafficking assays. Integrin-trafficking assays were performed as described previously[42].

Capture ELISA. Maxisorb 96-well plates (Life Technologies) were coated overnight with anti-β_1-integrin antibody (MAB1997, Chemicon; 1:250) in carbonate buffer at 4 °C. Unspecific binding was blocked by 5% BSA in PBS/0.1% Tween-20 (PBS-T) for 1–2 h at room temperature before adding 50 µl cell lysate for incubation overnight at 4 °C to capture integrins. Following extensive washes with PBS-T, plates were incubated with streptavidin–HRP in 1% BSA in PBS-T for 1 h at 4 °C. Biotinylated β_1 integrin was detected after several washing steps by chromogenic reaction with ABTS peroxidase substrate (Vector Laboratories).

Selective immunoprecipitations. Selective isolation of β_1 integrins on the cell surface and in endocytic vesicles was achieved by cell-surface immunoprecipitation. Cell-surface β_1 integrins of live cells were labelled with a rabbit anti-β_1-integrin antibody (home-made; 1:1,500) for 1 h on ice. After two washes with ice-cold PBS to remove unbound antibody, cells were incubated for 20 min in medium with or without 0.5 mM primaquine to inhibit integrin recycling to the cell surface[42]. Cells were then washed twice with PBS, lysed in immunoprecipitation buffer and cleared by centrifugation. β_1-integrin immune complexes were pulled down by incubation with protein G Sepharose (Sigma) for 2 h at 4 °C with gentle agitation. After several washes with lysis buffer, proteins were subjected to SDS–PAGE and western blot analysis.

DOI: 10.1038/ncb2501

SILAC-based peptide pulldowns. Pulldowns were performed as described previously[43] with β_1 wt cytoplasmic tail peptides (758–598: HDRREFAKFEKEKM-NAKWDTGENPIYKSAVTTVVNPKYEGK-OH), β_1 TT/AA tail peptide (HDR-REFAKFEKEKMNAKWDTGENPIYKSAVAAVVNPKYEGK-OH), β_1 Y795A tail peptide (HDRREFAKFEKEKMNAKWDTGENPIYKSAVTTVVNPKAEGK-OH), a scrambled peptide (EYEFEPDKVDTGAKGTKMAKNEKKFRNYTVHNIWESRK-VAP-OH) and α_5 peptide (KLGFFKRSLPYGTAMEKAQLKPPATSDA-OH). All peptides were desthiobiotinylated. Before use, peptides were immobilized on 75 µl Dynabeads MyOne Streptavidine C1 (10 mg ml^{-1}, Invitrogen).

After cell-lysate generation and incubation with tail peptides, proteins were eluted and precipitated as described previously[43]. The protein pellet was dissolved in SDS–PAGE sample buffer and separated on a 4–15% gradient SDS–PAGE gel. The gel was stained with Coomassie blue using the GelCode Blue Safe Protein Stain reagent (Thermo Scientific) and used for mass analysis.

Expression and purification of recombinant proteins. Plasmids encoding GST–SNX17 or GST–SNX17QW/AA were transformed into BL21(DE3) Arctic Express *Escherichia coli*, and protein expression was induced with 1 mM IPTG. Afterwards, cells were pelleted, lysed and centrifuged. Supernatants were incubated with glutathione Sepharose beads (GST-binding resin, Novagen) and GST-tagged proteins were eluted according to the manufacturer's instruction.

Plasmid coding for His-tagged Kindlin-2 was transformed into BL21 T1 pRARE bacteria. Supernatants were generated as described above, incubated with His-Select Ni Affinity gel (Sigma) and His-tagged Kindlin-2 was eluted and subjected to gel filtration for further purification.

For pulldowns, synthetic peptides were immobilized on 20 µl Dynabeads MyOne Streptavidine C1 (10 mg ml^{-1}, Invitrogen) for 3 h at 4 °C, incubated with 2% BSA in Mammalian Protein Extraction Reagent (Thermo Scientific) for 30 min to block unspecific binding before adding 50 ng recombinant GST-tagged SNX17 protein and further incubation on a rotator for 2 h at 4 °C. For competition experiments, 50 ng GST–SNX17 and 500 ng His–Kindlin-2 or 500 ng BSA were incubated with the tail peptides for 3 h at 4 °C. After three washes with RIPA buffer, proteins were eluted from the beads by boiling with 80 µl SDS–PAGE sample buffer for 5 min, separated by SDS–PAGE gel and blotted with SNX17 antibody.

Quantitative PCR. RNA was isolated from cells using the RNeasy mini kit (Qiagen) and 1 µg of total RNA was transcribed into cDNA using the iScriptcDNA Synthesis kit (Bio-Rad). Quantitative PCR assays were performed with the iCycleriQ (Bio-Rad) using SYBR green and the following primers: β_1 integrin-forward (5′-atgccaaatcttgcggagaat-3′), β_1 integrin-reverse (5′-tttgctgcgattggtgacatt-3′), β_3 integrin-forward (5′-ccacacgaggcgtgaact c-3′), β_3 integrin-reverse (5′-cttcaggttacatcggggtga-3′), GAPDH-forward (5′-tcgtggatctgacgtgccgcctg-3′), GAPDH-reverse (5′-caccaccctgttgctgtagccgtat-3′).

Immunofluorescence microscopy. For immunostaining, cells were cultured on glass coated with 10 µg ml^{-1} fibronectin (Calbiochem). For the detection of endosomes, cells were fixed with 4% PFA/PBS for 15 min on ice, washed with PBS and permeabilized with 0.01% saponin/PBS for 10 min on ice. Cells were blocked with 3% BSA/PBS for 1 h followed by incubation with the primary antibody in 3% BSA/0.01% saponin/PBS overnight at 4 °C and secondary antibodies for 1 h at room temperature in the dark. All other staining was performed as described previously[44].

To determine the endocytic trafficking of β_1 integrins from the cell surface by surface labelling, cells were washed with cold PBS and incubated with an anti-β_1-integrin antibody (102202, HMβ1-1, BioLegend; 1:400) for 30 min on ice. Surface-bound antibody was allowed to internalize for different times at 37 °C in regular growth medium. At each time point, the samples were washed with cold PBS and the remaining antibody at the cell surface was removed by two acid washes (0.2 M acetic acid/0.5 M NaCl/PBS) for 2 min on ice. Subsequently, the cells were fixed, permeabilized and stained as described above.

Images were collected at room temperature by confocal microscopy (DMIRE2; Leica) with a ×63/1.4 objective using the Leica Confocal Software (version 2.5, build 1227) or collected with an AxioImager Z1 microscope (Zeiss) with a ×63/1.4 oil objective.

Time-lapse video microscopy of cell spreading and migration. Cell spreading and single-cell migration assays were done as described previously[44]. Cell spreading was also measured with cells seeded on fibronectin-coated glass slides, fixed with 4% PFA at 37 °C at indicated time points and stained with phalloidin–Alexa488 for F-actin. Images were taken with an AxioImager Z1 microscope (Zeiss, Germany) with a ×20 objective and the spreading area was calculated using MetaMorph 7 (Molecular Devices) imaging software.

For single-cell migration, the acquired images were analysed using the manual tracking plugin of ImageJ and the Chemotaxis and Migration Tool (v2.0) of the QWT project.

Cell-wounding assays were performed with confluent monolayers of cells cultured in fibronectin-coated 6-well dishes. Cells were serum-starved overnight before wounds were applied with a 200 µl plastic micropipette followed by thorough washing with PBS. Wound closure was imaged in serum-free medium at 15 min intervals overnight. The acquired images were analysed using the manual tracking plugin of ImageJ and the Chemotaxis and Migration Tool (v2.0) of the QWT project.

Images of live cells were recorded at 37 °C and 5% CO_2 on a Zeiss Axiovert 200 M (Zeiss, Germany) equipped with ×10/.3, ×20/.4 and ×40/.6 objectives, a motorized stage (Märzhäuser) and an environment chamber (EMBL Precision Engineering) with a cooled CCD (charge-coupled device) camera (Roper Scientific). Image acquisition and microscope control were carried out with MetaMorph software (Molecular Devices).

Statistics. Statistical analysis was performed using the GraphPad Prism software (version 5.00, GraphPad Software). Statistical significance was determined by the unpaired *t*-test or Mann–Whitney *U*-test as indicated. Results are expressed as the mean ± s.d. unless indicated otherwise.

35. Czuchra, A., Meyer, H., Legate, K. R., Brakebusch, C. & Fässler, R. Genetic analysis of β_1 integrin 'activation motifs' in mice. *J. Cell Biol.* **174,** 889–899 (2006).
36. Ussar, S., Wang, H. V., Linder, S., Fässler, R. & Moser, M. The Kindlins: subcellular localization and expression during murine development. *Exp. Cell Res.* **312,** 3142–3151 (2006).
37. Azimifar, S. B. *et al.* Induction of membrane circular dorsal ruffles requires co-signalling of integrin-ILK-complex and EGF receptor. *J. Cell Sci.* **125,** 435–448 (2012).
38. Li, M. Z. & Elledge, S. J. Harnessing homologous recombination in vitro to generate recombinant DNA via SLIC. *Nat. Methods* **4,** 251–256 (2007).
39. Mates, L. *et al.* Molecular evolution of a novel hyperactive Sleeping Beauty transposase enables robust stable gene transfer in vertebrates. *Nat. Genet.* **41,** 753–761 (2009).
40. Pfeifer, A., Kessler, T., Silletti, S., Cheresh, D. A. & Verma, I. M. Suppression of angiogenesis by lentiviral delivery of PEX, a noncatalytic fragment of matrix metalloproteinase 2. *Proc. Natl Acad. Sci. USA* **97,** 12227–12232 (2000).
41. Montanez, E. *et al.* Analysis of integrin functions in peri-implantation embryos, hematopoietic system, and skin. *Methods Enzymol.* **426,** 239–289 (2007).
42. Roberts, M., Barry, S., Woods, A., van der Sluijs, P & Norman, J. PDGF-regulated rab4-dependent recycling of $\alpha_v\beta_3$ integrin from early endosomes is necessary for cell adhesion and spreading. *Current Biol.* **11,** 1392–1402 (2001).
43. Meves, A. *et al.* β_1 integrin cytoplasmic tyrosines promote skin tumorigenesis independent of their phosphorylation. *Proc. Natl Acad. Sci. USA* **108,** 15213–15218 (2011).
44. Böttcher, R. T. *et al.* Profilin 1 is required for abscission during late cytokinesis of chondrocytes. *EMBO J.* **28,** 1157–1169 (2009).

nature cell biology

DOI: 10.1038/ncb2501

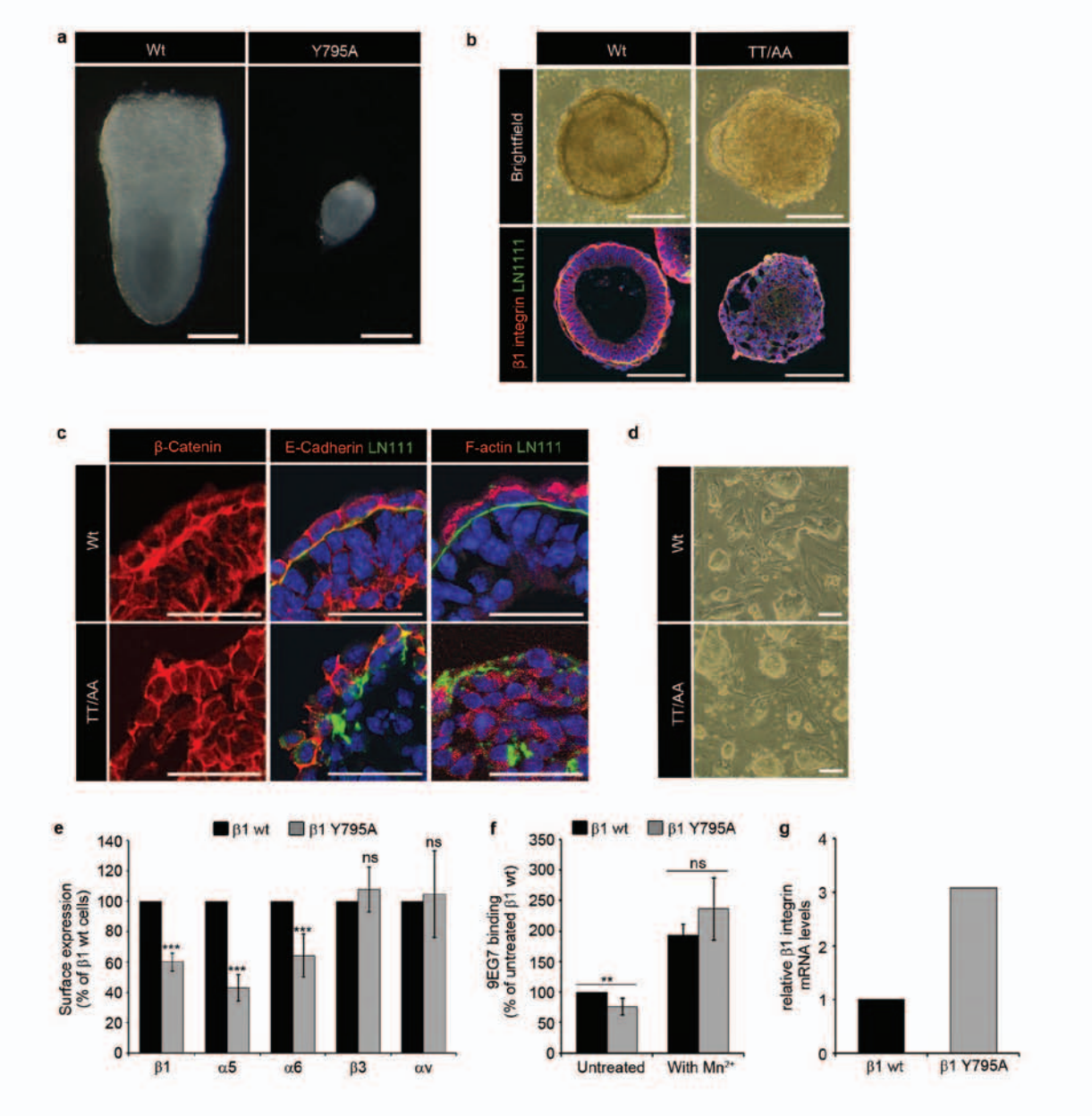

Figure S1 Defects of β1 TT/AA and β1 Y795A ES cells. **(a)** Brightfield images of E7.5 embryos without implantation chamber. **(b)** Upper panels show brightfield images of EBs on the 5th day of suspension culture. Lower panels show cryo-sections of EBs on the 5th day of suspension culture stained for β1 integrin (red) and laminin111 (green). Nuclei were counterstained with DAPI (blue). **(c)** Cryo sections of EBs on the 5th day of suspension culture stained for β-catenin, E-cadherin, F-actin and laminin111. Nuclei were counterstained with DAPI (blue). (**d**) ES cell colonies on feeder cells. (**e**) Expression of integrin subunits on ES cells determined by FACS (mean ± SD; n=5; ***p (student's t-test)≤0.0005; ns=not significant). **(f)** Integrin activation on ES cells measured by 9EG7 binding and corrected for total β1 integrin expression (mean ± SD; n=5; **p (student's t-test)=0.0043; ns=not significant). **(g)** Expression of β1 integrin mRNA in ES cells measured by qRT-PCR (n=2). Scale bar, 100 μm (a, b, d), 50 μm (c).

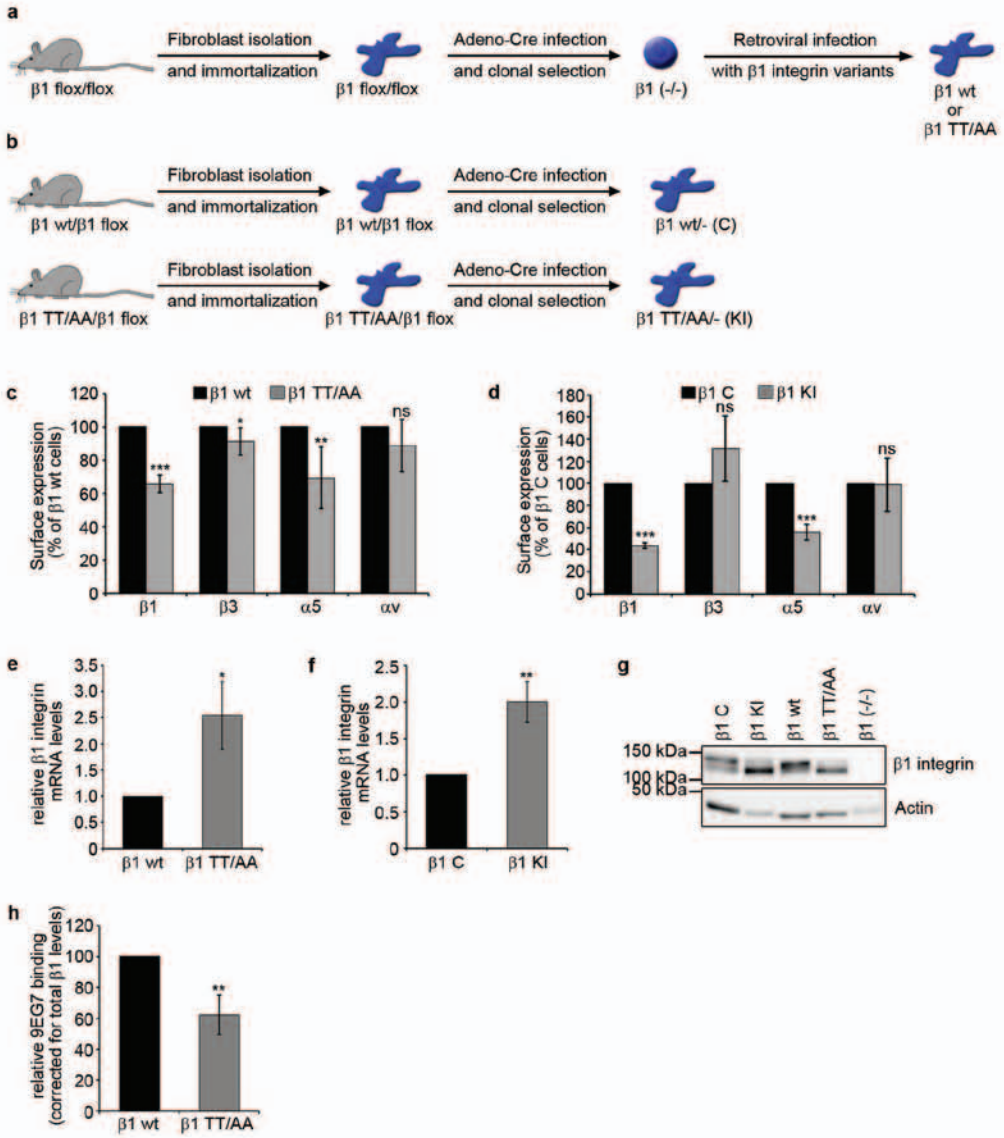

Figure S2 Characterization of fibroblasts expressing β1 TT/AA integrin. **(a, b)** Scheme depicting the generation of β1 wt and β1 TT/AA fibroblasts. β1 wt and β1 TT/AA fibroblasts were either obtained by retroviral expression of β1 variants in β1 null cells (a) or by immortalization of fibroblasts from mouse embryos (b). **(c, d)** Surface expression of different α and β integrin subunits on β1 wt and β1 TT/AA fibroblasts determined by FACS (mean ± SD; n=6 (c); n=4 (d); *p (student's t-test)<0.05, **p (student's t-test)=0.0022, ***p (student's t-test)<0.0001; ns=not significant). **(e, f)** β1 integrin mRNA levels determined by qRT-PCR (mean ± SD; n=3 with two independent cDNAs; *p (student's t-test)=0.015, **p (student's t-test)=0.0032). **(g)** Western blot analysis of fibroblast cell lines with antibodies against β1 integrin and actin. **(h)** β1 integrin activation measured by 9EG7 binding and corrected for β1 integrin expression (mean ± SD; n=4; **p (student's t-test)=0.0097).

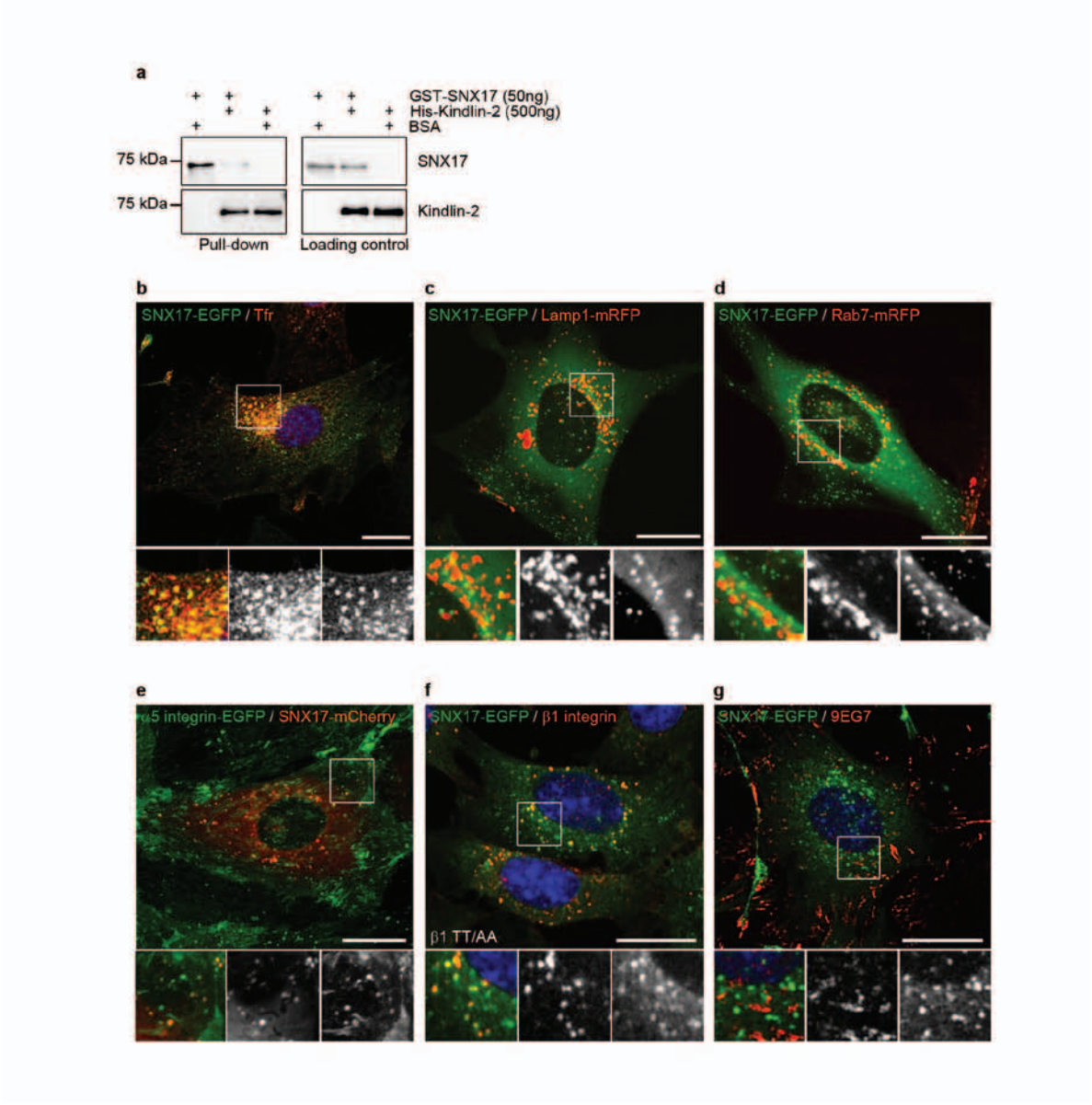

Figure S3 SNX17 localization in fibroblasts. **(a)** Streptavidin-bead pull-down assay with a biotinylated wild-type β1 integrin cytoplasmic tail peptide and recombinant GST-tagged SNX17 and His-tagged Kindlin-2. **(b)** Immunostaining of SNX17-EGFP expressing cells for Tfr (red). Nuclei were counterstained with DAPI (blue) (correlation coefficient 0.032 ± 0.121; mean ± SD of 13 cells analyzed). (**c, d**) SNX17-EGFP expressing cells were transfected with Lamp1-mRFP (c) and Rab7-mRFP (d) and the fluorescence distribution was determined in living cells by spinning disk confocal microscopy. Stills of movies are shown (correlation coefficient Rab7-mRFP -0.454 ± 0.106; mean ± SD of 15 cells analyzed). (**e**) Distribution of SNX17-mCherry and α5 integrin-EGFP in living cells determined by spinning disk confocal microscopy. A still of a movie is shown. (**f**) Distribution of β1 TT/AA integrins in SNX17-EGFP expressing cells after surface labeling with an anti-β1 integrin antibody and internalization for 15 min. Cells were fixed, stained and the fluorescence was determined with confocal microscopy. (**g**) Localization of active β1 integrins after surface labeling with a 9EG7 antibody and internalization for 15 min in SNX17-EGFP expressing cells. The fluorescence was determined with confocal microscopy. Scale bars, 20 μM.

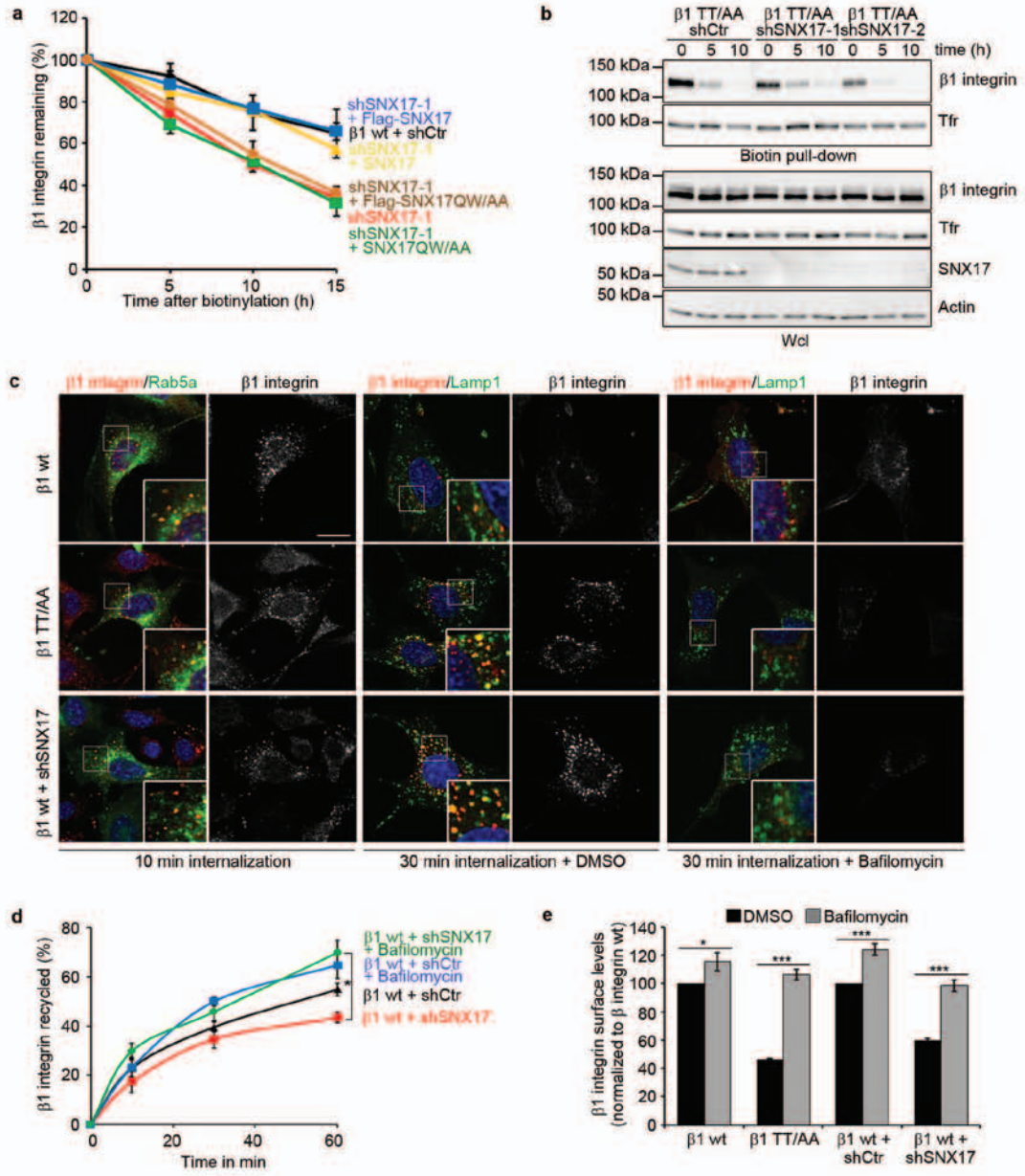

Figure S4 SNX17 regulates β1 integrin surface levels. **(a)** Stability of surface β1 integrin in the indicated cell lines determined by surface biotinylation followed by capture-ELISA (mean ± SD; n=3). SNX17 levels were restored in SNX17-depleted cells by re-expressing either siRNA-insensitive wt SNX17 or SNX17QW/AA. **(b)** SNX17-depleted β1 TT/AA expressing cells were surface biotinylated and incubated for the indicated time points, before biotinylated proteins were pulled-down with streptavidin-sepharose and analyzed by western blotting. (**c**) Localization of endogenous β1 integrin after surface labeling with an anti-β1 integrin antibody and internalization for 10 and 30 min in β1 wt, β1 TT/AA and SNX17-depleted cells, respectively treated with or without bafilomycin. Cells either expressed Rab5a-GFP or were fixed and stained with antibodies against Lamp1. Nuclei were counterstained with DAPI (blue). Scale bar, 20 μM. (**d**) Bafilomycin normalizes the recycling of β1 wt in SNX17-depleted cells. The quantity of biotinylated β1 integrin remaining within the cells was determined by capture-ELISA using β1 integrin specific antibodies (mean ± s.e.m.; n=3). (**e**) Quantification of β1 surface levels by FACS in indicated cell lines treated for 8 h with and without bafilomycin (mean ± SD; n=3; *p (student's t-test)=0.0133, ***p (student's t-test)<0.0006; ns=not significant).

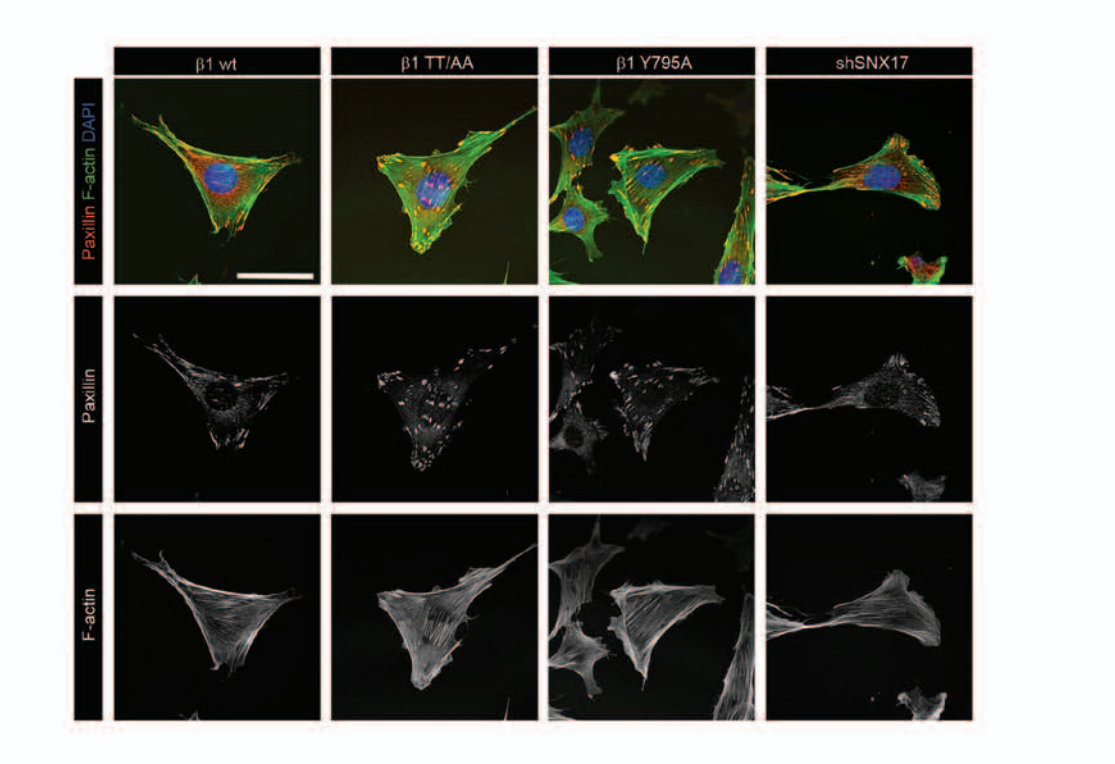

Figure S5 Focal adhesions and the actin cytoskeleton are not affected in β1 TT/AA, β1 Y795A and SNX17-depleted cells. β1 wt, β1 TT/AA, β1 Y795A and SNX17-depleted β1 wt cells were stained with an antibody against paxillin (red) and fluorescently labelled phalloidin to visualize F-actin (green). Nuclei were counterstained with DAPI (blue). Scale bar, 50 μM.

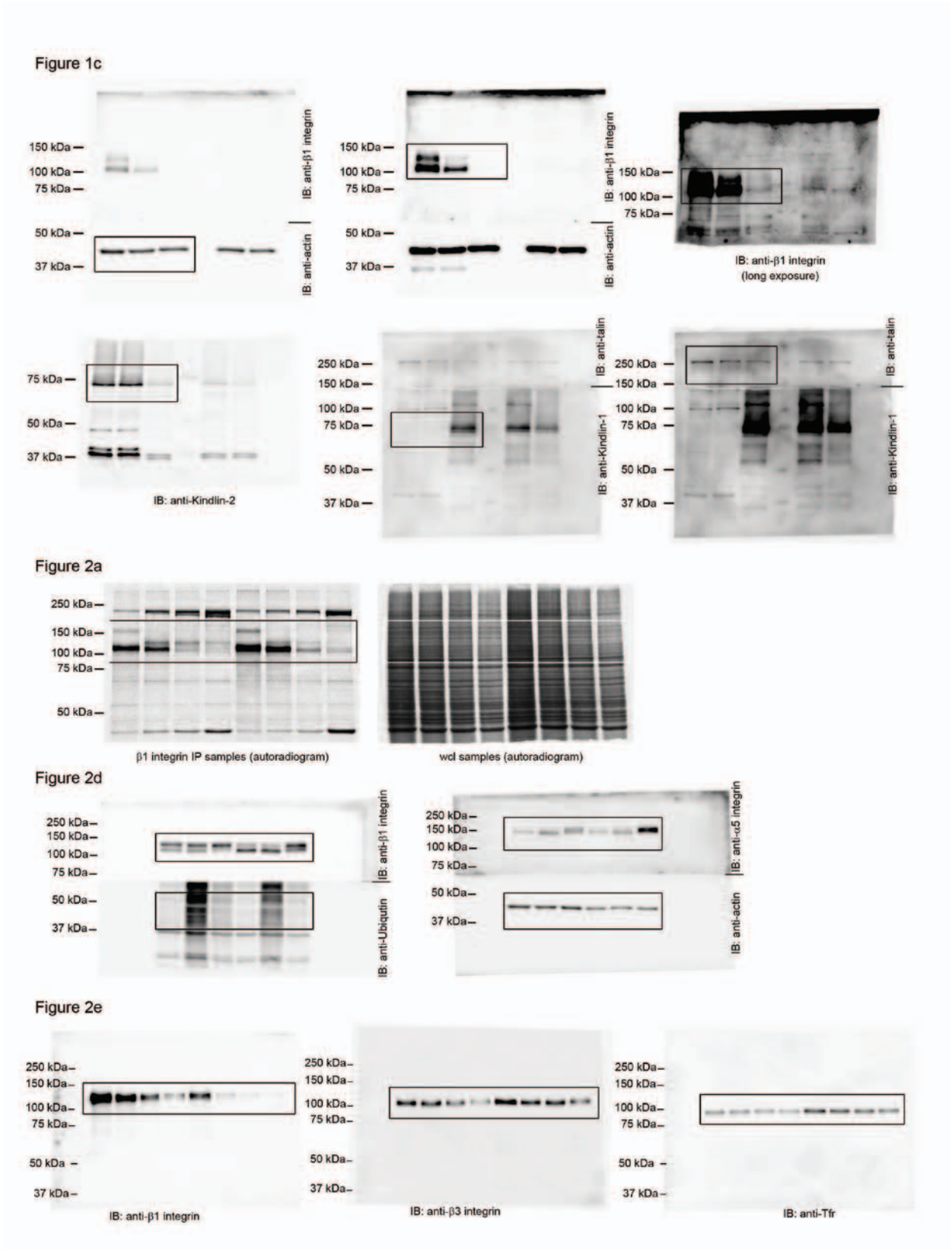

Figure S6 Full scans of the key immunoblots. Boxes indicate cropped images used in the figures and numbers indicate the molecular weight.

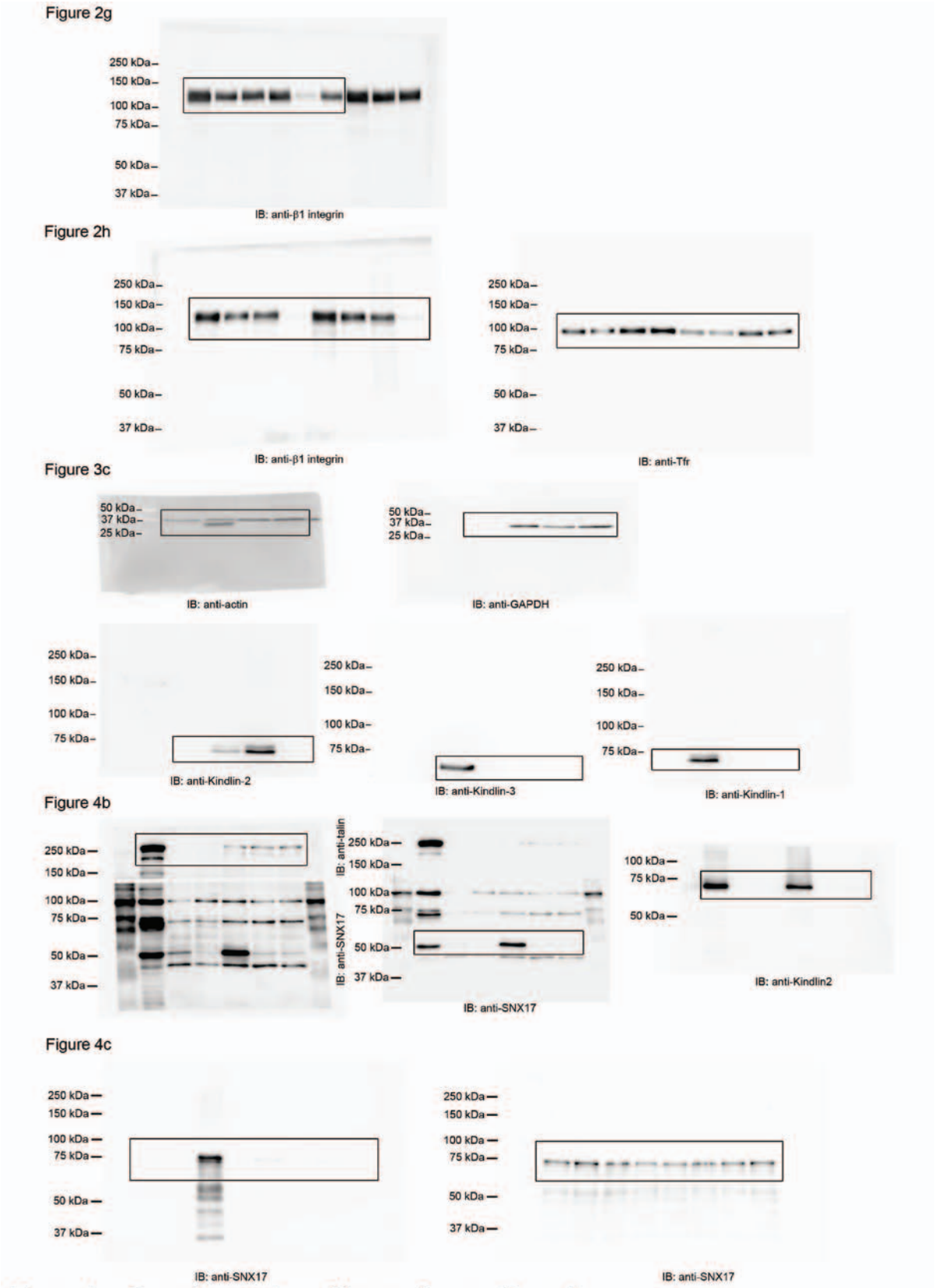

Figure S6 continued

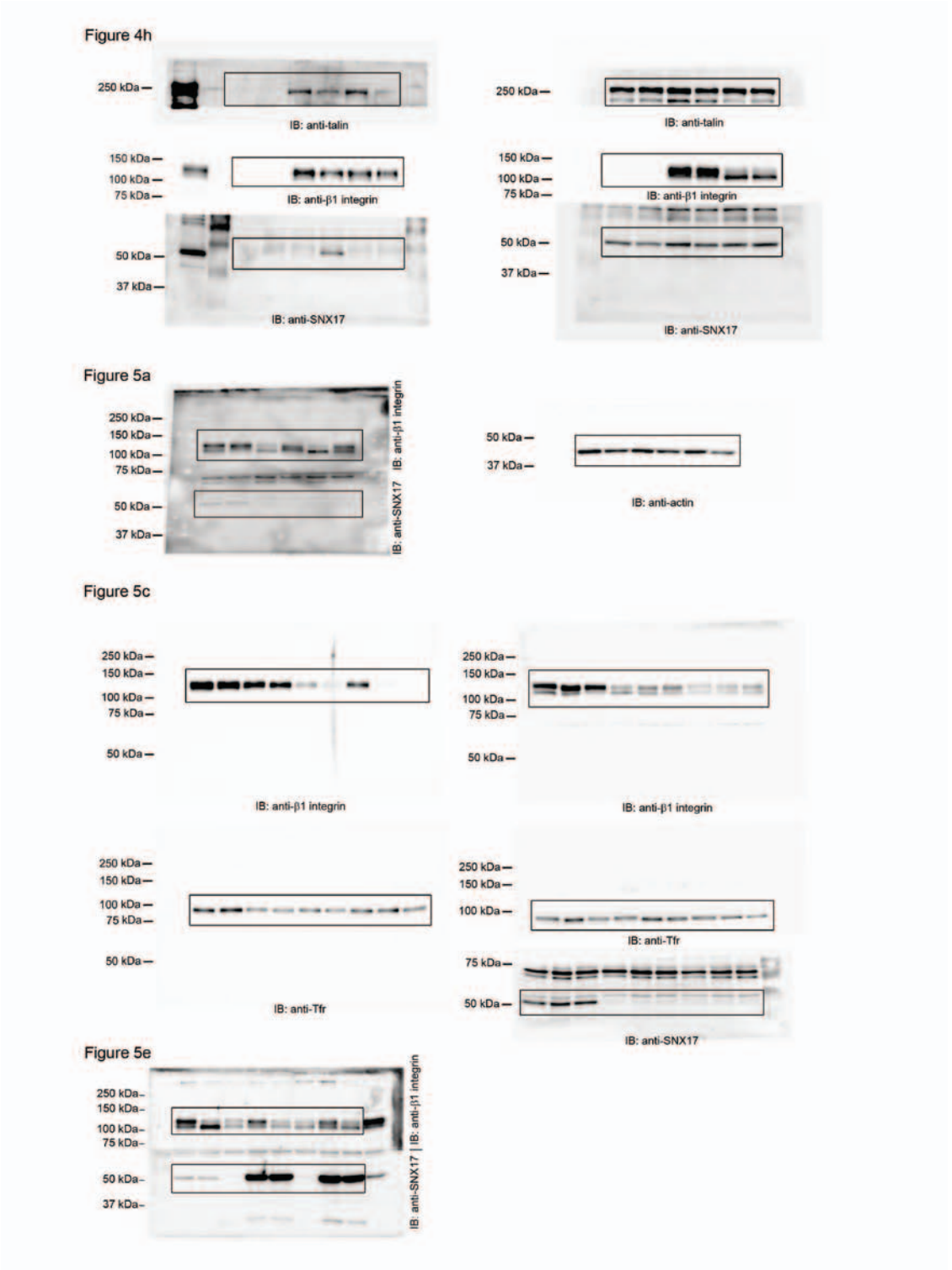

Figure S6 continued

Supplementary Movie 1 Time-lapse video recording of spreading β1 (-/-), β1 wt β1 TT/AA, and SNX17-depleted cells on FN (pictures taken every 10 min, imaging period 4 hrs).

Supplementary Movie 2 Time-lapse video recording of migrating β1 wt, β1 TT/AA, SNX17-depleted cells (shSNX17) and SNX17-depleted cells rescued with wild-type SNX17 (shSNX17 + SNX17) on FN (pictures taken every 10 min, imaging period 6 hrs).

Supplementary Table 1 List of β1 interactors from the SILAC-based β1 wt tail peptide versus scrambled peptide pull-down.
List of the proteins that showed an increased binding (>2.0 fold) to the β1 wt tail peptide against the scrambled peptide. Protein names, gene names, SILAC-ratios and intensities are listed.

Sorting Nexin 31 Binds Multiple β Integrin Cytoplasmic Domains and Regulates β1 Integrin Surface Levels and Stability

Hui-Yuan Tseng [1], Niko Thorausch [1], Tilman Ziegler [1], Alexander Meves [2], Reinhard Fässler [1] and Ralph T. Böttcher [1]

1 - Department of Molecular Medicine, *Max Planck Institute of Biochemistry, Am Klopferspitz 18, 82152 Martinsried, Germany*
2 - Department of Dermatology, *Mayo Clinic, Rochester, MN 55905, USA*

Correspondence to Ralph T. Böttcher: *Department of Molecular Medicine, Max Planck Institute of Biochemistry, 82152 Martinsried, Germany. Fax: +49 89 8578 2422. rboettch@biochem.mpg.de*
http://dx.doi.org/10.1016/j.jmb.2014.07.003
Edited by J. Sellers

Abstract

Trafficking of α5β1 integrin to lysosomes and its subsequent degradation is influenced by ligand occupancy and the binding of SNX17 via its protein 4.1, ezrin, radixin, moesin (FERM) domain to the membrane-distal NPxY motif in the cytoplasmic domain of β1 integrin in early endosomes. Two other sorting nexin (SNX) family members, namely SNX27 and SNX31, share with SNX17 next to their obligate phox domain a FERM domain, which may enable them to bind β integrin tails. Here we report that, in addition to SNX17, SNX31 but not SNX27 binds several β integrin tails in early endosomes in a PI3 (*p*hosphatidyl*i*nositide *3*)-kinase-dependent manner. Similarly like SNX17, binding of SNX31 with β1 integrin tails in early endosomes occurs between the FERM domain and the membrane-distal NPxY motif in the β1 integrin cytoplasmic domain. Furthermore, expression of SNX31 rescues β1 integrin surface levels and stability in SNX17-depleted cells. In contrast to SNX17, expression of SNX31 is restricted and found highly expressed in bladder and melanoma tissue. Altogether, these results demonstrate that SNX31 is an endosomal regulator of β integrins with a restricted expression pattern.

Introduction

Integrins constitute a major family of adhesion molecules. They are composed of an α subunit and a β subunit, which together mediate interactions of cells with proteins of the extracellular matrix. Although cell adhesion depends on integrin surface expression, the residence time of integrins on the cell surface is short and terminated by internalization followed by their routing into the endosomal network, where they are sorted into specific recycling or degradative pathways [1,2]. The endosomal trafficking of integrins regulates cell behavior by controlling integrin stability, integrin availability and distribution on the cell surface, and signaling of growth factor receptors that traffic together with integrins [1].

The pathways controlling the recycling of α5β1 integrin are heavily investigated and quite well understood. Less well known are the mechanisms underlying the degradation of α5β1 integrin or the consequences when integrin degradation is misregulated. The trafficking of α5β1 integrin to lysosomes and its subsequent degradation is influenced by ligand occupancy [3,4] and controlled by the binding of SNX17 [5,6]. Ligand-bound α5β1 integrin is ubiquitinylated, sorted to lysosomes, and degraded when CLIC3 is absent [3,4], while in the presence of CLIC3, lysosomally targeted α5β1 integrins recycle back to the plasma membrane [3]. Inactive α5β1 integrins are routed to early endosomes where they recruit SNX17 to the membrane-distal NPxY motif in the β1 integrin tails to prevent routing of β1 integrins to the lysosome resulting in their recycling back to the cell surface [5].

SNX17 belongs to the large family of sorting nexin (SNX) proteins characterized by the presence of a phox (PX) homology domain, which mediates the association with mono-phosphoinositide-enriched membranes of the early endocytic network [7,8]. SNX proteins are structurally classified into different subfamilies depending on their additional protein

domains [7,8]. The SNX-protein 4.1, ezrin, radixin, moesin (FERM) subfamily consists of three members, SNX17, SNX27, and SNX31 [9], and is defined by the presence of a FERM domain capable of binding NxxY motifs in integral membrane proteins [10]. The recruitment of SNX17 to NxxY motifs is required for the retrieval of β1 integrins and several other transmembrane proteins from the degradation pathway [5,6,11–14]. SNX27 is distinct from SNX17 and SNX31 as it harbors an additional PDZ domain that can engage PDZ binding motifs at the C-terminus of transmembrane proteins [15]. It has recently been shown that SNX27 prevents lysosomal routing of β2 adrenergic receptors and transmembrane proteins required for maintaining cellular nutrient homeostasis through binding to the SNX-BAR retromer [16,17]. Furthermore, loss of SNX27 was also shown to contribute to excitatory synaptic dysfunction in Down's syndrome patients by affecting glutamate receptor recycling [18]. Unlike SNX17 and SNX27, the functional properties of SNX31 are unknown. A genome-wide mutation study identified several driver coding mutations within SNX31 in human melanoma [19]. Whether they play a role in melanoma, however, is not known.

In the present study, we investigated whether the SNX-FERM subfamily members are able to bind integrins and control integrin stability. We report that (i) SNX17 and SNX31 but not SNX27 bind different β integrin cytoplasmic domains; (ii) this interaction depends on an intact FERM domain in SNX31 and the membrane-distal NPxY motif in the β1 integrin tail; (iii) SNX31 is highly expressed in bladder and primary skin melanoma; (iv) SNX31 is recruited to early endosomes in a PI3 (*p*hosphatidyl*i*nositide *3*)-kinase-dependent manner where it co-localizes with β1 integrins; and (v) SNX31 rescues β1 integrin surface levels and stability in SNX17-depleted mouse fibroblasts. Our findings show that both SNX17 and SNX31 are engaged in fine-tuning the surface levels of β1 integrins.

Results

SNX17 and SNX31 but not SNX27 bind various β integrin subunits

The SNX-FERM subfamily of PX domain containing proteins is defined by the presence of a FERM domain capable of binding NxxY motifs in integral membrane proteins [9] (Fig. 1a). A sequence alignment of its three murine family members, SNX17, SNX27, and SNX31, revealed that SNX17 and SNX31 are most closely related, sharing 37% identity, while SNX27 is more distantly related sharing 14% and 13% identity with SNX17 and SNX31, respectively (Fig. 1b and c). The identity within the FERM domain ranges between 22% and 36% (Fig. 1d).

SNX17 regulates turnover and recycling of α5β1 integrin through a direct binding of its FERM domain to the membrane-distal NxxY motif of β1 integrin cytoplasmic tails [5]. To test whether the other two members of the SNX-FERM subfamily, SNX27 and SNX31, also bind integrin tails, we expressed Flag-tagged SNX27 and Flag-tagged SNX31 in mouse fibroblasts either expressing endogenous SNX17 or depleted of SNX17 (Fig. 2a), lysed the cells, and performed pull-down experiments with several β integrin tail peptides (Fig. 2b–d). As expected, all wild-type β cytoplasmic tail peptides pulled down the integrin activating protein Talin [20] (Fig. 2b–d). As shown previously, SNX17 bound the β1 integrin tail [5], less efficiently the β2 integrin tail, and more strongly the β3, β5, and β6 integrin tails (Fig. 2b and c). Flag-tagged SNX31 showed robust binding to the β5 and β6 tails and less efficient binding to β1, β2, and β3 tails (Fig. 2b and d). In contrast, SNX27 bound neither β integrin tail peptide tested (Fig. 2c and d). Importantly, siRNA-mediated depletion of endogenous SNX17 did not change the binding profile of Flag-tagged SNX31 or Flag-tagged SNX27 (Fig. 2d).

The F3-FERM subdomain of Talin, Kindlin, and SNX17 is essential for β integrin tail binding [5,21,22]. A conserved QW motif present in the F3-FERM domain of SNX17 and SNX31 is crucial for the SNX17–β1 integrin interaction. To test whether the QW motif in SNX31 is also required for β integrin tail binding, we substituted both residues with alanines (QW356/357AA), stably expressed the mutant cDNA in mouse fibroblasts, and performed pull-down experiments with the β1 integrin tail peptide. The experiments revealed that Talin, SNX17, and wild-type SNX31 bound the β1 integrin wild-type tail peptide, while SNX31-QW/AA failed to bind the β1 tail peptide, indicating that SNX31 shares the integrin tail binding mode with SNX17 (Fig. 3a). As expected, we only observed background binding of the integrin tail binding proteins to the scrambled peptide (Fig. 3a). We also investigated whether SNX31 binding requires an intact proximal and/or distal NPxY motif in the β1 integrin tail by substituting the tyrosine residue with an alanine residue in either the membrane-proximal NPxY motif (β1 Y783A) or membrane-distal NxxY motif (β1 Y795A). As shown previously for SNX17 [5], Flag-tagged SNX31 binding was strongly reduced to β1 Y795A, while binding to β1 Y783A was only moderately reduced (Fig. 3b). To determine whether SNX31 directly interacts with the β1 integrin tail, we performed integrin tail peptide pull-down experiments with recombinant wild-type GST (*g*lutathione *S*-*t*ransferase)-tagged SNX31 or the integrin-binding-deficient GST-tagged SNX31-QW/AA. The results of the pull-down experiments revealed that SNX31 bound directly to β1 wild type while we observed very weak or no binding to β1 Y795A or scrambled peptides (Fig. 3c). Importantly, the QW/AA substitution in SNX31 abolished binding to wild-type β1 integrin tail (Fig. 3c). As

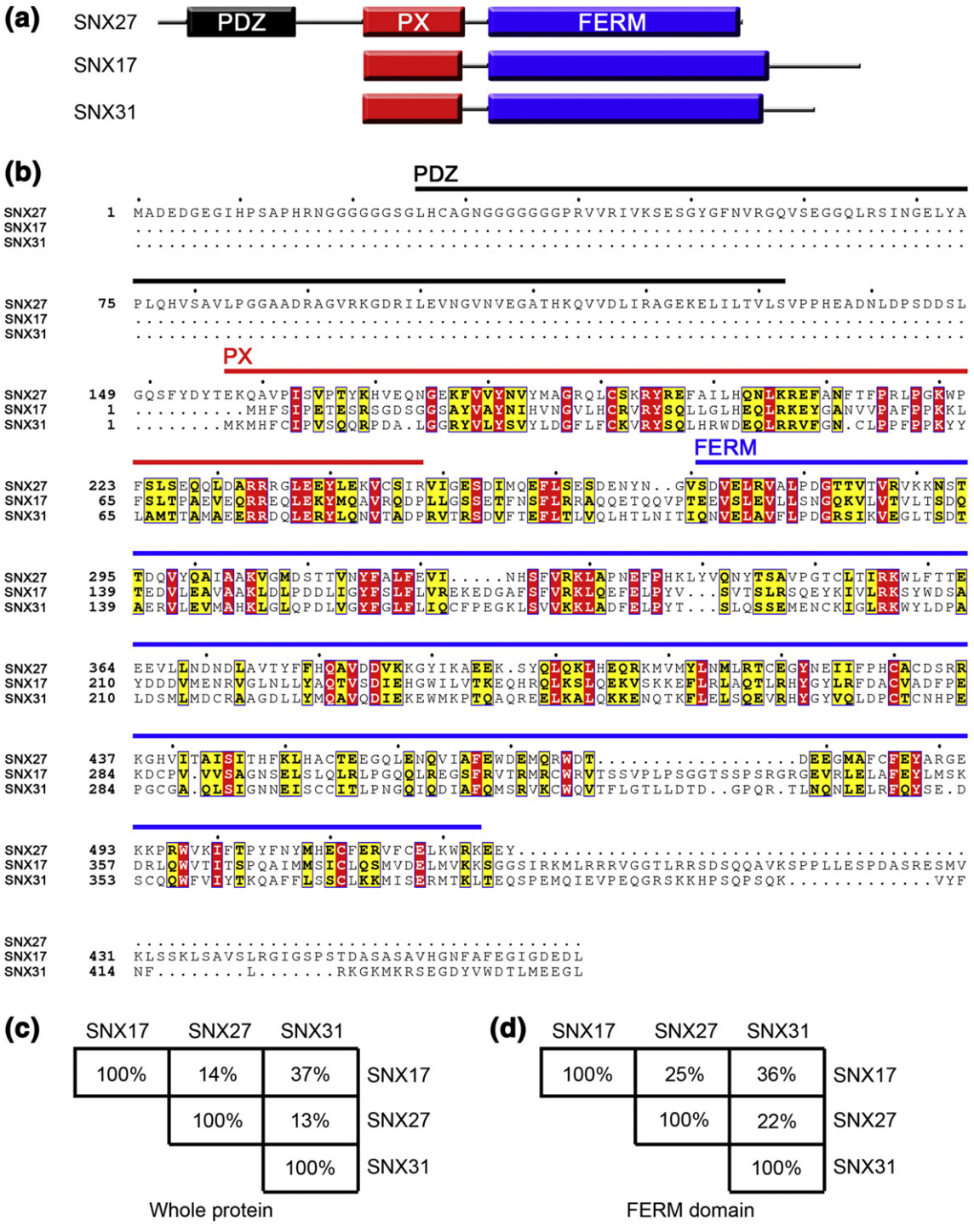

Fig. 1. Sequence alignment of the three murine SNX-FERM subfamily members. (a) Predicted domain structures of the three mouse SNX-FERM family members. (b) Sequence alignment of mouse SNX17, SNX27, and SNX31. The location of PX, FERM, and PDZ subdomains are indicated. Amino acids conserved in all three SNX-FERM proteins are shown in red, and amino acids similar across the three proteins are indicated in yellow. (c and d) Matrix of pairwise identity percentages of the three SNX-FERM family members using the entire sequences (c) or the FERM domains (d).

we cannot rule out that the SNX-FERM proteins bind differently to full-length integrins than to the cytoplasmic tail peptides, we finally investigated if the interaction of SNX31 with β1 integrins can also be demonstrated with the endogenous full-length β1 integrin. For this, we expressed either SNX17 only or

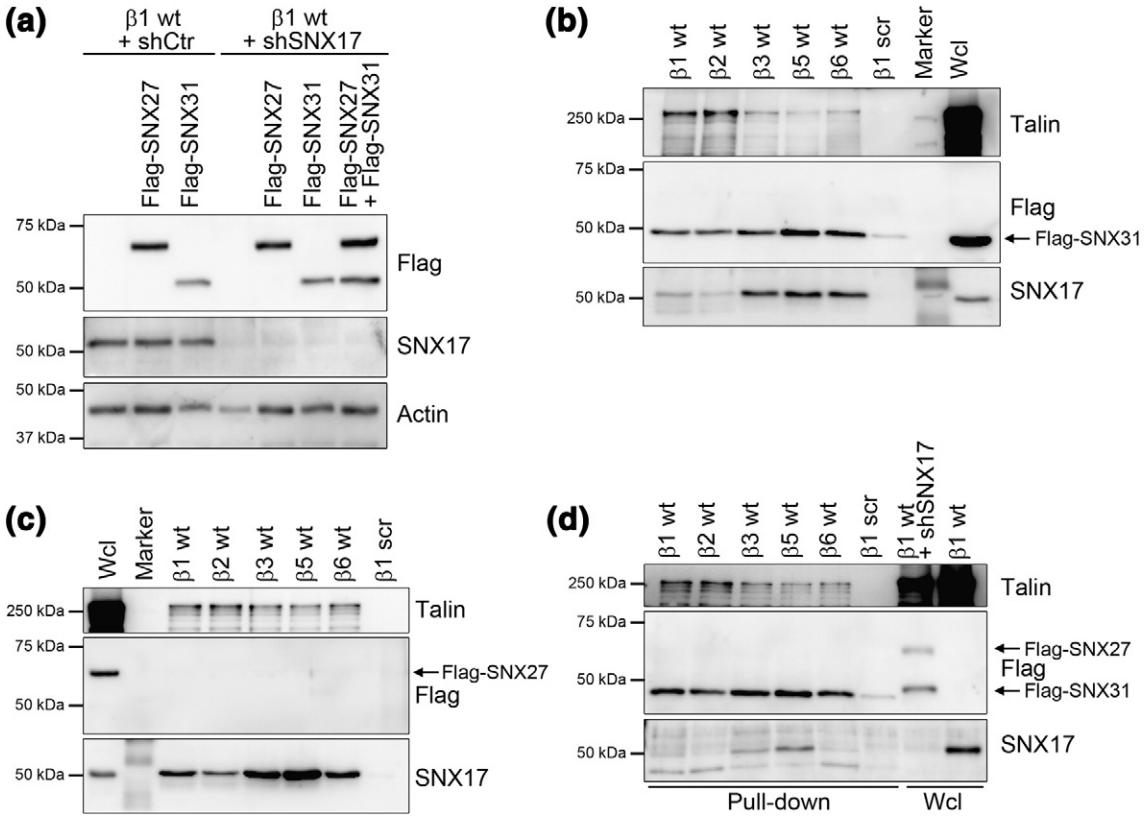

Fig. 2. SNX31 and SNX17 but not SNX27 interact with several β integrin cytoplasmic domains. (a) Western blot analysis of control mouse fibroblasts (shCtr) and SNX17 knockdown (shSNX17) cells used for pull-down experiments stably expressing different Flag-tagged SNX-FERM proteins with antibodies against the Flag-tag and SNX17. Actin served as loading control. (b and c) Biotinylated β integrin cytoplasmic tail peptides were analyzed for binding of endogenous SNX17, Flag-tagged SNX27, and Flag-tagged SNX31 by Western blotting. The indicated biotinylated β integrin cytoplasmic tail peptides were immobilized on Streptavidin beads and subsequently incubated with protein lysates of cells expressing Flag-tagged SNX31 (b) or Flag-tagged SNX27 (c). After washing, we analyzed the pulled-down proteins by Western blotting for the binding of the different FERM-SNX family members. Binding of Talin, a known β integrin cytoplasmic interactor, served as positive control showing the functionality of the tail peptides. Whole cell lysate was loaded next to the pull-down samples to show expression of the different proteins. Wcl, whole cell lysate; marker, molecular mass standard. (d) Western blot showing Flag-tagged SNX27 and Flag-tagged SNX31 binding to the biotinylated integrin tail peptides in lysates of SNX17-depleted cells. A second cell lysate sample was loaded to show the SNX17 depletion and the expression levels of Flag-tagged proteins. Wcl, whole cell lysate.

SNX17 together with Flag-tagged SNX31 in mouse fibroblasts and enriched the endosomal pool of antibody-labeled and internalized surface β1 integrins with primaquine, which was shown to inhibit recycling/exocytosis [23]. Immunoprecipitation of the endosomally enriched β1 integrins co-precipitated SNX17 and SNX31 while they did not bind to the transferrin receptor (TFR) under the same conditions (Fig. 3d). Interestingly, co-expression of Flag-tagged SNX31 reduced the amount of endogenous SNX17 bound to β1 integrins, showing that SNX31 can compete with SNX17 for β1 binding (Fig. 3d). In line with our peptide pull-down data, neither SNX17 nor SNX31 was co-immunoprecipitated with β1 Y795A integrin (Fig. 3d).

Altogether, these findings indicate that SNX17 and SNX31 but not SNX27 directly bind β integrin cytoplasmic domains. This interaction requires an intact SNX-FERM domain and the membrane-distal NxxY motif within the integrin cytoplasmic tail.

Expression pattern of *SNX31* in mouse tissues and human cell lines

The function, expression pattern, and subcellular localization of SNX31 are not known. We first analyzed RNA-seq expression data of coding RNAs from 27 different human tissues [24] and microarray data of 191 mouse samples [25] that indicated a restricted *SNX31* expression pattern. In human tissues, *SNX31* was highly expressed in bladder; weakly expressed in esophagus, heart, prostate, and testis; and absent in all other organs tested. Similarly, *SNX31* exhibited the highest expression in mouse bladder and was 30–100 times less expressed in the mouse prostate and

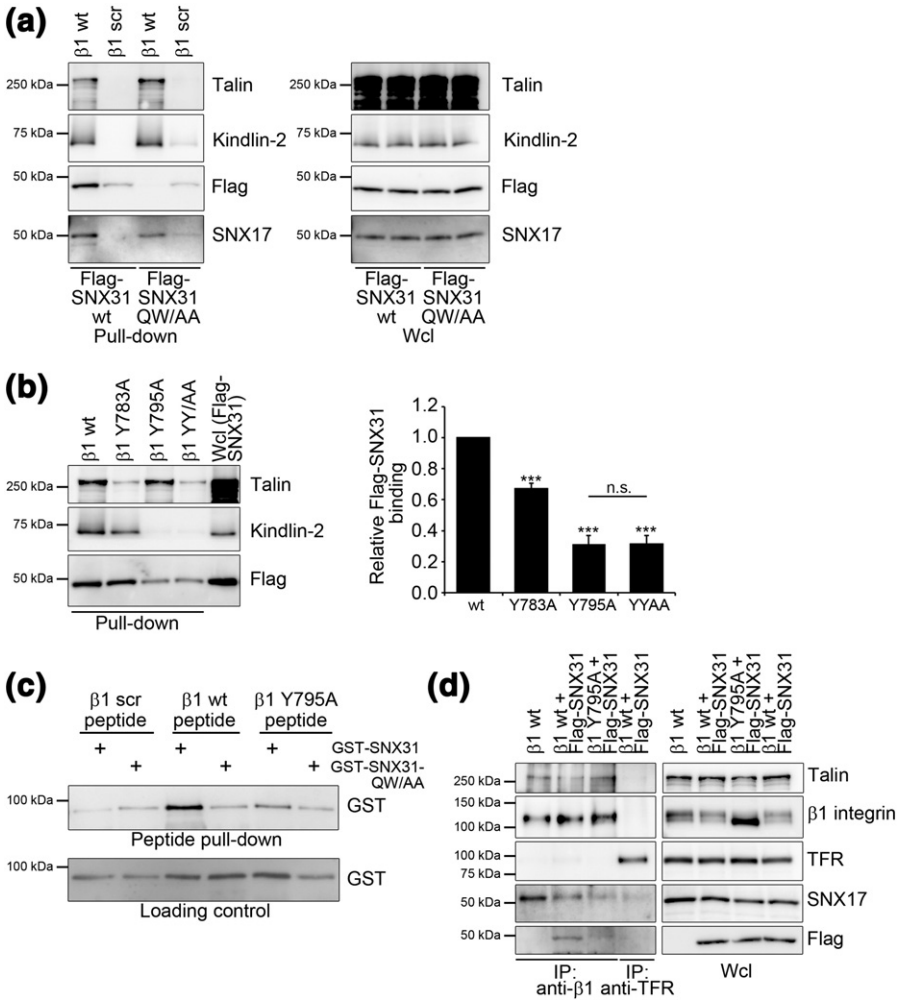

Fig. 3. SNX31 requires an intact FERM domain for β1 integrin tail binding. (a) Streptavidin-bead pull-down of biotinylated β1 integrin wild type and scrambled cytoplasmic tail peptides incubated with cell lysates containing wild-type Flag-tagged SNX31 or Flag-tagged SNX31-QW/AA. SNX31 binding to the β1 integrin cytoplasmic tail peptides was analyzed by Western blotting with an antibody against the Flag-tag. Binding of Talin, Kindlin-2, and SNX17 to the β1 integrin wild-type tail peptide indicated equal loading and functionality of the peptide. Wcl, whole cell lysate. (b) Streptavidin-bead pull-down of indicated wild type and mutant biotinylated β1 integrin tail peptides incubated with cell lysates expressing Flag-tagged SNX31 and subsequent Western blotting for Talin, Kindlin-2, and Flag-tagged SNX31. Bar graph shows the quantification of Flag-tagged SNX31 binding to the mutant biotinylated β1 integrin tail peptides relative to its binding to the β1 wild-type peptide. Western blot images were analyzed with ImageJ software for quantification [mean ± SEM (*s*tandard *e*rror of the *m*ean) ($n = 5$); ***p (student's t-test) < 0.001, n.s. = not significant]. (c) Streptavidin-bead pull-down assay with the indicated biotinylated β1 integrin cytoplasmic tail peptides and recombinant GST-tagged SNX31 or a GST-tagged SNX31-QW/AA. Synthetic peptides were immobilized on Streptavidin beads and incubated with 2% BSA for 30 min to block unspecific binding prior to adding 150 ng recombinant GST-tagged SNX31 or GST-tagged SNX31 QW/AA protein for 2 h at 4 °C. Protein binding to the β1 integrin cytoplasmic tail peptides was analyzed by Western blotting with an antibody against the GST-tag. (d) Co-immunoprecipitation of Flag-tagged SNX31 with endogenous, endosomally enriched wild-type β1 integrin. Cell surface β1 integrins (either β1 wild type or β1 Y795A integrin) or transferrin receptors were antibody labeled on ice followed by incubation of the cells for 10 min at 37 °C in medium with 0.2 mM primaquine to enrich for receptor antibody complexes in endosomes. After cell lysis, β1 integrin immune complexes were pulled-down, subjected to SDS-PAGE and Western blot analysis. Wcl, whole cell lysate.

cornea. To confirm this data and to elucidate the relative expression levels of the three subfamily members in different tissues, we performed quantitative reverse transcription (RT)-PCR on RNA samples derived from several mouse tissues and widely used human cancer cell lines. While *SNX17* and *SNX27* were expressed in all mouse tissues and human cell lines analyzed, high *SNX31* expression was restricted to the bladder and RT4 human urinary bladder cells (Fig. 4a–c). Significantly lower *SNX31* mRNA levels

were present in A2780 cells and vascular smooth muscle cells while *SNX31* transcripts were absent in primary mouse keratinocytes, immortalized mouse fibroblasts, and melanocytes (Fig. 4b and c).

Since whole exome sequencing of human melanomas identified several mutations in SNX31 [19], we decided to determine whether *SNX17* or *SNX31* mRNA expression changes during melanoma progression. To this end, we isolated total RNA from biopsies of benign melanocytic nevi and in-transit melanoma metastases and determined *SNX17* and *SNX31* mRNA levels by quantitative PCR (Fig. 5a). We found that *SNX17* expression was not significantly changed in benign nevi *versus* metastatic melanoma, while *SNX31* expression was decreased in metastatic melanoma. To further delineate whether *SNX17* or *SNX31* RNA levels correlate with metastasis, we measured their mRNA levels in biopsies of primary skin melanoma, which either have or lack sentinel lymph node (SLN) metastasis. While *SNX17* mRNA levels remained unchanged in primary melanoma with and without SLN metastasis, *SNX31* levels decreased in melanoma with SLN metastasis ($p < 0.0025$) (Fig. 5b).

Together, these results show that SNX31 exhibits a restricted expression pattern across tissues and cell lines and decreases in invasive primary melanoma.

SNX31 localizes to early endosomes in a PI3-kinase-dependent manner

SNX family members localize via their PX domains to PI(3)P-rich membranes [1,8]. While SNX17 and SNX27 were shown to be recruited to endosomes in a PX-domain-dependent manner [14,26], the distribution of SNX31 in cells is unknown. We determined the subcellular localization of SNX31 by transfecting HeLa cells with eGFP (*e*nhanced *g*reen *f*luorescent *p*rotein)-tagged SNX31 followed by immunostaining with antibodies against endosomal and lysosomal marker proteins. SNX31 overlapped with the early endosomal antigen 1 (EEA1), a marker for early endosomes, and weakly with transferrin receptor (TFR), a marker for recycling endosomes [Fig. 6a and b; correlation coefficients: 0.44 ± 0.10 (EEA1) and 0.19 ± 0.05 (TFR)]. In contrast, no apparent co-localization was observed with the lysosomal acid membrane

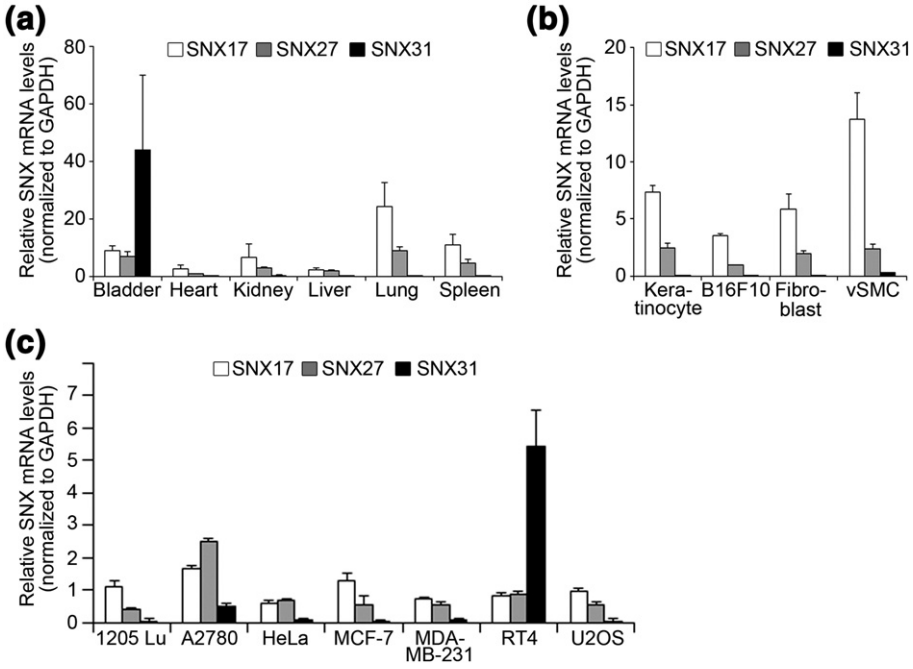

Fig. 4. *SNX31* mRNA levels in mouse tissues and human cell lines. *SNX17*, *SNX27*, and *SNX31* mRNA expression levels in mouse tissues (a), mouse cell lines (b), and human cell lines (c) measured by quantitative RT-PCR. (a) Total RNA was extracted from organs of 6-week-old C57BL/6 mice, reverse transcribed into cDNA, and the expression of the three SNX-FERM family members was determined by quantitative RT-PCR. Shown is the abundance of each transcript relative to GAPDH (mean ± SEM; $n = 3$). (b and c) Quantitative RT-PCR was performed for all three SNX-FERM family members with cDNA derived from total RNA obtained from the indicated cell lines. Shown is the abundance of each transcript relative to GAPDH (mean ± SEM; $n = 3$). B16F10 (melanocyte cell line), RT4 (urinary bladder cells), vSMC (vascular smooth muscle cell line), 1205LU (metastatic melanoma cell line), A2780 (ovarian carcinoma cell line), MDA-MB-231 and MCF-7 (breast adenocarcinoma cell lines), U2OS (osteosarcoma cell lines), and HeLa (cervical cancer cells).

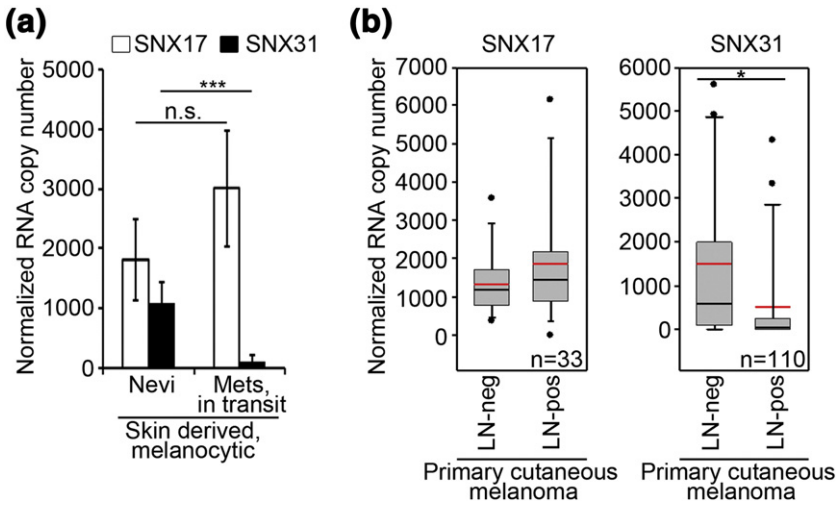

Fig. 5. *SNX31* expression during melanoma progression. (a and b) *SNX31* expression is reduced in metastasizing melanoma. (a) *SNX17* and *SNX31* RNA copy number in benign nevi and in-transit melanoma metastases. Total RNA was extracted from 6 benign nevi and 6 in-transit metastases of FFPE patient-derived biospecimens, pooled, and reverse transcribed into cDNA; the expression *SNX17* and *SNX31* was determined by quantitative RT-PCR. SNX copy number was normalized to 25,000 copies of housekeeping genes [mean ± SD; ***p (student's t-test) < 0.0001, n.s. = not significant]. (b) *SNX17* and *SNX31* RNA copy number in a consecutive series of 33 and 110 patients with primary cutaneous melanoma, respectively. All patients had an SLN biopsy performed to rule out metastasis to regional lymph nodes. *SNX17* and *SNX31* mRNA levels were determined by quantitative RT-PCR. SNX copy number was normalized to 25,000 copies of housekeeping genes. SNX31 copy number is reduced in melanoma that metastasize to SLN (*p < 0.0025 by Mann–Whitney U-test). Red line: average. Black line: mean.

protein 1 (Lamp1) and the late endosomal protein Rab7 [Fig. 6c and d; correlation coefficients: −0.01 ± 0.08 (Lamp1) and −0.02 ± 0.06 (Rab7)]. Co-transfection of eGFP and mCherry fusion proteins of SNX17, SNX27, and SNX31 revealed that all three subfamily members co-localize in the early endosome compartment [Fig. 6e and f; correlation coefficients: 0.56 ±0.07 (SNX17 *versus* SNX27) and 0.69 ± 0.08 (SNX31 *versus* SNX17)]. Since the early endosomal localization of SNX17 and of SNX27 depend on the interaction of their PX domains with PI(3)Ps [14,26], we tested whether the activity of PI3 kinases is required for SNX31 localization by treating HeLa cells with the PI3 kinase inhibitor wortmannin, which reduces the level of endosomal PI(3)P [27]. Live-cell microscopy and immunostainings revealed that wortmannin induced a rapid dislodgment of eGFP-tagged SNX17 and eGFP-tagged SNX31 from early endosomes (Fig. 7a, b, and d). In contrast, eGFP-tagged SNX27 was less sensitive to PI3 kinase inhibition and remained bound to intracellular membranes over a longer period of time (Fig. 7c and d). We also analyzed whether the localization of SNX-FERM proteins to endosomes requires the PX domain by substituting a conserved arginine residue in SNX17 (R36), SNX27 (R194), and SNX31 (R37) critical for PI(3)P binding [9] with glutamine. Subsequent immunostaining revealed that an intact PX domain is indeed necessary for endosomal localization as eGFP-tagged SNX17-R36Q, SNX27-R194Q, and SNX31-R37Q lost their typical punctate staining pattern and instead showed a uniform distribution throughout the cytoplasm (Fig. 7e). In line with our observation that eGFP-tagged SNX27 was less sensitive to PI3 kinase inhibition, we observed a weak residual endosomal pool of SNX27-R194Q while similar mutations in SNX17 and SNX31 completely abolished their endosomal localization (Fig. 7e).

Together, these data show that the SNX-FERM subfamily members SNX17, SNX27, and SNX31 associate via their PX domains with early endosomes in a PI3-kinase-dependent manner.

SNX31 rescues β1 integrin stability and surface levels in SNX17-depleted cells

β1 integrins are widely used to elucidate general mechanisms of integrin trafficking. Furthermore, it has been shown recently that SNX17 is an essential regulator of β1 integrin stability [5,6]. The interaction of SNX31 with β1 integrin tails *in vitro* and its localization to early endosomes suggest a role in β1 integrin trafficking and/or degradation. To test whether SNX31 and β1 integrins co-localize, we performed live-cell microscopy in mouse fibroblasts expressing eGFP-tagged SNX31. These experiments revealed that eGFP-tagged SNX31 and internalized antibody-labeled β1 integrins co-localized in puncta-like structures reminiscent of endosomes (Fig. 8a). Next we investigated whether SNX31 can rescue the

diminished β1 integrin stability in SNX17-depleted cells by stably re-expressing wild-type Flag-tagged SNX17, Flag-tagged SNX27, or Flag-tagged SNX31. As expected, depletion of SNX17 significantly decreased the pool of mature β1 integrin (molecular mass: 125 kDa) in whole cell lysates (Fig. 8b) and the β1 integrin surface levels (Fig. 8c). The reduction in β1 integrin levels was accompanied with a decrease in α5 integrin levels (Fig. 8b). Importantly, expression of Flag-tagged SNX31 in SNX17-depleted cells normalized the pool of mature β1 integrin and α5 integrin levels in cell lysates and β1 integrin on the cell surface, while the integrin-binding-deficient Flag-tagged SNX31-QW/AA or Flag-tagged SNX27 showed no effect (Fig. 8b and c). To elucidate whether re-expressed SNX31 normalized β1 integrin surface levels by improving protein stability, we determined the degradation kinetics of the surface β1 integrins by surface labeling with

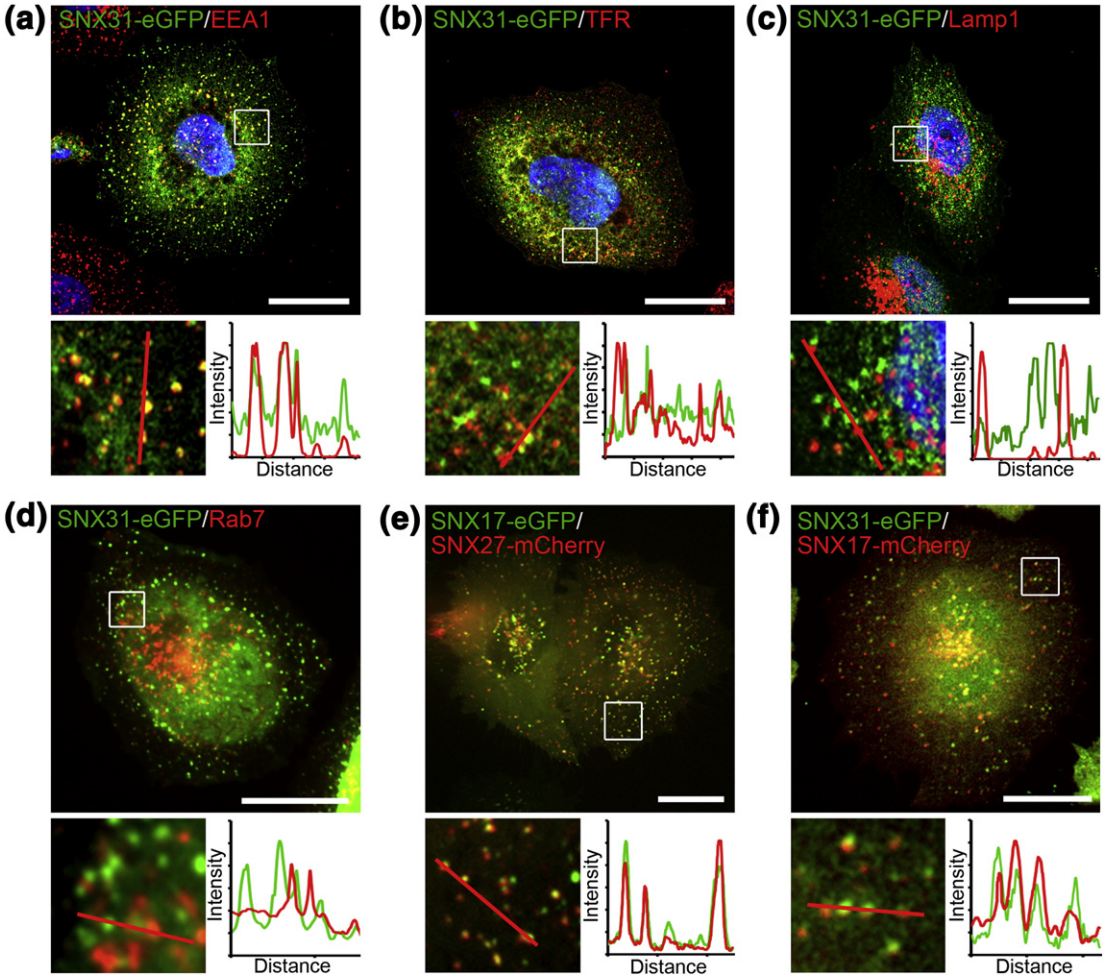

Fig. 6. SNX31 localizes to early endosomes. (a–c) HeLa cells transiently transfected with eGFP-tagged SNX31 were seeded onto fibronectin (5 μg/ml) overnight, fixed and stained with antibodies against EEA1 (a), transferrin receptor (TFR) (b), and Lamp1 (c). Nuclei were counterstained with DAPI (blue). Images were obtained by laser scanning confocal microscopy. Scale bars represent 20 μm. Correlation coefficients: 0.44 ± 0.10 (EEA1) (n = 13), 0.19 ± 0.05 (TFR) (n = 14), and −0.01 ± 0.08 (Lamp1) (n = 11); mean ± SD. Fluorescence intensity line scan profiles were generated along the red lines using LSM software. (d) Co-expression of SNX31 and Rab7 in HeLa cells. HeLa cells were transiently transfected with eGFP-tagged SNX31 and mRFP-tagged Rab7, seeded onto fibronectin overnight before fluorescence distribution was determined in living cells by spinning disk confocal microscopy. A still of a movie is shown. The scale bar represents 20 μm. Correlation coefficient: −0.02 ± 0.06; mean ± SD (n = 11). (e and f) Co-localization of SNX-FERM family members in living cells. HeLa cells were transiently transfected with eGFP-tagged SNX17 and mCherry-tagged SNX27 (e) or eGFP-tagged SNX31 and mCherry-tagged SNX17 (f). Twenty-four hours after transfection, cells were seeded onto fibronectin-coated (5 μg/ml) glass-bottom dishes and fluorescence distribution was determined using spinning disk confocal microscopy. A still of a movie is shown. Fluorescence intensity line scan profiles were generated along the red lines using LSM software. Scale bars represent 20 μm. Correlation coefficients: 0.56 ± 0.07 (SNX17 *versus* SNX27) (n = 6) and 0.69 ± 0.08 (SNX31 *versus* SNX17) (n = 11); mean ± SD.

biotin followed by capture ELISA. While β1 integrins were rapidly degraded in SNX17-depleted fibroblasts, expression of Flag-tagged SNX31 rescued β1 integrin stability, although less efficiently compared to Flag-tagged SNX17. In contrast, Flag-tagged SNX31-QW/AA and Flag-tagged SNX27 had no effect (Fig. 8d).

These findings indicate that SNX31 can compensate the loss of SNX17 and prevent β1 integrin degradation.

Discussion

Integrins are constantly endocytosed from the plasma membrane and sorted in early endosomes for degradation or recycling back to the plasma membrane [1]. A key player of β1 integrin endosomal sorting is the SNX-FERM protein SNX17, which directly binds β1 integrin tails in early endosomes and thereby prevents degradation by a still unknown mechanism. In the present study, we investigated whether the other two members of the SNX-FERM subfamily, SNX27 and SNX31, share the properties of SNX17. We found that this is the case for SNX31, while SNX27 neither interacts with β integrin tails nor stabilizes cell surface β1 integrins. SNX31 is a novel SNX family member highly expressed in bladder and in primary melanoma where it is frequently mutated [19].

The tails of α and β integrins bind a large number of proteins, which enable integrin activation, clustering, signaling, endocytosis, and recycling [28]. Since integrin tails are short, protein binding is often mutually exclusive and either occurs at temporally distinct stages of adhesion site maturation or in different subcellular compartments. The Kindlin binding site in the membrane-distal NPxY motif of β1 integrin tails is occupied by Kindlin at the plasma membrane to increase integrin affinity for its ligands and by SNX17 in early endosomes to prevent degradation [5,16,29,30]. We found that SNX31 is also able to bind the membrane-distal NPxY motif of integrin β1 tails in endosomes where it rescues β1 integrin stability in SNX17-depleted cells. The FERM domain is key for binding β integrin tails. Many NxxY integrin tail binding proteins including Talin, Kindlins, SNX17, and SNX31 contain FERM domains. A third SNX member, SNX27, also contains a FERM domain but is unable to bind β integrin tail peptides and to stabilize β1 integrins. Although we cannot rule out that SNX27 interacts with full-length integrins, our findings are in agreement with the inability of SNX27 to bind integrins in peptide arrays [10] and to influence β1 integrin surface levels in HeLa cells [6]. In contrast to SNX17 and SNX31, SNX27 shows preferential binding to phosphorylated NxxY motifs in peptides and receptors [10]. The levels of phosphorylated β1 integrin in non-transformed cells are not detectable [31], which might explain why SNX27 fails to associate with NxxY motifs in integrins and hence fails to influence their behavior.

In SNX17 knockdown cells, re-expression of SNX17 or expression of SNX31 regulated β1 integrin levels in comparable manners. Bladder and melanoma cells express SNX31 and SNX17 that both bind to the membrane-distal NPxY motif on the β1 integrin tail. Therefore, it is conceivable that SNX17 and SNX31 compete for β1 integrin binding in early endosomes. This could provide cells with back-up proteins that are functionally interchangeable. Alternatively, it could be that SNX17 and SNX31 regulate the stability of different integrin heterodimers when co-expressed in cells depending on their relative expression levels and their affinity for different β integrins and co-regulatory proteins. In line with this hypothesis, we observed differential binding patterns of SNX17 and SNX31 to different β integrin tail peptides. A similar finding was made with the three members of the Kindlin family, which bind specific β integrin tails to regulate their function; for example, the β1 and β3 integrin tails associate with Kindlin-1 and Kindlin-2, while the β5 integrin tail binds Kindlin-1 but not Kindlin-2 [32,33]. Unfortunately, we were unable to deplete SNX31 with several siRNAs or shRNAs in bladder carcinoma RT4 cells that co-express SNX17 and SNX31. It therefore remains to be analyzed if SNX17 and SNX31 exhibit a similar specificity for binding β integrin subunits in living cells or regulate the stability of distinct integrins.

Fig. 7. SNX31 localization to early endosomes is PI3 kinase dependent. (a–c) Montage showing eGFP-tagged SNX17 (a), eGFP-tagged SNX31 (b), and eGFP-tagged SNX27 (c) localization in HeLa cells before and after addition of DMSO or the PI3 kinase inhibitor wortmannin. HeLa cells transiently transfected with eGFP-tagged SNX-FERM family members were seeded on fibronectin-coated (5 μg/ml) glass-bottom dishes and fluorescence distribution was determined using spinning disk confocal microscopy. Wortmannin (0.4 μM) was added 90 s after start of the recording and cells were imaged for additional 8 min. Inverted images from selected time points of these time lapse recordings are shown. Note the disappearance of vesicular staining accompanied with an increase of diffuse cytoplasmic signal after wortmannin treatment. (d) Quantification of vesicular staining of eGFP-tagged SNX17, eGFP-tagged SNX31, and eGFP-tagged SNX27 before and 8 min after DMSO or wortmannin (0.4 μM) treatment. Values are provided as percentage of vesicular staining compared to cells before treatment [mean ± SEM, 10 cells in four independent experiments; ***p (Mann–Whitney U-test) < 0.001, **p (Mann–Whitney U-test) = 0.0015, n.s. = not significant]. (e) HeLa cells were transiently transfected with eGFP-tagged wild-type SNX-FERM family members or versions carrying point mutations in the PX domain. The cells were seeded on fibronectin and incubated for 24 h before fixation and immunostaining with an antibody against EEA1. Nuclei were counterstained with DAPI (blue). Images were obtained by laser scanning confocal microscopy. Scale bars represent 20 μm.

SNX17 and SNX31 are the only β integrin tail interactors known so far that regulate lysosomal degradation of integrins. Rab21 and p120RasGAP bind to several integrin α subunits and their knockdowns affect integrin recycling without decreasing integrin protein levels [34,35]. Although other proteins such as syntaxin 6 or CLIC3 were shown in cell depletion studies to regulate lysosomal β1 integrin degradation [3,36,37], their loss is more likely affecting more general aspects of endosome properties such as vesicle fusion or maintenance of intracellular membranes rather than specific functions of integrins. The mechanism by which

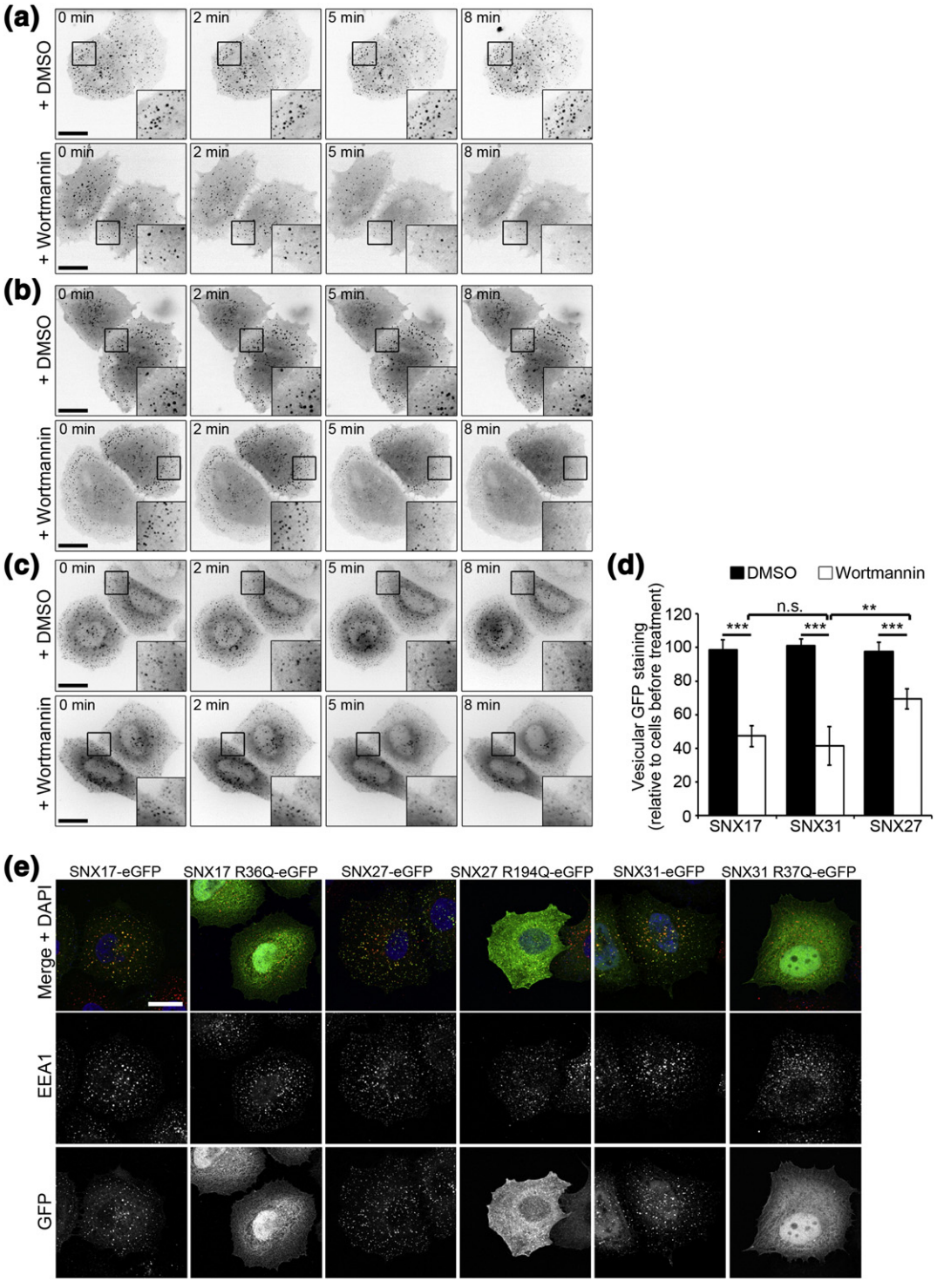

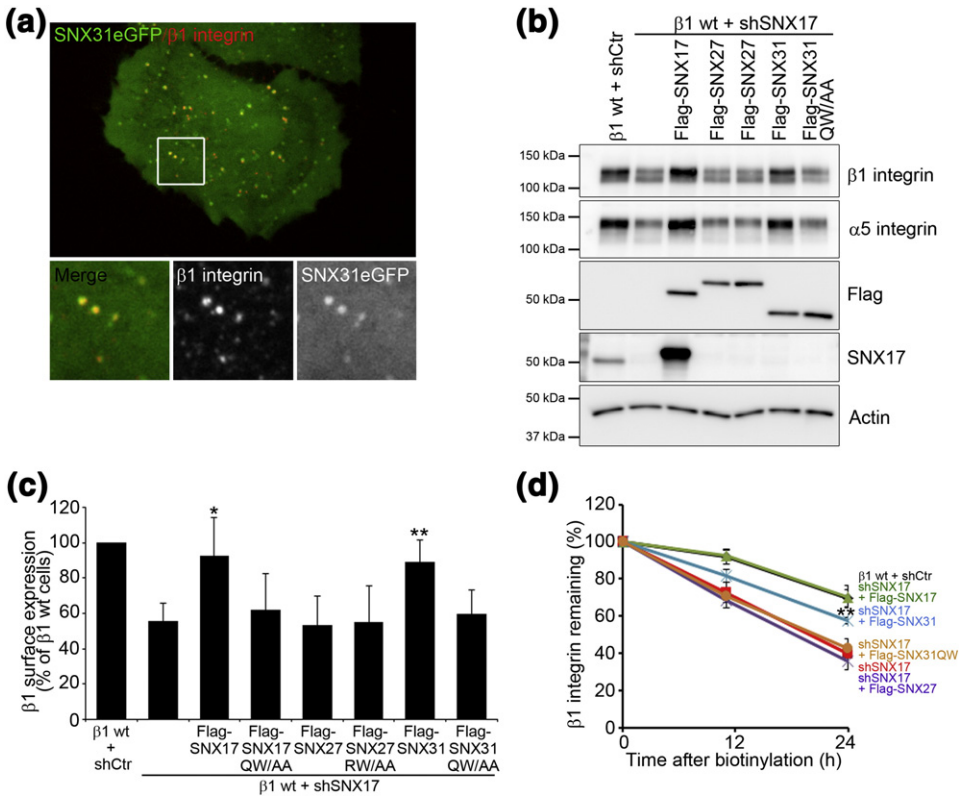

Fig. 8. SNX31 compensates for the loss of SNX17. (a) Co-localization of endogenous β1 integrin and eGFP-tagged SNX31. Mouse fibroblasts expressing eGFP-tagged SNX31 were grown on fibronectin-coated (5 μg/ml) glass-bottom dishes. Cells were incubated on ice and endogenous β1 integrin was surface labeled for 1 h with a fluorescently labeled anti-β1 integrin antibody. Surface-bound antibody was allowed to internalize for 15 min at 37 °C and subsequently imaged in living cells by spinning disk confocal microscopy. A still of a movie is shown. (b) Control mouse fibroblasts (shCtr), SNX17 knockdown (shSNX17) cells, and rescue cell lines stably expressing different SNX-FERM proteins were analyzed for their β1 and α5 integrin expression levels by Western blotting. Actin served as loading control. (c) Quantification of β1 integrin surface levels in the indicated cell lines determined by FACS [mean ± SD, $n = 4$; $^{**}p$ (student's t-test) = 0.0059, $^{*}p$ (student's t-test) = 0.0206]. (d) SNX31 prevents degradation of cell surface β1 integrins in the absence of SNX17. The indicated cell lines were surface biotinylated for 1 h on ice and then incubated for 0 h, 12 h, and 24 h at 37 °C. Cells were lysed at each time point and biotinylated β1 integrin was determined by capture-ELISA [mean ± SD; $n = 3$; $^{**}p$ (student's t-test) = 0.002].

SNX17 and SNX31 prevent lysosomal degradation of β1 integrin is unclear. SNX27 prevents lysosomal routing of transmembrane proteins such as β2 adrenergic receptor or the glucose transporter GLUT1 by recruiting the SNX-BAR retromer, a protein complex that transports transmembrane proteins from endosomes to the *trans*-Golgi network [16,17,38]. Since SNX17 and SNX31 do not interact with the SNX-BAR retromer [16], the mechanisms that prevent integrin degradation must be fundamentally different.

Our expression analyses revealed that *SNX17* and *SNX27* transcripts were detectable in all tissues and cell lines analyzed while *SNX31* expression was highly restricted with high expression in bladder and in melanoma. Malignant melanoma is a highly metastatic cancer that is considered one of the most aggressive and treatment-resistant human cancers [39]. A recent study identified several driver coding mutations within SNX31 in human melanoma [19]. While the identified mutations were distributed over the entire protein, several accumulated in the FERM domain of SNX31. However, the consequences of the mutations for SNX31 function have not been analyzed. Our expression data further support a role of SNX31 in melanoma formation and metastasis; *SNX31* expression is significantly lower in in-transit melanoma metastases compared to benign melanocytic nevi and *SNX31* levels are also decreased in melanoma with SLN metastasis. Interestingly, melanoma cells seem to loose SNX31 expression after immortalization as we failed to detect *SNX31* mRNA in all mouse and human melanoma cell lines tested. How the reduced SNX31

expression levels or mutations within its FERM domain affect melanoma pathology is unknown and it remains to be elucidated whether it is the consequence of aberrant trafficking of integrins and/or other transmembrane cargo.

Materials and Methods

Antibodies

The following antibodies were used for Western blotting and cell staining: Actin (A-2066, Sigma), β1 integrin (MAB1997, Chemicon), EEA1 (BD Transduction Laboratories), Flag M2-HRP (Sigma), GST (71097-3, Novagen), Kindlin-2 (K3269, Sigma), Lamp1 (Abcam), SNX17 (10275-1-AP, Proteintech), Talin (T3287, clone 8d4, Sigma), transferrin receptor (13-6800, Invitrogen), and transferrin receptor (ab63335, Abcam). 4′,6-Diamidino-2-phenylindole (DAPI) (Sigma) was used for immunohistochemistry.

The following antibodies were used for flow cytometry: β1 integrin PE (HMbeta1-1, BioLegend) and β1 integrin biotin (Ha2/5, BD Pharmingen).

Plasmids

Point mutations into SNX31 (QW356/357AA, R37Q), SNX17 (R36Q), and SNX27 (RW498/499AA, R194Q) cDNA were introduced by site-directed mutagenesis. For stable expression of the mouse SNX31 (wild type, QW356/357AA) and the human SNX27 (wild type, RW498/499AA) cDNAs, we cloned the cDNAs into the retroviral expression vector pCLMFG or pLZRS. For expression of eGFP-tagged SNX17, SNX27 and SNX31 cDNAs were cloned into the pEGFP(N1 and N3) vector (Clonetech). SNX17 expression plasmids have been described before [5]. For recombinant expression of GST-tagged SNX31, Flag-tagged SNX31, and Flag-tagged SNX31, QW360/361AA cDNA was cloned into the pGEX-6P-1 vector (GE Healthcare).

Cell lines

β1(-/-), β1 wild type and SNX17 knockdown mouse fibroblast cell lines have been described mouse fibroblast [5]. Cell lines were cultured in Dulbecco's modified Eagle's medium supplemented with 10% (v/v) serum at 37 °C and 10% CO_2. Human RT4 cells were a kind gift from Roman Nawroth (Technical University of Munich) and were cultured in RPMI supplemented with 10% (v/v) serum and 1% (v/v) non-essential amino acids.

Transient and stable transfection/transduction

Cells were transiently transfected with Lipofectamine 2000 (Invitrogen) according to the manufacturer's protocol. To generate stable cell lines, we produced VSV-G (*v*esicular *s*tomatitis *v*irus *G* glycoprotein) pseudotyped retroviral vectors by transient transfection of 293T (human embryonic kidney) cells. Viral particles were concentrated from cell culture supernatant as previously described [40] and used for infection.

Turnover of surface integrins and capture ELISA

The half-life of surface proteins was determined by biotinylation as previously described [5]. Briefly, fibroblasts were grown to 80% confluence, washed twice in cold PBS (*p*hosphate-*b*uffered *s*aline), and surface-biotinylated with 0.2 mg/ml sulfo-NHS-LC-biotin (Thermo Scientific) in PBS for 45 min at 4 °C. Following washes with cold PBS, we incubated the cells in Dulbecco's modified Eagle's medium containing 0.2% fetal bovine serum for 0, 11, and 24 h at 37 °C. Cells were lysed in a low volume of lysis buffer [75 mM Tris, 200 mM NaCl, 7.5 mM ethylenediaminetetraacetic acid and 7.5 mM ethylene glycol bis(β-aminoethyl ether) *N,N*′-tetraacetic acid, 1.5% Triton X-100, 0.75% Igepal CA-630, and protease inhibitors]. Lysates were passed through a 27-gauge needle 10 times and centrifuged 10 min at 4 °C. We used 50 µl of the supernatant for capture ELISA.

For capture ELISA, Maxisorb 96-well plates (Life Technologies) were coated overnight with anti-β1 integrin antibody (MAB1997, Chemicon) in 50 mM carbonate buffer (pH 9.6) at 4 °C. Prior to adding the cell lysate, we blocked unspecific binding with 5% BSA (*b*ovine *s*erum *a*lbumin) in PBS/0.1% Tween-20 (PBS-T) for 1–2 h at room temperature. We incubated 50 µl cell lysate overnight at 4 °C to capture integrins. Following extensive washes with PBS-T, we incubated plates with Streptavidin-HRP in 1% BSA in PBS-T for 1 h at 4 °C. Biotinylated β1 integrin was detected after several washing steps by chromogenic reaction with ABTS peroxidase substrate (Vector Laboratories).

Quantitative PCR

RNA was isolated from cells using the RNeasy mini kit (Qiagen) and 500 ng of total RNA was transcribed into cDNA using the iScript cDNA Synthesis kit (Bio-Rad). Quantitative PCR assays were performed with the LightCycler 480 II (Roche) using SYBR green and the following primers: human SNX17-forward AGTACAT GCAAGCTGTTCGG, human SNX17-reverse AGCT ACAGCCTCCAGGACAT, human SNX27-forward AATGGTGTGTCCGACGTAGA, human SNX27-reverse TTTGCTGCGATAGCCTGATA, human SNX31-forward TGCTGGCAGTGGTTTGTTAT, human SNX31-reverse CTGCTGGCTTTGTTGAATGT, human GAPDH-forward AGGGCTGCTTTTAACTCTGGT, human GAPDH-reverse CCCCACTTGATTTTGGAGGGA, mouse SNX17-forward CATTGCTCGAGTCACCAGAC, mouse SNX17-reverse CATCCAGGCAGCTGAGATTA, mouse SNX27-forward AGAGCTCTCAGGGAGGAACA, mouse SNX27-reverse GTTTGGAGCAATGAAGGGAT, mouse SNX31-forward GCCAACCTAGCCAGAAAGTC, mouse SNX31-reverse AAGTGGATAAATGCCTGGATG, mouse GAPDH-forward TCCTGCACCACCAACTGCTTAGC, and mouse GAPDH-reverse TGGATGCAGGGATGATGTTCTGG.

Study of patient-derived pigmented lesions was approved by the internal review board of Mayo Clinic (IRB11-6390). We selected 6 benign nevi and 6 in-transit metastasis of FFPE (*f*ormalin *f*ixed, *p*araffin-*e*mbedded) patient-derived biospecimens randomly from the Mayo Clinic Tissue Archive. Primary skin melanoma that was included here had an invasion depth (Breslow) of $\geq$1 mm

or 0.75–0.99 mm plus any of the following three risk factors: mitotic index > 0 mm [2], tumor ulceration present, or patient age < 40 years. All included primary melanoma patients had an SLN biopsy performed within 90 days of their diagnosis. Consecutive patients were from 2008 to 2012. FFPE blocks were effaced and up to 100 microns of tissue was collected. RNA was extracted and reverse transcribed into cDNA using commercially available kits. Quantitative PCR was performed using standard techniques. RNA copy number was determined by running standards of diluted and linearized DNA containing the desired amplicon and ranging from 5 to 5 million in copy number. SNX copy number was normalized to 25,000 copies of housekeeping genes. Oligonucleotides for SNX amplification were as follows: SNX17-forward: AGCCAGCAAGCAGTG AAGTC; SNX17-reverse: TCAGGTGACTCAAGCAGTGG; SNX31-forward: TAACCATGGACCCAAACGTG; SNX31-reverse: CTCAACGAAGACATCACTTCTCA.

Peptide pull-downs

Pull-downs were performed with the following peptides: β1 wild-type cytoplasmic tail peptide (HDRREFAKFEKE KMNAKWDTGENPIYKSAVTTVVNPKYEGK-OH), β1 scrambled peptide (EYEFEPDKVDTGAKGTKMAKNE KKFRNYTVHNIWESRKVAP-OH), β2 wild-type cytoplasmic tail peptide (TDLREYRRFEKEKLKSQWNNDNPLFK SATTTVMNPKFAES), β3 wild-type cytoplasmic tail peptide (HDRKEFAKFEEERARAKWDTANNPLYKEATS TFTNITYRGT), β5 wild-type cytoplasmic tail peptide (HDRREFAKFQSERSRARYEMASNPLYRKPISTHTVD FAFNKFNKSYNGSVD-OH), and β6 wild-type cytoplasmic tail peptide (HDRKEVAKFEAERSKAKWQTGTNPLYRG STSTFKNVTYKHREKHKAGLSSDG -OH). All peptides were desthiobiotinylated. Prior to use, peptides were immobilized on Dynabeads MyOne Streptavidin C1 (10 mg/ml, Invitrogen) for 3 h at 4 °C.

Fibroblasts expressing Flag-tagged SNX27 and Flag-tagged SNX31 were lysed on ice in Mammalian Protein Extraction Reagent (Thermo Scientific) and 0.5–1 mg of cell lysate was incubated with the indicated peptides overnight at 4 °C. After three washing steps with lysis buffer, we boiled the beads in SDS-PAGE sample buffer and loaded the supernatant on a 8% SDS-PAGE gel.

Expression and purification of GST-tagged proteins

Plasmids encoding GST-tagged SNX31 or GST-tagged SNX31-QW/AA were transformed into Rosetta competent bacteria. Protein expression was induced with 1 mM IPTG and the cells were grown for 3 h at 30 °C. Bacteria were pelleted, washed once with PBS, resuspended in TBS (50 mM Tris–HCl, with 150 mM NaCl, pH 7.4) containing protease inhibitors (Protease Inhibitor Cocktail Tablets, Merck), sonicated with a tip sonicator, and thereafter incubated with 100 µg/ml Lysozyme (Sigma) and 50 µg/ml DNase I (Sigma) at 4 °C for 3 h. Lysates were centrifuged with 14,000 rpm at 4 °C for 20 min. Supernatants were then incubated with 1 ml glutathione Sepharose beads (GST-binding resin) for 3 h at 4 °C. GST-tagged proteins were bound and eluted according to manufacturer's instruction.

For pull-downs, synthetic peptides were immobilized on Dynabeads My One Streptavidin C1 (10 mg/ml, Invitrogen) for 3 h at 4 °C, incubated with 2% BSA in Mammalian Protein Extraction Reagent (Thermo Scientific) for 30 min to block unspecific binding prior to adding 150 ng recombinant GST-tagged SNX31 protein, and further incubated on a rotator for 2 h at 4 °C. After 3 washes with Mammalian Protein Extraction Reagent, proteins were eluted from the beads by boiling with 70 µl SDS-PAGE sample buffer for 5 min, separated by SDS-PAGE gel, and blotted with antibodies against the GST-tag.

Selective immunoprecipitation

Selective isolation of β1 integrins in endocytic vesicles by cell surface immunoprecipitation has been described previously [5]. Briefly, cell surface β1 integrins of live cells were labeled with an anti-β1 integrin antibody (1:1500, homemade) or with an anti-transferrin receptor antibody (1:1000, Abcam) for 1 h on ice followed by two washes with ice-cold PBS to remove unbound antibody. To enrich β1 integrin and transferrin receptor antibody complexes in endosomes, we incubated cells for 10 min in medium with 0.2 mM primaquine. After two PBS washes, cells were lysed in IP buffer [50 mM Tris–HCl (pH 7.5), 150 mM NaCl, 1% Triton X-100, 0.1% sodium deoxycholate, 1 mM ethylenediaminetetraacetic acid, and protease inhibitors] and cleared by centrifugation. The receptor immune complexes were pulled-down by incubation with Protein G Sepharose (Sigma) for 2 h at 4 °C with gentle agitation and subjected to SDS-PAGE and Western blot analysis.

Immunofluorescence

For immunostaining, we cultured cells on glass coverslips coated with 10 µg/ml fibronectin (Calbiochem). Cells were fixed with 4% PFA/PBS for 15 min on ice, washed with PBS, and permeabilized with 0.01% saponin/PBS for 10 min on ice. After blocking unspecific binding with 3% BSA/PBS for 1 h, we incubated the fixed cells with the primary antibody in 3% BSA/0.01% saponin/PBS overnight at 4 °C. After several PBS washes, the fluorescently labeled secondary antibodies were incubated for 1 h at room temperature in the dark. Images were collected at room temperature by Zeiss LSM 780 confocal microscope (Zeiss, Germany) equipped with a 100×/1.4 objective.

To determine the endocytic trafficking of β1 integrins from the cell surface by surface labeling, we seeded cells on fibronectin-coated (5 µg/ml) glass cover dishes (Cellview, Advance TC, Greiner). Cells were washed with cold PBS and incubated with an anti-β1 integrin antibody (HMbeta1-1, BioLegend) for 30 min on ice. Surface-bound antibody was allowed to internalize for 15 min at 37 °C in regular growth medium and subsequently imaged with a 63×/1.4 objective on a Zeiss Observer Z1 microscope equipped with a CSU10 spinning disc scanhead (Yokogawa) and a Coolsnap HQ2 camera (Roper scientific) run by Metamorph software (Molecular Devices, Downingtown, PA). The system was implemented by Visitron Systems.

Sequence alignment

Sequence alignment was made with CLUSTAL Omega und ESPript 3.0 (ESPript[†]) [41]. The matrix of pairwise identity percentages was generated using the LALIGN software.

Analysis of RNA-seq and microarray data

RNA-seq of coding RNA from 27 different human tissues [24] and the GeneAtlas MOE430 gcrma of 191 mouse samples [25] were analyzed via the EMBL-EBI expression atlas‡ and BioGPS§, respectively.

Statistics

Statistical analysis was performed using the GraphPad Prism software (version 5.00, GraphPad Software). Statistical significance was determined by two-tailed student's *t*-test or Mann–Whitney *U*-test as indicated. Results are expressed as the mean ± SD if not indicated otherwise.

Acknowledgments

We thank Dr Roman Nawroth (Technical University of Munich) for providing the RT4 cells and Hildegard Reiter for expert technical assistance. This work was funded by the German Center for Cardiovascular Research and the Deutsche Forschungsgemeinschaft (SFB 914, project A5).

Received 31 January 2014;
Received in revised form 17 June 2014;
Accepted 3 July 2014
Available online 11 July 2014

Keywords:
protein turnover;
SNX17;
SNX27;
integrin trafficking;
melanoma

†http://espript.ibcp.fr.
‡https://www.ebi.ac.uk/gxa/home.
§http://www.biogps.org.

Abbreviations used:
FERM, protein 4.1, ezrin, radixin, moesin; PX, phox; SLN, sentinel lymph node; SNX, sorting nexin; EEA1, early endosomal antigen 1; Lamp1, lysosomal acid membrane protein 1; DAPI, 4′,6-diamidino-2-phenylindole.

References

[1] Caswell PT, Vadrevu S, Norman JC. Integrins: masters and slaves of endocytic transport. Nat Rev Mol Cell Biol 2009;10:843–53.
[2] Valdembri D, Serini G. Regulation of adhesion site dynamics by integrin traffic. Curr Opin Cell Biol 2012;24:582–91.
[3] Dozynkiewicz MA, Jamieson NB, Macpherson I, Grindlay J, van den Berghe PVE, Thun, von A, et al. Rab25 and CLIC3 collaborate to promote integrin recycling from late endosomes/lysosomes and drive cancer progression. Dev Cell 2012;22:131–45.
[4] Lobert VH, Brech A, Pedersen NM, Wesche J, Oppelt A, Malerød L, et al. Ubiquitination of alpha 5 beta 1 integrin controls fibroblast migration through lysosomal degradation of fibronectin-integrin complexes. Dev Cell 2010;19:148–59.
[5] Böttcher RT, Stremmel C, Meves A, Meyer H, Widmaier M, Tseng H-Y, et al. Sorting nexin 17 prevents lysosomal degradation of β1 integrins by binding to the β1-integrin tail. Nat Cell Biol 2012;14:584–92.
[6] Steinberg F, Heesom KJ, Bass MD, Cullen PJ. SNX17 protects integrins from degradation by sorting between lysosomal and recycling pathways. J Cell Biol 2012;197:219–30.
[7] Cullen PJ. Endosomal sorting and signalling: an emerging role for sorting nexins. Nat Rev Mol Cell Biol 2008;9:574–82.
[8] Teasdale RD, Collins BM. Insights into the PX (phox-homology) domain and SNX (sorting nexin) protein families: structures, functions and roles in disease. Biochem J 2012;441:39–59.
[9] Ghai R, Mobli M, Norwood SJ, Bugarcic A, Teasdale RD, King GF, et al. Phox homology band 4.1/ezrin/radixin/moesin-like proteins function as molecular scaffolds that interact with cargo receptors and Ras GTPases. Proc Natl Acad Sci USA 2011;108:7763–8.
[10] Ghai R, Bugarcic A, Liu H, Norwood SJ, Skeldal S, Coulson EJ, et al. Structural basis for endosomal trafficking of diverse transmembrane cargos by PX-FERM proteins. Proc Natl Acad Sci USA 2013;110:E643–52.
[11] Burden JJ, Sun X-M, García ABG, Soutar AK. Sorting motifs in the intracellular domain of the low density lipoprotein receptor interact with a novel domain of sorting nexin-17. J Biol Chem 2004;279:16237–45.
[12] Knauth P, Schlüter T, Czubayko M, Kirsch C, Florian V, Schreckenberger S, et al. Functions of sorting nexin 17 domains and recognition motif for P-selectin trafficking. J Mol Biol 2005;347:813–25.
[13] Stockinger W, Sailler B, Strasser V, Recheis B, Fasching D, Kahr L, et al. The PX-domain protein SNX17 interacts with members of the LDL receptor family and modulates endocytosis of the LDL receptor. EMBO J 2002;21:4259–67.
[14] Williams R, Schlüter T, Roberts MS, Knauth P, Bohnensack R, Cutler DF. Sorting nexin 17 accelerates internalization yet retards degradation of P-selectin. Mol Biol Cell 2004;15:3095–105.
[15] Balana B, Maslennikov I, Kwiatkowski W, Stern KM, Bahima L, Choe S, et al. Mechanism underlying selective regulation of G protein-gated inwardly rectifying potassium channels by the psychostimulant-sensitive sorting nexin 27. Proc Natl Acad Sci USA 2011;108:5831–6.
[16] Steinberg F, Gallon M, Winfield M, Thomas E, Bell AJ, Heesom KJ, et al. A global analysis of SNX27-retromer assembly and cargo specificity reveals a function in glucose and metal ion transport. Nat Cell Biol 2013;15:461–71.
[17] Temkin P, Lauffer B, Jäger S, Cimermancic P, Krogan NJ, Zastrow von M. SNX27 mediates retromer tubule entry and endosome-to-plasma membrane trafficking of signalling receptors. Nat Cell Biol 2011;13:715–21.
[18] Wang X, Zhao Y, Zhang X, Badie H, Zhou Y, Mu Y, et al. Loss of sorting nexin 27 contributes to excitatory synaptic dysfunction by modulating glutamate receptor recycling in Down's syndrome. Nat Med 2013;19:473–80.
[19] Hodis E, Watson IR, Kryukov GV, Arold ST, Imielinski M, Theurillat J-P, et al. A landscape of driver mutations in melanoma. Cell 2012;150:251–63.

[20] Calderwood DA, Fujioka Y, de Pereda JM, García-Alvarez B, Nakamoto T, Margolis B, et al. Integrin beta cytoplasmic domain interactions with phosphotyrosine-binding domains: a structural prototype for diversity in integrin signaling. Proc Natl Acad Sci USA 2003;100:2272–7.
[21] Montanez E, Ussar S, Schifferer M, Bösl M, Zent R, Moser M, et al. Kindlin-2 controls bidirectional signaling of integrins. Genes Dev 2008;22:1325–30.
[22] Tadokoro S, Shattil SJ, Eto K, Tai V, Liddington RC, de Pereda JM, et al. Talin binding to integrin beta tails: a final common step in integrin activation. Science 2003;302:103–6.
[23] van Weert AW, Geuze HJ, Groothuis B, Stoorvogel W. Primaquine interferes with membrane recycling from endosomes to the plasma membrane through a direct interaction with endosomes which does not involve neutralisation of endosomal pH nor osmotic swelling of endosomes. Eur J Cell Biol 2000;79:394–9.
[24] Fagerberg L, Hallström BM, Oksvold P, Kampf C, Djureinovic D, Odeberg J, et al. Analysis of the human tissue-specific expression by genome-wide integration of transcriptomics and antibody-based proteomics. Mol Cell Proteomics 2014;13:397–406.
[25] Lattin JE, Schroder K, Su AI, Walker JR, Zhang J, Wiltshire T, et al. Expression analysis of G protein-coupled receptors in mouse macrophages. Immunome Res 2008;4:5.
[26] Chia PZC, Gleeson PA. The regulation of endosome-to-Golgi retrograde transport by tethers and scaffolds. Traffic 2011;12:939–47.
[27] Rameh LE, Cantley LC. The role of phosphoinositide 3-kinase lipid products in cell function. J Biol Chem 1999;274:8347–50.
[28] Legate KR, Fässler R. Mechanisms that regulate adaptor binding to beta-integrin cytoplasmic tails. J Cell Sci 2009;122:187–98.
[29] Margadant C, Kreft M, de Groot D-J, Norman JC, Sonnenberg A. Distinct roles of talin and kindlin in regulating integrin α5β1 function and trafficking. Curr Biol 2012;22:1554–63.
[30] Meves A, Stremmel C, Böttcher RT, Fässler R. β1 integrins with individually disrupted cytoplasmic NPxY motifs are embryonic lethal but partially active in the epidermis. J Invest Dermatol 2013;133:2722–31.
[31] Meves A, Geiger T, Zanivan S, DiGiovanni J, Mann M, Fässler R. Beta1 integrin cytoplasmic tyrosines promote skin tumorigenesis independent of their phosphorylation. Proc Natl Acad Sci USA 2011;108:15213–8.
[32] Bandyopadhyay A, Rothschild G, Kim S, Calderwood DA, Raghavan S. Functional differences between kindlin-1 and kindlin-2 in keratinocytes. J Cell Sci 2012;125:2172–84.
[33] Rognoni E, Widmaier M, Jakobson M, Ruppert R, Ussar S, Katsougkri D, et al. Kindlin-1 controls Wnt and TGF-β availability to regulate cutaneous stem cell proliferation. Nat Med 2014;20:350–9.
[34] Mai A, Veltel S, Pellinen T, Padzik A, Coffey E, Marjomäki V, et al. Competitive binding of Rab21 and p120RasGAP to integrins regulates receptor traffic and migration. J Cell Biol 2011;194:291–306.
[35] Pellinen T, Arjonen A, Vuoriluoto K, Kallio K, Fransen JAM, Ivaska J. Small GTPase Rab21 regulates cell adhesion and controls endosomal traffic of beta1-integrins. J Cell Biol 2006;173:767–80.
[36] Riggs KA, Hasan N, Humphrey D, Raleigh C, Nevitt C, Corbin D, et al. Regulation of integrin endocytic recycling and chemotactic cell migration by syntaxin 6 and VAMP3 interaction. J Cell Sci 2012;125:3827–39.
[37] Tiwari A, Jung J-J, Inamdar SM, Brown CO, Goel A, Choudhury A. Endothelial cell migration on fibronectin is regulated by syntaxin 6-mediated alpha5beta1 integrin recycling. J Biol Chem 2011;286:36749–61.
[38] Seaman MNJ. The retromer complex—endosomal protein recycling and beyond. J Cell Sci 2012;125:4693–702.
[39] Tsao H, Chin L, Garraway LA, Fisher DE. Melanoma: from mutations to medicine. Genes Dev 2012;26:1131–55.
[40] Pfeifer A, Kessler T, Silletti S, Cheresh DA, Verma IM. Suppression of angiogenesis by lentiviral delivery of PEX, a noncatalytic fragment of matrix metalloproteinase 2. Proc Natl Acad Sci USA 2000;97:12227–32.
[41] Gouet P, Robert X, Courcelle E. ESPript/ENDscript: extracting and rendering sequence and 3D information from atomic structures of proteins. Nucleic Acids Res 2003;31:3320–3.

Kank family proteins comprise a novel type of talin activator

Zhiqi Sun, Hui-Yuan Tseng, Sally J. Deeb, Dirk Dedden, Maik Veelders, Naoko Mizuno, Matthias Mann, Reinhard Fässler

Max Planck Institute of Biochemistry, Martinsried, Germany

Key words: integrin, adhesion, talin, actin

Running title: Kank proteins are talin activators

Abstract

We developed an integrative adhesome analysis by combining a focal adhesion enrichment index with integrin tail interactome to identify novel FA proteins. Using this approach we identified the evolutionarily conserved Kank protein family as novel FA proteins. Interestingly, Kank2 concentrates at the lateral border of FAs (which we term the FA belt), a previously unrecognized FA sub-compartment. Mechanistically, Kank directly binds the talin R7 domain through its evolutionarily conserved KN motif and promotes talin activation in a force- and F-actin-independent manner. Consequently, Kank2 induces and/or maintains the formation of active integrins and destabilizes talin-actin connection. Our data identify Kank family proteins as novel type of talin activator, which specifically stabilize integrin-talin complexes that are uncoupled from the actomyosin system.

Introduction

Mesenchymal migration relies on integrin receptors, a large family of α/β heterodimers that couple the extracellular matrix (ECM) to the actin cytoskeleton [1]. To allow cell adhesion and migration, integrins have to be activated. Integrin activation is characterized by shifting the unbound form of the integrin from a low to a high affinity conformation followed by ligand binding [2]. Ligand bound integrins then cluster and assemble a mechano-sensitive macro-protein complex (called the adhesome) around their cytoplasmic domains [3, 4]. The initial adhesion complex are small, short-lived nascent adhesions (NAs) formed at the periphery of cell protrusions. A limited number of NAs subsequently couple to F-actin and actomyosin-mediated pulling forces reinforce the integrin-ligand interaction and promote the recruitment of more proteins to form large, mature focal adhesions (FAs). The dynamic engagement between integrin and actomyosin serves as a molecular clutch that promotes both forward membrane protrusion and rearward traction force to drive cell migration [5].

Talin and kindlin directly bind to β integrin cytoplasmic tails and play key roles in integrin activation and coupling to actin [6]. Talin is a large, ~270 kD protein composed of an N-terminal FERM (protein 4.1, ezrin, radixin, moesin) domain, also called talin head domain (THD), and a long C-terminal rod domain consisting of 13 helical bundles (R1-R13 domains). The THD is divided into four subdomains (F0, F1, F2, F3). The F3 subdomain of the THD binds β integrin tails and negatively charged lipids on the plasma membrane, and mediates integrin activation. The rod domain contains two F-actin binding sites, several binding sites for RIAM, numerous binding sites for vinculin and a dimerization domain at the extreme C-terminus [7]. The F-actin binding through talin rod couples the integrin/talin complexes to actomyosin, which is required for adhesion re-enforcement and rigidity sensing.

Talin cycles between plasma membrane, where it activates integrins, and cytosol, where it adopts an auto-inhibited form, presumably as a compact globular dimer [8] with an intramolecular interaction between the F3 subdomain and the R9 domain [9, 10]. Since this interaction masks the integrin binding site, talin requires an activation step that disrupts the auto-inhibitory head-rod interaction. A prime candidate for talin activation is the Rap1 effector protein RIAM (Rap1–GTP-interacting adapter molecule), which binds the R8 helical bundle [11], relieves the autoinhibitory interaction and recruits talin to the plasma membrane [12, 13]. A second, potential talin activator is PtdIns(4,5)P_2 [10]. A splice isoform of phosphatidylinositol 4-phosphate 5-kinase type Iγ (PIPKIγ90) locally synthesizes

PtdIns(4,5)P_2 upon recruitment to FAs through direct binding to talin F3 subdomain [14]. Finally, the actin retrograde flow was shown to induce the high affinity state of αLβ2 (LFA-1) on T cells [15], although it is not clear whether talin is the target of the actin flow. However, it is clear from genetic studies that talin activation is a highly redundant process, as neither RIAM- nor PIPKIγ90-deficient mice have apparent phenotypes [16, 17].

In the present paper we developed a FA enrichment index to identify novel FA proteins through high-resolution quantitative mass spectrometry (MS). We identified the evolutionarily conserved Kank protein family as novel FA proteins. Kank family proteins consist of 4 members (Kank1-4) characterized by an N-terminal Kank (KN) motif, several central coil-coil domains and C-terminal ankyrin repeats [18]. Kank1 was shown to restrict microtubule outgrowth at cell cortex by recruiting Kif21a to liprin β1 [19]. Overexpressed Kank proteins inhibit stress fiber formation and migration probably by downregulating RhoA [20]. A single Kank ortholog in *C.elegans*, called VAB19, controls epidermis-muscle attachment [21], neuronal migration [22] and basement membrane sliding during vulval morphogenesis [23]. The Kank3 knockdown in zebrafish leads to epidermal detachment [24]. We found that Kank localizes to the outer border of FAs (which we term the FA belt) and to central fibrillar adhesion, and induces and/or maintains the formation of active integrins at sites lacking actomyosin coupling. Mechanistically, Kank directly binds the talin R7 domain through its evolutionarily conserved KN motif and promotes talin activation in a force- and F-actin-independent manner. Our data identify Kank as novel talin activator, which specifically stabilizes integrin-talin complex that are uncoupled from the actomyosin system.

Results

Kank is a novel FA protein

To identify highly enriched proteins in integrin adhesion sites, we seeded mouse kidney-derived fibroblasts for 3 hours on FN, isolated whole cell lysates and the crosslinked FA fraction and quantified their proteome using high-resolution mass spectrometry combined with the label free protein quantification algorithm (MaxLFQ) (suppl. Fig. 1a). We identified 7954 proteins in the total proteome and 2378 proteins in the corresponding FA-enriched protein fractions. Proteins that were highly abundant in the total proteome were over-represented in the FA-enriched subproteome (suppl. Fig. 1b) pointing to an abundance-dependent unspecific enrichment. We used the false discovery rate (FDR) controlled 2D annotation enrichment algorithm to systematically compare the relative abundance of functional categories between the total proteome and the FA-enriched subproteome and found that proteins involved in cell adhesion including the known adhesome proteins as well as ECM components were strongly enriched in the FA-enriched subproteome, while proteins from intracellular organelles and cytosol such as the endoplasmic reticulum, mitochondria, proteasome were significantly underrepresented in the FA-enriched protein fraction (suppl. Fig. 1c). To identify true FA proteins, we determined the enrichment for each protein of the FA fraction relative to the total proteome abundance (FA enrichment index; FAEI) by calculating ratios of MS-intensity in the FA-enriched subproteome and the total proteome (n=2378; Table S1, suppl. Fig. 1a). The FAEI fits a typical Gaussian distribution (Fig. 1a) with a correlation coefficient of R2 >0.98. Among the proteins in the upper 10% quartile of the FAEI distribution (Table S1), were several novel proteins that have been shown to regulate potentially integrin-regulated processes such as cell adhesion or migration. They include the Kank family member Kank2 (Fig. 1a), three kinases (Csnk1a1, Taok1 and CDK11b) and two phosphatases (Ptp4a2 and Ppp1cc, Table S1).

To identify novel adhesome proteins that associate with β1 integrin tails, we overlaid the FAEI with MS results of β1 integrin tail peptide pulldowns from whole cell lysate. Several known FA proteins enriched with β1 tail peptide pulldown including talin, kindlin and the members of the IPP complex showed high FAEI scores. Proteins such as Dab2 [25], known to bind β1 tails during endocytosis, or SNX17 [26], known to bind β1 tails in the endosomal compartment displayed a low FAEI score. Interestingly, Kank2 was among the proteins that showed a high FAEI score and strong β1 tail binding (Fig. 1a, b). Unlike kindlin2 or c-Src, which preferentially bind β1 and β3 integrin tails respectively, Kank2 bound β1 and

β3 tails with similar efficiencies (Fig. 1c). Immunostaining with polyclonal anti-Kank2 antibodies revealed Kank2-positive puncta closely attached to mature FAs (Fig.1d arrow heads). The nuclear signal is likely unspecific, as it remained in Kank2-depleted cells (data not shown). Interestingly, Kank2-specific immunostaining signals were absent from small NAs. The absence of Kank2 from NAs was confirmed by inhibiting myosin-II with blebbistatin. While blebbistatin-treated cells showed no Kank2 co-localisation with paxillin in NAs at protruding cell membranes (Fig. 1d), Kank2 and paxillin overlapped in thin and long trailing tails (Fig. 1d). Using line intensity profile measurements we observed that endogenous Kank2 puncta peaked at the outer border of FAs (termed FA belt) where conventional FA proteins including talin, kindlin-2, ILK, paxillin and vinculin showed ~50% of their plateau intensity (Fig. 1e-g).

To test whether the localisation of Kank2 to the FA belt depends on the presence of a specific FN-binding integrin class, we overexpressed Kank2-GFP in cells expressing α5β1 and/or αvβ3 and αvβ5 integrins [27], seeded them on FN and determined Kank2 localisation. The experiments revealed that overexrpessed Kank2-GFP localized to the FA belt in β1 as well as αv-class integrin expressing fibroblasts (suppl. Fig 1d), indicating that FA belt localization of Kank2 is integrin class-independent.

Kank is targeted to FAs via the KN motif

To determine the protein domain(s) of Kank2 that is(are) responsible for Kank2 recruitment to FA belt, we generated GFP-tagged Kank2 expression constructs lacking evolutionarily conserved domains (Fig. 2a): the Kank2ΔKN-GFP lacked the Kank (KN) motif; the Kank2ΔCoil-GFP lacked the liprin-binding coiled-coil domain; the Kank2(1-670)-GFP lacked the Kif21a-binding C-terminal ankyrin repeats; and the Kank2ΔKNΔCoil-GFP lacked the KN and coil-coil domains. The constructs were stably transduced into FN-cultured, Kank2-depleted cells (Fig. 2b), and immunostained for paxillin and for F-actin with phalloidin. Similar to endogenous Kank2, full length Kank2-GFP localized to the belt of paxillin-positive FAs and to fibrillar adhesions. In sharp contrast, Kank2ΔKN-GFP did not concentrate on FA belts and fibrillar adhesion but accumulated outside FAs (Fig. 2c-e) co-localizing with liprin β1 (suppl. Fig. 2a). Kank2ΔCoil-GFP and Kank2(1-670)-GFP localized to FA belts and to fibrillar adhesions (Fig. 2c-e), indicating that liprin β1 or Kif21a are not required for FA belt localization of Kank2. Interestingly however, Kank2 could recruit liprin-β1 to FA belt through the coiled-coil domain (suppl. Fig.2a). Kank2ΔKNΔCoil-GFP was diffusely distributed throughout the cytosol (Fig. 2c). To test whether the KN

motif alone is sufficient for FA belt localization, we transduced Kank2-depleted cells with a GFP-tagged KN construct and found a complete overlap of GFP with paxillin (Fig. 2c). These findings indicate (i) that the KN motif is essential to localize Kank2 to FA belts and fibrillar adhesions, (ii) that neither the coil-coil nor the ankyrin repeats are required for Kank2 targeting to the FA belt or exclusion from the FA center, and (iii) that the KN motif peptide is not sufficient to restrict Kank2 localisation to the FA belt.

To test whether the Kank2-KN motif associates with β1 integrin cytoplasmic tails, we performed β1 tail pull downs with lysates from Kank2-depleted cells expressing the GFP-tagged Kank2 expression constructs (Fig. 2a,b) and found that Kank2-GFP and KN-GFP but not GFP or Kank2ΔKN-GFP associated with β1 integrin tail peptides (Fig. 2f,g). In line with the high sequence conservation of the KN motifs from Kank1-4, the GFP-tagged KN motifs from Kank1, Kank3 and Kank4 localized to paxillin-positive FAs (suppl. Fig. 2b). Interestingly, when expressed at similar levels as judge by GFP intensity, Kank1-GFP and Kank3-GFP localized to FA belts, while Kank4-GFP did not show a clear FA belt localization, probably due to its additional diffused localization in the cytoplasm (suppl. Fig. 2c).

The talin rod binds the KN motif of Kank2

Pull down experiments of Kank2 with different wild type and mutant integrin tail peptides from wild type fibroblast lysates revealed that β2 integrin tails had the highest affinity for Kank2, β1 tails an intermediate affinity and β5 tails the lowest affinity (Fig. 3a). Interestingly, the binding profile of Kank2 overlapped with that of talin but not kindlin-2 (Fig. 3a), suggesting that talin and Kank2 are co-recruited to integrin tails. In line with this hypothesis, β1 tails, in which the tyrosine-783 was substituted with alanine (β1-Y783A), neither pulled down Kank2 nor talin, but still kindlin-2 (Fig. 3a). To identify novel Kank2 interacting proteins, we expressed GFP alone or GFP-tagged Kank2 in fibroblasts, performed GFP pull-downs and determined their interactors by MS. In line with a previous report, we identified liprin β1 as a binding partner of Kank2 [19]. Furthermore, talin-1 and two dynein light chain isoforms (Dynll1/LC8a and Dynll2/LC8b) were also among Kank2 interacting proteins (Fig. 3b). Strikingly, while β1 integrin tails specifically recruited talin and Kank2 in tyrosine 783-dependent manner, deletion of talin-1 and talin-2 genes in fibroblasts completely abolished Kank2 recruitment to β1 integrin tails (Fig. 3c), indicating that Kank2 recruitment to integrin tails is indeed talin-dependent. To test whether Kank2 forms a complex with talin through the KN motif, we performed GST pull downs with

recombinant GST-KN motif and recombinant talin head domain (THD) or full length talin-1 (suppl. Fig. 3a). These experiments revealed that the GST-KN motif efficiently pulled down full length talin-1 but not the THD (Fig. 3d) indicating that Kank2 is recruited to β integrin tails through a direct interaction between the KN motif and the talin rod. Fluorescence correlation microscopy measurements revealed a binding affinity of 230±70 nM (mean ± error represents 95% confidence interval) between recombinant full length talin and fluorescently labelled KN peptide (suppl. Fig. 3b). To further narrow down the KN-binding site on the talin rod we expressed different GFP-tagged Talin rod domains in fibroblasts, prepared cell lysates, incubated the cell lysates with the recombinant GST-KN motif and immunoprecipitated protein complexes with anti-GFP antibodies. The experiments revealed that the R7R8 domains of the talin rod bind the GST-KN motif (suppl. Fig. 3c). Altogether these findings show that the KN motif of Kank2 can directly bind the R7R8 domains of Talin.

Kank2 induces Talin and β1 integrin activation

The R7R8 domains were shown to bind RIAM, actin and vinculin [28], all of which can induce and/or maintain the active, integrin binding state of talin. Therefore, we tested whether Kank2 binding to the R7R8 domains also controls talin-integrin interactions. First, we incubated normal fibroblast cell lysates with bacterially expressed, recombinant GST-KN polypeptides or chemically synthesized KN peptides and subsequently performed β1 integrin tail pulldowns. The experiments revealed that GST-KN as well as the synthesized KN peptide efficiently displaced endogenous Kank2 from β1 integrin tail peptides and strongly increased talin binding but affected neither kindlin2 nor Dab2 binding (Fig. 4a; suppl. Fig. 4a-d). Second, we depleted Kank2 using specific shRNA and found that Kank2 depletion decreased binding of endogenous talin to β1 integrin tail peptides by ~30% (Fig. 4b), while overexpression of full length Kank2-GFP but not Kank2ΔKN-GFP increased talin binding to β1 integrin tails in a dose-dependent manner (suppl. Fig. 4e, f). Third, we incubated equal molar (10nM) recombinant full length talin protein with either GST-KN or GST and performed integrin tail peptide pulldown assays *in vitro*. We observed that the GST-KN protein but not GST significantly increased talin binding to β1 integrin tails and that GST-KN was co-recruited with talin to β1 integrin tail (Fig. 4c). Finally, co-expression of talin-GFP with Cherry-tagged Kank2, Kank2ΔKN and Kank2-KN in Kank2-depleted fibroblasts revealed that Kank2 as well as Kank2-KN enhanced localization of talin-GFP to kindlin2-positive adhesion sites, while Kank2ΔKN or Cherry left talin-1-GFP to a large

extent in the cytosol (Fig. 4d,e). These findings clearly indicate that Kank2 induces and/or maintains talin binding to integrin β tails through the KN motif.

Since the activation of talin is a pre-requisite for integrin activation we next tested whether Kank2 regulates integrin activation. To this end, we overexpressed Kank2-GFP, Kank2ΔKN-GFP, KN-GFP or GFP in fibroblasts, seeded them on FN and immunostained them with the activation epitope reporting antibody 9EG7. We found that overexpressed Kank2-GFP or KN-GFP co-localized with 9EG7-positive β1 integrins and increased active β1 integrin clusters in the central cell area, while overexpression of Kank2ΔKN-GFP had no influence on the active integrin clusters at the ventral cell cortex compared with GFP alone (Fig.4f,g).

Kank2 regulates Talin turnover, adhesion remodeling and cell migration

It has been shown that overexpression of Kank2 proteins suppressed stress fiber formation [18]. We next co-stained 9EG7 epitope with phalloidin in cell expressing GFP or Kank2-GFP. We noticed that Kank2-GFP strongly co-localized with active integrin clusters that were apparently not linked with thick stress fibers (suppl. Fig.5a). While Kank2-GFP overexpression consistently increased active β1 integrin clusters, the phalloidin-stained F-actin in 9EG7-positive area is significantly reduced (suppl. Fig.5b, c), suggesting that Kank2 may dislodged F-actin from talin. It has been has been shown that talin binding to F-actin plays the dominant role in immobilizing talin within adhesion sites [29, 30]. To test whether Kank2 regulates talin turnover, we performed fluorescence recovery after photobleaching (FRAP) in central adhesion sites of Kank-2-deplted fibroblasts expressing Kank2-mCherry, Kank2ΔKN-mCherry, KN-mCherry or mCherry alone. While neither Kank2ΔKN, nor the KN motif alone affected the mobile fraction of talin in comparison with mCherry control, expression of full length Kank2 increased the mobile fraction of Talin from 63.8±9.0% to 92.4±7.5% (Fig. 5a-c) suggesting that talin is almost completely decoupled from F-actin by full length Kank2. Interestingly, however, when we calculated the recovery rates of talin-GFP by measuring κ ($1/\tau_{1/2}$) we noticed that full length Kank2 but not Kank2ΔKN reduced the recovery rates of Talin by ~50% (Fig.5b,d), which indicates that Talin associated with Kank2 undergoes a more stable association to β integrin tails. While the KN motif alone did not change the mobile fraction of Talin in adhesion sites, it reduced Talin recovery rates in comparison to mCherry, although not to the same extent as full length Kank2 (Fig. 5d).

Next we examined whether Kank2-induced talin turnover changes adhesion dynamics. To this end, we expressed talin-TagRFP in Kank2-depleted cells rescued with either Kank2-GFP or Kank2ΔKN-GFP and imaged individual adhesion sites over a period of 10 min. In Kank2 expressing cells, talin- TagRFP-positive central adhesions underwent rapid lateral sliding movements and shape remodeling (Fig. 5e; suppl. Movie 1). In sharp contrast, in cells expressing Kank2ΔKN, talin-TagRFP-positive central adhesions remained largely immobile before disassembly (Fig. 5e; suppl. Movie 2). As revealed in color-overlaid time lapse images, Kank2-GFP but Kank2ΔKN-GFP induced adhesion sliding throughout the cell (Fig, 5f). Tracking the mass center of the adhesion sites revealed that expression of full length Kank2 induced a significantly higher adhesion sliding velocity in comparison to expression of Kank2ΔKN (Fig, 5g). Moreover, we observed rapid extensional growth of the adhesion structure in cells expressing full length Kank2 (suppl. Fig. 5d; suppl. Movie 3), suggesting that Kank2 is able to promote de novo assembly of adhesion structure. Altogether these findings suggest that Kank2 regulates talin turnover and adhesion remodeling both by stabilizing talin-integrin complexes and by destabilizing talin-actin linkage.

Increased adhesion sliding is correlated with reduced migration [31]. To test whether Kank2 influences integrin-mediated 2D random cell migration, we depleted ~90% of Kank2 using 2 independent shRNA in fibroblasts (Fig. 6a). Kank2 depletion significantly increased cell migration velocity (Fig. 6b), while directional persistence or β1 integrin expression remained unaffected (Fig.6a and data not shown). Conversely, overexpression of Kank2 (Fig. 6c) reduced migration velocity, regardless whether serum was present or absent during the experiment (Fig. 6d). Finally, the accelerated migration speed of Kank2 knockdown cells was normalized by re-expressing full length Kank2-AcGFP but not Kank2ΔKN-AcGFP or Kank2-KN-AcGFP as measured by mean square displacement (Fig. 6.e,f). Together these result indicate that Kank2 suppresses cell migration by stabilizing talin-integrin complex in the absence of stress fiber coupling.

Discussion

Recent advances in focal adhesion isolation and proteomic analysis provided comprehensive profiling of integrin adhesome [4]. However, the protein enrichment analysis based on spectral counting or label free quantification (LFQ) in biochemical fractions are biased by the protein abundance in the raw material [32]. By normalizing the LFQ intensities in purified FA with total expression level, we derived the FA enrichment index (FAEI), which reflects the enrichment of each protein in the FA fraction regardless of its expression level. Combined with β1 integrin tail interactome, we identified Kank2 as a novel component in integrin binding complex. The evolutionarily conserved Kank family proteins have been implicated in cell-ECM adhesion. For instance, Kank homologue, vab19 in *C.elegans* act synergistically with integrin to restrict basement membrane sliding during vulval morphogenesis [23]. Importantly, mutations of Kank1, Kank2 and Kank4 in human lead to nephrotic syndrome [33], which is often caused by defects in integrin-mediated adhesion or hyper-activated Rho GTPase [34, 35]. Kank1 deletion results in cerebral palsy type 2, spastic quadriplegic (CPSQ2) which could be due to neuronal migration defects [36].

Kank2 is connected to integrin through talin as Kank2 recruitment to integrin tail was abolished in talin-1 and talin-2 double knockout cells. We found direct interaction between KN motif in Kank2 and R7 domain in talin rod. Talin is autoinhibited in the cytoplasm by intramolecular interaction between F3 domain in talin head the R9 in talin rod. Its activation is thought to be mediated by Rap1-RIAM complex and $PI(4,5)P_2$ at the plasma membrane. Activated talin couples integrin with actomyosin system through direct and indirect F-actin binding. The affinity between KN motif and full length Talin measured with FCS is 230±70nmol, in the same range of talin auto-inhibitory interaction. R7 and R8 domains have unique folding with R8 domain inserted in R7 domain. Strikingly, Kank2 binding to talin induced talin activation. Notably, Kank-mediated talin activation could be reconstituted in either cell lysate or recombinantly *in vitro* in a force and F-actin-independent manner. Accordingly, Kank2 promotes translocation of overexpressed talin from cytosol to adhesion sites in KN motif-dependent manner. Consistent with the role of talin in integrin activation, overexpression of Kank2 but not KN motif deletion mutant induced more active β1 integrin clusters in adherent cells. Since R7R8 domain also contains high affinity binding sites for RIAM, vinculin and F-actin, all of which are implicated in talin activation, our data indicate that R7R8 fusion domain contains talin activation motifs where protein interactions disturb talin auto-inhibitory conformation.

Whether other proteins (e.g. DLC1 and synemin) [37, 38] that also bind R7R8 domain have similar talin activation activity needs further investigation.

Intriguingly, endogenous and ectopically expressed Kank2 as well as other Kank homologs concentrate at the lateral border of focal adhesions (FA belt) and fibrillar adhesions but not in nascent adhesions. This localization relies on the interaction with talin as KN motif deletion mutant failed to associate with adhesion border but localized to liprin-β1-positive cortical complex ~200nm away from FA border. Thus Kank2 marks the FA belt as a novel FA sub-compartment. The FA belt localization of Kank2 is independent of integrin subtype since Kank2 concentrates at FA belt in cell expressing only α5β1 integrin or αVβ3/β5 integrins. Notably, KN motif alone was not restricted to FA border but also penetrated into the center of FA, indicating that an unknown structural or functional feature in full length Kank2 excludes it from FA center. It has been shown that RIAM and vinculin compete for talin binding and localize to nascent adhesion and focal adhesion respectively in mutually exclusive manner [39, 40]. Similarly, Kank2 may be excluded from FA center by steric hindrance with other talin interacting molecules.

FA center is linked to thick stress fibers and exerts mechanical tension. Overexpression of Kank proteins has been shown to attenuate stress fiber formation at least partially through down-regulating RhoA activity probably by recruiting RhoGDI [33]. We hypothesize that Kank proteins may locally dislodge F-actin from talin-integrin complex. In comparison with the dynamic interaction between talin head domain and integrin, the F-actin binding through talin rod plays a dominant role in talin immobilization within FA. Our FRAP analysis of talin dynamics revealed that Kank2 but not KN motif deletion mutant increased the talin mobile fraction from ~65% to ~94%. Thus Kank2 almost induced complete mobilization of talin within adhesion, indicating that it destabilized talin's linkage to F-actin. On the other hand, Kank2 but not KN motif deletion mutant slowed the talin recovery rate in the mobile fraction, indicating a reduced off-rate due to stabilized talin-integrin complex. Consistent with its FA center localization, KN motif reduced talin recovery rate but failed to mobilize talin. These data suggests that Kank2 uncoupled talin-mediated integrin activation from actomyosin linkage. Consistent with this hypothesis, Kank2 co-localized with active β1 integrin clusters that appeared not linked to stress fibers. Mechanistically it is difficult to envision how Kank2 controls talin coupling to F-actin. Since Kank2 interacts with central region in Talin rod, calpain-dependent cleavage between talin head and rod is unlikely to be the cause. Kank2 binding may directly pose steric hindrance for F-actin binding on talin.

Post-translational modification may also be involved since methylation of Talin C-terminal F-actin binding site by methyltransferase Ezh2 partially liberates Talin from F-actin [41]. Kank2 may also locally inhibit RhoA activity through RhoGDI and thus suppress F-actin filament assembly.

Integrin-mediated cell migration is driven by the molecular clutch between integrins and actomyosin system [5]. The migration velocity is determined by the balance between clutch engagement and adhesiveness [42, 43]. Stationary fibroblasts exhibit more sliding adhesions, reflecting uncoupled actomyosin connection to ECM and reduced catch-bond interaction [31]. DNA hairpin-based digital force sensor revealed that certain adhesion plaques in the cell do not apply force to their ECM ligands [44]. Consistent with our FRAP analysis, Kank2-GFP and talin-1-TagRFP positive adhesion structures underwent rapid sliding movement and shape deformation, suggesting a slip-bond behavior. In sharp contrast, in cells expressing mutant Kank2 lacking KN motif, talin-1-TagRFP-labeled adhesions remained static and underwent only slight uniaxial movement likely along stress fiber. Our observations suggest that Kank2 could maintain adhesive structure with a slip-bond interface and prevented its conversion to a catch-bond interface. While the catch-bond interface applies pulling force to drive cell migration, slip-bond interface provides frictional adhesiveness that inhibits cell migration. In this sense, the excessive basement membrane sliding in vab-19 mutant in *C.elegans* may be caused by reduced cell adhesiveness and increase cell traction force on the ECM. Indeed, Kank2 overexpression strongly suppressed random cell migration velocity. Conversely, Kank2 knockdown led to increase cell migration speed. Although KN motif alone is able to activate talin, it is required in the full length Kank2 but not sufficient by itself to reduce cell migration velocity in Kank2-depleted cells.

Besides regulating talin activation and talin-actin linkage, Kank proteins may control cell migration by regulating local ECM degradation. We have identified liprin-β1 and two dynein light chain subunits dynll1 and dynll2 as Kank2 binding partners. Kank1 has been shown to interact with liprin-β1 and restrict cortical microtubule (MT) growth by recruiting Kif21a [19]. Although we did not find Kif21a in Kank2 interactome probably due to its low expression in fibroblasts, dynein motors are also involved in MT capture on cell cortex [45]. Liprin-β1 forms large protein complex containing at least liprin-α, ELKS and LL5, which captures MT plus end protein CLASPs and mediates focal exocytosis of MT1-MMP around FAs [19, 46-48]. Local metalloprotease exocytosis then facilitates FA disassembly. Although

liprin interaction is not required for Kank2's FA belt localization, Kank2 could recruit liprin-β1 to FA belt. Moreover, in the absence of talin binding, Kank2ΔKN mutant fully colocalized with liprin-β1. Thus, Kank2 is not only able to participate into both integrin-talin and liprin complex but also further bridge these two complexes. Whether Kank proteins coordinate integrin activation with local exocytosis will be investigated in the future.

Despite the importance of talin activation, neither PIPKIγ90 knockout mice nor RIAM knockout mice display obvious developmental defect [16, 17], suggesting that Talin activation mechanisms may be highly redundant in vivo. Moreover, RIAM knockdown decreased melanoma cell migration [49] whereas a Talin mutant with disrupted auto-inhibition led to delayed dorsal epidermal closure in drosophila [50]. Together with these observations, our data support the existence of redundant and more importantly, functionally distinct talin activation mechanisms. Different talin activation modes have different migratory effects according to differential actomyosin or membrane coupling.

References

1. Hynes, R.O. Integrins: bidirectional, allosteric signaling machines. *Cell* **110**, 673-687 (2002).
2. Luo, B.H., Carman, C.V. & Springer, T.A. Structural basis of integrin regulation and signaling. *Annu Rev Immunol* **25**, 619-647 (2007).
3. Schiller, H.B. & Fassler, R. Mechanosensitivity and compositional dynamics of cell-matrix adhesions. *EMBO reports* **14**, 509-519 (2013).
4. Winograd-Katz, S.E., Fassler, R., Geiger, B. & Legate, K.R. The integrin adhesome: from genes and proteins to human disease. *Nature reviews. Molecular cell biology* **15**, 273-288 (2014).
5. Gardel, M.L., Schneider, I.C., Aratyn-Schaus, Y. & Waterman, C.M. Mechanical integration of actin and adhesion dynamics in cell migration. *Annual review of cell and developmental biology* **26**, 315-333 (2010).
6. Calderwood, D.A., Campbell, I.D. & Critchley, D.R. Talins and kindlins: partners in integrin-mediated adhesion. *Nature reviews. Molecular cell biology* **14**, 503-517 (2013).
7. Critchley, D.R. Biochemical and structural properties of the integrin-associated cytoskeletal protein talin. *Annual review of biophysics* **38**, 235-254 (2009).
8. Goult, B.T. *et al.* Structural studies on full-length talin1 reveal a compact auto-inhibited dimer: implications for talin activation. *Journal of structural biology* **184**, 21-32 (2013).
9. Song, X. *et al.* A novel membrane-dependent on/off switch mechanism of talin FERM domain at sites of cell adhesion. *Cell research* **22**, 1533-1545 (2012).
10. Goksoy, E. *et al.* Structural basis for the autoinhibition of talin in regulating integrin activation. *Molecular cell* **31**, 124-133 (2008).
11. Chang, Y.C. *et al.* Structural and mechanistic insights into the recruitment of talin by RIAM in integrin signaling. *Structure* **22**, 1810-1820 (2014).
12. Han, J. *et al.* Reconstructing and deconstructing agonist-induced activation of integrin alphaIIbbeta3. *Current biology : CB* **16**, 1796-1806 (2006).
13. Lafuente, E.M. *et al.* RIAM, an Ena/VASP and Profilin ligand, interacts with Rap1-GTP and mediates Rap1-induced adhesion. *Developmental cell* **7**, 585-595 (2004).
14. Legate, K.R. *et al.* Integrin adhesion and force coupling are independently regulated by localized PtdIns(4,5)2 synthesis. *The EMBO journal* **30**, 4539-4553 (2011).
15. Comrie, W.A., Babich, A. & Burkhardt, J.K. F-actin flow drives affinity maturation and spatial organization of LFA-1 at the immunological synapse. *The Journal of cell biology* **208**, 475-491 (2015).
16. Legate, K.R., Montag, D., Bottcher, R.T., Takahashi, S. & Fassler, R. Comparative phenotypic analysis of the two major splice isoforms of phosphatidylinositol phosphate kinase type Igamma in vivo. *Journal of cell science* **125**, 5636-5646 (2012).
17. Stritt, S. *et al.* Rap1-GTP-interacting adaptor molecule (RIAM) is dispensable for platelet integrin activation and function in mice. *Blood* **125**, 219-222 (2015).
18. Kakinuma, N., Zhu, Y., Wang, Y., Roy, B.C. & Kiyama, R. Kank proteins: structure, functions and diseases. *Cellular and molecular life sciences : CMLS* **66**, 2651-2659 (2009).
19. van der Vaart, B. *et al.* CFEOM1-associated kinesin KIF21A is a cortical microtubule growth inhibitor. *Developmental cell* **27**, 145-160 (2013).
20. Kakinuma, N., Roy, B.C., Zhu, Y., Wang, Y. & Kiyama, R. Kank regulates RhoA-dependent formation of actin stress fibers and cell migration via 14-3-3 in PI3K-Akt signaling. *The Journal of cell biology* **181**, 537-549 (2008).

21. Ding, M., Goncharov, A., Jin, Y. & Chisholm, A.D. C. elegans ankyrin repeat protein VAB-19 is a component of epidermal attachment structures and is essential for epidermal morphogenesis. *Development* **130**, 5791-5801 (2003).
22. Yang, Y., Lee, W.S., Tang, X. & Wadsworth, W.G. Extracellular matrix regulates UNC-6 (netrin) axon guidance by controlling the direction of intracellular UNC-40 (DCC) outgrowth activity. *PloS one* **9**, e97258 (2014).
23. Ihara, S. *et al.* Basement membrane sliding and targeted adhesion remodels tissue boundaries during uterine-vulval attachment in Caenorhabditis elegans. *Nature cell biology* **13**, 641-651 (2011).
24. Boggetti, B. *et al.* NBP, a zebrafish homolog of human Kank3, is a novel Numb interactor essential for epidermal integrity and neurulation. *Developmental biology* **365**, 164-174 (2012).
25. Ezratty, E.J., Bertaux, C., Marcantonio, E.E. & Gundersen, G.G. Clathrin mediates integrin endocytosis for focal adhesion disassembly in migrating cells. *The Journal of cell biology* **187**, 733-747 (2009).
26. Bottcher, R.T. *et al.* Sorting nexin 17 prevents lysosomal degradation of beta1 integrins by binding to the beta1-integrin tail. *Nature cell biology* **14**, 584-592 (2012).
27. Schiller, H.B. *et al.* beta1- and alphav-class integrins cooperate to regulate myosin II during rigidity sensing of fibronectin-based microenvironments. *Nature cell biology* **15**, 625-636 (2013).
28. Gingras, A.R. *et al.* Central region of talin has a unique fold that binds vinculin and actin. *The Journal of biological chemistry* **285**, 29577-29587 (2010).
29. Himmel, M. *et al.* Control of high affinity interactions in the talin C terminus: how talin domains coordinate protein dynamics in cell adhesions. *The Journal of biological chemistry* **284**, 13832-13842 (2009).
30. Rossier, O. *et al.* Integrins beta1 and beta3 exhibit distinct dynamic nanoscale organizations inside focal adhesions. *Nature cell biology* **14**, 1057-1067 (2012).
31. Smilenov, L.B., Mikhailov, A., Pelham, R.J., Marcantonio, E.E. & Gundersen, G.G. Focal adhesion motility revealed in stationary fibroblasts. *Science* **286**, 1172-1174 (1999).
32. Mellacheruvu, D. *et al.* The CRAPome: a contaminant repository for affinity purification-mass spectrometry data. *Nature methods* **10**, 730-736 (2013).
33. Gee, H.Y. *et al.* KANK deficiency leads to podocyte dysfunction and nephrotic syndrome. *The Journal of clinical investigation* (2015).
34. Gee, H.Y. *et al.* ARHGDIA mutations cause nephrotic syndrome via defective RHO GTPase signaling. *The Journal of clinical investigation* **123**, 3243-3253 (2013).
35. Tian, X. *et al.* Podocyte-associated talin1 is critical for glomerular filtration barrier maintenance. *The Journal of clinical investigation* **124**, 1098-1113 (2014).
36. Lerer, I. *et al.* Deletion of the ANKRD15 gene at 9p24.3 causes parent-of-origin-dependent inheritance of familial cerebral palsy. *Human molecular genetics* **14**, 3911-3920 (2005).
37. Li, G. *et al.* Full activity of the deleted in liver cancer 1 (DLC1) tumor suppressor depends on an LD-like motif that binds talin and focal adhesion kinase (FAK). *Proceedings of the National Academy of Sciences of the United States of America* **108**, 17129-17134 (2011).
38. Sun, N., Critchley, D.R., Paulin, D., Li, Z. & Robson, R.M. Identification of a repeated domain within mammalian alpha-synemin that interacts directly with talin. *Experimental cell research* **314**, 1839-1849 (2008).
39. Goult, B.T. *et al.* RIAM and vinculin binding to talin are mutually exclusive and regulate adhesion assembly and turnover. *The Journal of biological chemistry* **288**, 8238-8249 (2013).

40. Lee, H.S., Anekal, P., Lim, C.J., Liu, C.C. & Ginsberg, M.H. Two modes of integrin activation form a binary molecular switch in adhesion maturation. *Molecular biology of the cell* **24**, 1354-1362 (2013).
41. Gunawan, M. *et al.* The methyltransferase Ezh2 controls cell adhesion and migration through direct methylation of the extranuclear regulatory protein talin. *Nature immunology* (2015).
42. Palecek, S.P., Loftus, J.C., Ginsberg, M.H., Lauffenburger, D.A. & Horwitz, A.F. Integrin-ligand binding properties govern cell migration speed through cell-substratum adhesiveness. *Nature* **385**, 537-540 (1997).
43. Gupton, S.L. & Waterman-Storer, C.M. Spatiotemporal feedback between actomyosin and focal-adhesion systems optimizes rapid cell migration. *Cell* **125**, 1361-1374 (2006).
44. Blakely, B.L. *et al.* A DNA-based molecular probe for optically reporting cellular traction forces. *Nat Methods* **11**, 1229-1232 (2014).
45. Hendricks, A.G. *et al.* Dynein tethers and stabilizes dynamic microtubule plus ends. *Current biology : CB* **22**, 632-637 (2012).
46. Stehbens, S.J. *et al.* CLASPs link focal-adhesion-associated microtubule capture to localized exocytosis and adhesion site turnover. *Nature cell biology* **16**, 561-573 (2014).
47. Grigoriev, I. *et al.* Rab6 regulates transport and targeting of exocytotic carriers. *Developmental cell* **13**, 305-314 (2007).
48. Lansbergen, G. *et al.* CLASPs attach microtubule plus ends to the cell cortex through a complex with LL5beta. *Developmental cell* **11**, 21-32 (2006).
49. Colo, G.P. *et al.* Focal adhesion disassembly is regulated by a RIAM to MEK-1 pathway. *Journal of cell science* **125**, 5338-5352 (2012).
50. Ellis, S.J. *et al.* Talin autoinhibition is required for morphogenesis. *Current biology : CB* **23**, 1825-1833 (2013).

Figure legends

Figure 1. Identification of Kank2 as a novel component in integrin complex.

(a) Histogram of focal adhesion enrichment index (FAEI). (b) Scatter plot of β1 integrin tail peptide binding proteins overlay with coloration according to FAEI. The $\log_2$ SILAC ratio of proteins are plotted as the forward pulldown (x axis) against the reverse labelling pulldown (y axis). (c) Westernblot analysis of proteins complex assembled around β1 and β3 integrin tail peptides. (d) Mouse kidney fibroblasts are plated on fibronectin for 3hours, then treated with or without blebbistatin for 1hour, fixed and immunostained for endogenous Kank2, paxillin (Pxn, red), F-actin with phalloidin (blue) and DAPI (grey). Scale bar, 10μm. (e) Line profile analysis of focal adhesion stained with anti-Talin and anti-vinculin antibody together with Kank2. (f) Theoretical definition of the lateral border of focal adhesion and distance to FA border in line profile analysis. (g) Measurement of the distance between Kank2-postive puncta and FA border using different conventional FA protein markers including ILK, kindlin, vinculin, talin and paxillin. The Kank2-positive puncta structures locates at the lateral border of focal adhesion in line profile analysis.

Figure 2. KN motif is essential for Kank2 localization at FA border and recruitment to integrin tail complex.

(a) Domain organization of Kank2 protein and illustration of truncation/deletion mutant design. (b) Westernblot analysis of the expression level of endogenous Kank2 and reconstituted GFP-tagged Kank2 constructs using anti-Kank2 antibody and ant-GFP antibody in cell with stable Kank2 knockdown and reconstitutions with GFP-tagged Kank2 truncation/deletion mutants. Vinculin is used as loading control. (c) Immunofluorescence of GFP-tagged Kank2 constructs (green) co-stained with anti-Paxillin antibody (Pxn, red), phalloidin (blue) and DAPI (grey). Scale bar, 10μm. (d) Line profile analysis for localization of full length Kank2 and Kank2ΔKN mutant. (e) Quantification of the distance between indicated Kank2 wild type and mutants' localization to FA border indicates KN motif is required for FA association. Student t-test ***P<0.0001. (f)&(g) Integrin tail peptide pulldown and westernblot analysis showed that GFP-tagged full length Kank2 and KN motif along but not Kank2ΔKN mutant or GFP control could be recruited to integrin tail complex. Kank2 constructs were detected with anti-GFP antibody. Kindlin2 was used as positive control.

Figure 3. Kank2 is recruited to integrin tail complex through direct interaction with Talin.

(a) Westernblot (upper panel) and densitometry analysis (lower panel) of the recruitments of endogenous Kank2, kindlin2 and talin to wildtype β1, β2, β5 integrin tail and β1 integrin tail with tyrosine to alanine mutation at the position of tyrosine 783 in full length β1 integrin (β1 Y783A). β1 scrambled peptide (β1 scr) was used as universal control. Note that the binding profiles of Kank2 and talin completely overlapped with each other. (b) Scatter plot of LFQ-intensity ratio between Kank2-GFP pulldown and GFP control pulldown identified Ppfibp1, Dynll1, Dynll2 and talin-1 as strongest Kank2 binding partners. (c) Westernblot (upper panel) and densitometry analysis (lower panel) of the recruitments of endogenous Kank2, kindlin2 and talin to wildtype β1 tail and β1 Y783A mutant tail peptides from wildtype cells (Talin-1/2 flox/flox) or talin knockout cells (Talin-1/2 DKO). Kank2 recruitment to integrin tail strictly depends on the presence of talin. Student t-test ***P<0.0001. (d) GST pulldown of GST-KN fusion protein or GST control with full length recombinant talin-1 or talin-head domain (THD).

Figure 4. Kank2 activates talin and promote integrin activation

(a) Westernblot (left panel) and densitometry analysis (right panel) of the recruitments of endogenous Kank2, talin, kindlin-2 and Dab2 to β1 integrin tail peptide in the presence of exogenous KN-GST or GST recombinant protein. GST-KN recombinant protein replaced endogenous Kank2 but promoted Talin recruitment without affecting kindlin-2 or Dab2 binding. (b) Westernblot (left panel) and densitometry analysis (right panel) of the recruitments of endogenous Kank2, talin and kindling-2 to β1 integrin tail in control cells or Kank2-knockdown cells. (c) Westernblot (left panel) and densitometry analysis (right panel) show that purified GST-KN promotes recombinant talin-1 binding to β1 integrin tail in vitro. (d) Talin-AcGFP (shown in rainbow LUT) was co-transfected with Cherry-tagged full length Kank2, Kank2ΔKN mutant, KN motif along or cherry control into Kank2 knockdown cells. Cells are fixed and stained for kindling-2 (blue). Scale bar, 10μm. (e) Quantification of talin-AcGFP intensity ratio between kindling-2-positive adhesion area and kindling-2-negative cytosolic region in (d) revealed that Kank2 promoted talin localization to adhesion sites through KN motif. (f) Kank2 knockdown cells were transfected with GFP-tagged full length Kank2, Kank2ΔKN mutant, KN motif along or GFP control (green), plated on fibronectin and stained for active integrin with 9EG7 antibody (shown in rainbow LUT). Scale bar, 10μm. (g) Kank2 promote active integrin cluster

formation through KN motif. 9EG7 staining intensity per cell area is quantified from (f). Student t-test *P<0.05, **P<0.01, ***P<0.0001.

Figure 5. Kank2 regulate Talin turnover and adhesion dynamics.

(a) Representative timelapse images of Talin-1-AcGFP (shown in rainbow LUT) in FRAP experiments. Talin-1-AcGFP was co-transfected with Cherry-tagged full length Kank2 or Kank2ΔKN mutant into Kank2 knockdown cells. AcGFP signal is bleached in region of interest (ROI, red circle). (b) Fluorescence recovery curves corresponding to FRAP experiments in (a). Mean fluorescence intensity in ROI is plotted as the percentage of the initial intensity after normalization to cytosolic background. Fluorescent recovery curves from 6 FRAP experiments are fitted with one-phase association model (mean±s.d.). (c) Full length Kank2 but not Kank2ΔKN mutant or KN motif along increased talin-1 mobile fraction in adhesion sites. Mobile fraction is quantified from 10 independent FRAP experiment (mean ± sd. one-way ANOVA Tukey test, ***P<0.001). (d) Full length Kank2 and KN motif along but not Kank2ΔKN mutant reduced talin-1-AcGFP recovery rate. Recovery rate is quantified from 10 independent FRAP experiment (mean ± sd. one-way ANOVA Tukey test, *P<0.05, **P<0.01, ***P<0.0001). (e) Timelapse images of talin-1-TagRFP (rainbow LUT) and Kank2-GFP or Kank2ΔKN-GFP. Talin-1-Tag-RFP was co-transfected with Cherry-tagged full length Kank2 or Kank2ΔKN mutant into Kank2 knockdown cells. Scale bar, 5μm. (f) Color overlay of talin timelapse images from 0min (red), 5min (green) and 10min (blue). (g) Sliding velocities of talin-positive adhesion sites were plotted as box and whisker (min to max). Student t-test ***P<0.001.

Figure 6. Kank2 regulates cell migration through talin.

(a) Westernblot analysis of Kank2 and β1 integrin (Itgb1) expression in cells expressing scrambled shRNA control or two different Kank2 shRNA. B-actin is used as loading control. (b) Kank2 knockdown increased velocity of 2-D random migration on fibronectin. Data is illustrated as box and whisker (minimal to maximal value). Student t-test ***P<0.0001. (c) Westernblot analysis of Kank2 and β1 integrin (Itgb1) expression in cells expressing GFP control or Kank-GFP fusion protein. B-actin is used as loading control. (d) Kank2 overexpression decreased velocity of 2-D random migration on fibronectin with or without serum stimulation. Data is illustrated as box and whisker (minimal to maximal value). Student t-test ***P<0.0001. (e) Single cell tracking is plotted for Kank2 knockdown cells rescued with wild type Kank2, Kank2 lacking KN motif, KN motif alone or GFP control. (f)

Mean square displacement analysis showed that only full length Kank2 restored normal cell migration speeds in Kank2 knockdown cells.

Supplementary figure legends

Suppl. Figure 1

(a) Experiment work flow for mass spectrometry analysis and focal adhesion enrichment index (FAEI) calculation. (b) Histogram of LFQ intensity distribution of total proteome for all quantified proteins in whole cell lysates and those identified in isolated adhesion revealed that adhesion isolation method tends to enrich high abundance proteins. (c) False discovery rate (FDR) controlled 2D annotation enrichment analysis of the relative abundance of functional categories between the total proteome and the FA-enriched subproteome. (d) Kank2-EGFP was overexpressed in cells expressing only α5β1 or αvβ3/β5 integrins and stained for paxillin (Pxn, red), F-actin with phalloidin (blue) and DAPI (grey). Scale bar, 10μm.

Suppl. Figure 2

(a) Immunofluorescence of GFP-tagged Kank2 constructs (green) co-stained with anti-paxillin antibody (Pxn, blue), anti-liprin β1 antibody (red) and DAPI (grey). Scale bar, 10μm. (b) GFP-tagged KN motifs from Kank1, Kank3 and Kank4 are transfected into Kank2 knockdown cells and co-stained with anti-Paxillin antibody (Pxn, red), F-actin with phalloidin (blue) and DAPI (grey). Scale bar, 10μm. (c) GFP-tagged Kank1, Kank3 and Kank4 are transfected into normal fibroblasts and co-stained with anti-paxillin antibody (Pxn, red), F-actin with phalloidin (blue) and DAPI (grey). Scale bar, 10μm.

Suppl. Figure 3

(a) SDS-PAGE analysis of purified full length talin-1, talin head domain, GST-KN fusion protein and GST. (b) Fluorescence correlation spectroscopy measurement of complex formation between atto488-leabeled KN peptide and full length talin-1. (c) Different GFP-tagged talin rod truncations were overexpressed. Cell lysates were mixed with GST-KN motif and immunoprecipitated with anti-GFP antibody and analyzed with westerblot.

Suppl. Figure 4

(a-d) Westernblot (a, c) and densitometry analysis (b, d) of the recruitments of endogenous Kank2, talin, kindlin-2 to β1 integrin tail peptide in the presence of recombinant KN-GST (a, b) or chemically synthesized KN peptide (c, d). GST-KN recombinant protein and KN peptide replaced endogenous Kank2 but promoted talin recruitment without affecting kindlin-2 binding in a dose-dependent manner. (e, f) Westernblot and densitometry analysis of the recruitments of talin to β1 integrin tail in the

presence of different doses of overexpressed full length Kank2 or Kank2ΔKN mutant. Student t-test ***P<0.0001.

Suppl. Figure 5

(a) Kank2 knockdown cells reconstituted with GFP control or Kank2-GFP were stained for active integrin with 9EG7 antibody (red) and F-actin with phalloidin (grey). Lower enlarged boxed region shows that Kank2 strongly colocalized with 9EG7 but not phalloidin (see arrow heads). (b) Kank2 promote active integrin cluster formation. 9EG7 staining intensity per cell area is quantified from (a). Student t-test ***P<0.0001. (c) Quantification of F-actin linked to active β1 integrin. Phalloidin intensity in 9EG7-positive area is quantified from (a) and plotted as box and whisker (min to max). Student t-test ***P<0.001. (d) Timelapse images of Talin-1-TagRFP (rainbow LUT) and Kank2-GFP. Scale bar, 5μm.

Supplementary material and methods

Focal adhesion isolation

Focal adhesion isolation with chemical crosslinking was performed as previously described with minor modification. Serum-starved cells were plated on plastic dishes coated with10 µg ml−1 fibronectin at density of 1.5X106 cells per 10cm dish for 3hours. Cells were washed with PBS and crosslinked with 0.5mM DSP and 0.05mM DPDPB at r.t. for 5min and the crosslinker was quenched and washed with buffer containing 134mM NaCl, 50mM TrisHCl. Crosslinked cells were lysed with RIPA buffer (50mM Tris-Hcl pH7.5, 150mM NaCl, 1% Triton-X100, 0.2% SDS, 0.5% sodium deoxycholic acid, and EDTA-free protease inhibitor cocktail) for 30min at 4˚C. Plates were sprayed with high pressure water for 60 second to remove cellular material that was not covalently bound. Crosslinked materials were released in 3ml of lysis buffer (150mM NaCl, 50mMTrisHCl 7.5, 0.1%SDS) at 60°C for 60 minutes and precipitated with cold acetone. Protein pellets were re-dissolved in lysis buffer. Whole cell lysates were collected immediately after crosslinking and quenching in 100mM TrisHCl pH7.5, 4%SDS, 100mM DTT. Samples were snap-freezed in liquid nitrogen for further mass spectrometry sample processing. Experiments were performed in triplicate.

Mass spectrometry analysis

For focal adhesion enrichment index analysis, isolated focal adhesion fractions and total cell lysates were collected in parallel and samples were processed in FASP method. To calculate the FA enrichment index (FAEI), proteins with at least one valid LFQ intensity value in three replicates were filtered and matched according to uniprot ID. After imputation of missing values from normal distribution, ratios between average LFQ intensity in FA and average LFQ intensity in total proteome were calculated and fitted with a Gaussian distribution. FAEI is derived by normalizing mean value of Gaussian distribution to 0.

For in gel digestion and mass spectrometry analysis of EGFP pulldown samples, the samples were loaded on a gel and run for approximately 1 cm length and stopped mainly to incorporate all the proteins onto the gel rather than separating the proteins. Then the whole lane up to where the gel was run was then cut into 1mmX1mm pieces and subjected to a standard in-gel digestion protocol. Briefly the gel pieces were destained in ethanol followed by sequential reduction and alkylation with 10 mM dithiothreitol (DTT) and 40 mM

chloroacetamide (CAA). The gel pieces were then dried and incubated with digestion buffer containing 12.5 ng/µl of trypsin in 25mM Tris pH 8.5. Following overnight digestion the peptides were extracted and purified in StageTips and analyzed in LTQ-Orbitrap XL mass spectrometer. The raw data were processed using MaxQuant computational platform version 1.5.0.26.

Antibodies.

The following antibodies were used for western blotting (WB) and immunofluorescence (IF): GFP (A11122, Life Technologies, 1:1,1000 for WB), Kank2 (HPA015643, Sigma; 1:2,000 for WB and 1:800 for IF), Dab2 (610464, BD Transduction Laboratories, 1:1,000 for WB), actin (A-2066, Sigma; 1:3,000 for WB), β1 integrin (MAB1997, MB1.2, Chemicon; 1:800 for IF), GAPDH (CB1001, 6C5, Calbiochem; 1:5,000 for WB), Kindlin-2 (MAB2617, EMD Millipore 1:1,000 for WB and 1:800 for IF), paxillin (610051, 349, BD Transduction Laboratories, 1:800 for IF), talin-1 (T3287, 8d4, Sigma; 1:1,000 for WB, 1:200 for IF), talin-head specific antibody (sc-15336, Santa Cruz Biotechnology; 1:1000 for WB). A home-made β1-integrin antibodies was used for western blotting (1:10,000 for WB), Phalloidin (Alexa Fluor 546 and Alexa Fluor 647 conjugated, Molecular Probes; 1:50 for IF) was used to stain F-actin. DAPI (Sigma) was used to stain nuclei.

Plasmids and constructs.

cDNA encoding mouse Kank1 and Kank2 were cloned into pEGFP-N1 vector (Clontech) between XhoI and EcoRI sites. Mouse Kank3 was cloned into pEGFP-N1 vector between BglII and EcoRI sites. Mouse Kank4 was cloned into pEGFP-N1 vector between XhoI and AgeI sites. For retrovirus mediated overexpression, DNA fragment encoding Kank2 full length, Kank2ΔKN (a.a.31-56 deleted), Kank2ΔLID (a.a.181-240 deleted), Kank2ΔKNΔLID (a.a.31-56 and a.a.181-240 deleted), Kank2-1-670 (a.a 1-670) and KN motif (a.a. 29-72) were amplified via PCR and inserted between XhoI and EcoRI sites in pRetroQ-AcGFP-N1 vector. To generate NIH3T3 cells stably expressing Kank2-EGFP, AcGFP fragment was replaced with Kank2-EGFP or EGFP fragments from pEGFP-N1-Kank2 with XhoI and NotI cutting sites.

Plasmids for Talin-AcGFP and Talin-TagRFP expression in mammalian cells were generated from pLPCXmod-Talin-1-Ypet (gift from Dr. Carsten Grashoff). Ypet was replaced with either AcGFP sequence or TagRFP-T sequence. Various Talin rod

truncations were amplified with PCR and inserted between XhoI and EcoRI sites in pEGFP-N1 vector.

For retrovirus mediated stable knockdown of mouse Kank2, two shRNA targeting ATACTGTATTCTTGAGTCA (shKank2#1) and AGCCAGAAAGCCAAGCTAC (shKank2#2) in mouse Kank2 3'UTR region were cloned into pSuper.Retro.puro vector (OligoEngine) according to the manufacturer's instruction.

For recombinant protein production, cDNA encoding Kank2 KN motif (a.a 29-72) was inserted into pGEX-6P1 (GE Healthcare) between EcoRI and BamHI sites. Plasmid for recombinant Talin-1 head domain (a.a 405) was cloned in pCoofy vector. Plasmid for full length Talin-1 recombinant protein production (pET101-Talin-FL) was described before [citation].

Cell lines.

Mouse kidney fibroblasts carrying floxed αv and β1 alleles were cultured as previously described and used for focal adhesome analysis. Mouse kidney fibroblasts containing floxed β1-integrin allele were cultured as previously described. NIH3T3 mouse fibroblasts and hTert-RPE1 cells were cultured according to the recommendation of ATCC.

Transient and stable transfection/transduction.

Cells were transiently transfected with Lipofectamine 2000 (Invitrogen) according to the manufacturer's protocol. To generate stable cell lines, VSV-G pseudotyped retroviral vectors were produced by transient transfection of HEK293T (human embryonic kidney) cells. Viral particles were concentrated from cell culture supernatant as described previously and used for infection.

Expression and purification of recombinant proteins.

For GST fusion protein of KN motif, plasmids encoding GST–KN or GST alone were transformed into BL21 (DE3) and protein expression was autoinduced over night at 37˚C. 5g biomass was lysed with high pressure homogenizer in GST binding buffer (TrisHCl 50mM, NaCl 150mM, EDTA 1mM, DTT 1mM, pH 7.5). Protease inhibitor (AEBSF-HCl 1mM, Aprotinin 2μg/ml, Leupeptin 1μg/ml, Pepstatin 1μg/ml) and nuclease (Benzonase) were added during the cell lysis. After clarification, supernatant were incubated with Glutathione Sepharose 4 Fast Flow (GE Healthcare) for 3.5hour at 4˚C followed by 3 times

washing with GST binding buffer and elution with 50 mM Glutathione in the binding buffer. Elute fractions containing were pooled and desalted (Sephadex G-25 in Hi Prep 26/10) in buffer (TrisHCl 50mM, NaCl 150mM, 0.1mM DTT) and further purified with size-exclusion chromatography (Superdex 75 PC 3.2/30) in desalting buffer.

Full length talin recombinant protein production was optimized based on previously published protocol. Briefly, pET101-Talin-FL was transformed into BL21 (DE3) Gold and induced 1 mM IPTG at 18˚C overnight. After lysis with high pressure homogenizer in lysis buffer (50mM TrisHCl pH7.8, 500mM NaCl, 30mM imidazole, 1mM DTT) and clarification of the supernatant, full length Talin was purified by Ni-NTA affinity chromatography (Ni SepharoseHigh Performance, GE Healthcare). Elute fractions with 500mM imidazole in lysis buffer were pooled and loaded on anion exchange (HiTrap Q HP, 6% highly cross linked agarose; strong anion -N+(CH3)3, GE Healthcare) in MES buffer (20mM MES pH6.3, 1mM DTT, gradient from 100mM KCl to 100mM KCl). Elute fractions were pooled and concentrated (Amicon Ultra 15, MWCO 100kD) and further purified by size-exclusion chromatography (Superdex 200 10/300 GL, GE Healthcare) in 50mM TrisHCl pH7.8, 150mM KCl, 1mM DTT. Purified fractions were stored in presence of 50% glycerol in -80˚C.

Talin-1-head (a.a. 1-405) was cloned into pCoofy vector. The recombinant production of talin-1-head (a.a. 1-405) in E. coli Rosetta cells (Merck Millipore) was autoinduced at 24 °C for 22 h. After cell lysis and clarification of the supernatant, talin-1-head was purified by Ni-NTA affinity chromatography (Qiagen). Elute fractions containing talin-1-head were pooled, cleaved with SenP2 protease and purified by size-exclusion chromatography (Superdex 200 26/600, GE Healthcare) yielding unmodified murine talin dead domain.

Immunoprecipitation and GST pulldown

For immunoprecipitation of EGFP tagged proteins, cells were lysed in M-PER buffer and 1mg cells lysates in were immunoprecipitated with µMACS GFP Isolation Kit (Miltenyi Biotec) according to the manufacturer's protocol. Elutes were separated in SDS-PAGE for westernbloting or in-gel digestion and mass spectrometry analysis.

For GST pulldown experiments, full length Talin and Talin-head recombinant protein were re-buffered in the GST binding buffer (137mM NaCl, 13mM KCl, 0.05% Tween-20, 50mM TrisHCl pH7.5) with Zebra Desalt Spin Columns (Thermo Scientific). 200nM GST or GST-

KN fusion proteins were incubated with 100nM full length Talin or 300nM Talin head for 30min at 4˚C and then incubated with Glutathione Sepharose (GE Healthcare) for another 1.5hour at 4˚C. Resin was washed three times with the GST binding buffer and eluted in 2X laemmli buffer at 95˚C for 2min. Samples were analyzed in westernblot using antibody against Talin head and GST.

Fluorescence correlation spectroscopy (FCS)

The diffusion time as a function of talin protein concentration was measured by fluorescence correlation spectroscopy (FCS). FCS experiments were performed on a custom-build confocal microscopy. Prior to the experiment, the known diffusion coefficient of AlexaFluor 488 in water was used to calibrate the confocal volume (D = 400 $\mu m^2/s$). To analyze the interactions between the atto488 fluorescently-labeled KN peptide and talin, the peptide was diluted to a final concentration of ~1 nM in buffer (20 mM HEPES, 150 mM KCl, 0.5 mM EDTA, 1 mM DTT, pH 7.5) and 32 μM of talin was added. The reaction was incubated at room temperature for 3 minutes before subject to the FCS measurement. Lower concentrations in solution of talin were made by subsequent dilution in buffer containing 1nM of atto488-labeled KN peptide. The full dilution series was repeated three times. The fluctuation of fluorescence arising from the fluorescent KN-talin complexes was monitored and auto-correlated using all three measurements and diffusion time was estimated by fitting with a single diffusing species.

Integrin peptide pulldowns.

Peptide pulldowns were performed as described previously with minor modifications with β1 wt cytoplasmic tail peptides (HDRREFAKFEKEKMNAKWDTGENPIYKSAVTTVVNPKYEGK-OH), β1 Y795A tail peptide (HDRREFAKFEKEKMNAKWDTGENPIYKSAVTTVVNPKAEGK-OH), β3 tail peptide (HDRKEFAKFEEERARAKWDTANNPLYKEATSTFTNITYRGT-OH), β5 tail peptide (HDRREFAKFQSERSRARYEMASNPLYRKPISTHTVDFAFNKFNKSYNGSVD-OH), β2 tail peptide (TDLREYRRFEKEKLKSQWNN-DNPLFKSATTTVMNPKFAES-OH), a scrambled peptide (EYEFEPDKVDTGAKGTKMAKNEKKFRNYTVHNIWESRKVAP-OH). All peptides were desthiobiotinylated. Before use, peptides were immobilized on 20 μl Dynabeads MyOne Streptavidine C1 (10 mg ml−1, Invitrogen) in washing buffer containing 137mM NaCl, 13mM KCl, 50mM TrisHCl at pH 7.4, 0.05% Tween-20 for 2hours at 4˚C. Beads were washed twice with washing buffer and once with M-PER buffer. 0.5mg

cell lysate at 1mg/ml collected in M-PER buffer was incubated with the beads for 5hours at 4˚C. After incubation with tail peptides, proteins were eluted with 2X laemmli buffer at 95˚C for 5min. For in vitro Talin activation assay, 10nM recombinant talin diluted in the peptide pulldown washing buffer for 15min and then incubated with 10nM GST or GST-KN motif for 1hour together with the Dynabeads at 4˚C. Beads were washed three times with the washing buffer and eluted with 2X laemmli buffer at 95˚C for 5min.

Immunofluorescence microscopy.

For immunostaining, cells were cultured on glass coated with 10 μg ml−1 fibronectin (Calbiochem) for 5hours in complete culture medium before fixed with cold methanol:acetone (1:1) for 5min at -20˚C (for endogenous Talin staining) followed by 15min rehydration in PBS at r.t. or with 2% PFA/PBS for 15min at r.t. For PFA fixed samples, fixed cells were permeabilized with 0.1% Triton-X100/PBS for 30min at r.t. Cells were blocked with 5%BSA/PBS for 1 h at r.t. followed by incubation with the primary antibodies in 5%BSA/PBS overnight at 4˚C and secondary antibodies for 1 h at r.t. Images were collected at room temperature on a ZEISS (Jena, Germany) LSM780 confocal laser scanning microscope equipped with a ZEISS Plan-APO 63x/NA1.46 oil immersion objective.

Fluorescence recovery after photobleaching and fluorescence live cell imaging

Fluorescence recovery after photobleaching (FRAP) and fluorescence live cell imaging were performed on a ZEISS (Jena, Germany) LSM780 confocal laser scanning microscope equipped with a ZEISS Plan-APO 63x/NA1.46 oil immersion objective with environmental control (5% CO2 and humidification). Cells were transfected with indicated plasmids and cultured on 10 μg ml−1 fibronectin coated glass-bottom live cell imaging chamber (ibidi) for 24 hours. For FRAP experiments, region of interest was bleached with full laser power at 488nm for 30 iterations and fluorescence recovery was monitored for 5min with 20second interval with 1% laser power. No significant photobleaching was observed during the post-bleaching phase. FRAP data was extracted with build-in package in Carl Zeiss ZEN software and analyzed in GraphPad Prism 6. FRAP curves were fitted in one phase association model: Y=Y0 + (Plateau-Y0)*(1-exp(-K*x)). For fluorescence live cell imaging, cells were imaged for 10min with 20second interval with 1% laser power.

Time-lapse video microscopy of 2D-random cell migration.

Indicated cells were seeded sparsely on 6-well plate coated with 5μg/ml fibronectin in the absence of serum for 2hours, then the cell migrations were recorded at 37 °C and 5% CO2 for 6hours with 5min time interval on a Zeiss Axiovert 200 M (Zeiss, Germany) equipped with ×10/.3, ×20/.4 and ×40/.6 objectives, a motorized stage (Märzhäuser) and an environment chamber (EMBL Precision Engineering) with a cooled CCD (charge-coupled device) camera (Roper Scientific). Image acquisition and microscope control were carried out with MetaMorph software (Molecular Devices). The acquired images were analyzed using the manual tracking plugin of ImageJ and the Chemotaxis and Migration Tool (ibidi).

Statistics.

Statistical analysis was performed in GraphPad Prism software (version 5.00, GraphPad Software). Results are illustrated as the mean±sd. unless otherwise indicated.

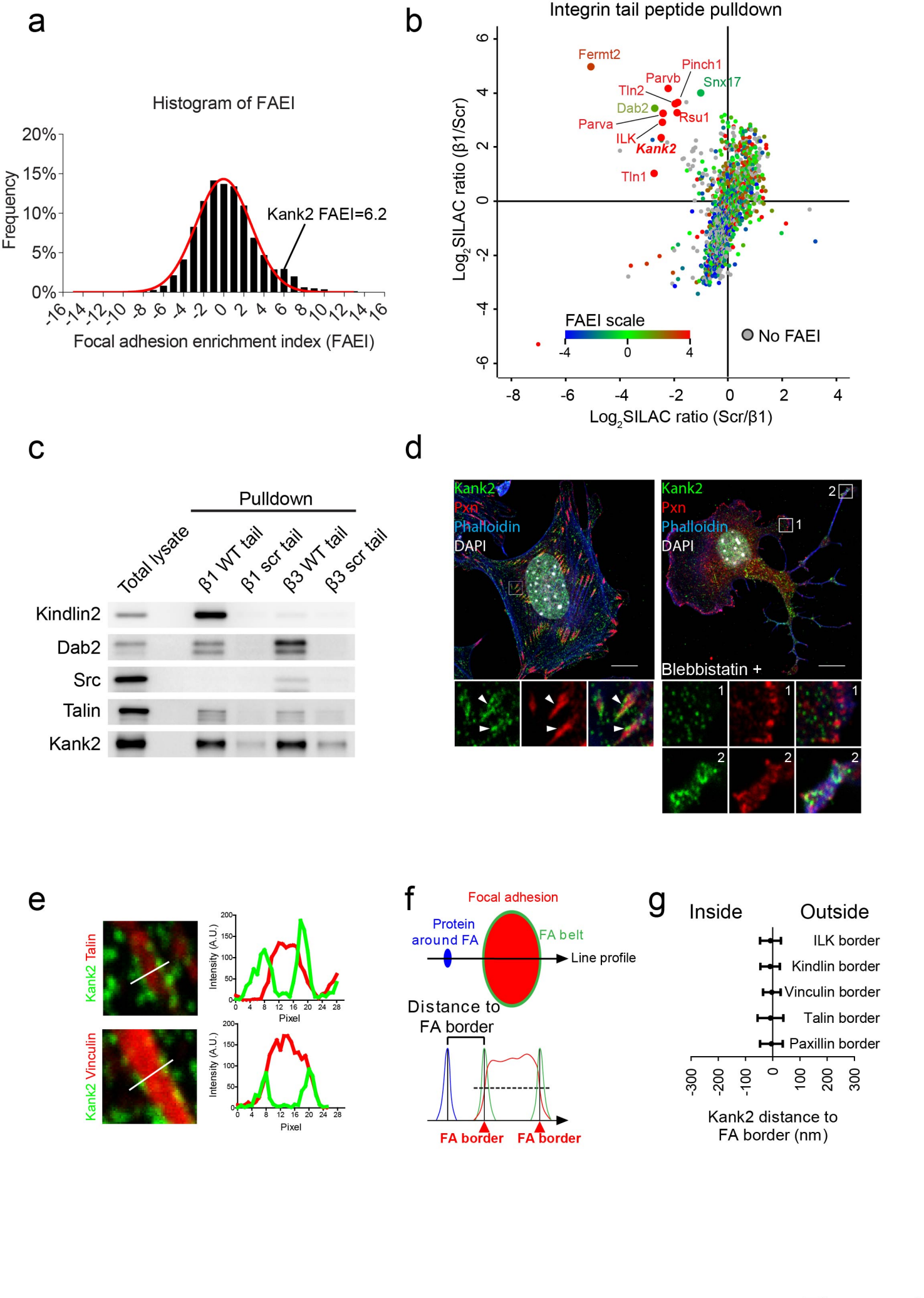
a
Histogram of FAEI
Frequency
20%
15%
10%
5%
0%
Kank2 FAEI=6.2
-16 -14 -12 -10 -8 -6 -4 -2 0 2 4 6 8 10 12 14 16
Focal adhesion enrichment index (FAEI)
b
Integrin tail peptide pulldown
Fermt2
Pinch1
Parvb
Snx17
Tln2
Dab2
Rsu1
Parva
ILK
Kank2
Tln1
FAEI scale
-4 0 4
No FAEI
Log2SILAC ratio (β1/Scr)
Log2SILAC ratio (Scr/β1)
c
Pulldown
Total lysate
β1 WT tail
β1 scr tail
β3 WT tail
β3 scr tail
Kindlin2
Dab2
Src
Talin
Kank2
d
Kank2
Pxn
Phalloidin
DAPI
Blebbistatin +
e
Kank2 Talin
Kank2 Vinculin
Intensity (A.U.)
Pixel
f
Focal adhesion
Protein around FA
FA belt
Line profile
Distance to FA border
FA border
FA border
g
Inside
Outside
ILK border
Kindlin border
Vinculin border
Talin border
Paxillin border
-300 -200 -100 0 100 200 300
Kank2 distance to FA border (nm)

Figure 1

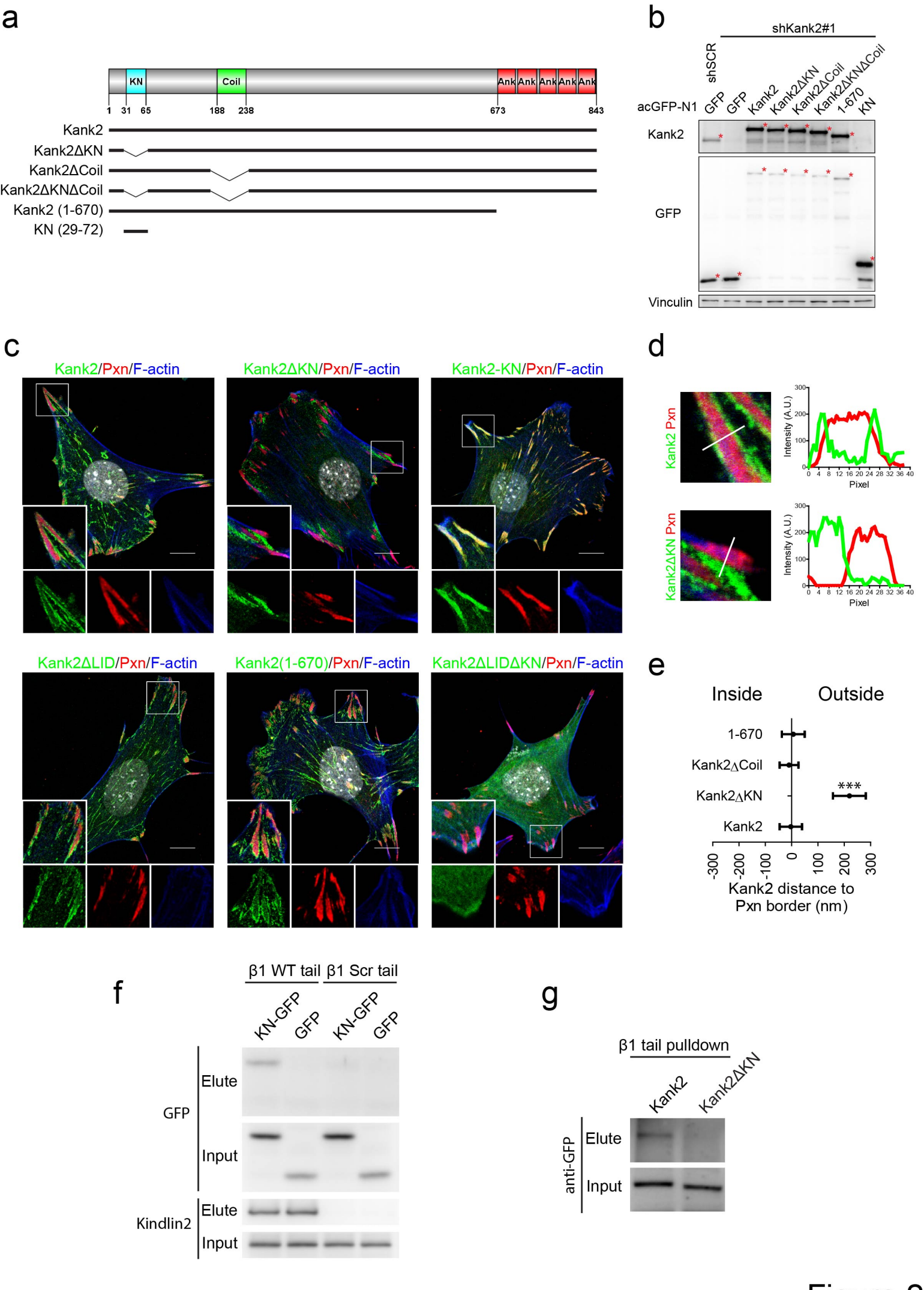
a
KN
Coil
Ank
1
31
65
188
238
673
843
Kank2
Kank2ΔKN
Kank2ΔCoil
Kank2ΔKNΔCoil
Kank2 (1-670)
KN (29-72)
b
shKank2#1
shSCR
acGFP-N1
GFP
GFP
Kank2
Kank2ΔKN
Kank2ΔCoil
Kank2ΔKNΔCoil
1-670
KN
Kank2
GFP
Vinculin
c
Kank2/Pxn/F-actin
Kank2ΔKN/Pxn/F-actin
Kank2-KN/Pxn/F-actin
Kank2ΔLID/Pxn/F-actin
Kank2(1-670)/Pxn/F-actin
Kank2ΔLIDΔKN/Pxn/F-actin
d
Kank2 Pxn
Kank2ΔKN Pxn
Intensity (A.U.)
Pixel
e
Inside
Outside
1-670
Kank2ΔCoil
Kank2ΔKN
Kank2
***
-300
-200
-100
0
100
200
300
Kank2 distance to
Pxn border (nm)
f
β1 WT tail
β1 Scr tail
KN-GFP
GFP
KN-GFP
GFP
GFP
Elute
Input
Kindlin2
Elute
Input
g
β1 tail pulldown
Kank2
Kank2ΔKN
anti-GFP
Elute
Input

Figure 2

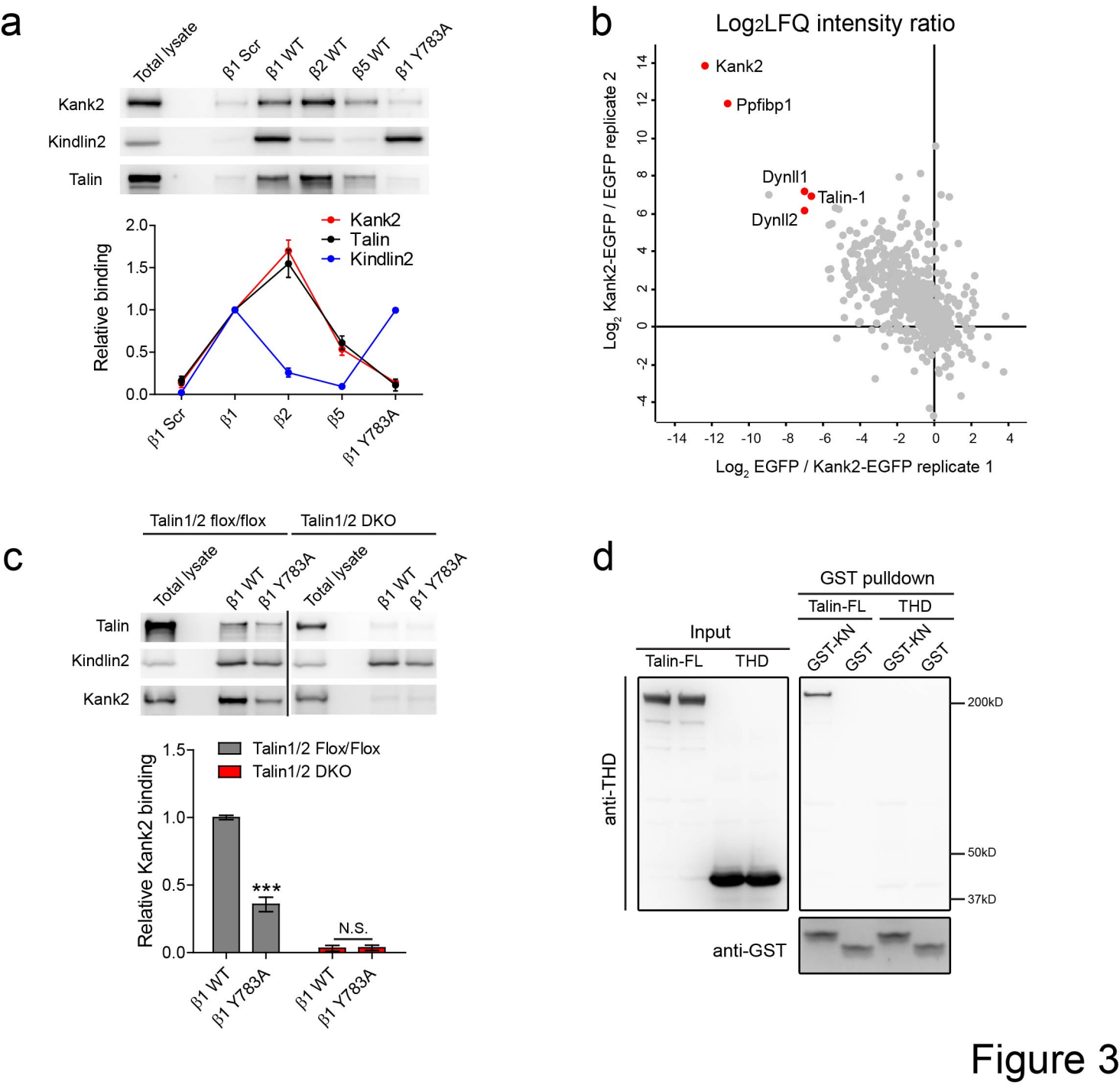
a
Total lysate
β1 Scr
β1 WT
β2 WT
β5 WT
β1 Y783A
Kank2
Kindlin2
Talin
Relative binding
Kank2
Talin
Kindlin2
β1 Scr
β1
β2
β5
β1 Y783A
b
Log2LFQ intensity ratio
Kank2
Ppfibp1
Dynll1
Talin-1
Dynll2
Log2 Kank2-EGFP / EGFP replicate 2
Log2 EGFP / Kank2-EGFP replicate 1
c
Talin1/2 flox/flox
Talin1/2 DKO
Total lysate
β1 WT
β1 Y783A
Talin
Kindlin2
Kank2
Relative Kank2 binding
Talin1/2 Flox/Flox
Talin1/2 DKO
***
N.S.
β1 WT
β1 Y783A
d
GST pulldown
Talin-FL
THD
Input
GST-KN
GST
anti-THD
200kD
50kD
37kD
anti-GST

Figure 3

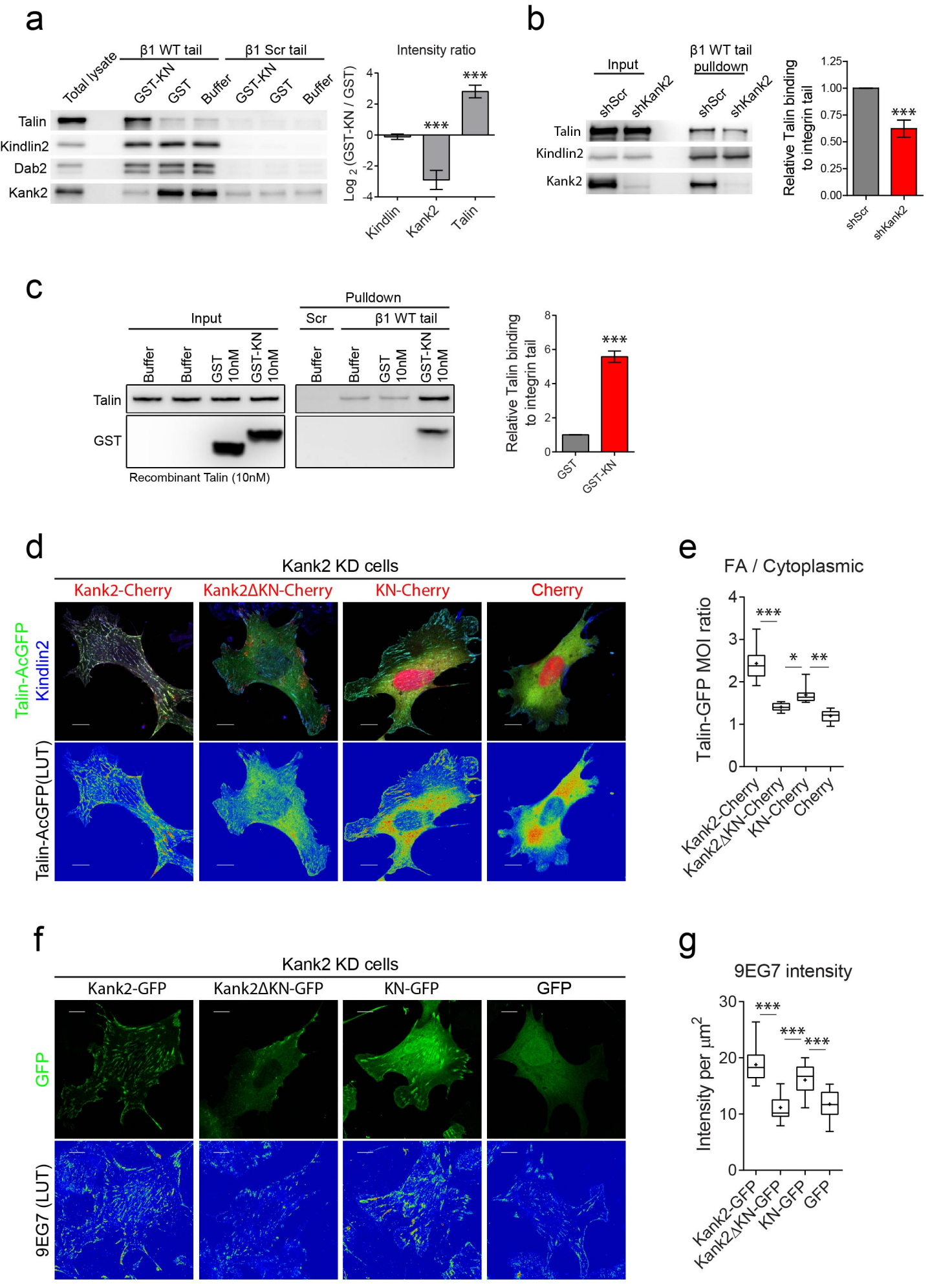
a
Total lysate
β1 WT tail
β1 Scr tail
GST-KN
GST
Buffer
GST-KN
GST
Buffer
Talin
Kindlin2
Dab2
Kank2
Intensity ratio
Log 2 (GST-KN / GST)
***
***
Kindlin
Kank2
Talin
b
Input
β1 WT tail pulldown
shScr
shKank2
shScr
shKank2
Talin
Kindlin2
Kank2
Relative Talin binding to integrin tail
***
shScr
shKank2
c
Pulldown
Input
Scr
β1 WT tail
Buffer
Buffer
GST 10nM
GST-KN 10nM
Buffer
Buffer
GST 10nM
GST-KN 10nM
Talin
GST
Recombinant Talin (10nM)
Relative Talin binding to integrin tail
***
GST
GST-KN
d
Kank2 KD cells
Kank2-Cherry
Kank2ΔKN-Cherry
KN-Cherry
Cherry
Talin-AcGFP
Kindlin2
Talin-AcGFP(LUT)
e
FA / Cytoplasmic
Talin-GFP MOI ratio
***
*
**
Kank2-Cherry
Kank2ΔKN-Cherry
KN-Cherry
Cherry
f
Kank2 KD cells
Kank2-GFP
Kank2ΔKN-GFP
KN-GFP
GFP
GFP
9EG7 (LUT)
g
9EG7 intensity
Intensity per μm2
***
***
***
Kank2-GFP
Kank2ΔKN-GFP
KN-GFP
GFP

Figure 4

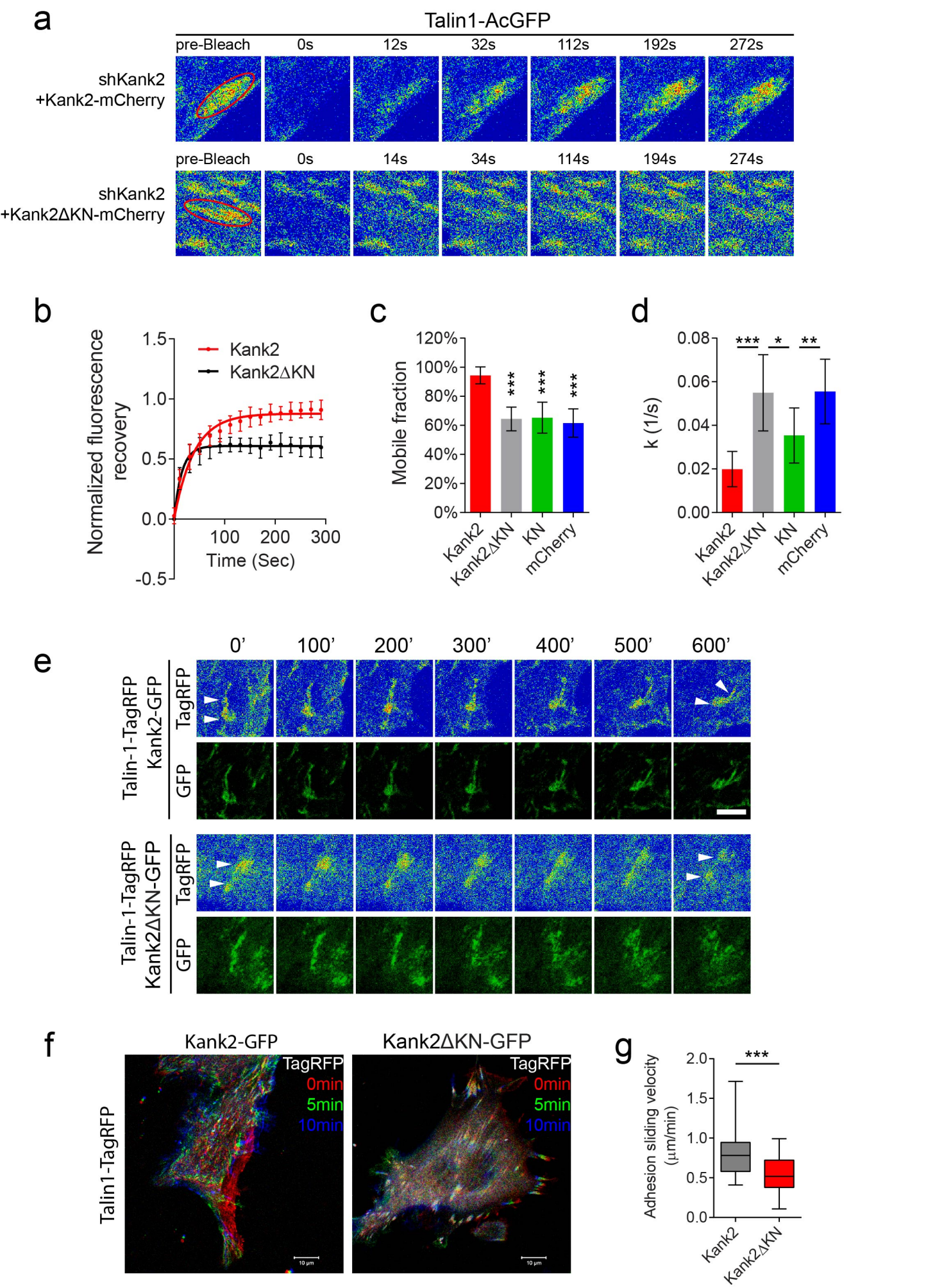
a
Talin1-AcGFP
pre-Bleach
0s
12s
32s
112s
192s
272s
shKank2
+Kank2-mCherry
pre-Bleach
0s
14s
34s
114s
194s
274s
shKank2
+Kank2ΔKN-mCherry
b
Normalized fluorescence recovery
Kank2
Kank2ΔKN
Time (Sec)
c
Mobile fraction
Kank2
Kank2ΔKN
KN
mCherry
d
k (1/s)
Kank2
Kank2ΔKN
KN
mCherry
e
0'
100'
200'
300'
400'
500'
600'
Talin-1-TagRFP
Kank2-GFP
TagRFP
GFP
Talin-1-TagRFP
Kank2ΔKN-GFP
TagRFP
GFP
f
Kank2-GFP
Kank2ΔKN-GFP
Talin1-TagRFP
TagRFP
0min
5min
10min
g
Adhesion sliding velocity (μm/min)
Kank2
Kank2ΔKN

Figure 5

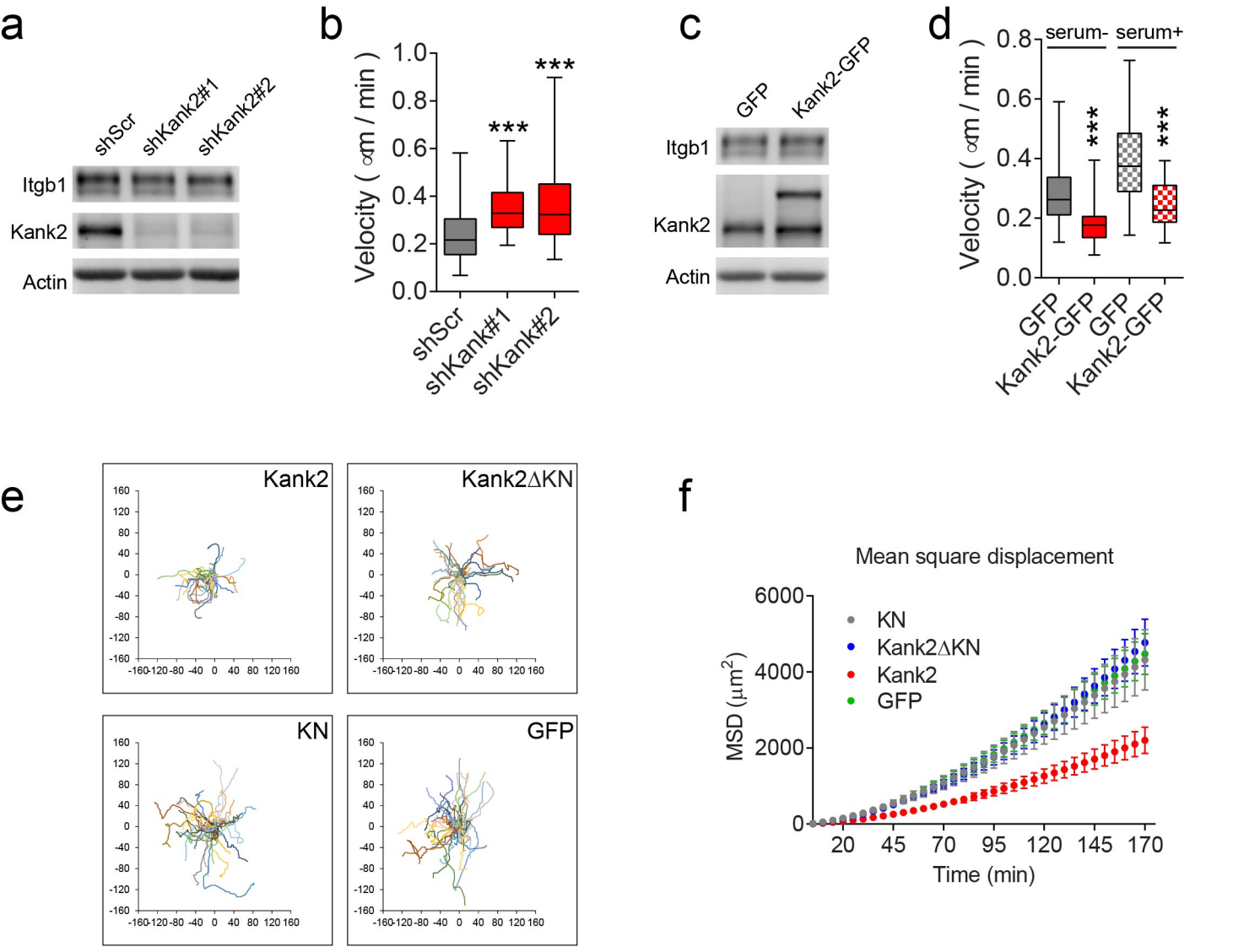
a
shScr
shKank2#1
shKank2#2
Itgb1
Kank2
Actin
b
Velocity (∝m / min)
1.0
0.8
0.6
0.4
0.2
0.0
***
***
shScr
shKank#1
shKank#2
c
GFP
Kank2-GFP
Itgb1
Kank2
Actin
d
serum-
serum+
Velocity (∝m / min)
0.8
0.6
0.4
0.2
0.0
***
***
GFP
Kank2-GFP
GFP
Kank2-GFP
e
Kank2
Kank2ΔKN
KN
GFP
160
120
80
40
0
-40
-80
-120
-160
-160-120-80 -40 0 40 80 120 160
f
Mean square displacement
MSD (μm2)
6000
4000
2000
0
KN
Kank2ΔKN
Kank2
GFP
20
45
70
95
120
145
170
Time (min)

Figure 6

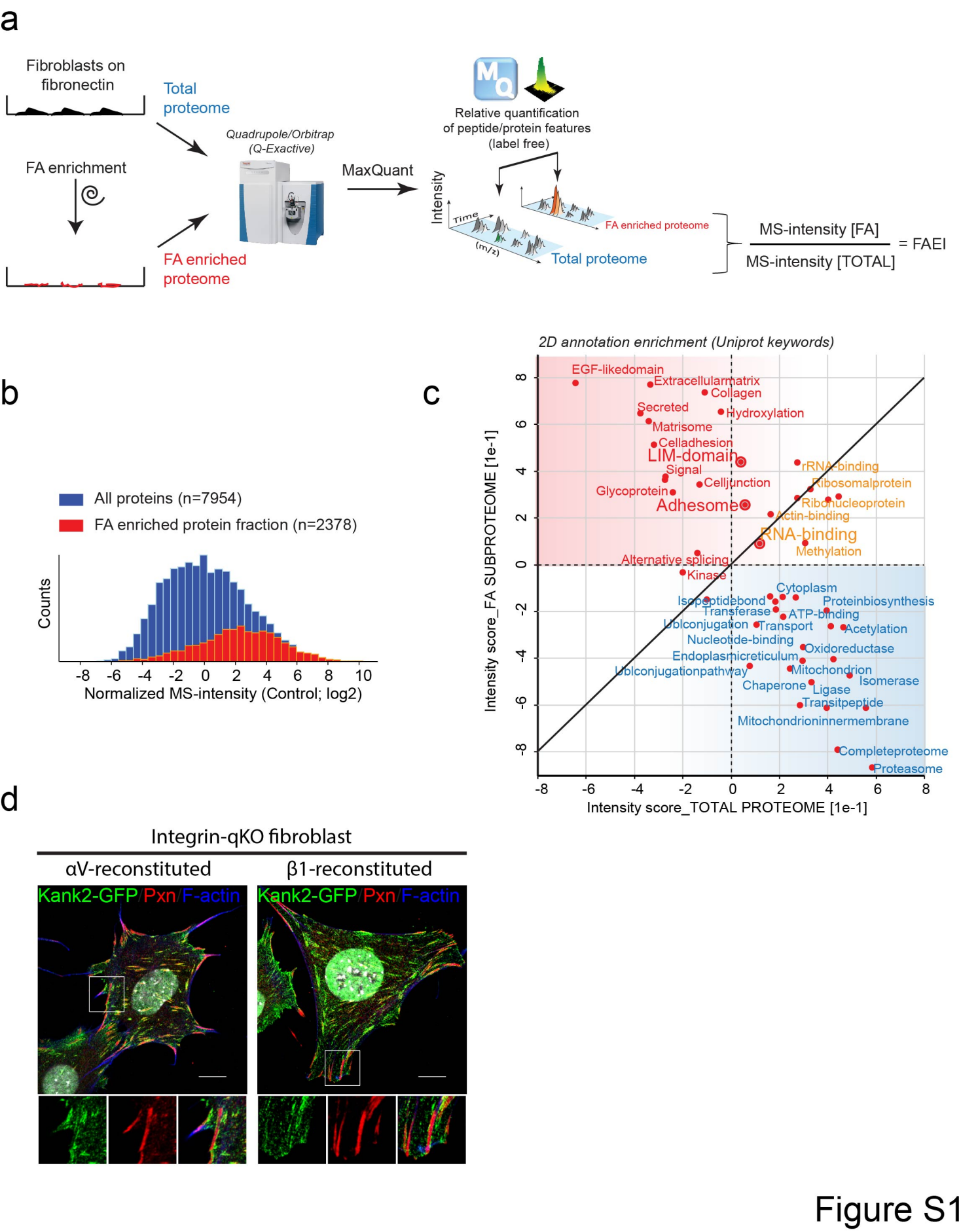
a
Fibroblasts on fibronectin
Total proteome
FA enrichment
Quadrupole/Orbitrap (Q-Exactive)
FA enriched proteome
MaxQuant
Relative quantification of peptide/protein features (label free)
Intensity
Time
(m/z)
FA enriched proteome
Total proteome
MS-intensity [FA] / MS-intensity [TOTAL] = FAEI
b
All proteins (n=7954)
FA enriched protein fraction (n=2378)
Counts
Normalized MS-intensity (Control; log2)
c
2D annotation enrichment (Uniprot keywords)
Intensity score_FA SUBPROTEOME [1e-1]
Intensity score_TOTAL PROTEOME [1e-1]
EGF-likedomain
Extracellularmatrix
Collagen
Secreted
Hydroxylation
Matrisome
Celladhesion
LIM-domain
Signal
Celljunction
Glycoprotein
Adhesome
rRNA-binding
Ribosomalprotein
Ribonucleoprotein
Actin-binding
RNA-binding
Methylation
Alternative splicing
Kinase
Cytoplasm
Isopeptidebond
Proteinbiosynthesis
Transferase
ATP-binding
Ubl conjugation
Transport
Acetylation
Nucleotide-binding
Oxidoreductase
Endoplasmicreticulum
Ubl conjugationpathway
Mitochondrion
Isomerase
Chaperone
Ligase
Transitpeptide
Mitochondrioninnermembrane
Completeproteome
Proteasome
d
Integrin-qKO fibroblast
αV-reconstituted
β1-reconstituted
Kank2-GFP/Pxn/F-actin
Kank2-GFP/Pxn/F-actin

Figure S1

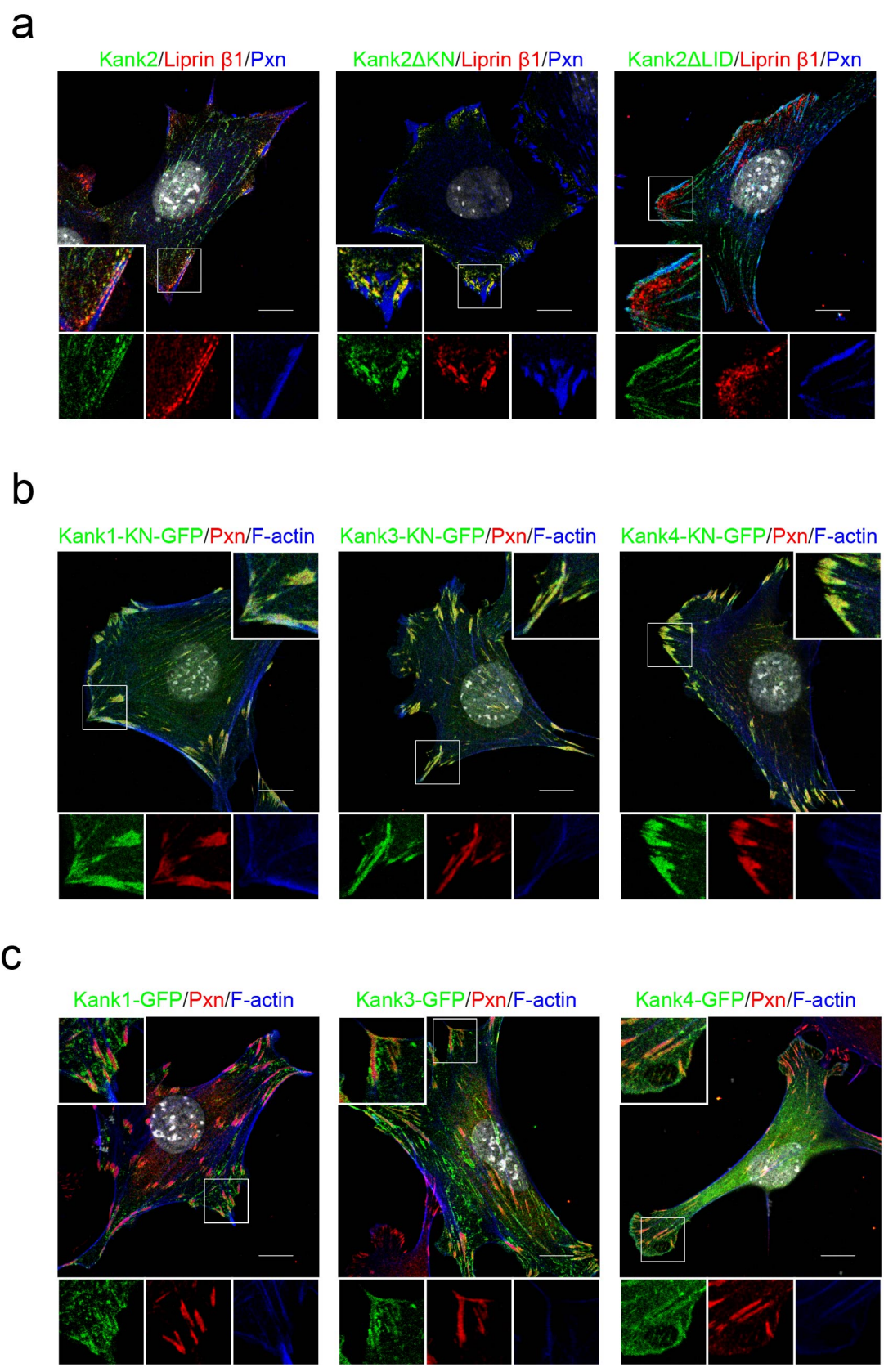
a
Kank2/Liprin β1/Pxn
Kank2ΔKN/Liprin β1/Pxn
Kank2ΔLID/Liprin β1/Pxn
b
Kank1-KN-GFP/Pxn/F-actin
Kank3-KN-GFP/Pxn/F-actin
Kank4-KN-GFP/Pxn/F-actin
c
Kank1-GFP/Pxn/F-actin
Kank3-GFP/Pxn/F-actin
Kank4-GFP/Pxn/F-actin

Figure S2

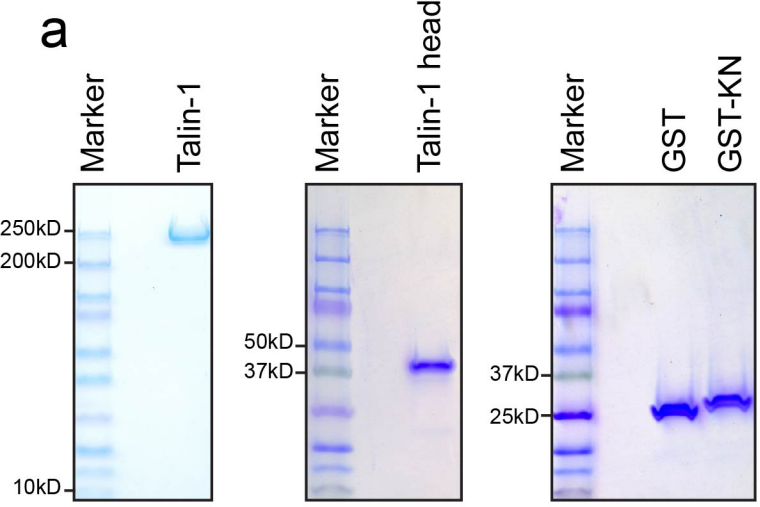
a
Marker
Talin-1
250kD
200kD
10kD
Marker
Talin-1 head
50kD
37kD
Marker
GST
GST-KN
37kD
25kD

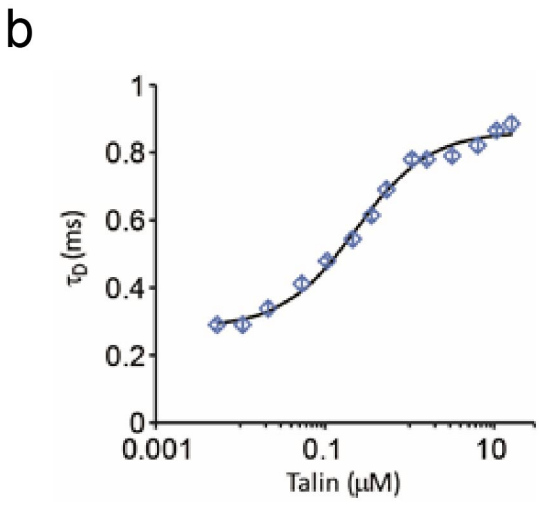
b
1
0.8
0.6
0.4
0.2
0
τD (ms)
0.001
0.1
10
Talin (μM)

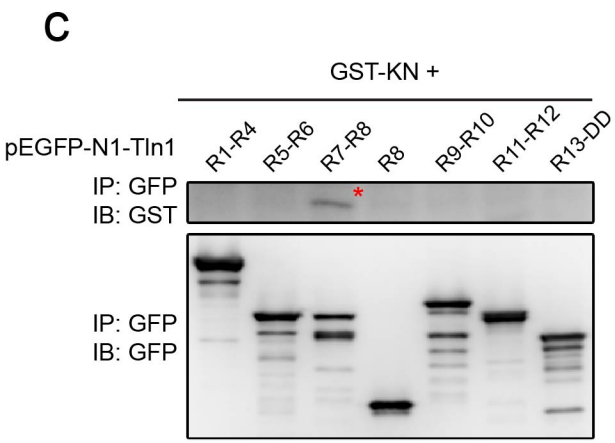
c
GST-KN +
pEGFP-N1-Tln1
R1-R4
R5-R6
R7-R8
R8
R9-R10
R11-R12
R13-DD
IP: GFP
IB: GST
*
IP: GFP
IB: GFP

Figure S3

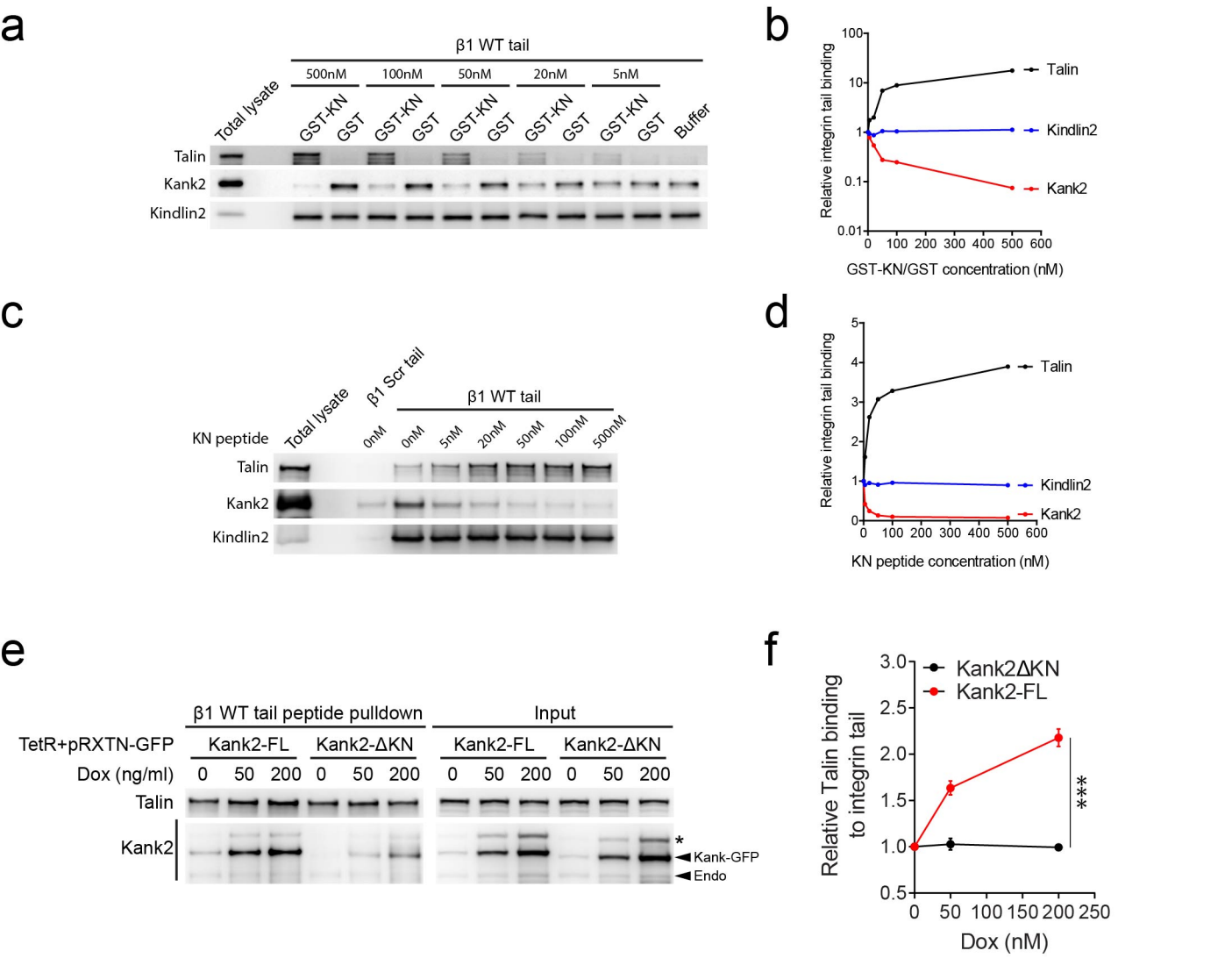
a
β1 WT tail
500nM
100nM
50nM
20nM
5nM
Total lysate
GST-KN
GST
Buffer
Talin
Kank2
Kindlin2
b
Relative integrin tail binding
Talin
Kindlin2
Kank2
GST-KN/GST concentration (nM)
c
β1 Scr tail
β1 WT tail
KN peptide
0nM
5nM
20nM
50nM
100nM
500nM
d
KN peptide concentration (nM)
e
β1 WT tail peptide pulldown
Input
TetR+pRXTN-GFP
Kank2-FL
Kank2-ΔKN
Dox (ng/ml)
0
50
200
Kank-GFP
Endo
f
Kank2ΔKN
Kank2-FL
Relative Talin binding to integrin tail
***
Dox (nM)

Figure S4

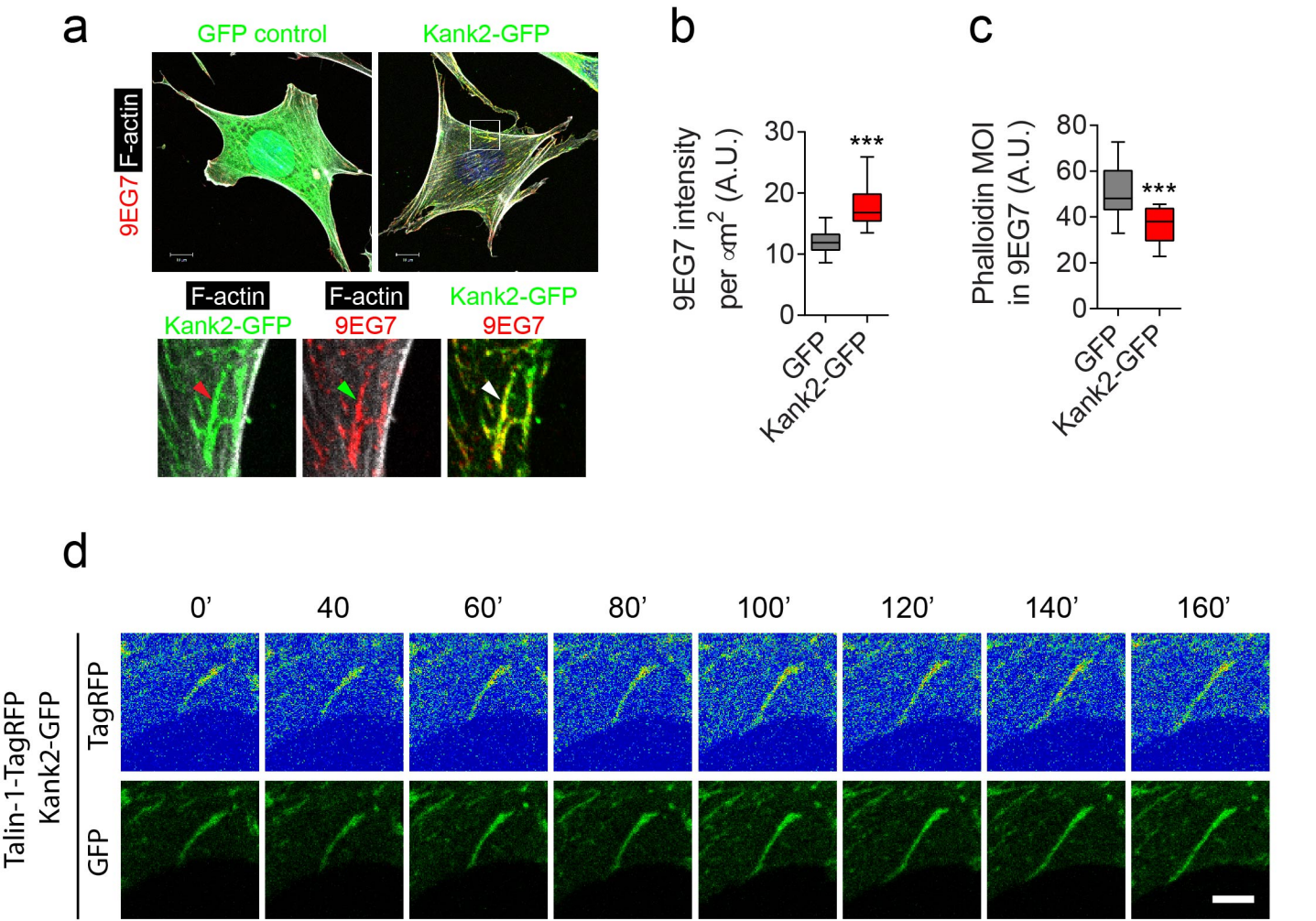
a
GFP control
Kank2-GFP
9EG7 F-actin
F-actin
Kank2-GFP
F-actin
9EG7
Kank2-GFP
9EG7
b
9EG7 intensity per μm² (A.U.)
30
20
10
0
***
GFP
Kank2-GFP
c
Phalloidin MOI in 9EG7 (A.U.)
80
60
40
20
0
***
GFP
Kank2-GFP
d
0'
40
60'
80'
100'
120'
140'
160'
Talin-1-TagRFP
Kank2-GFP
TagRFP
GFP

Figure S5

Integrin α3β1 regulates kidney collecting duct development via TRAF6-dependent K63-linked polyubiquitination of Akt

Eugenia M. Yazlovitskaya[a], Hui-Yuan Tseng[b], Olga Viquez[a], Tianxiang Tu[a], Glenda Mernaugh[a], Karen K. McKee[c], Karen Riggins[a], Vito Quaranta[d], Amrita Pathak[e], Bruce D. Carter[e], Peter Yurchenco[c], Arnoud Sonnenberg[f], Ralph T. Böttcher[b], Ambra Pozzi[a,d,g], and Roy Zent[a,d,g,h]

[a]Division of Nephrology and Hypertension, Department of Medicine, [d]Department of Cancer Biology, [e]Department of Biochemistry, and [g]Department of Cell and Developmental Biology, Vanderbilt University School of Medicine, Nashville, TN 37232; [b]Department of Molecular Medicine, Max Planck Institute of Biochemistry, 82152 Martinsried, Germany; [c]Department of Pathology and Laboratory Medicine, Robert Wood Johnson Medical School, Piscataway, NJ 08854; [f]Division of Cell Biology, Netherlands Cancer Institute, 1066 CX Amsterdam, Netherlands; [h]Veterans Affairs Hospital, Nashville, TN 37232

ABSTRACT **The collecting system of the kidney develops from the ureteric bud (UB), which undergoes branching morphogenesis, a process regulated by multiple factors, including integrin–extracellular matrix interactions. The laminin (LM)-binding integrin α3β1 is crucial for this developmental program; however, the LM types and LM/integrin α3β1–dependent signaling pathways are poorly defined. We show that α3 chain–containing LMs promote normal UB branching morphogenesis and that LM-332 is a better substrate than LM-511 for stimulating integrin α3β1–dependent collecting duct cell functions. We demonstrate that integrin α3β1–mediated cell adhesion to LM-332 modulates Akt activation in the developing collecting system and that Akt activation is PI3K independent but requires decreased PTEN activity and K63-linked polyubiquitination. We identified the ubiquitin-modifying enzyme TRAF6 as an interactor with the integrin β1 subunit and regulator of integrin α3β1–dependent Akt activation. Finally, we established that the developmental defects of TRAF6- and integrin α3–null mouse kidneys are similar. Thus K63-linked polyubiquitination plays a previously unrecognized role in integrin α3β1–dependent cell signaling required for UB development and may represent a novel mechanism whereby integrins regulate signaling pathways.**

Monitoring Editor
Mark H. Ginsberg
University of California, San Diego

Received: Jul 10, 2014
Revised: Mar 17, 2015
Accepted: Mar 17, 2015

This article was published online ahead of print in MBoC in Press (http://www.molbiolcell.org/cgi/doi/10.1091/mbc.E14-07-1203) on March 25, 2015.

Address correspondence to: Roy Zent (roy.zent@vanderbilt.edu).

Abbreviations used: BrdU, 5-bromodeoxyuridine; CD, collecting duct; DMSO, dimethyl sulfoxide; FAK, focal adhesion kinase; GFP, green fluorescent protein; HA, hemagglutinin; H&E, hematoxylin and eosin; IgG, immunoglobulin G; LM, laminin; PBS, phosphate-buffered saline; PDK1, phosphoinositol-dependent kinase 1; PI3K, phosphoinositide 3-kinase; PIP_2, $PI(4,5)P_2$; PIP_3, $PI(3,4,5)P_3$; siRNA, small interfering RNA; TNF, tumor necrosis factor; TRAF6, TNF receptor–associated factor 6; UB, ureteric bud; WT, wild type.

INTRODUCTION

The kidney develops from two distinct embryonic components: the ureteric bud (UB), which forms the multibranched collecting system, and the metanephric mesenchyme, which gives rise to the nephrons. The formation of the collecting system occurs by iterative branching morphogenesis of the UB, a process regulated by multiple factors, including integrin-dependent cell–extracellular matrix (ECM) interactions.

Laminins (LMs), trimeric proteins consisting of α, β, and γ chains, are the principal ECM components that regulate UB development. There are five α chains, four β chains, and three γ chains, which can form 15 LM trimers (Aumailley *et al*., 2005). The γ1, α5, and α3 LM chains are expressed in UB-derived structures (Zent *et al*., 2001;

Supplemental Material can be found at:
http://www.molbiolcell.org/content/suppl/2015/03/23/mbc.E14-07-1203v1.DC1.html

Chen *et al.*, 2004; Miner and Yurchenco, 2004). The γ1 chain, found in 10 of the LMs, is critical for UB development, as mice lacking this chain in the UB have a severe kidney branching morphogenesis defect (Yang *et al.*, 2011). The LM α5 chain, found in LM-511 and LM-521, is also necessary for normal UB development, as LM α5–null mice have a mild branching morphogenesis defect (Liu *et al.*, 2009). The role of the α3 chain–containing LMs (LM-332, LM-321, and LM-311) in UB development in vivo is less well defined, as their importance in branching morphogenesis has only been shown utilizing LM-332 inhibitory antibodies in an ex vivo organ culture model (Zent *et al.*, 2001).

Integrins are heterodimeric transmembrane matrix receptors consisting of αβ subunits that exhibit different ligand-binding properties. Twenty-four integrins are found in mammals, and four of them—α3β1, α6β1, α6β4, and α7β1—primarily bind to LMs. While integrins α3β1, α6β1, and α6β4 are expressed in the developing UB (Zent *et al.*, 2001), integrin α3β1 is the major receptor that mediates UB formation (Liu *et al.*, 2009). The global integrin α3–null mouse, which dies at birth, presents with an abnormal renal papilla outgrowth evident at embryonic day 18.5 (E18.5; Kreidberg *et al.*, 1996). Specific deletion of the integrin α3 subunit in the UB using the Hoxb7Cre/green fluorescent protein (GFP) mouse results in adult mice with absent or dramatically flattened papillae (Liu *et al.*, 2009). This abnormality was proposed to be due to alterations in expression of Wnt7b and Wnt4 in vivo (Liu *et al.*, 2009). Integrin α3β1–dependent phosphoinositide 3-kinase (PI3K)/Akt signaling was shown to control expression of Wnts in collecting duct (CD) cells, suggesting this signaling pathway modulates Wnts in UB development (Liu *et al.*, 2009). However, the mechanism whereby integrin α3β1 regulates the Akt signaling pathway is currently unknown.

The PI3K/Akt pathway, which plays a central role in multiple biological functions, is stimulated downstream of numerous cell receptors, including growth factor receptors and integrins. Activation of this pathway is complex. PI3K phosphorylates $PI(4,5)P_2$ (PIP_2) to form $PI(3,4,5)P_3$ (PIP_3), which is required for the recruitment of Akt from the cytosol to the plasma membrane (Cantley, 2002). The dual-specificity protein phosphatase PTEN negatively regulates this process by dephosphorylating PIP_3 to PIP_2 (Song *et al.*, 2012). Src-induced phosphorylation of Akt at Tyr315/Tyr326 is required to precondition Akt for membrane binding (Jiang and Qiu, 2003). At the membrane, Akt is phosphorylated on Thr308 within its catalytic domain by phosphoinositol-dependent kinase 1 (PDK1) and at Ser473 within its C-terminal regulatory domain by mammalian target of rapamycin complex 2 (mTORC2), resulting in its full activation (Guertin and Sabatini, 2007; Bayascas, 2008).

A less well-recognized mechanism of regulation of Akt activity is polyubiquitination. Specifically, K63-linked polyubiquitination, executed by the E3 ligase tumor necrosis factor (TNF) receptor–associated factor 6 (TRAF6), promotes Akt translocation to the membrane and is essential for Akt phosphorylation (Yang *et al.*, 2009, 2010). Of the six known TRAF proteins, TRAF6 has several unique features that contribute to its diverse physiological functions. Unlike other TRAFs, which mediate signaling only from the TNF receptor superfamily, TRAF6 also participates in signal transduction from the Toll-like receptor/interleukin-1 receptor superfamily (Wu and Arron, 2003) and other receptors, including TGF-β receptors (Landstrom, 2010). TRAF6 induces K63-linked polyubiquitination of itself and downstream signaling molecules (Wang *et al.*, 2012). It is unclear how the K63-linked polyubiquitination of Akt results in its recruitment to the plasma membrane and its subsequent activation. Moreover, the role of TRAF6-mediated K63-linked polyubiquitination in integrin-dependent signaling is undefined.

The contribution of integrin α3β1 to the development of the kidney collecting system has been investigated; however, the involvement of its LM substrates and the signaling pathways mediated by LM/α3β1 integrin interactions are poorly defined. In this study, we show that the α3 chain containing LMs is essential for normal UB branching morphogenesis. We also demonstrate that integrin α3β1 mediates renal CD cell functions by activating Akt via a mechanism that is PI3K independent but requires K63-linked polyubiquitination. Finally, we show that the ubiquitin ligase TRAF6 interacts with the integrin β1 subunit and regulates integrin-dependent Akt activation. Thus we conclude that K63-linked polyubiquitination plays a previously unrecognized role in regulating integrin α3β1–dependent cell signaling that is required for UB development.

RESULTS

The LM α3 chain is required for normal UB development

The γ1 and α5 LM chains have been shown to be required for normal UB development in vivo (Liu *et al.*, 2009; Yang *et al.*, 2011); however, the role for the α3-containing LMs is undefined. We previously showed that LM-332 is expressed in early development of the rat UB (Zent *et al.*, 2001). We verified that α3-containing LMs are expressed in the developing mouse UB in E15 and E19 mouse kidneys by performing immunohistochemistry with antibodies directed against the LM α3 chain, found in LM-311, LM-321, and LM-332, and the LM γ2 chain that is specific for LM-332 (Figure 1, A–D). We subsequently defined the role of LM α3 chain in UB development by examining kidneys of LM α3–null mice, which die at birth due to a skin-blistering condition, on an undefined background, (Ryan *et al.*, 1999). We found that 40% of these mice (12/30) had developed one kidney when examined at birth (postnatal day 1 [P1]). This phenotype was lost as the mice were bred onto a pure C57/Bl6 background. However, examination of embryonic kidneys of LM α3–null mice on this background revealed mild hypoplasia/dysplasia of the papilla at E18 (Figure 1, E and F), which became more evident in newborn mice (Figure 1, G and H) and is manifested by fewer but more dilated tubules in the papilla. LM α3 deletion also significantly decreased tubule proliferation in the papilla (Figure 1, I–K), suggesting that a proliferative defect accounts in part for the abnormal phenotype. Thus α3-containing LMs appear to play a distinct role in UB development in vivo.

Deleting the integrin α3 subunit in the UB causes branching morphogenesis defects and renal papilla dysplasia/hypoplasia and impairs Akt and p38 MAPK signaling

Deletion of the β1 integrin subunit in the UB results in a severe branching morphogenesis defect in vivo (Zhang *et al.*, 2009), and organ culture experiments predicted that integrin α3β1 is a major contributor to UB development (Zent *et al.*, 2001). However, when the integrin α3 subunit was specifically deleted in the UB using the Hoxb7Cre mouse, only a mild to moderate CD defect characterized by absence or flattening of the papilla was noted (Liu *et al.*, 2009). Owing to this discrepant result, we used Hoxb7Cre;Itgα3$^{flox/flox}$ mice that were generated using different targeting strategies (Kobayashi *et al.*, 2005; Sachs *et al.*, 2006) to those published (Liu *et al.*, 2009; see *Materials and Methods* for details). These mice had a normal lifespan despite complete deletion of the integrin α3 subunit in the UB (Figure 2M). The kidneys had a mild UB branching morphogenesis defect that was first evident at E15 (Figure 2, A and B). At E18 and P1, the papillae of kidneys from Hoxb7Cre;Itgα3$^{flox/flox}$ mice were hypoplastic/dysplastic with fewer and more dilated CDs when compared with kidneys from controls

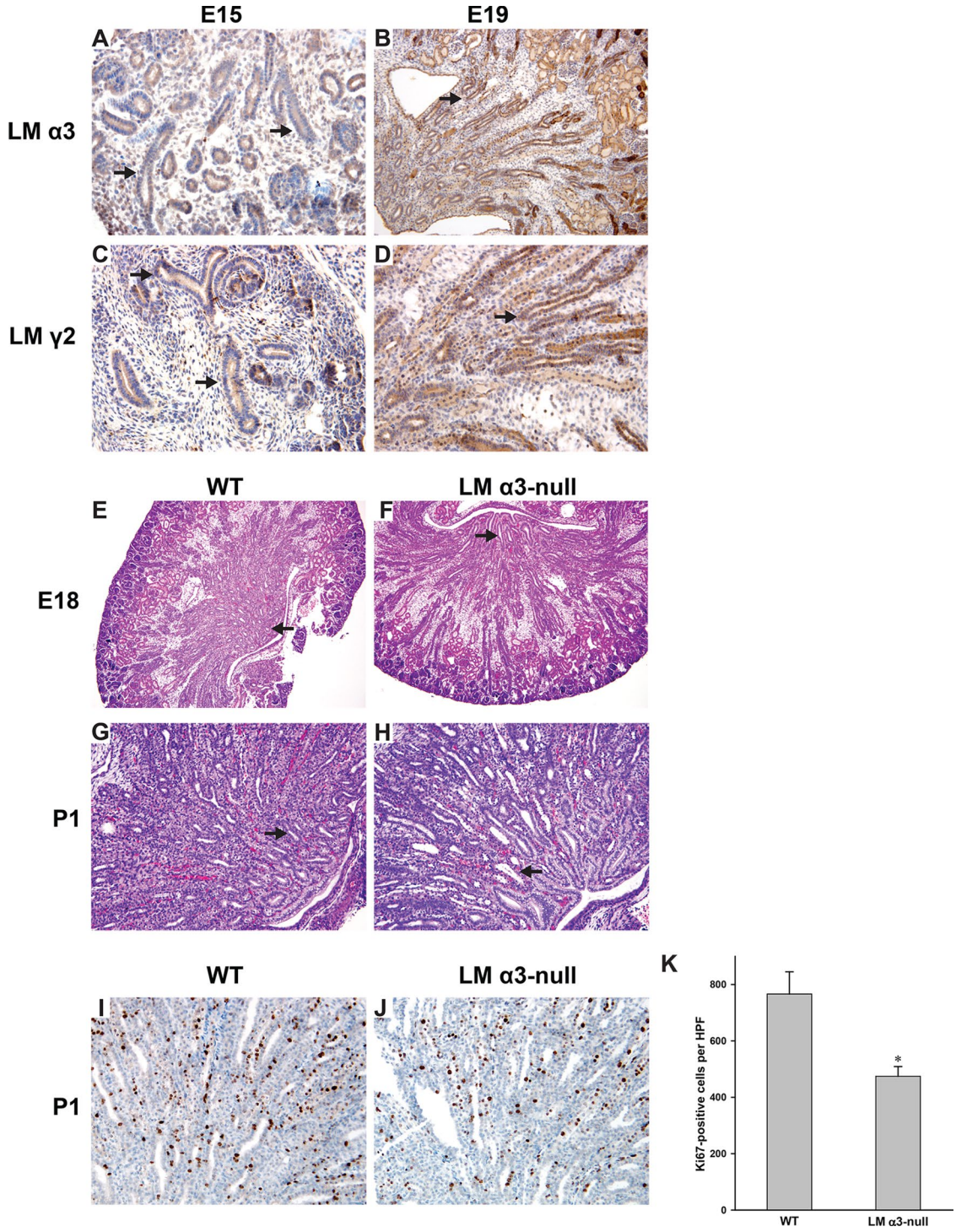

FIGURE 1: The LM α3 chain is required for normal UB development. (A–D) Embryonic mouse kidneys (E15, E19) stained with antibody against the LM α3 or LM γ2 chain. The UB is designated by the arrows (100× magnification). (E–H) H&E-stained kidneys of WT and LM α3–null mice at E18 and postnatal day 1 (P1). Magnification is 40× (E and F) and 100× (G and H). The arrows indicate the hypoplastic dysplastic papilla with dilated CDs present in the LM α3–null relative to WT mice. (I and J) Embryonic mouse kidneys (E19) stained with Ki67 antibody (100× magnification). (K) Bar graph of the average numbers of Ki67-positive tubular cells per HPF 100× magnification field of inner medullary CDs (6 HPF, 3 mice of each genotype) with SEM, *, $p < 0.05$ between WT and LM α3–null.

(Figure 2, C–H). Hypoplastic/dysplastic papillae persisted into adulthood of the Hoxb7Cre;Itgα3$^{flox/flox}$ mice (Figure 2, I–L).

As deleting the β1 integrin subunit in the UB resulted in markedly decreased activating phosphorylation of focal adhesion kinase (FAK), Akt, ERK1/2, and p38 MAPK (Zhang *et al.*, 2009), we examined whether similar abnormalities occurred in the developing collecting system of Hoxb7Cre;Itgα3$^{flox/flox}$ mice. As for the β1-null mice, we noted a decrease in Akt and p38 phosphorylation in the UB of Hoxb7Cre;Itgα3$^{flox/flox}$ mice; however, FAK (unpublished data) and ERK1/2 (Figure 2M) activation were

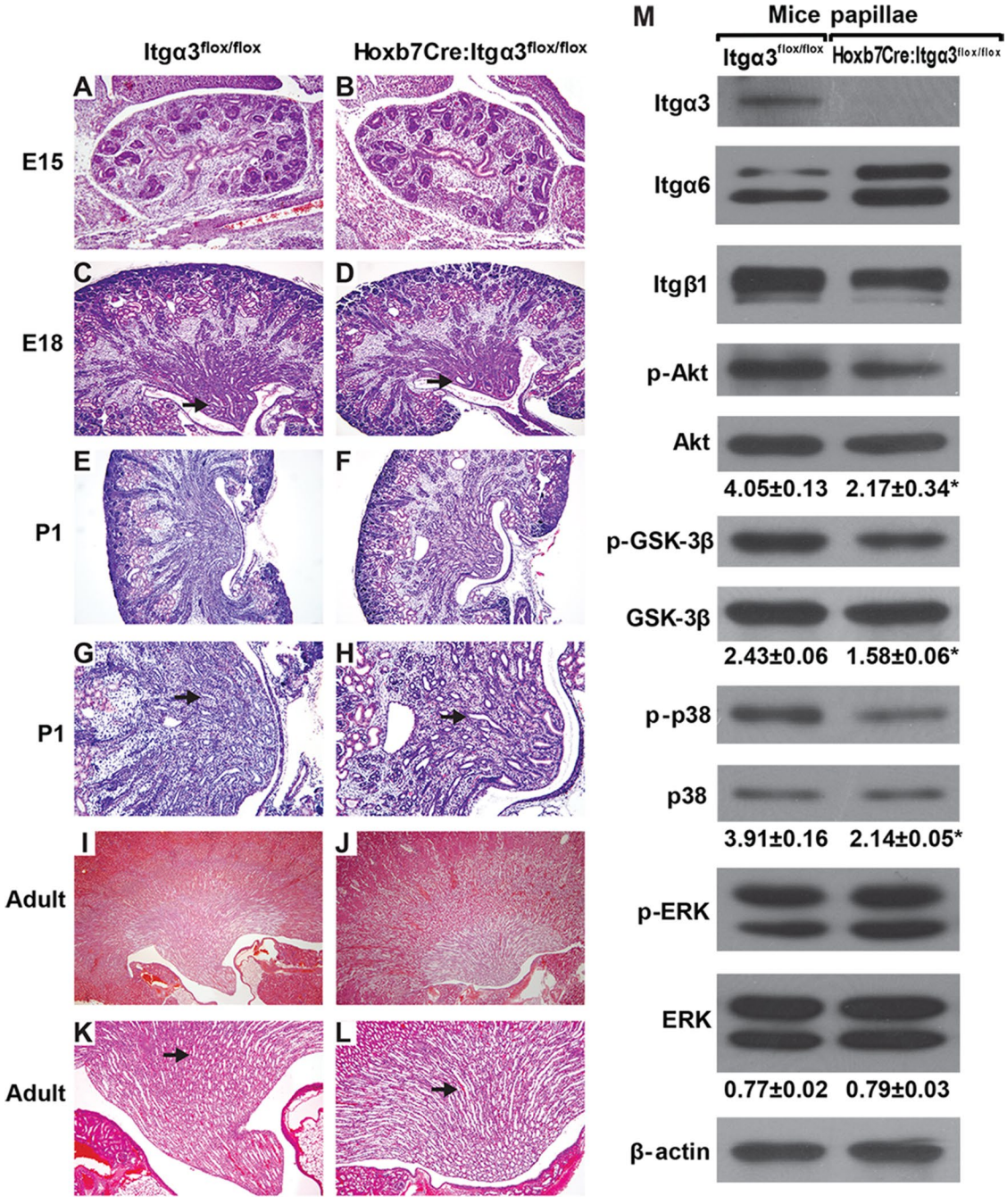

FIGURE 2: Hoxb7Cre:Itgα3$^{flox/flox}$ mice have defective UB development and decreased activation of Akt, GSK-3β, and p38 MAPK. (A–L) H&E stained kidneys of WT mice (Itgα3$^{flox/flox}$) and mice lacking integrin α3 in the UB (Hoxb7:Itgα3$^{flox/flox}$) at various stages of development. Magnification is 40× (A–F, I, and J) and 100× (G, H, K, and L). Note the mild branching defect from E15 onward and the hypoplastic papilla, which is characterized by fewer but dilated CDs in the Hoxb7:Itgα3$^{flox/flox}$ mice from E18 onward (arrows). (M) Lysates of papillae (20 μg total protein/lane) from 3-d-old Itgα3$^{flox/flox}$ and Hoxb7:Itgα3$^{flox/flox}$ mice were analyzed by Western blotting for levels of integrin subunits α3, α6, and β1; phospho-Akt^{Ser473}, phospho-GSK-3β, phospho-p38, and phospho-ERK1/2. Bands of phosphorylated and total proteins as well as β-actin (loading control) were measured by densitometry. The amount of phosphorylated proteins was normalized to total protein and β-actin levels and presented as mean ±SEM from at least three animals; *, $p < 0.05$ between Hoxb7:Itgα3$^{flox/flox}$ and Itgα3$^{flox/flox}$ samples.

unaffected. Consistent with diminished Akt activation, there was decreased Akt-dependent phosphorylation of glycogen synthase kinase 3 beta (GSK-3β) at Ser9 (Figure 2M). These data suggest that integrin α3 subunit regulates a limited number of integrin β1–dependent signaling pathways in the developing kidney collecting system, specifically the Akt and p38 MAPK pathways. Of note, deletion of α3 integrin subunit resulted in decreased expression of β1 and increased expression of α6 integrin subunits (Figure 2M). These data suggest that α3 is the major integrin subunit that interacts with the β1 subunit in the renal papilla and that there is compensatory expression of the integrin α6 subunit upon its deletion.

Integrin α3–null CD cells have severe adhesion, migration, proliferation, and signaling defects on LM-332

To study the mechanisms whereby LM/integrin α3β1 interactions regulate collecting system development, we isolated CD cells from Itgα3$^{flox/flox}$ mice (Itgα3$^{f/f}$) and deleted the integrin α3 subunit in vitro by infecting the cells with adeno-cre (Itgα3$^{-/-}$). As seen in the renal papilla, integrin α3 deletion led to increased integrin α6 and decreased integrin β1 expression (Figure 3, A and B). Interestingly, the increased α6 integrin subunit was associated with β1 and the level of integrin α6β4 was unchanged (Figure 3C). There was no change in expression of α1, α2, α5, or αv integrin subunits (unpublished data), suggesting that the expression levels of the collagen- and arginine–glycine–aspartic acid (RGD)-binding integrins were unaffected. Thus, as in the renal papilla, α3 appears to be the principal integrin subunit that interacts with the β1 subunit in CD cells, and there is compensatory expression of the integrin α6 subunit upon its deletion.

On the basis of our in vivo studies and those of others demonstrating that Hoxb7Cre;Itgα3$^{flox/flox}$ mice have similar phenotypes to LM α5– and α3–null mice (Miner and Li, 2000; Liu *et al.*, 2009; Figure 1), we defined whether integrin α3β1 controls CD cell adhesion, migration, and proliferation by interacting with LM-511 and/or LM-332. Severe defects in all these cell functions were detected for Itgα3$^{-/-}$ CD cells plated on LM-332. In contrast, the defects on LM-511, while significant, were not as severe (Figure 3, D–G), suggesting that LM-332 is a preferred substrate for integrin α3β1. To confirm the specific role of integrin α3β1 and the α6-containing integrins on CD cell adhesion to LM-332 and LM-511, we performed adhesion assays in the presence of a blocking anti-Itgα6 antibody (Figure 3H). Blocking α6-containing integrins did not affect adhesion of Itgα3$^{f/f}$ CD cells to LM-332 but decreased adhesion of these cells to LM-511. Adhesion of Itgα3$^{-/-}$ CD cells to both LMs was decreased by the addition of anti-Itgα6 antibody (Figure 3H). Thus α6-containing integrins play a role in CD cell binding to LM-511 in the presence and absence of integrin α3β1; however, they only affect CD cell adhesion to LM-332 in the absence of integrin α3β1. LM-332 and LM-511 were verified as specific substrates for integrin α3β1, as no differences between Itgα3$^{f/f}$ and Itgα3$^{-/-}$ cells were found when these assays were performed on collagen I, fibronectin, vitronectin, or LM-111 (Supplemental Figure 2).

Integrin α3β1–dependent adhesion to LM-332 and LM-511 activates Akt and p38 signaling pathways in CD cells

As our in vivo data demonstrated decreased Akt and p38 activation in the Hoxb7Cre;Itgα3$^{flox/flox}$ mice (Figure 2M), we performed in vitro replating assays to define whether the defects observed in cell function were mediated by abnormalities in integrin α3β1-LM–dependent signaling. Itgα3$^{-/-}$ CD cells failed to significantly increase Akt phosphorylation when plated on LM-332 or LM-511 (Figure 4A). A similar defect in Akt-dependent phosphorylation of GSK-3β was also seen when Itgα3$^{-/-}$ CD cells were plated on LM-332 or LM-511 (Figure 4A). It is important to note that the basal levels of Akt and Akt-dependent GSK-3β phosphorylation were significantly higher in Itgα3$^{-/-}$ than in Itgα3$^{f/f}$ CD cells (an approximately twofold difference; Figure 4A). There were also less marked but significant abnormalities in p38 signaling characterized by less-sustained activation in Itgα3$^{-/-}$ CD cells plated on either LM-332 or LM-551 compared with Itgα3$^{f/f}$ CD cells (Figure 4A). No difference in ERK1/2 activation was seen between the two CD cell populations. These results suggest that integrin α3β1 mediates LM-dependent activation of both Akt and p38 pathways; however, the effects on Akt are more profound. As with cell adhesion, migration, and proliferation (Figure 3, D–G), integrin α3β1 induced these signaling pathways more strongly when it interacted with LM-332 than with LM-511.

The role of p38 MAPK on integrin α3β1–dependent CD cell adhesion and migration on LM-332 was investigated by inhibiting its activity with SB203580 in Itgα3$^{f/f}$ CD cells. Inhibition of p38 MAPK, which was verified by decreased phosphorylation of MAPK-APK2, a specific downstream target of p38 MAPK (Figure 4B), resulted in a severe adhesion and migration defect (Figure 4, C and D). These data confirmed a role of p38 MAPK for integrin α3β1–dependent adhesion to and migration on LM-332.

Akt signaling pathway is critical for integrin α3β1–dependent CD cell adhesion and migration on LM-332

Because deleting the integrin α3 subunit caused increased basal Akt signaling and the inability to activate this pathway further, we defined the functional significance of Akt activation on integrin α3β1–dependent CD cell adhesion and migration on the preferred integrin α3β1 substrate LM-332. This was done by inhibiting its activity using two distinct Akt small interfering RNAs (siRNAs) or Akt inhibitor IV in Itgα3$^{f/f}$ CD cells (Figure 5, A and B) and then defining the ability of these cells to adhere and migrate (Figure 5, C and D). These treatments resulted in a significant decrease in cell adhesion to and migration on LM-332 (Figure 5, C and D). We confirmed that adhesion of CD cells to LM-332 was dependent on Akt signaling by restoring normal basal cell adhesion by transducing the cells with an adenovirus expressing constitutively active myristoylated Akt (Figure 5E). Analysis of signaling pathway activation revealed that Akt inhibitor IV treatment prevented phosphorylation of Akt and its downstream target GSK-3β (Figure 5B).

Integrin α3β1–dependent CD cell adhesion to and migration on LM-332 requires PI3K-independent Akt activation

A key regulator of Akt activity is PI3K, which phosphorylates PIP_2 to PIP_3 to create membrane sites for the Akt pleckstrin homology domain binding that allows for Akt recruitment to the plasma membrane, where it is activated (Cantley, 2002). To determine whether PI3K activity plays a role in integrin α3β1–dependent adhesion to and migration on LM-332, we inhibited PI3K activity by infecting the Itgα3$^{fl/fl}$ cells with adenovirus carrying a catalytic subunit deletion PI3K mutant, ad-delta p85 (Figure 6A). Surprisingly, both cell adhesion and migration were not affected by this form of PI3K inhibition (Figure 6, B and C). Similar results were obtained with the selective PI3K inhibitor LY294002 (Figure 6, B and C). Signaling pathway analysis revealed that LY294002 prevented Akt phosphorylation at the PI3K/PDK1-dependent Thr308 site (Figure 6D); however, phosphorylation of Ser473, which is performed by mTORC2 and serves as an indication of full Akt activation (Cantley, 2002; Guertin and Sabatini, 2007), was not affected (Figure 6D). Taken together, these data demonstrate that, in CD cells, Akt activity required for integrin α3β1–dependent adhesion to and migration on LM-332 is PI3K independent.

We next defined the mechanisms whereby integrin α3β1 regulates PI3K-independent activation of Akt in response to adhesion to LM by measuring the PIP_3 levels in Itgα3$^{f/f}$ and Itgα3$^{-/-}$ CD cells upon plating on LM-332. Basal levels of PIP_3 in Itgα3$^{-/-}$ CD cells were significantly higher than those detected in Itgα3$^{f/f}$ CD cells (Figure 6E). However, following plating on LM-332, Itgα3$^{f/f}$ CD cells showed a dramatic increase in PIP_3 levels (~1000-fold). In contrast, decreased levels of PIP_3 were noted in Itgα3$^{-/-}$ CD cells (Figure 6E).

In addition to PI3K, the amount of PIP_3 in cellular membranes is regulated by PTEN (Cantley, 2002; Song *et al.*, 2012). We therefore determined whether PTEN is responsible for the observed differences in PIP_3 levels. Indeed, the higher basal amount of PIP_3 in

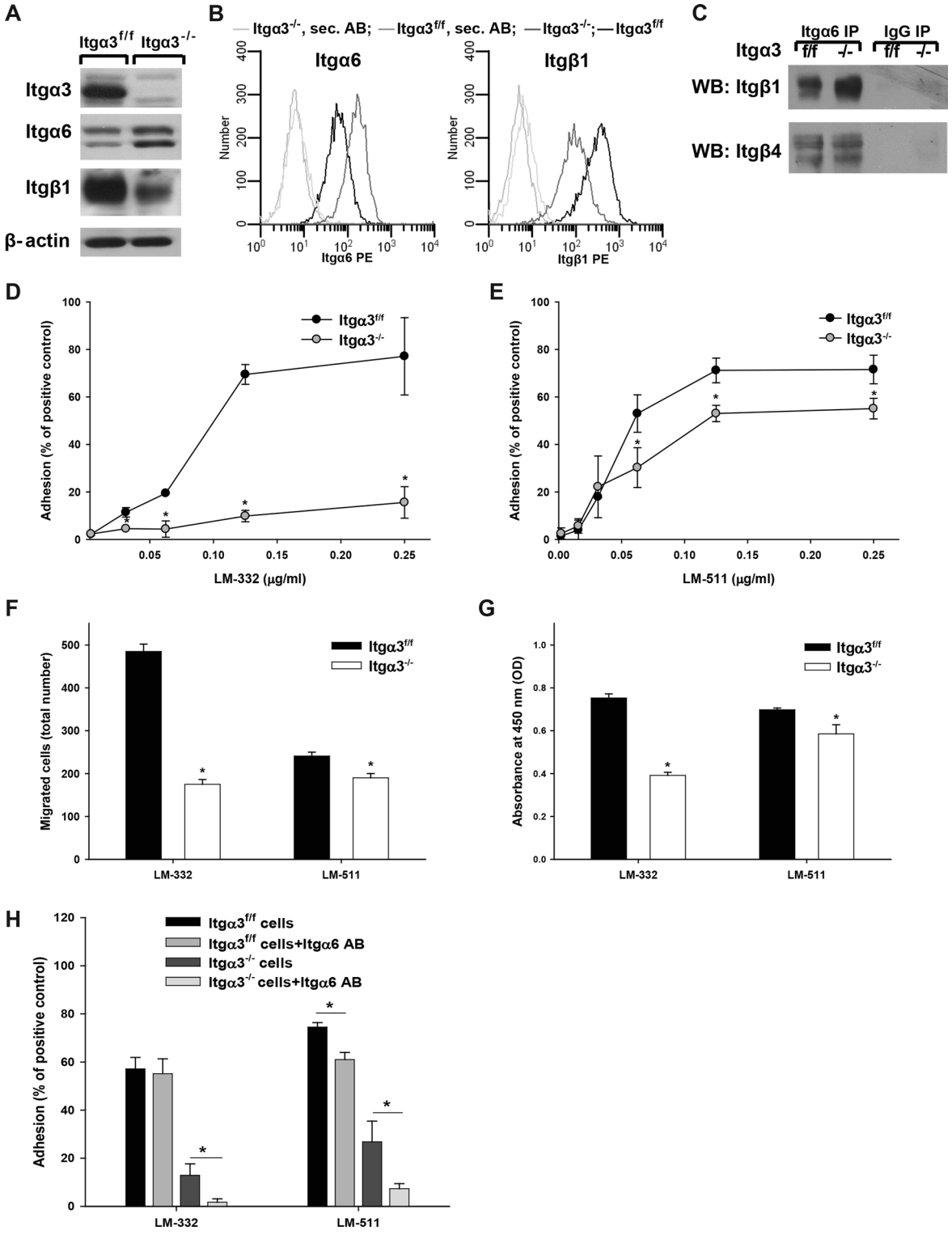

FIGURE 3: Integrin α3β1 promotes CD cell adhesion, migration, and proliferation on LM-332 and LM-511. (A) Lysates from Itgα3$^{-/-}$ and Itgα3$^{f/f}$ CD cells (20 μg total protein/lane) were immunoblotted for integrin β1, α3, and α6 subunits. β-actin served as a loading control. (B) Surface expression of integrin β1, α3, and α6 subunits was determined on Itgα3$^{-/-}$ and Itgα3$^{f/f}$ CD cells by flow cytometry using R-phycoerythrin (PE). (C) Lysates from Itgα3$^{-/-}$ and Itgα3$^{f/f}$ CD cells (100 μg total protein) were immunoprecipitated with anti-Itgα6 antibody or normal rabbit IgG and immunoblotted for integrin subunits β1 and β4. Adhesion (D and E), migration (F), and proliferation (G) of Itgα3$^{f/f}$ and Itgα3$^{-/-}$ CD cells on LM-332 and LM-511 were evaluated as described in *Materials and Methods*. Mean measurements ±SEM of four to six independent experiments are shown; *, $p \leq 0.05$ between Itgα3$^{f/f}$ and Itgα3$^{-/-}$ CD cells. (H) Itgα3$^{f/f}$ and Itgα3$^{-/-}$ CD cells were treated with blocking anti-Itgα6 antibody and plated on LM-332. Adhesion was evaluated as described in *Materials and Methods*. Mean measurements ± SEM of three independent experiments are shown; *, $p \leq 0.05$ between CD cells and CD cells treated with blocking anti-Itgα6 antibody.

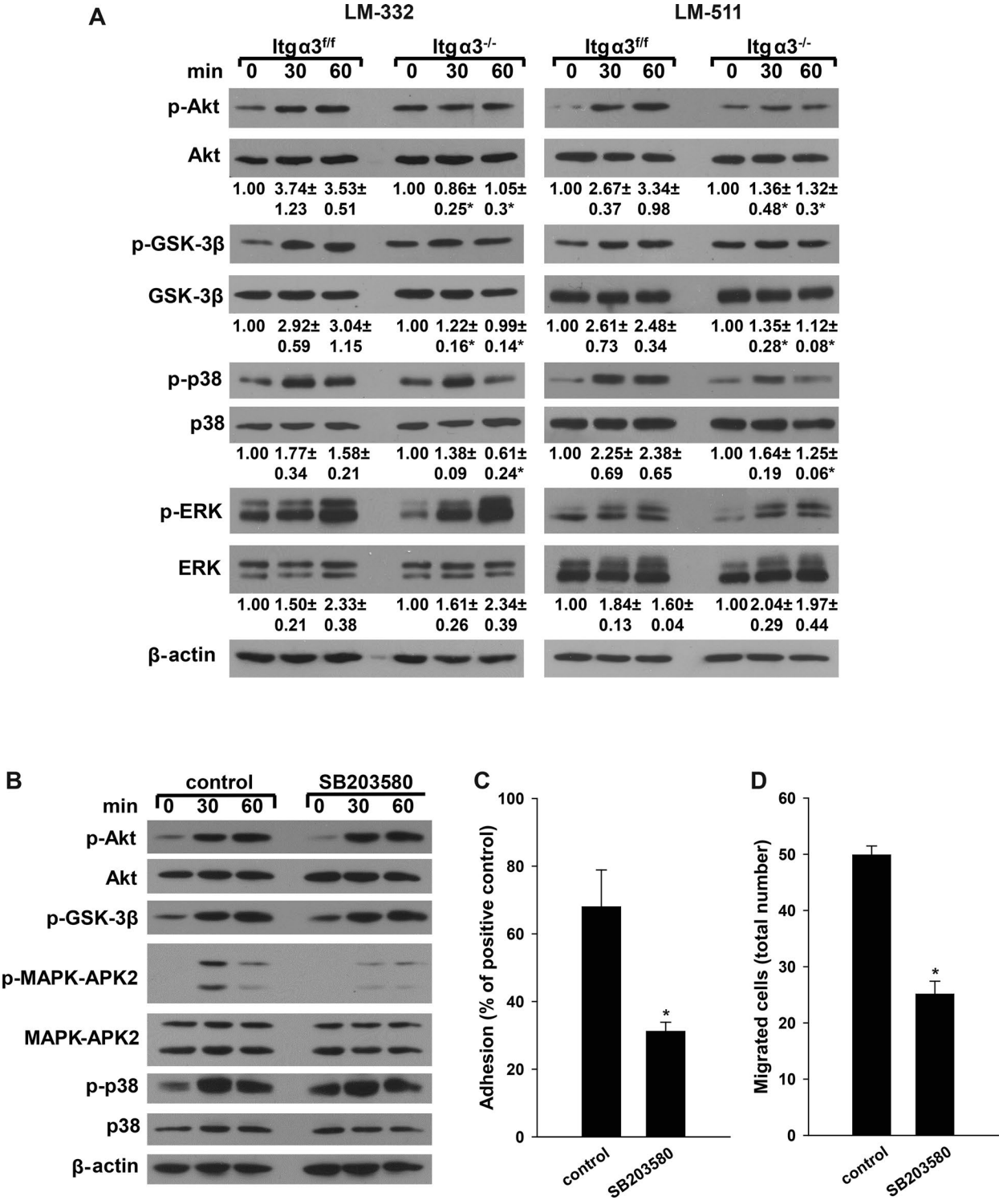

FIGURE 4: Integrin α3β1–dependent adhesion induces activation of Akt and p38 pathways. (A) Itgα3$^{f/f}$ and Itgα3$^{-/-}$ CD cells were plated in serum-free medium on LM-332 or LM-511 (both at 1 μg/ml). Cells were lysed at 30 and 60 min after plating, and lysates were analyzed by Western blotting for levels of phosphorylated Akt^{Ser473}, GSK-3β, p38, and ERK1/2 (20 μg total protein/lane). Levels of phosphorylated proteins were measured by densitometry, normalized to total protein and β-actin levels, and expressed as fold change relative to cells left in suspension, "0" time point. Values are the mean ± SEM of three independent experiments; *, $p \leq 0.05$ between Itgα3$^{f/f}$ and Itgα3$^{-/-}$ CD cells. (B–D) Itgα3$^{f/f}$ CD cells were treated with dimethyl sulfoxide (DMSO; control) or the p38 inhibitor SB203580 (10 μM) for 1 h, after which the cells were trypsinized; resuspended in serum-free medium; and subjected to replating (B), adhesion (C), or migration (D) assays on LM-332 (1 μg/ml). (B) Cell signaling was evaluated by immunoblotting cell lysates for phosphorylated Akt^{Ser473}, GSK-3β, p38, and MAPK-APK2 (20 μg total protein/lane). β-actin served as a loading control. Adhesion (C) and migration (D) were evaluated as described in *Materials and Methods*. Mean measurements ± SEM of three independent experiments are shown; *, $p \leq 0.05$ between Itgα3$^{f/f}$ treated with DMSO and SB203580.

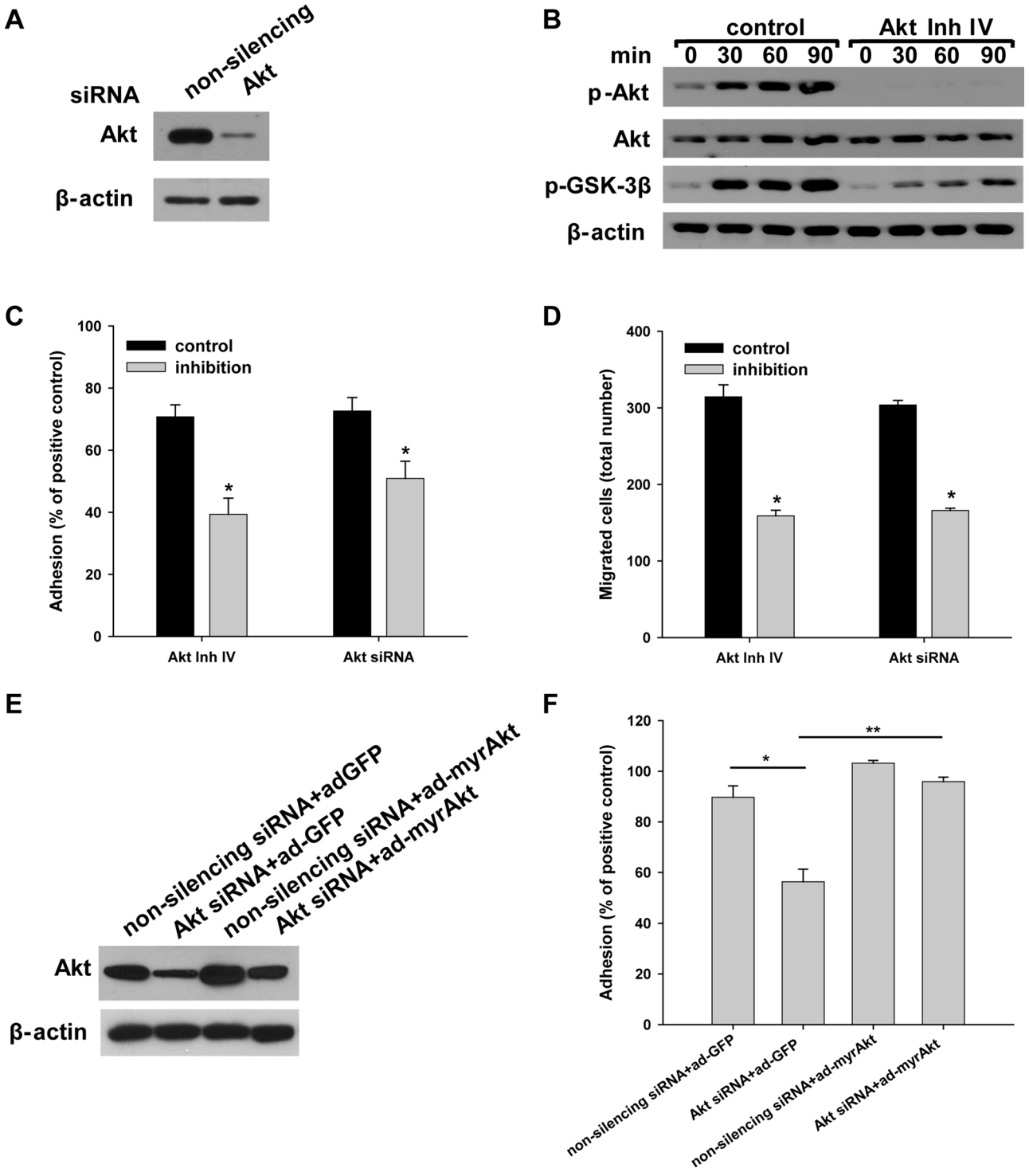

FIGURE 5: Integrin α3β1–dependent adhesion and migration on LM-332 are regulated by Akt activation. Itgα3$^{f/f}$ CD cells were transfected with nonsilencing or Akt siRNA (100 nM for 48 h) (A and C–F) or treated with the Akt inhibitor IV (5 μM for 1 h) or DMSO (control) (B–D). The effect of the siRNA on AKT expression is shown by immunoblotting cell lysates for total Akt, with β-actin serving as a loading control (A). (B–D) Control cells or cells treated with Akt inhibitor IV were subjected to replating, after which cell lysates were immunoblotted for phosphorylated Akt^{Ser473} and GSK-3β and total Akt (20 μg total protein/lane), with β-actin serving as a loading control (B). Treated and untreated cells were evaluated for adhesion (C) or migration (D) on LM-332 (1 μg/ml) and evaluated as described in *Materials and Methods*. Mean measurements ± SEM of four to six independent experiments are shown; *, $p \leq 0.05$ between control Itgα3$^{f/f}$ cells and Itgα3$^{f/f}$ cells with inhibitors. (E and F) Itgα3$^{f/f}$ CD cells were transfected with either nonsilencing or Akt siRNA, with control (ad-GFP) or myristilated Akt (100 plaque-forming units/cell for 24 h) (myrAkt) (E) and subjected to an adhesion assay as described in C (F). Mean measurements ± SEM of four to six independent experiments are shown; *, $p \leq 0.05$ between control Itgα3$^{f/f}$ cells and Itgα3$^{f/f}$ cells transfected with Akt siRNA; *, $p \leq 0.05$ between Itgα3$^{f/f}$ cells with Akt siRNA and Itgα3$^{f/f}$ cells with Akt siRNA and myristilated Akt.

Itgα3$^{-/-}$ CD cells (Figure 6E) correlated with lower basal PTEN levels (Figure 6F) and higher basal Akt activity (Figure 4A). Following plating on LM-332, PTEN levels decreased in Itgα3$^{f/f}$ CD cells but increased in Itgα3$^{-/-}$ CD cells (Figure 6F). By contrast, PIP_3 levels and Akt activity increased in Itgα3$^{f/f}$ CD cells, but decreased in Itgα3$^{-/-}$ CD cells (Figures 6E and 4A). These data suggest that integrin α3β1 regulates PIP_3 levels and, in turn, Akt activation by regulating PTEN levels.

There are two signaling events in the canonical pathway of Akt activation that precede and follow the membrane-anchoring step: Src-dependent Akt phosphorylation preconditions Akt for membrane binding, and PDK1-mediated phosphorylation activates membrane-bound Akt (Cantley, 2002; Jiang and Qiu, 2003; Bayascas, 2008). No differences in Src or PDK1 activation were noted between Itgα3$^{f/f}$ and Itgα3$^{-/-}$ CD cells plated on LM-332 (Figure 6F), suggesting that these kinases were not responsible for the differences in Akt activation between the two cell populations. As Src and PDK1 activities are regulated by PI3K, these data further confirm that integrin α3β1 regulates Akt activity via a PI3K-independent mechanism(s).

Integrin α3β1–dependent K63-linked polyubiquitination of Akt is mediated by TRAF6

K63-linked polyubiquitination of Akt is also an essential step in Akt activation (Yang *et al.*, 2009, 2010). While the mechanism is unclear, it has been postulated that K63-linked polyubiquitination increases Akt binding to PI(3,4,5)P3 on the membrane or creates docking sites for Akt to interact with other signaling proteins (Wang *et al.*, 2012). We therefore checked for differences in K63-linked polyubiquitination between Itgα3$^{f/f}$ and Itgα3$^{-/-}$ CD cells plated on LM-332 by immunoblotting for K63-linked polyubiquitination of Akt immunoprecipitates (Figure 7A). K63-linked polyubiquitination of Akt increased over time when Itgα3$^{f/f}$ CD cells were plated on LM-332, while no significant change was noted in the Itgα3$^{-/-}$ CD cells (Figure 7A). Of note, the basal level of Akt K63-linked polyubiquitination was significantly higher in Itgα3$^{-/-}$ than in Itgα3$^{f/f}$ CD cells (an approximately twofold difference; Figure 7A). To verify the specificity of the Akt K63-linked polyubiquitination, we measured Akt K48-linked polyubiquitination in Itgα3$^{f/f}$ and Itgα3$^{-/-}$ CD cells and found that this was unaffected by adhesion to LM-332 (Figure 7B). Thus integrin α3β1–dependent CD cell adhesion to LM specifically increases K63-linked polyubiquitination of Akt.

TRAF6 was recently identified as a unique E3 ligase for Akt that is responsible for K63-linked Akt polyubiquitination, which facilitates Akt membrane recruitment and subsequent Akt phosphorylation and activation (Yang *et al.*, 2009; Wang *et al.*, 2012). We therefore determined whether the ubiquitination activity of TRAF6 was altered by integrin α3β1–dependent adhesion to LM-332 by measuring TRAF6 K63-linked autopolyubiquitination (Lamothe *et al.*, 2007). This was indeed the case, as K63-linked polyubiquitination of TRAF6 increased significantly when Itgα3$^{f/f}$ CD cells adhered to LM-332, while no increase above basal levels was seen in Itgα3$^{-/-}$ CD cells (Figure 7C). Of note, the basal level of TRAF6 K63-linked polyubiquitination was significantly higher in Itgα3$^{-/-}$ than in Itgα3$^{f/f}$ CD cells (an approximately twofold difference; Figure 7C), which would explain the increased basal Akt ubiquitination and activation observed in Itgα3$^{-/-}$ CD cells (see Figure 4A for details).

The functional significance of TRAF6 activity for integrin α3β1–dependent Akt activation was then defined by down-regulating its expression in Itgα3$^{f/f}$ CD cells using an siRNA approach (Figure 7D). Reduced TRAF6 expression resulted in a severe defect in Akt phosphorylation (Figure 7D) and decreased K63-linked polyubiquitination of Akt when Itgα3$^{f/f}$ CD cells were plated on LM-332 (Figure 7E). We next defined the functional effects of down-regulating TRAF6 on integrin α3β1–dependent cell adhesion to LM-332 and found that decreased TRAF6 expression significantly decreased Itgα3$^{f/f}$ CD cells adhesion to this substrate (Figure 7F). As this decreased adhesion was similar to that induced by the Akt inhibitor IV (Figure 7F), we postulated that TRAF6 might regulate cell adhesion by altering the activation state of Akt. This possibility was confirmed by the fact that introduction of a constitutively active Akt (ad-myrAkt) restored the adhesion defects caused by TRAF6 down-regulation (Figure 7F).

TRAF6 deficiency causes renal papilla dysplasia/hypoplasia and defects in Akt signaling

Our in vitro data suggested that integrin α3β1 regulates Akt activation by altering TRAF6 function in CD cells. We therefore investigated whether TRAF6-dependent activation of Akt regulates kidney collecting system development in vivo by analyzing the phenotype of kidneys from TRAF6-deficient (KO) mice. Previous investigation of these animals has demonstrated that TRAF6 is essential for normal bone formation (Lomaga *et al.*, 1999), establishment of the immune system and inflammatory response (Lomaga *et al.*, 1999; Naito *et al.*, 1999), development of the central neuron system (Lomaga *et al.*, 2000) and epidermal appendixes (Naito *et al.*, 1999). The kidneys of TRAF6 KO newborn mice were noticeably smaller than wild-type (WT) animals (Figure 8, A and B). When we examined the kidneys of TRAF6 KO newborn mice in detail, we noted a slight branching morphogenesis defect in the renal collecting system and a mildly dysplastic papilla (Figure 8, C and D) resembling the defects observed in the Hoxb7Cre;Itgα3$^{flox/flox}$ (Figure 2, E–H) and the constitutive Itgα3-null mice (Kreidberg *et al.*, 1996). As deleting the α3 integrin subunit in the UB resulted in markedly decreased activation of Akt signaling (Figure 2M), we examined whether similar abnormalities occurred in the developing collecting system of TRAF6 KO mice. As in Hoxb7Cre;Itgα3$^{flox/flox}$ mice, we noted a decrease in Akt activation of phosphorylation in the collecting system of the TRAF6 KO mice (Figure 8E). Consistent with decreased Akt activation, there was decreased Akt-dependent phosphorylation of GSK-3β at Ser9 (Figure 8E). These data suggest that TRAF6 regulates activity of the Akt signaling pathway in the developing kidney collecting system.

TRAF6 forms a complex with α3β1 integrin and Akt

Finally, we defined how α3β1 integrin and TRAF6 interact with each other to mediate K63-linked polyubiquitination of Akt. This question was addressed by immunoprecipitating integrin α3 or β1 subunits from Itgα3$^{f/f}$ and Itgα3$^{-/-}$ CD cells grown on uncoated cell culture plates. The immunoprecipitates were immunoblotted for integrin β1 and α3 subunits or TRAF6 (Figure 9, A and B). The β1 integrin subunit was present in α3 immunoprecipitates from Itgα3$^{f/f}$ but not Itgα3$^{-/-}$ CD cells (Figure 9A). TRAF6 was not detected in Itgα3 immunoprecipitates from Itgα3$^{f/f}$ or Itgα3$^{-/-}$ CD cells (Figure 9A). We believe this is a result of very low immunoprecipitation efficiency. In this regard, Figure 9A shows that ~5% of integrin α3 immunoprecipitates with the anti-Itgα3 antibody, which allows us to detect bound integrin β1. However, since TRAF6 likely binds inferiorly to integrin α3β1 via the cytoplasmic tail of integrin β1, it does not allow for TRAF6 detection. As expected, there were fewer β1 and no α3 integrin subunits in the Itgβ1 immunoprecipitates from Itgα3$^{-/-}$ compared with Itgα3$^{f/f}$ CD cells (Figure 9B). TRAF6 was immunoprecipitated from lysates of Itgα3$^{f/f}$ but not Itgα3$^{-/-}$ CD cells (Figure 9B). We next defined the integrin subunit to which TRAF6 binds by performing affinity chromatography of CD cell lysates with His-tagged β1, α3, or α5 (used as negative control) transmembrane and

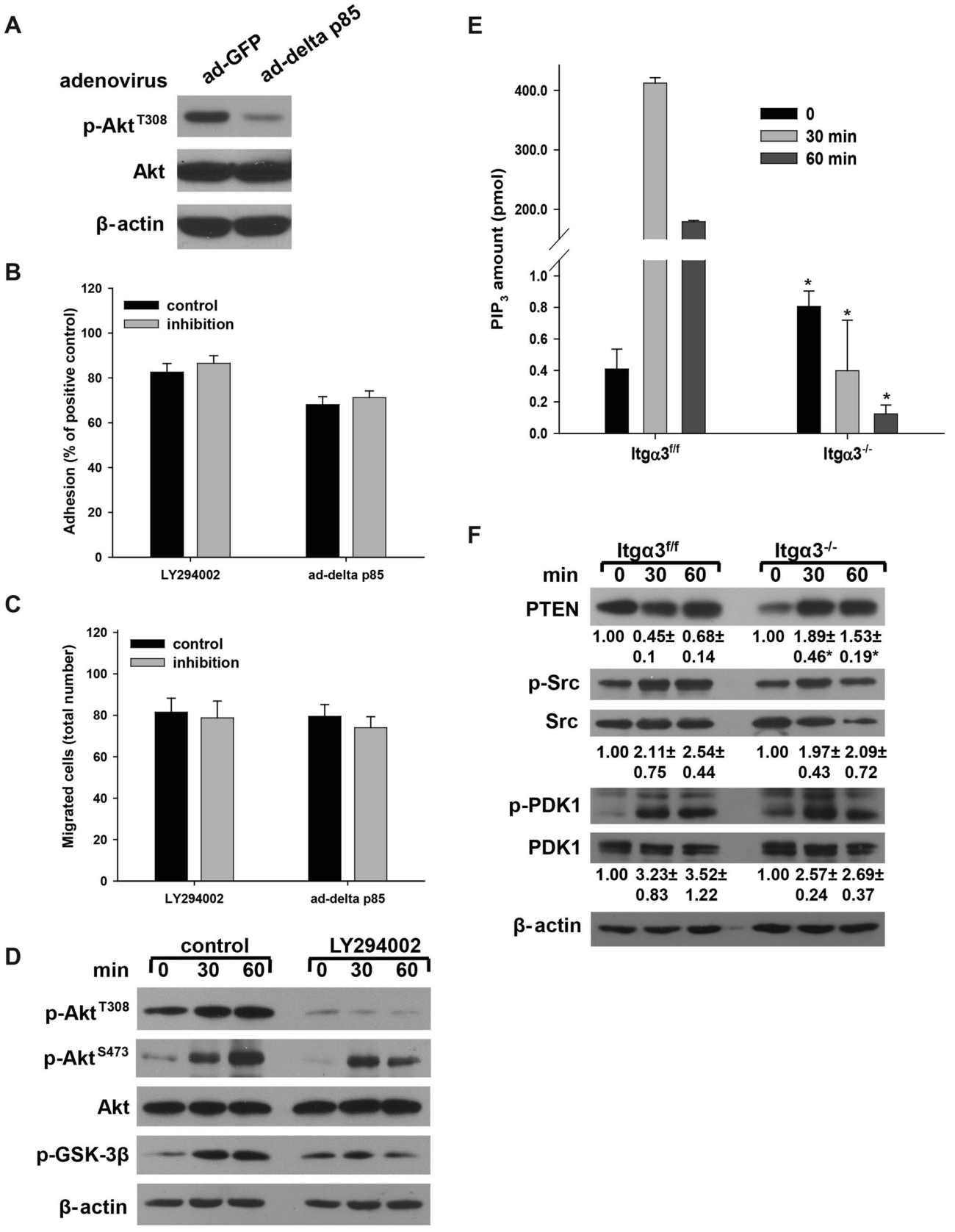

FIGURE 6: Integrin α3β1–dependent CD cell adhesion to and migration on LM-332 requires PI3K-independent Akt activation. (A–D) Itgα3$^{f/f}$ CD cells were infected with ad-GFP or ad-delta p85 (100 plaque-forming units/cell for 24 h) (A); or treated with DMSO (control) or the PI3K inhibitor LY294002 (25 μM for 1 h). Cells were subjected to adhesion (B), migration (C), or the replating assay on LM-332 (1 μg/ml) for evaluation of phospho-Akt^{Thr308}, phospho-Akt^{Ser473}, and phospho-GSK-3β. β-actin served as a loading control. Western blot of cellular lysates shows that infection with ad-delta

cytoplasmic tail peptides. Interestingly, TRAF6 and kindlin 2 (which is known to bind specifically to β1 integrin) bound to integrin β1 but not to α3 or α5 cytoplasmic tails (Figure 9C). Together these data suggest that TRAF6 binds to the cytoplasmic tail of the β1 integrin subunit, and this interaction requires the presence of the α3 integrin subunit in cells expressing intact β1 integrin.

We next defined whether TRAF6 associates with Akt and whether this association is regulated by integrin α3β1 interactions with LM. When CD cells were plated on LM-332, more Akt coimmunoprecipitated with TRAF6 in a time-dependent manner in Itgα3$^{f/f}$ compared with Itgα3$^{-/-}$ cells. These data suggest that that TRAF6 and Akt form a complex following integrin α3β1–dependent adhesion (Figure 9D).

DISCUSSION

Integrin α3β1 plays an important role in UB development in vivo due to its interactions with α5-containing LMs, and in vitro studies suggested these effects are mediated by its ability to regulate PI3K/Akt-dependent Wnt signaling (Liu *et al.*, 2009). In this study, we show that α3-containing LMs, in addition to the α5 LMs, play a crucial part in UB development and that integrin α3β1 regulates both Akt and p38 activation in the UB in vivo. We also demonstrate that LM-332 is the preferred ligand for mediating integrin α3β1–dependent CD cell functions and signaling. Finally, and most importantly, we establish that the integrin β1 cytoplasmic tail interacts with TRAF6, which is an E3 ligase for K63-linked polyubiquitination, and this interaction regulates integrin α3β1–dependent Akt activation and cell functions. Thus these studies define a novel functionally important LM–integrin α3β1 interaction in UB development and identify K63-linked polyubiquitination as a critical new mechanism whereby integrins modulate cell signaling.

We previously demonstrated that LM-332 is expressed during initial UB formation and that it plays a significant role in in vitro cell and organ culture models of UB development (Zent *et al.*, 2001). Consistent with these findings, we demonstrate in this study that the α3 and γ2 LM chains are expressed during UB development and that deleting the α3 LM chain results in a severe renal development abnormality in outbred mice (with 40% of mice not developing one kidney) and a mild to moderate branching defect in pure C57/Bl6 mice. Interestingly, no phenotype was observed in the developing UB of the LM γ2–null mice (unpublished data), suggesting functional redundancy of the α3 LMs in UB development. The mild to moderate phenotype in LM α3–null mice is similar to that seen in LM α5–null mice (Liu *et al.*, 2009) and much less severe than when the LM γ1 chain was selectively deleted in the developing UB (Yang *et al.*, 2011). Our finding that LM α3 plays a role in UB development might explain the less severe than expected phenotype in the LM γ1–null mice, as LM-332 could be compensating for the LM γ1 deletion (Yang *et al.*, 2011).

When we deleted the integrin α3 subunit in the UB, we observed a mild to moderate branching morphogenesis defect at E15 that persisted into adulthood. These results differ slightly from previous observations that the UB of constitutive integrin α3–null kidneys at E15 was indistinguishable from WT mice and that a difference was seen only at E18, when the null kidneys demonstrated a failure of papillary outgrowth (Kreidberg *et al.*, 1996; Liu *et al.*, 2009). These discrepancies could be due to differences in mouse backgrounds or because the Hoxb7Cre and integrin α3$^{flox/flox}$ mice were generated using different strategies.

Deleting the α3 integrin subunit in the UB in vivo and in CD cells resulted in decreased expression of the β1 and increased expression of the α6 integrin subunits, suggesting that α3 is the major integrin subunit that interacts with the β1 subunit in the renal papilla and there is compensatory expression of the integrin α6 subunit upon its deletion. The increased α6 expression might explain the mild phenotypic defects observed when the integrin α3 subunit is deleted from the UB (Kreidberg *et al.*, 1996; Liu *et al.*, 2009) and why it is significantly less severe than that seen when kidneys or isolated UBs are grown in the presence of α3-blocking antibodies (Zent *et al.*, 2001). This possibility is further supported by our in vitro data showing that α6β1 integrin contributes to increased CD cell binding to LM-332 and LM-511, especially in the absence of integrin α3β1 expression. Although it is not proven, we speculate that the α6β1 compensation occurs through a distinct TRAF6-independent mechanism.

We show that LM-332 is the preferred LM for CD cell adhesion, migration, proliferation, and adhesion-dependent cell signaling. These data are consistent with findings demonstrating a role for LM-332 in regulating proliferation and cyst formation of cells isolated from a patient with autosomal polycystic kidney disease (Joly *et al.*, 2003) and adhesion and migration of Madin-Darby canine kidney cells (Mak *et al.*, 2006; Moyano *et al.*, 2010; Greciano *et al.*, 2012). These in vitro data also support the idea that LM-332 is a preferred ligand for integrin α3β1 signaling in renal tubule development, maintenance, and recovery from injury (Joly *et al.*, 2003, 2006).

We report that integrin α3β1 primarily regulates Akt and p38 signaling, as activation of these two pathways was diminished in the developing UB of Hoxb7Cre;Itg α3$^{flox/flox}$ mice and when Itgα3$^{-/-}$ CD cells were plated on LM-332 and LM-511. These data contrast with the Hoxb7Cre;Itgβ1$^{flox/flox}$ mice and Itgβ1$^{-/-}$ CD cells, where phosphorylation of FAK and ERK1/2, as well as of Akt and p38, was severely affected (Zhang *et al.*, 2009). Our results suggest that integrins other than α3β1 play additional roles in UB development and that specific β1-containing integrins regulate the precision of signaling in the kidney collecting system.

We show that integrin α3β1–LM-332 interactions induce Akt activation by mechanisms that are independent of PI3K, Src, and PDK1, but dependent on PTEN and K63 polyubiquitination (Figure 10). Our data suggest that PTEN is responsible for the low basal levels of PIP_3 and Akt activity in Itgα3$^{f/f}$ cells, which dramatically increase upon integrin α3β1 binding to LM-332, while we observe opposite effects in Itgα3$^{-/-}$ CD cells under the same conditions. These results are consistent with previous studies demonstrating

p85 resulted in marked decrease in phospho-Akt^{Thr308} (D). Adhesion and migration were evaluated as described in *Materials and Methods*. Mean measurements ± SEM of three independent experiments are shown. (E and F) Itgα3$^{f/f}$ and Itgα3$^{-/-}$ CD cells were plated on LM-332 (1 μg/ml) as described in Figure 4A. PIP_3 levels were detected using the PIP_3 Mass ELISA Kit as described in *Materials and Methods*. Mean measurements ± SEM of three independent experiments are shown; *, $p \leq 0.05$ between Itgα3$^{f/f}$ and Itgα3$^{-/-}$ CD cells (E). Cell lysates (20 μg total protein/lane) were analyzed by Western blotting for levels of total PTEN and phosphorylated and total Src and PDK1 (20 μg total protein/lane) (F). Levels of phosphorylated and total proteins were evaluated as described in Figure 4A. Values are the means ± SEM of three independent experiments; *, $p \leq 0.05$ between Itgα3$^{f/f}$ and Itgα3$^{-/-}$ CD cells.

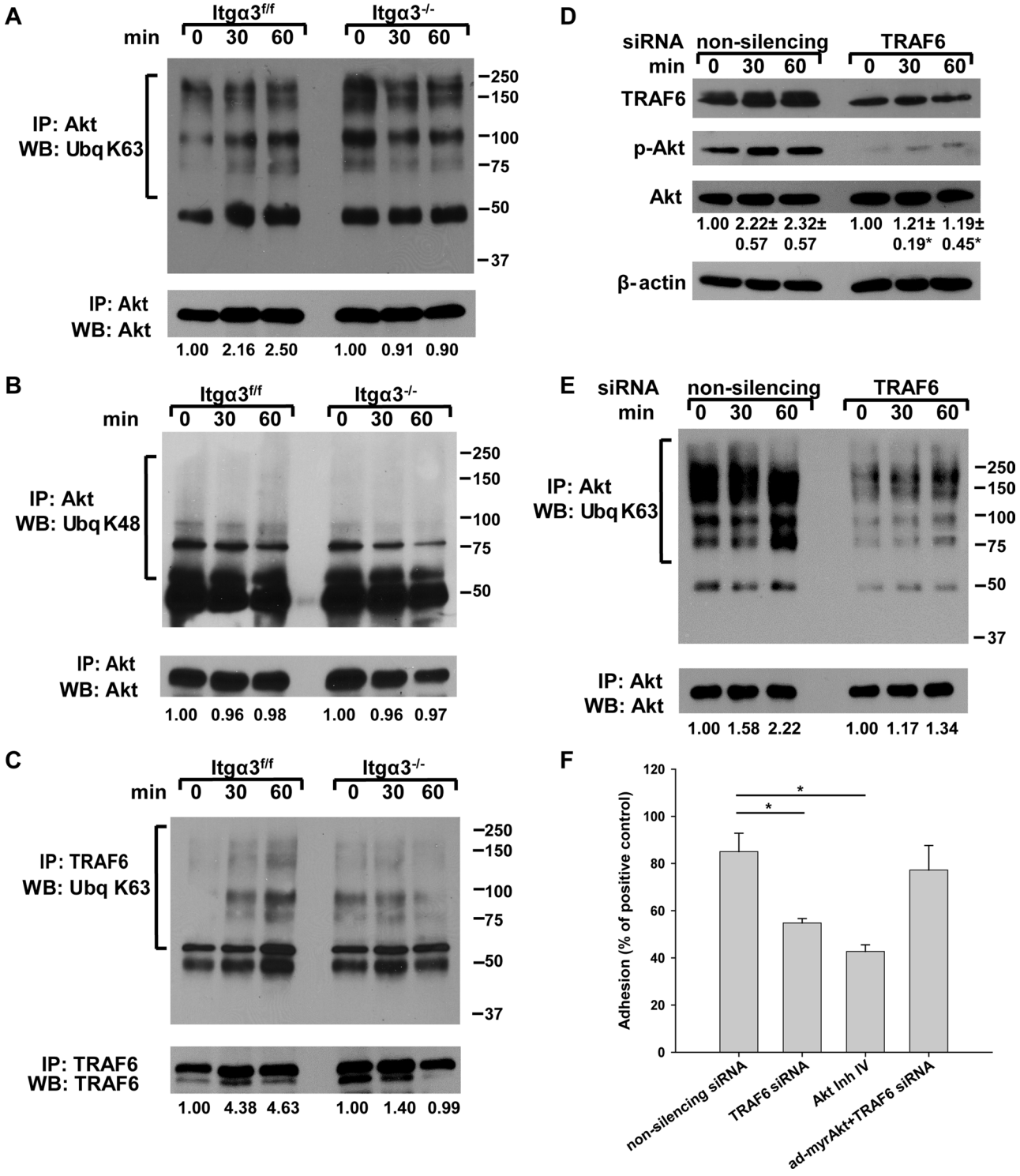

FIGURE 7: Akt activation by integrin α3β1 is regulated by TRAF6-dependent K63-linked polyubiquitination. (A–C) Itgα3$^{f/f}$ and Itgα3$^{-/-}$ CD cells were plated on LM-332 (1 μg/ml) as described in Figure 4A. Cell lysates (100 μg total protein) were immunoprecipitated with anti-Akt antibodies and immunoblotted for K63-linked ubiquitination and Akt (A) or K48-linked ubiquitination and Akt (B). Cell lysates (100 μg total protein) were immunoprecipitated with antibodies to TRAF6 and immunoblotted for K63 ubiquitination or TRAF6 (C). Levels of ubiquitinated proteins were measured by densitometry, normalized to total protein, and expressed as fold change relative to cells left in suspension (0 time point). A representative of three experiments with quantification at the bottom is shown. (D and E) Itgα3$^{f/f}$ CD cells were transfected with nonsilencing or TRAF6 siRNA (20 nM for 48 h) and subjected to the replating assay on LM-332 (1 μg/ml). Cell lysates (40 μg total protein/lane) were immunoblotted for TRAF6, phospho-Akt^{Ser473}, and Akt (D). Levels of phosphorylated and total proteins were evaluated as described in Figure 4A. Values are the means ± SEM of three independent experiments; *, $p \leq 0.05$ between cells transfected with nonsilencing and TRAF6 siRNA. The same cell lysates (200 μg total protein) were immunoprecipitated with antibodies to Akt and immunoblotted for K63-linked

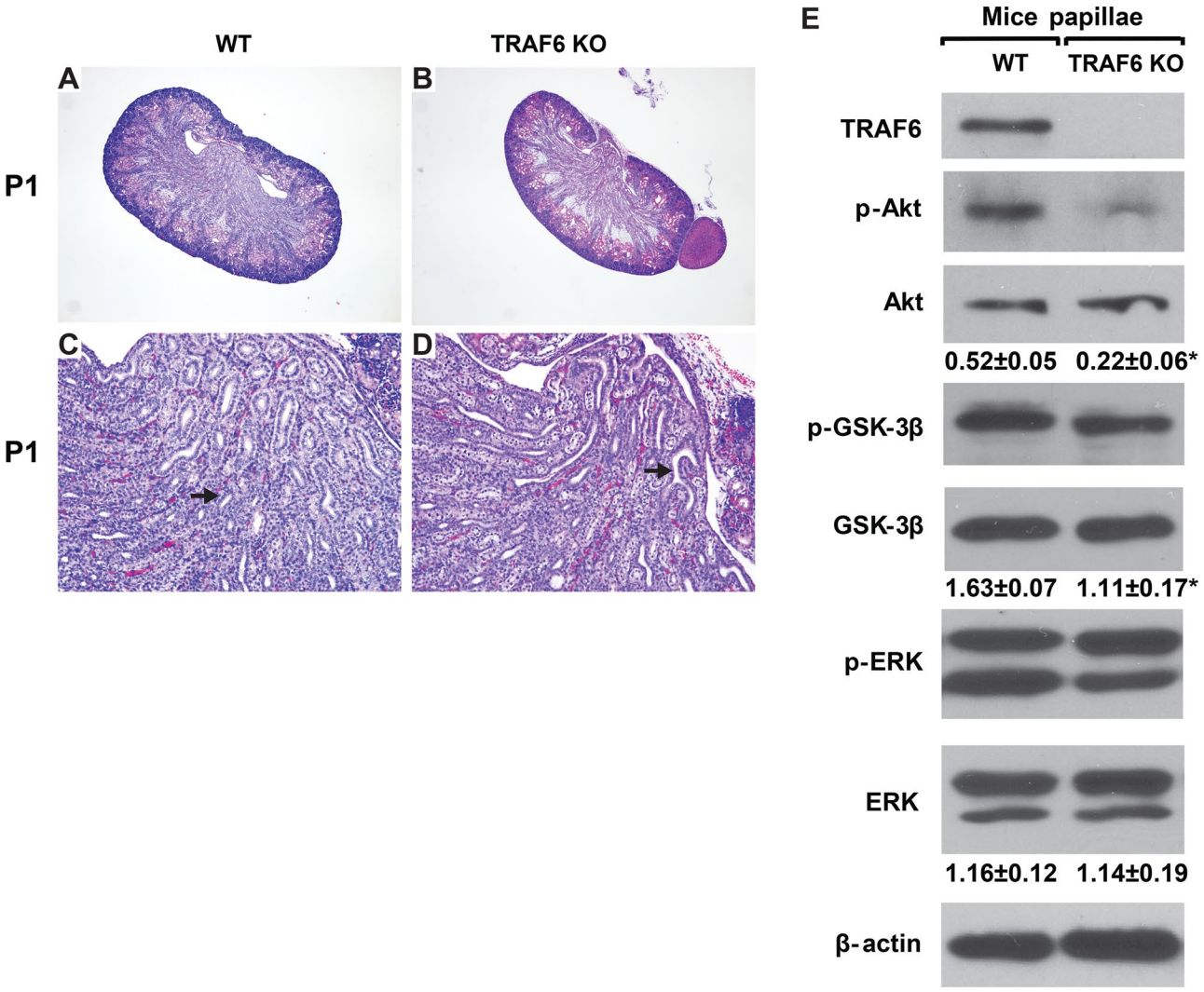

FIGURE 8: TRAF6 KO mice have defective UB development and decreased activation of Akt signaling. (A–D) H&E stained kidneys of newborn (P1), WT mice (TRAF6 WT), and TRAF6-deficient mice (TRAF6 KO). Magnification 40× (A and B) and 100× (C and D). Note the mild branching defect and hypoplastic papilla in the TRAF6 KO mice (arrows). (E) Lysates of papillae from newborn WT and TRAF6 KO mice (20 μg total protein) were analyzed by Western blotting for levels of TRAF6, phospho-Akt^{Ser473}, and phospho-GSK-3β. β-actin was used as a loading control. The amount of phosphorylated proteins was evaluated as in Figure 2. *, $p \leq 0.05$ between WT and TRAF6 KO mice.

that the collagen-binding β1 integrins can regulate PTEN expression in fibroblasts (Xia *et al.*, 2008; Nho and Kahm, 2010), which suggests that this might be a generalized mechanism whereby β1 integrin regulates Akt activation. It is yet to be determined how integrin α3β1 regulates PTEN in CD cells.

We demonstrate that K63-linked polyubiquitination is a novel mechanism whereby integrin α3β1–LM-332 interactions induce Akt activation (Figure 10). These results are consistent with the observations that TRAF6-dependent K63-linked polyubiquitination assists in Akt translocation to the membrane and is essential for Akt activating phosphorylation following growth factor and cytokine stimulation (Yang *et al.*, 2009, 2010). We also show that TRAF6 regulates integrin α3β1–dependent signaling. TRAF6 E3 ligase activity was increased upon integrin α3β1–dependent adhesion to LM and it was required for Akt activating phosphorylation and cell adhesion to LM. These data are consistent with evidence that TRAF6 K63-linked autopolyubiquitination is the regulatory mechanism for TRAF6 activation and that TRAF6-dependent K63-linked polyubiquitination is a

polyubiquitination or Akt (E). Changes in protein ubiquitination were evaluated as described in A. A representative of three experiments with quantification at the bottom is shown. (F) Itgα3$^{f/f}$ CD cells were transfected with nonsilencing or TRAF6 siRNA (20 nM for 48 h), or treated with Akt inhibitor IV (5 μM for 1 h), and/or transduced with ad-myrAkt (100 plaque-forming units/cell for 24 h) and subjected to adhesion assay. Adhesion was evaluated as described in *Materials and Methods*. Mean measurements ± SEM of three independent experiments are shown; *, $p \leq 0.05$ between cells transfected with nonsilencing and TRAF6 siRNA or treated with the Akt inhibitor IV.

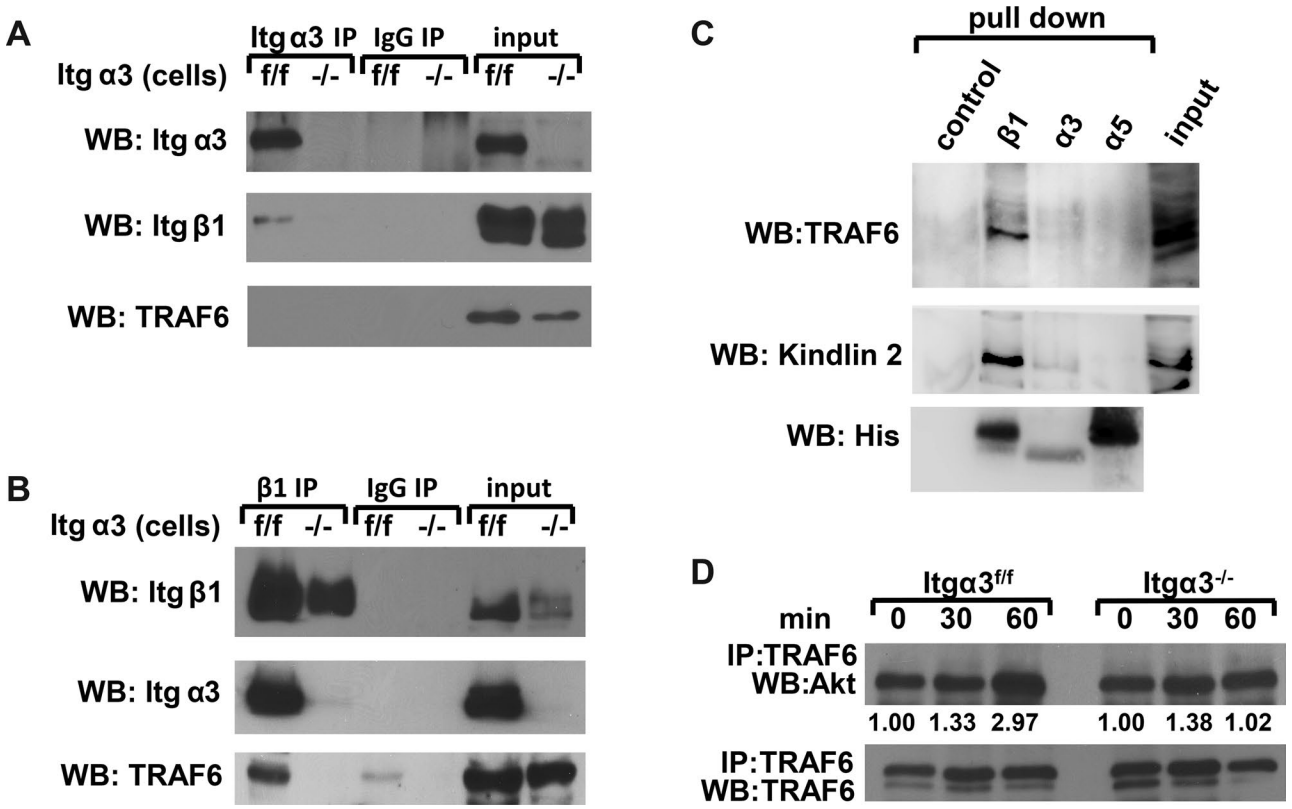

FIGURE 9: TRAF6 forms a complex with α3β1 integrin and Akt. (A and B) Cell lysates from Itgα3$^{f/f}$ and Itgα3$^{-/-}$ CD cells (1.0 mg total protein) were immunoprecipitated with protein G-Sepharose–coupled antibody to α3 (A) or β1 (B) integrin subunits. Immunoprecipitates were subjected to Western blot analysis with antibodies to TRAF6 or α3 or β1 integrin subunits. Input was 20 μg total protein lysates (2%). (C) Ni-NTA magnetic agarose beads (control), α3-TM-Cyto domains, α5-TM-Cyto domains, or β1-TM-Cyto domains bound to Ni-NTA magnetic agarose beads were incubated with Itgα3$^{f/f}$ cell lysates and then immunoblotted with antibodies to TRAF6, kindlin 2, or His. (D) Itgα3$^{f/f}$ and Itgα3$^{-/-}$ CD cells were trypsinized and replated on LM-332 (1 μg/ml) as described in Figure 4A. Cell lysates (200 μg total protein) were immunoprecipitated with antibodies to TRAF6 and immunoblotted for Akt or TRAF6. Levels of Akt and TRAF6 were measured by densitometry, normalized to TRAF6 levels, and expressed as fold change relative to cells left in suspension (0 time point). Values shown are representative of three experiments.

key requirement for Akt activation downstream of other receptors such as the TNFα receptor (Chen, 2012). Our in vivo data from TRAF6 KO mice confirm that the regulatory role of TRAF6 for Akt activity in the renal collecting system is associated with developmental abnormalities. Thus it is plausible that our in vitro mechanism delineating that α3β1 integrin controls TRAF6-dependent K63-linked polyubiquitination of Akt (Figure 10) explains the phenotype of the Hoxb7Cre;Itgα3$^{flox/flox}$ mice.

Finally, we found that TRAF6 is present in integrin β1 immunoprecipitates from Itgα3$^{f/f}$ but not Itgα3$^{-/-}$ CD cells and that this interaction is independent of integrin α3β1 binding to ligand. Affinity chromatography with free integrin tails showed that TRAF6 binds only to the integrin β1 but not the α3 cytoplasmic tail. These data suggest that, although the TRAF6/α3β1 integrin complex forms through an interaction of TRAF6 and the β1 integrin subunit in CD cells, the α3 integrin subunit is required. These data may explain the interesting observation that there were increased basal levels of Akt activating phosphorylation, Akt K63–linked polyubiquitination, and TRAF6 K63–linked polyubiquitination in Itgα3$^{-/-}$ compared with Itgα3$^{f/f}$ CD cells. We speculate that, in Itgα3$^{-/-}$ CD cells, integrin α3β1 does not interact with TRAF6 and therefore cannot alter its activity. By contrast, in cells expressing the α3 integrin subunit, integrin α3β1 acts as a repressor of TRAF6 activity when the integrin is not bound to LM. After the cells adhere to LM, TRAF6 is activated in an integrin-dependent manner by mechanisms that are yet to be determined.

In conclusion, this study demonstrates that integrin α3β1 interactions with both α3- and α5-containing LMs regulate UB development by functionally modulating the Akt signaling pathway. In addition, we show that K63-linked polyubiquitination plays a previously unrecognized role in integrin α3β1–dependent cell signaling required for UB development and that this may be a novel general mechanism whereby integrins regulate signaling pathways.

MATERIALS AND METHODS

Reagents, adenovirus vectors, siRNAs, and antibodies

Human laminin 332 (LM-332) was produced, purified, and evaluated as previously described (Tripathi *et al.*, 2008). LM-111 was produced as previously described (McKee *et al.*, 2007, 2009). Collagen I was purchased from BD Biosciences (San Jose, CA); fibronectin and vitronectin were purchased from Sigma-Aldrich (St. Louis, MO). Akt inhibitor IV, PI3K inhibitor LY294002, and p38 inhibitor SB203580 were purchased from Calbiochem (San Diego, CA).

LM-511 was produced as a heterotrimer of mouse LM α5, hemagglutinin (HA)-tagged human LM β1, and human LM γ1, as

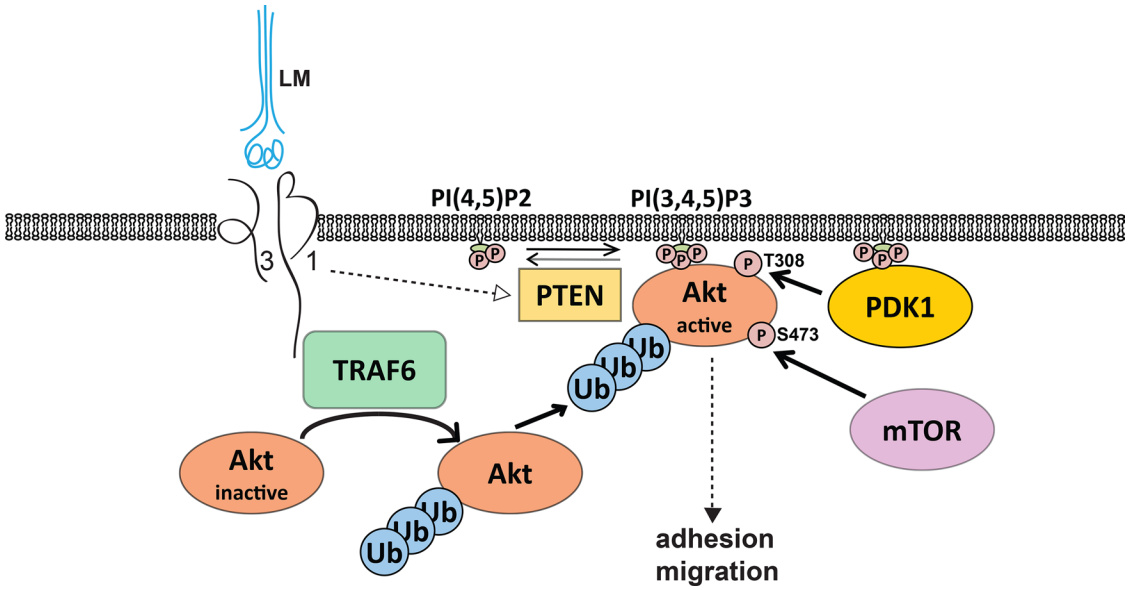

FIGURE 10: LM-332/integrin α3β1 interactions induce Akt activation by TRAF6-mediated K63-linked polyubiquitination. Integrin α3β1 interactions with LM induce the formation of a TRAF6/α3β1 integrin complex through binding of TRAF6 to the cytoplasmic tail of β1 integrin subunit. This complex is required for TRAF6 activation and triggers K63-linked polyubiquitination of Akt, which facilitates Akt translocation to the cellular membrane. Integrin α3β1 interactions with LM also induce PTEN inactivation that results in an increase of PIP_3 and Akt anchoring to the membrane, where it is phosphorylated and fully activated.

previously described (McKee *et al.*, 2007). The complete mouse LM α5 cDNA in an LZ10 plasmid (kindly provided by Jeffrey Miner, Washington University, St. Louis, MO) was excised with *Eco*R1 and ligated into the expression vector pcDNA3.1 puro. HEK293 cells stably expressing the human β1 LM subunit containing an N-terminal HA tag and the γ1 LM subunit (McKee *et al.*, 2007, 2009) were transfected with the LM α5 construct. Stable clones secreting the LM into media were selected and expanded. Recombinant LM-511 protein was purified by affinity chromatography from conditioned medium of HEK293 cells on an HA matrix (E6779; Sigma-Aldrich) and eluted per manufacturer's conditions with 0.1 M glycine (pH 2.8). Protein was concentrated in Amicon ultra 15 filters (100K mwco, ufc900024; Millipore, Billerica, MA) and dialyzed in 50 mM Tris (pH 7.4), 90 mM NaCl, and 0.125 mM EDTA. The homogeneity of purified LM-511 was confirmed by Coomassie blue staining of SDS–PAGE (Supplemental Figure 1A). The correct folding of LM-511was confirmed by a polymerization assay (Supplemental Figure 1B; McKee *et al.*, 2007), and LM-511activity was assessed by binding with recombinant α7β1 and α6β1 integrins (Supplemental Figure 1C; McKee *et al.*, 2012).

Adenoviruses with vectors encoding GFP, ad-GFP, the dominant-negative catalytic subunit deletion mutant PI3K, ad-delta p85, and constitutively active myristoylated Akt (ad-myrAkt) were propagated in HEK293 cells, purified by column chromatography, quantitated, and used for cell infection based on particle yield as previously described (Tan *et al.*, 2006).

SignalSilence Akt siRNA I (sequence [5′-3′] UGCCCUUCUACAACCAGGA) and SignalSilence Akt1 siRNA I (mouse-specific, sequence [5′-3′] GCUCAAGAAGGACCCUACA) were purchased from Cell Signaling Technology (Danvers, MA). Silencer Select predesigned TRAF6 siRNAs (sequences [5′-3′] CAUUAAGGAUGAUACAUUAtt and AGAAAAGAGUUGUAGUUUUtt) and Silencer Select Negative control #1 siRNA were bought from Ambion (Carlsbad, CA).

The following antibodies were used in Western immunoblot analyses: integrin α3 (AB1920 [Millipore, Temecula, CA] and AF2787 [R&D Systems]); integrin β1 (AB1952; Millipore); integrin β4 (AF4054; R&D Systems); integrin α6 (3750), phospho-Akt^{Thr308} (9275), phospho-Akt^{Ser473} (9271), total Akt (9272), phospho-GSK-3β^{Ser9} (9322), total GSK-3β (9315), phospho-p38$^{Thr180/Tyr182}$ (9211), total p38 (9212), phospho-ERK1/2$^{Thr202/Tyr204}$ (9101), total ERK1/2 (9102), phospho-PDK1^{Ser241} (3438) and total PDK1 (5662), phospho-Src^{Tyr416} family (2101), total Src (2108), PTEN (9552), K48-linkage specific polyubiquitin (8081), and K63-linkage specific polyubiquitin (5621) (all from Cell Signaling Technologies); TRAF6 (ab94720; Abcam, Cambridge, MA); kindlin 2 (MAB2617; Millipore); and His (620-0203; Bio-Rad). Antibodies for TRAF6 (H-274; Santa Cruz Biotechnology), Akt (4685; Cell Signaling), integrin β1 (MAB1997; Millipore), integrin α3 (AF2787; R&D Systems), and integrin α6 (H-87; Santa Cruz Biotechnology) were used for immunoprecipitation. Antibody to β-actin (A4700, Sigma-Aldrich) was used to evaluate protein loading. Anti-mouse β1 (550530), α1 (555001), α2 (553819), α5 (553350), α6 (555734), and αv (550024) integrin antibodies were purchased from BD Biosciences. R-phycoerythrin–conjugated secondary antibodies were purchased from Invitrogen (Carlsbad, CA). Antibodies to integrin α6 (555734; BD Biosciences) were used in adhesion assays.

Laminin subunits α3 and γ2 global knockout mice

All animal experiments were approved by the Vanderbilt University Institutional Animal Use and Care Committee. LM α3 global knockout mice were kindly provided by W. Carter (University of Washington; Ryan *et al.*, 1999). LM γ2 knockout mice were a gift from J. Uitto (Thomas Jefferson University; Meng *et al.*, 2003).

TRAF6-deficient mice

Generation of the global TRAF6 KO mice on 129SV background was previously described (Naito *et al.*, 1999). The genotyping was verified by PCR amplification of the genomic DNA with the

following primers: forward primer, 5′-CGTGCCATGTAATGCATTCTG-3′; reverse primer, 5′-CGAGATGTCTCAGTTCCATC-3′; and reverse mutant primer to amplify the TRAF6 gene deleted sequence, 5′-CACTCAGCACCATTTCCTAACCT-3′. Mice were bred as heterozygotes, and age-matched WT and TRAF6 KO littermates were used in experiments.

Generation of HoxB7Cre:Itgα3$^{flox/flox}$ mice

Integrin α3$^{flox/flox}$ (Itgα3$^{flox/flox}$) mice (Sachs *et al.*, 2006), were crossed with the HoxB7Cre mice (generous gift of A. McMahon, University of Southern California; Kobayashi *et al.*, 2005). Age-matched littermates homozygous for the integrin *Itgα3$^{flox/flox}$* gene, but lacking Cre (Itgα3$^{flox/flox}$ mice), were used as controls. The expression of integrin α3 and activation of signaling pathways in the developing mouse CDs was determined using Western immunoblot analysis.

Western blot analysis

Papillae from individual 3-d-old pups were isolated and lysed using a Polytron homogenizer in T-PER reagent (Thermo Scientific, Waltham, MA) with protease inhibitors and phosphatase inhibitors cocktail 1 and 2 (Sigma-Aldrich). Cell lysates were prepared using M-PER reagent (Thermo Scientific). Lysates were centrifuged at 17,000 × *g* for 15 min at 4°C, and total protein concentration was determined using BCA reagent (Thermo Scientific). Protein extracts were subjected to Western immunoblot analysis and developed using the Western Lightning Chemiluminescence Plus detection system (Perkin Elmer-Cetus, Wellesley, MA) according to the manufacturer's protocol. Densitometry was performed using the ImageJ program. For quantification of levels of protein phosphorylation, OD of bands for phosphoprotein was normalized to total protein and β-actin.

Morphological and immunohistochemical analysis

Whole mouse embryos or kidneys were removed, fixed, stained with hematoxylin and eosin (H&E) and evaluated by light microscopy as previously described (Mathew *et al.*, 2012). For analysis of LM-332 expression, tissue sections were treated with antigen-retrieval citra buffer for 10 min, blocked with 5% normal goat serum in phosphate-buffered saline (PBS) for 1 h at room temperature, and incubated with primary rabbit anti-rat LMγ2 antibody (Giannelli *et al.*, 1999). After incubation with biotinylated anti-rabbit antibody for 1 h at room temperature, LM332 was visualized using ABC reagent (a preformed avidin/biotinylated enzyme complex that was developed with 3,3′-diaminobenzidine horseradish peroxidase substrate). Slides were counterstained with hematoxylin. Similarly, tissue sections were probed with rabbit anti-rat LMα3 antibody (M3.3). Ki67 staining and scoring was performed as previously described (Mathew *et al.*, 2012).

Generation of integrin α3$^{-/-}$ CD cells

CD cells were isolated from 5- to 6-wk-old Itgα3$^{flox/flox}$ mice as described by Husted *et al.* (1988) and immortalized with pSV40 plasmid. Loci for the α3 integrin subunit in CD cells were deleted with adenovirus expressing Cre recombinase. CD cells were grown in DMEM/F12 containing 10% fetal bovine serum and 1% penicillin/streptomycin.

Flow cytometry analysis

Flow cytometry analysis was performed as previously described (Zhang *et al.*, 2009). CD cells were incubated with anti-mouse β1, β4, α1, α2, α6, and αv integrin antibodies followed by fluorescein isothiocyanate–conjugated secondary antibodies.

Cell adhesion

Cell adhesion assays were performed in 96-well plates as previously described (Chen *et al.*, 2004). Cells (1×10^5) were seeded in serum-free medium onto plates containing different concentrations of ECM for 60 min. Nonadherent cells were removed; the remaining cells were fixed, stained with crystal violet, and solubilized; and the optical densities of the cell lysates were read at 570 nm (OD_{570}). Adhesion was calculated as percent of positive control (adhesion to serum).

Cell migration

Cell migration was assayed as previously described (Chen *et al.*, 2004). Transwells with 8-μm pores were coated with different ECM components, and 1×10^5 cells were added to the upper well in serum-free medium. Cells that migrated through the filter after 4 h were counted.

Cell proliferation

Cell proliferation was assessed by measuring incorporation of 5-bromodeoxyuridine (BrdU) in an enzyme-linked immunosorbent assay–based 5-Bromo-2′-deoxy-uridine Labeling and Detection Kit III (Roche Applied Science, Indianapolis, IN) as previously described (Linkous *et al.*, 2010). BrdU incorporation was quantified by a change of absorbance (OD) at 405 nm.

Cell replating assays

Cell replating assays were performed on CD cells that were trypsinized, washed, suspended in serum-free DMEM, plated on LM-332 or LM-511 (1 μg/ml), and harvested 0, 30, and 60 min later. Cells were washed in PBS and lysed using M-PER reagent with protease and phosphatase inhibitor cocktails (Sigma-Aldrich). Protein extracts (20–40 μg) were subjected to Western immunoblot analysis.

When chemical inhibitors were used, they were added 1 h before the assays. Adenoviral infection of cells was performed at 10–100 plaque-forming units/cell as previously described (Tan *et al.*, 2006), and the assays were performed 24 h later. For silencing experiments, cells were transfected with nonsilencing siRNA (20 nM, transfection control) or Akt siRNA (100 nM) or TRAF6 siRNA (20 nM) using Lipofectamine RNAiMAX according to the manufacturer's instructions. Transfected cells were used 48 h later.

Evaluation of PIP_3 levels

CD cells were subjected to the replating assay using 150-mm cell culture plates coated with LM-332 (1 mg/ml) and were harvested at 0, 30, and 60 min after plating. Lipids were extracted using a modified Bligh and Dyer method as previously described (Yazlovitskaya *et al.*, 2008). PIP_3 levels were detected using the PIP_3 Mass ELISA Kit (Echelon, Salt Lake City, UT) according to the manufacturer's instructions.

Immunoprecipitation

For immunoprecipitation, antibody or corresponding normal immunoglobulin G (IgG) were covalently bound to protein A/G Sepharose (Thermo Scientific) as previously described (Persons *et al.*, 1999). Immunoprecipitations were performed with 0.1 mg (for integrin α6), 0.2 mg (for Akt and TRAF6), or 1.0 mg (for integrins α3 or β1) of total cell lysates overnight at 4°C with rotating, after which the bound immune complexes were washed, resuspended in SDS–PAGE sample buffer, heated at 95°C for 10 min, cleared by centrifugation, and subjected to Western immunoblot analysis. For immunoprecipitation of integrins α3 or β1, cells were grown on uncoated cell culture surfaces where integrin α3β1 is not ligated by ligand.

Pull-down assay

N-terminally 6×His-tagged integrin β1-TM-Cyto (transmembrane-cytoplasmic domains, mouse residues from 719 to 798 of the full-length protein), α5-TM-Cyto (mouse residues from 993 to 1053 of the full-length protein), and α3-TM-Cyto (mouse residues from 991 to 1053 of the full-length protein) were cloned into a pET15b vector and transformed into BL21 (DE3) Arctic Express *Escherichia coli*. After protein induction with 1 mM isopropyl β-D-1-thiogalactopyranoside, cells were pelleted by centrifugation, resuspended in TBS buffer (Tris 50 mM, NaCl 150 mM, pH 7.4) with 100 µg/ml lysozyme and 50 µg/ml DNase, and rotated at 4°C for 2 h. Cell lysates were treated with Empigen (30% solution; 1 ml per 10 ml of lysate) at 4°C for 1 h with rotation and centrifuged. Supernatants were incubated with Ni-NTA magnetic agarose beads (Qiagen) at 4°C for 3 h, washed three times with TBS buffer, and incubated with CD cell lysates (lysis buffer: 1% NP40, Tris 50 mM, NaCl 150 mM, pH 7.4, protease inhibitor cocktail [Sigma-Aldrich]) overnight at 4°C. After three washes with lysis buffer, proteins were eluted from the beads by being boiled with 80 µl SDS–PAGE sample buffer for 5 min and were subjected to Western blot analyses with antibodies to TRAF6, kindlin 2, or His.

Statistical analyses

The mean and SEM of each treatment group were calculated for all experiments. At least four independent experiments (some in triplicates each) were performed. Student's *t* test was used to compare two groups. All statistical tests were two-sided, and statistical analysis was done with the use of SigmaStat software (Systat Software, San Jose, CA). Statistical significance was defined as $p \leq 0.05$.

ACKNOWLEDGMENTS

We thank William Carter for the LM α3–null mice and Jouni Uitto for the LM γ2–null mice. We thank Catherine Alford for her technical help with cell sorting and flow cytometry and Reinhard Fassler and Marc Schmidt-Supprian for constructive criticism of the project. This work was supported by VA Merit Review 1I01BX002025 (Ambra Pozzi [A.P.]) and 1I01BX002196 (R.Z.) and National Institutes of Health Grants R01-CA162433 (A.P.), R01-DK095761 (A.P.), RO1-DK083187 (R.Z.), RO1-DK075594 (R.Z.), R01-DK066921 (R.Z.), and R01-DK36425 (P.Y.). A.S. is supported by the Netherlands Kidney Foundation. H.-Y.T. and R.T.B. are supported by the Max Planck Society and the Deutsche Forschungsgemeinschaft (DFG; SFB 914).

REFERENCES

Aumailley M, Bruckner-Tuderman L, Carter WG, Deutzmann R, Edgar D, Ekblom P, Engel J, Engvall E, Hohenester E, Jones JC, *et al.* (2005). A simplified laminin nomenclature. Matrix Biol 24, 326–332.

Bayascas JR (2008). Dissecting the role of the 3-phosphoinositide-dependent protein kinase-1 (PDK1) signalling pathways. Cell Cycle 7, 2978–2982.

Cantley LC (2002). The phosphoinositide 3-kinase pathway. Science 296, 1655–1657.

Chen D, Roberts R, Pohl M, Nigam S, Kreidberg J, Wang Z, Heino J, Ivaska J, Coffa S, Harris RC, *et al.* (2004). Differential expression of collagen- and laminin-binding integrins mediates ureteric bud and inner medullary collecting duct cell tubulogenesis. Am J Physiol Renal Physiol 287, F602–F611.

Chen ZJ (2012). Ubiquitination in signaling to and activation of IKK. Immunol Rev 246, 95–106.

Giannelli G, Pozzi A, Stetler-Stevenson WG, Gardner HA, Quaranta V (1999). Expression of matrix metalloprotease-2-cleaved laminin-5 in breast remodeling stimulated by sex steroids. Am J Pathol 154, 1193–1201.

Greciano PG, Moyano JV, Buschmann MM, Tang J, Lu Y, Rudnicki J, Manninen A, Matlin KS (2012). Laminin 511 partners with laminin 332 to mediate directional migration of Madin-Darby canine kidney epithelial cells. Mol Biol Cell 23, 121–136.

Guertin DA, Sabatini DM (2007). Defining the role of mTOR in cancer. Cancer Cell 12, 9–22.

Husted RF, Hayashi M, Stokes JB (1988). Characteristics of papillary collecting duct cells in primary culture. Am J Physiol 255, F1160–F1169.

Jiang T, Qiu Y (2003). Interaction between Src and a C-terminal proline-rich motif of Akt is required for Akt activation. J Biol Chem 278, 15789–15793.

Joly D, Berissi S, Bertrand A, Strehl L, Patey N, Knebelmann B (2006). Laminin 5 regulates polycystic kidney cell proliferation and cyst formation. J Biol Chem 281, 29181–29189.

Joly D, Morel V, Hummel A, Ruello A, Nusbaum P, Patey N, Noel LH, Rousselle P, Knebelmann B (2003). β4 integrin and laminin 5 are aberrantly expressed in polycystic kidney disease: role in increased cell adhesion and migration. Am J Pathol 163, 1791–1800.

Kobayashi A, Kwan KM, Carroll TJ, McMahon AP, Mendelsohn CL, Behringer RR (2005). Distinct and sequential tissue-specific activities of the LIM-class homeobox gene Lim1 for tubular morphogenesis during kidney development. Development 132, 2809–2823.

Kreidberg JA, Donovan MJ, Goldstein SL, Rennke H, Shepherd K, Jones RC, Jaenisch R (1996). Alpha 3 beta 1 integrin has a crucial role in kidney and lung organogenesis. Development 122, 3537–3547.

Lamothe B, Besse A, Campos AD, Webster WK, Wu H, Darnay BG (2007). Site-specific Lys-63-linked tumor necrosis factor receptor-associated factor 6 auto-ubiquitination is a critical determinant of I kappa B kinase activation. J Biol Chem 282, 4102–4112.

Landstrom M (2010). The TAK1-TRAF6 signalling pathway. Int J Biochem Cell Biol 42, 585–589.

Linkous AG, Yazlovitskaya EM, Hallahan DE (2010). Cytosolic phospholipase A2 and lysophospholipids in tumor angiogenesis. J Natl Cancer Inst 102, 1398–1412.

Liu Y, Chattopadhyay N, Qin S, Szekeres C, Vasylyeva T, Mahoney ZX, Taglienti M, Bates CM, Chapman HA, Miner JH, Kreidberg JA (2009). Coordinate integrin and c-Met signaling regulate *Wnt* gene expression during epithelial morphogenesis. Development 136, 843–853.

Lomaga MA, Henderson JT, Elia AJ, Robertson J, Noyce RS, Yeh WC, Mak TW (2000). Tumor necrosis factor receptor-associated factor 6 (TRAF6) deficiency results in exencephaly and is required for apoptosis within the developing CNS. J Neurosci 20, 7384–7393.

Lomaga MA, Yeh WC, Sarosi I, Duncan GS, Furlonger C, Ho A, Morony S, Capparelli C, Van G, Kaufman S, *et al.* (1999). TRAF6 deficiency results in osteopetrosis and defective interleukin-1, CD40, and LPS signaling. Genes Dev 13, 1015–1024.

Mak GZ, Kavanaugh GM, Buschmann MM, Stickley SM, Koch M, Goss KH, Waechter H, Zuk A, Matlin KS (2006). Regulated synthesis and functions of laminin 5 in polarized Madin-Darby canine kidney epithelial cells. Mol Biol Cell 17, 3664–3677.

Mathew S, Lu Z, Palamuttam RJ, Mernaugh G, Hadziselimovic A, Chen J, Bulus N, Gewin LS, Voehler M, Meves A, *et al.* (2012). β1 integrin NPXY motifs regulate kidney collecting-duct development and maintenance by induced-fit interactions with cytosolic proteins. Mol Cell Biol 32, 4080–4091.

McKee KK, Capizzi S, Yurchenco PD (2009). Scaffold-forming and adhesive contributions of synthetic laminin-binding proteins to basement membrane assembly. J Biol Chem 284, 8984–8994.

McKee KK, Harrison D, Capizzi S, Yurchenco PD (2007). Role of laminin terminal globular domains in basement membrane assembly. J Biol Chem 282, 21437–21447.

McKee KK, Yang DH, Patel R, Chen ZL, Strickland S, Takagi J, Sekiguchi K, Yurchenco PD (2012). Schwann cell myelination requires integration of laminin activities. J Cell Sci 125, 4609–4619.

Meng X, Klement JF, Leperi DA, Birk DE, Sasaki T, Timpl R, Uitto J, Pulkkinen L (2003). Targeted inactivation of murine laminin γ2-chain gene recapitulates human junctional epidermolysis bullosa. J Invest Dermatol 121, 720–731.

Miner JH, Li C (2000). Defective glomerulogenesis in the absence of laminin α5 demonstrates a developmental role for the kidney glomerular basement membrane. Dev Biol 217, 278–289.

Miner JH, Yurchenco PD (2004). Laminin functions in tissue morphogenesis. Annu Rev Cell Dev Biol 20, 255–284.

Moyano JV, Greciano PG, Buschmann MM, Koch M, Matlin KS (2010). Autocrine transforming growth factor-β1 activation mediated by integrin αVβ3 regulates transcriptional expression of laminin-332 in Madin-Darby canine kidney epithelial cells. Mol Biol Cell 21, 3654–3668.

Naito A, Azuma S, Tanaka S, Miyazaki T, Takaki S, Takatsu K, Nakao K, Nakamura K, Katsuki M, Yamamoto T, Inoue J (1999). Severe osteopetrosis, defective interleukin-1 signalling and lymph node organogenesis in TRAF6-deficient mice. Genes Cells 4, 353–362.

Nho RS, Kahm J (2010). β1-integrin-collagen interaction suppresses FoxO3a by the coordination of Akt and PP2A. J Biol Chem 285, 14195–14209.
Persons DL, Yazlovitskaya EM, Cui W, Pelling JC (1999). Cisplatin-induced activation of mitogen-activated protein kinases in ovarian carcinoma cells: inhibition of extracellular signal-regulated kinase activity increases sensitivity to cisplatin. Clin Cancer Res 5, 1007–1014.
Ryan MC, Lee K, Miyashita Y, Carter WG (1999). Targeted disruption of the LAMA3 gene in mice reveals abnormalities in survival and late stage differentiation of epithelial cells. J Cell Biol 145, 1309–1323.
Sachs N, Kreft M, van den Bergh Weerman MA, Beynon AJ, Peters TA, Weening JJ, Sonnenberg A (2006). Kidney failure in mice lacking the tetraspanin CD151. J Cell Biol 175, 33–39.
Song MS, Salmena L, Pandolfi PP (2012). The functions and regulation of the PTEN tumour suppressor. Nat Rev Mol Cell Biol 13, 283–296.
Tan J, Geng L, Yazlovitskaya EM, Hallahan DE (2006). Protein kinase B/Akt-dependent phosphorylation of glycogen synthase kinase-3β in irradiated vascular endothelium. Cancer Res 66, 2320–2327.
Tripathi M, Nandana S, Yamashita H, Ganesan R, Kirchhofer D, Quaranta V (2008). Laminin-332 is a substrate for hepsin, a protease associated with prostate cancer progression. J Biol Chem 283, 30576–30584.
Wang G, Gao Y, Li L, Jin G, Cai Z, Chao JI, Lin HK (2012). K63-linked ubiquitination in kinase activation and cancer. Front Oncol 2, 5.
Wu H, Arron JR (2003). TRAF6, a molecular bridge spanning adaptive immunity, innate immunity and osteoimmunology. Bioessays 25, 1096–1105.
Xia H, Diebold D, Nho R, Perlman D, Kleidon J, Kahm J, Avdulov S, Peterson M, Nerva J, Bitterman P, Henke C (2008). Pathological integrin signaling enhances proliferation of primary lung fibroblasts from patients with idiopathic pulmonary fibrosis. J Exp Med 205, 1659–1672.
Yang DH, McKee KK, Chen ZL, Mernaugh G, Strickland S, Zent R, Yurchenco PD (2011). Renal collecting system growth and function depend upon embryonic γ1 laminin expression. Development 138, 4535–4544.
Yang WL, Wang J, Chan CH, Lee SW, Campos AD, Lamothe B, Hur L, Grabiner BC, Lin X, Darnay BG, Lin HK (2009). The E3 ligase TRAF6 regulates Akt ubiquitination and activation. Science 325, 1134–1138.
Yang WL, Wu CY, Wu J, Lin HK (2010). Regulation of Akt signaling activation by ubiquitination. Cell Cycle 9, 487–497.
Yazlovitskaya EM, Linkous AG, Thotala DK, Cuneo KC, Hallahan DE (2008). Cytosolic phospholipase A2 regulates viability of irradiated vascular endothelium. Cell Death Differ 15, 1641–1653.
Zent R, Bush KT, Pohl ML, Quaranta V, Koshikawa N, Wang Z, Kreidberg JA, Sakurai H, Stuart RO, Nigam SK (2001). Involvement of laminin binding integrins and laminin-5 in branching morphogenesis of the ureteric bud during kidney development. Dev Biol 238, 289–302.
Zhang X, Mernaugh G, Yang DH, Gewin L, Srichai MB, Harris RC, Iturregui JM, Nelson RD, Kohan DE, Abrahamson D, *et al*. (2009). β1 integrin is necessary for ureteric bud branching morphogenesis and maintenance of collecting duct structural integrity. Development 136, 3357–3366.

Supplemental Materials

Molecular Biology of the Cell

Yazlovitskaya et al.

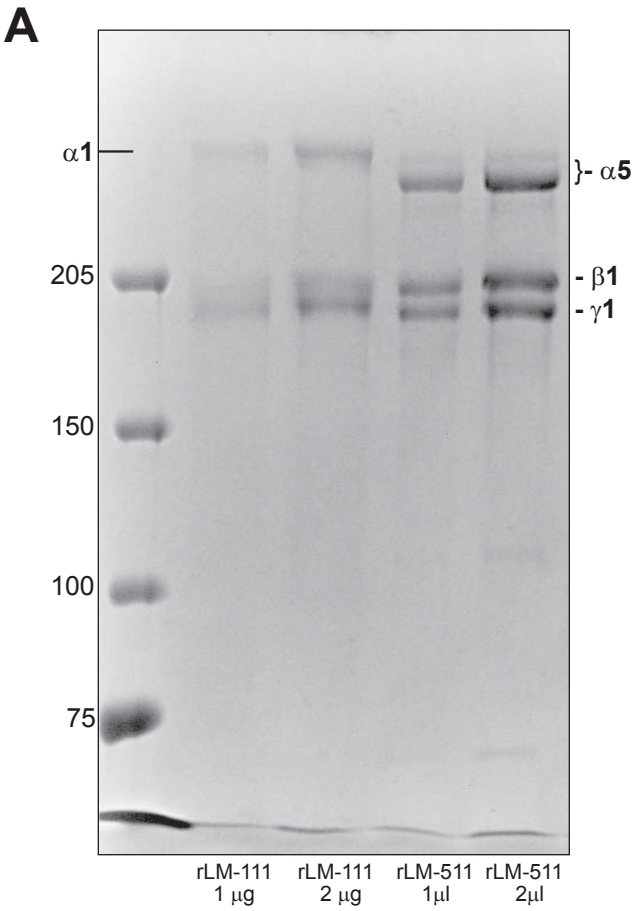

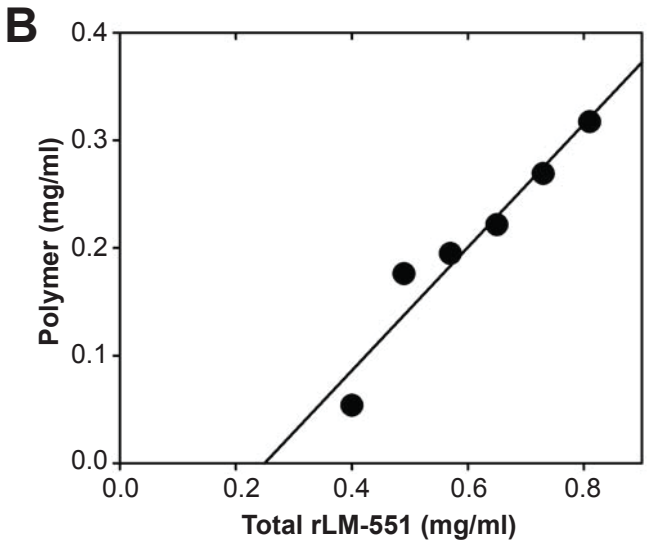

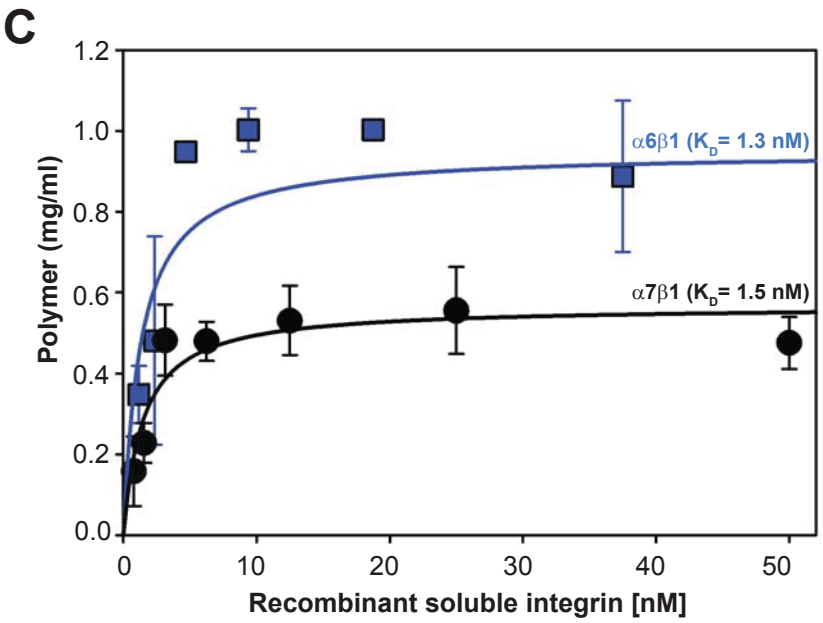

Supplementary Fig. 1

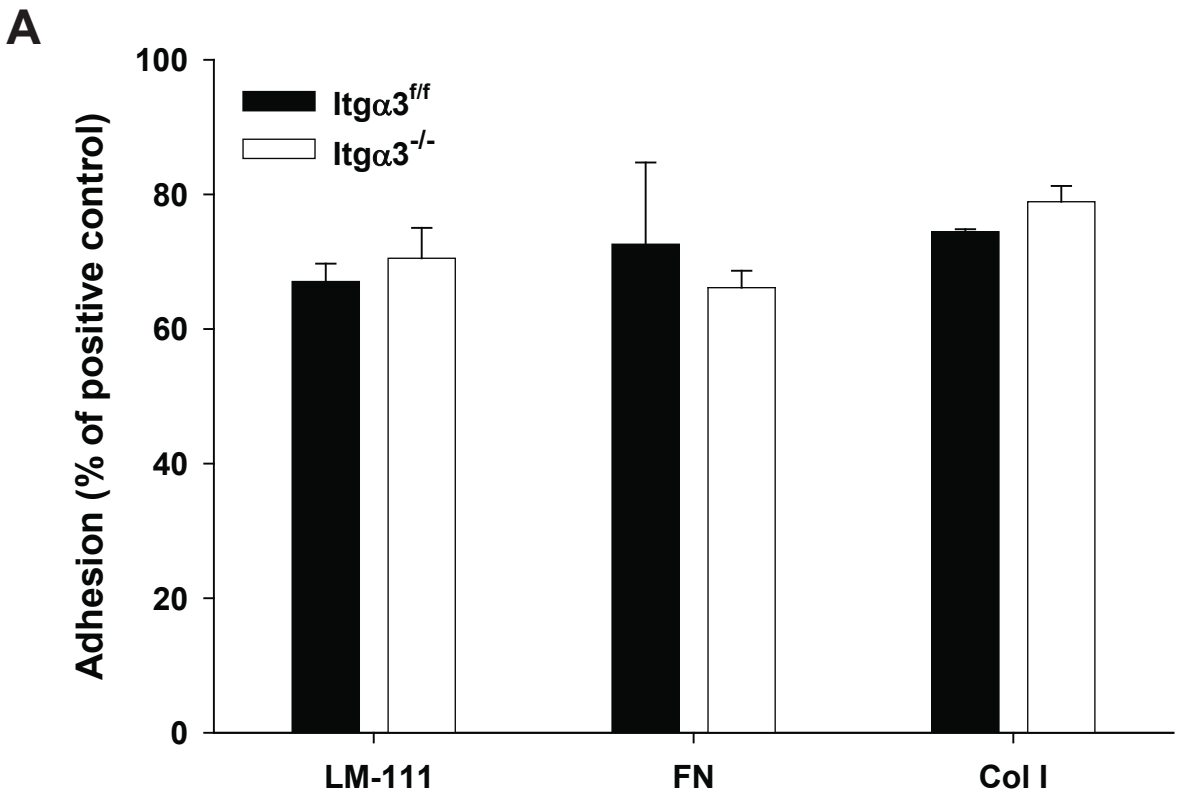

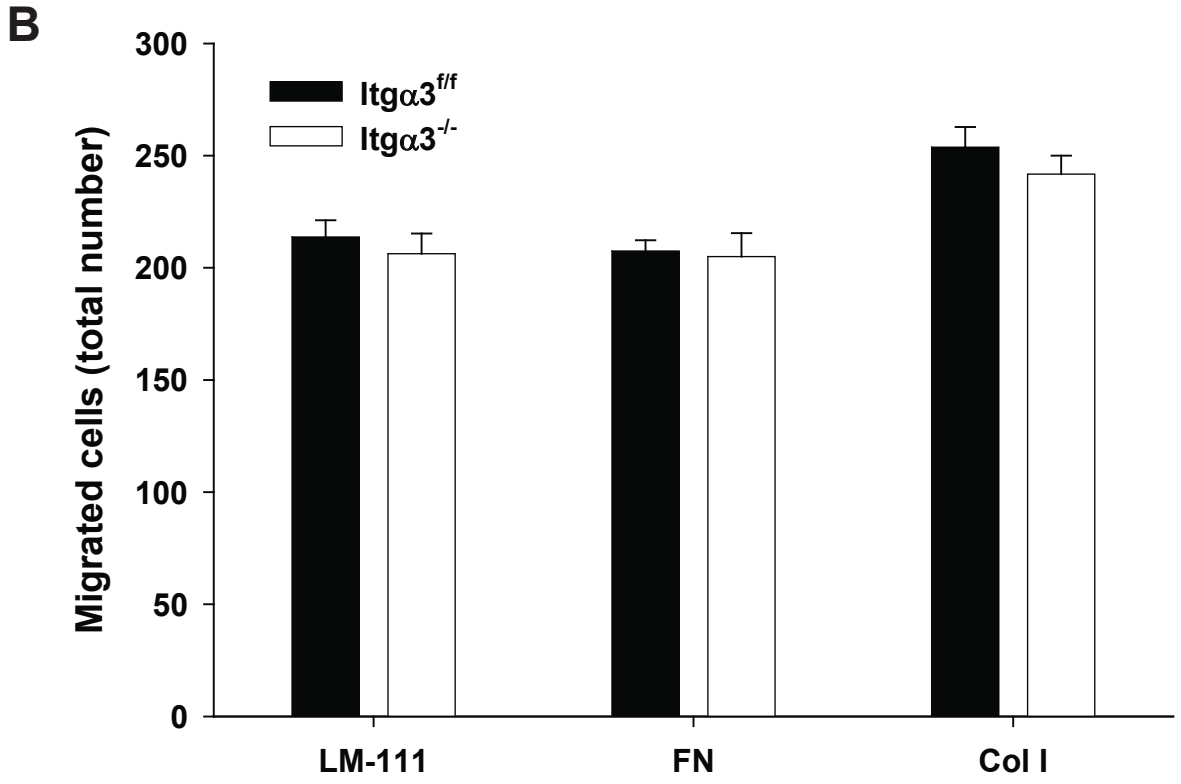

Supplementary Fig. 2

Supplementary Figure 1. Characterization of produced LM-511. (A) The homogeneity of purified LM-511 was confirmed by Coomassie blue staining of SDS-PAGE (7.5%, reduced). (**B**) The correct folding of LM-511was confirmed by a polymerization assay. Recombinant LM511 was incubated in the presence of 1 mm calcium at 37 °C followed by centrifugation. Shown is a plot of the concentration of polymer as a function of total laminin concentration. (**C**) LM-511activity was assessed by binding with recombinant integrins α7β1 (circles) and α6β1 (squares). The LM-511 was coated onto high binding dishes (Costar) at 10 nM in 40 mM sodium bicarbonate buffer, pH 9.6. The plate was blocked with TTBS (50mM Tris pH 7.4, 90mM NaCl, 0.02% tween 20, + 1% BSA and 1mM MnCl2), then soluble integrin was bound in the same buffer for 2 hours at room temperature. The bound integrin was detected with biotinylated rabbit anti-Velcro antibody (ACID/BASE coiled coil, 1:1000 dilution), followed by HRP-conjugated streptavidin (1 mg/ml) and then developed with TMB (Thermo Scientific).

Supplementary Figure 2. **Integrin α3β1 is not essential for CD cell adhesion and migration on LM-111, fibronectin (FN) and collagen I (Col I).** Adhesion **(A)** and migration **(B)** on LM-111, FN and Col I were evaluated as described in Methods. Mean measurements ±SEM of 4-6 independent experiments are shown.